

Doctoral Dissertation

**Urban Climate Challenges in Growing Cities of Southeast Asia:
Urban Heat Islands and Global Warming**

ANDHANG RAKHMAT TRIHAMDANI

Graduate School for International Development and Cooperation
Hiroshima University

September 2017

**Urban Climate Challenges in Growing Cities of Southeast Asia:
Urban Heat Islands and Global Warming**

D140185

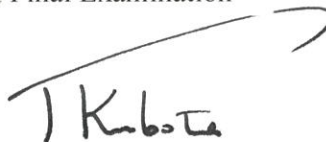
ANDHANG RAKHMAT TRIHAMDANI

A Dissertation Submitted to
the Graduate School for International Development and Cooperation
of Hiroshima University in Partial Fulfillment
of the Requirement for the Degree of
Doctor of Engineering

September 2017

We hereby recommend that the dissertation by Mr. ANDHANG RAKHMAT TRIHAMDANI entitled "Urban Climate Challenges in Growing Cities of Southeast Asia: Urban Heat Islands and Global Warming" be accepted in partial fulfillment of the requirements for the degree of DOCTOR OF ENGINEERING.

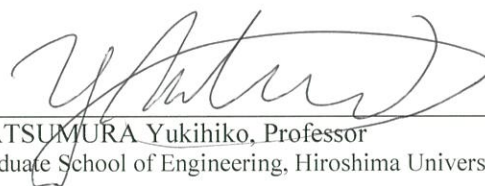
Committee on Final Examination



KUBOTA Tetsu, Associate Professor
Chairperson



ZHANG Junyi, Professor



MATSUMURA Yukihiro, Professor
Graduate School of Engineering, Hiroshima University

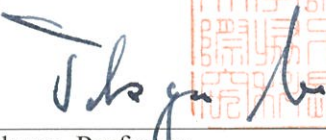


LEE Han Soo, Associate Professor



TANAKA Takahiro, Associate Professor
Graduate School of Engineering, Hiroshima University

Approved



BABA Takuya, Professor
Dean

Date 19 July 2017

Date September 1. 20 17

Contents

| | Page |
|--|-------|
| Abstract..... | vii |
| Acknowledgements..... | ix |
| List of Figures..... | xi |
| List of Tables..... | xix |
| List of Acronyms..... | xxi |
| List of Publications and Awards..... | xxiii |
| Chapter 1 - Introduction | |
| 1.1 Research background..... | 1 |
| 1.1.1 The growing cities in Southeast Asia..... | 1 |
| 1.1.2 Urbanisation and its environmental impact..... | 3 |
| 1.1.3 UHI effect..... | 5 |
| 1.1.4 Global warming..... | 6 |
| 1.1.5 The impact of urban warming..... | 7 |
| 1.2 The case study cities..... | 8 |
| 1.2.1 Hanoi, Vietnam..... | 9 |
| 1.2.2 Johor Bahru, Malaysia..... | 12 |
| 1.3 Research objectives..... | 16 |
| 1.4 Structure of thesis..... | 17 |
| References..... | 18 |
| Chapter 2 - Literature Review | |
| 2.1 UHI in general..... | 23 |
| 2.2 UHI studies in the tropics..... | 25 |
| 2.3 Impacts of land use changes on UHIs..... | 27 |
| 2.4 Influences of global warming on urban climate..... | 28 |
| 2.5 Studies on the impacts of urban warming..... | 30 |
| 2.5.1 Impact on building energy consumption..... | 30 |
| 2.5.2 Impacts on indoor and outdoor thermal comfort..... | 30 |
| 2.5.3 Impact on health..... | 31 |
| 2.6 Countermeasures to UHI..... | 31 |

| | | |
|------------|---|----|
| 2.6.1 | Cooling effect of greenery on urban climate | 32 |
| 2.6.2 | Cooling effect of cool materials on urban climate..... | 34 |
| 2.6.3 | Influences of anthropogenic heat emission on urban climate..... | 35 |
| 2.7 | Summary..... | 38 |
| References | | 39 |

Chapter 3 - Methodology

| | | |
|------------|---|----|
| 3.1 | Overall research approach | 49 |
| 3.2 | Numerical simulation using WRF | 50 |
| 3.2.1 | Overview..... | 50 |
| 3.2.2 | The governing equations..... | 52 |
| 3.2.3 | Numerical methods..... | 53 |
| 3.2.4 | Horizontal and vertical grid..... | 54 |
| 3.2.5 | Time integration..... | 55 |
| 3.2.6 | Initial conditions | 55 |
| 3.2.7 | Boundary conditions | 56 |
| 3.2.8 | Nesting..... | 56 |
| 3.2.9 | Parameterisations..... | 56 |
| 3.2.10 | WRF program workflows..... | 57 |
| 3.3 | Observational weather records | 59 |
| 3.4 | Experiments for validation and sensitivity testing of the parameterisations | 61 |
| 3.5 | Coupling WRF with Urban-Canopy Model (UCM)..... | 62 |
| 3.5.1 | Solar fluxes | 63 |
| 3.5.2 | Longwave fluxes..... | 64 |
| 3.5.3 | Sensible heat flux..... | 65 |
| 3.5.4 | Wind speed in the canyon..... | 65 |
| 3.5.5 | Surface temperature | 66 |
| 3.6 | Input weather data for global warming condition..... | 66 |
| 3.6.1 | IPCC AR5 RCP scenario | 66 |
| 3.6.2 | GCMs..... | 67 |
| 3.6.3 | Direct Dynamical Downscaling (DDD) method..... | 69 |
| 3.7 | WRF domain set-ups | 70 |
| 3.7.1 | WRF domain set-up of Hanoi case study | 70 |
| 3.7.2 | WRF domain set-up of JB case study | 71 |
| 3.8 | Building simulation using TRNSYS | 72 |
| 3.8.1 | Overview..... | 72 |
| 3.8.2 | The numerical solver and components used..... | 73 |
| 3.8.3 | Input weather data for TRNSYS simulation..... | 76 |
| References | | 78 |

Chapter 4 - Impacts of land use changes on urban climate: Case studies of Hanoi and Johor Bahru

| | | |
|-------|---|-----|
| 4.1 | Objectives | 81 |
| 4.2 | Scenarios for numerical experiments..... | 81 |
| 4.2.1 | Simulation scenarios for Hanoi case study | 81 |
| 4.2.2 | Land use proportion in current and master plan conditions of Hanoi..... | 83 |
| 4.2.3 | Simulation scenarios for JB case study..... | 84 |
| 4.2.4 | Land use proportions in current and master plan conditions of JB..... | 85 |
| 4.3 | WRF model configuration and validation | 86 |
| 4.3.1 | WRF configuration and validation of Hanoi case study | 86 |
| 4.3.2 | WRF configuration and validation of JB case study | 88 |
| 4.4 | Results and discussion | 91 |
| 4.4.1 | Hanoi case study | 91 |
| 4.4.2 | JB case study..... | 98 |
| 4.4.3 | Energy balance analysis of Hanoi and JB case studies..... | 103 |
| | Summary | 106 |
| | References | 107 |

Chapter 5 - Influence of global warming on urban climate: A case study of Hanoi

| | | |
|-------|--|-----|
| 5.1 | Objectives | 109 |
| 5.2 | Scenarios for numerical experiments..... | 109 |
| 5.3 | Results and discussion | 110 |
| 5.3.1 | Urban climate in 2030s | 110 |
| 5.3.2 | Contributions of land use changes and global warming to the future urban warming | 114 |
| 5.4 | Summary..... | 116 |
| | References | 118 |

Chapter 6 - Cooling effect of the green spaces: A case study of Hanoi

| | | |
|-------|--|-----|
| 6.1 | Objectives | 119 |
| 6.2 | Assessment of the cooling effect of proposed green spaces | 119 |
| 6.2.1 | WRF configuration | 119 |
| 6.2.2 | Scenarios for numerical experiments..... | 121 |
| 6.2.3 | Model validation | 122 |
| 6.3 | Proposal for new configuration of green spaces | 123 |
| 6.3.1 | Scenarios for numerical experiments..... | 123 |
| 6.4 | Cooling impacts of increasing the green coverage ratio in Hanoi Master Plan 2030 | 124 |
| 6.4.1 | Overview..... | 124 |
| 6.4.2 | WRF configuration | 125 |

| | | |
|-------|---|-----|
| 6.4.3 | Scenarios for numerical experiments..... | 125 |
| 6.5 | Results and discussion | 127 |
| 6.5.1 | The cooling effect of the proposed green spaces | 127 |
| 6.5.2 | Assessment of the new configurations of the green spaces | 136 |
| 6.5.3 | Effects of the further urban greening through GCR and vegetation type | 140 |
| 6.6 | Summary..... | 150 |

Chapter 7 – Influence of anthropogenic heat release on urban climate: A case study of Johor Bahru

| | | |
|------------|---|-----|
| 7.1 | Objectives | 151 |
| 7.2 | Scenarios for numerical experiments..... | 151 |
| 7.3 | Calculation of anthropogenic heat emission for current condition..... | 152 |
| 7.3.1 | Anthropogenic heat releases from traffic..... | 152 |
| 7.3.2 | Anthropogenic heat releases from buildings..... | 157 |
| 7.3.3 | Anthropogenic heat releases from human metabolism..... | 162 |
| 7.4 | Calculation of anthropogenic heat emission for BaU and CM scenarios | 164 |
| 7.4.1 | Anthropogenic heat releases from traffic..... | 164 |
| 7.4.2 | Anthropogenic heat releases from buildings..... | 164 |
| 7.4.3 | Anthropogenic heat releases from human metabolism..... | 167 |
| 7.5 | Total anthropogenic heat emission for current, BaU and CM scenarios | 167 |
| 7.6 | WRF-UCM configuration..... | 168 |
| 7.7 | Model validation..... | 168 |
| 7.8 | Results and discussion | 170 |
| 7.9 | Summary..... | 173 |
| References | | 174 |

Chapter 8 - Impacts of urban warming on thermal comfort and cooling load in residential buildings: A case study of Hanoi

| | | |
|------------|---|-----|
| 8.1 | Urban houses in Hanoi..... | 175 |
| 8.2 | Energy saving techniques for residential buildings in Vietnam | 176 |
| 8.3 | Objectives | 177 |
| 8.4 | Simulation conditions | 178 |
| 8.5 | Model validation..... | 180 |
| 8.6 | Results and discussion | 182 |
| 8.6.1 | Impacts of future urban warming on indoor thermal environments | 182 |
| 8.6.2 | Cooling effect of energy saving techniques on indoor thermal environments | 183 |
| 8.6.3 | Effect of energy-saving techniques on cooling load reduction..... | 185 |
| 8.7 | Summary..... | 187 |
| References | | 188 |

Chapter 9 – Countermeasures to urban warming for growing cities of Southeast Asia

| | | |
|-------|---|-----|
| 9.1 | The potential factors causing future urban warming | 189 |
| 9.2 | The UHI mitigation measures through urban greening and reduction of anthropogenic heat emission | 191 |
| 9.3 | Adaptation to urban warming in buildings | 192 |
| 9.4 | Recommendations..... | 193 |
| 9.4.1 | Tackling global warming or UHI? Global or local? | 193 |
| 9.4.2 | Focus on the reduction of nocturnal air temperature | 193 |
| 9.4.3 | Adaptation measures at building scale..... | 194 |
| 9.5 | Remarks | 195 |

Chapter 10 – Conclusions

| | | |
|------------|---|-----|
| 10.1 | Key findings of this study..... | 197 |
| 10.2 | Limitations and suggestion for the future research..... | 200 |
| References | | 200 |

| | | |
|-------------------|---|------|
| Appendix A | Creation process of the LULC datasets for WRF simulation | A-1 |
| Appendix B | Analysis of weather data in Hanoi..... | A-5 |
| Appendix C | Creation process of the LULC datasets for WRF simulation for JB | A-7 |
| Appendix D | Historical weather analysis for JB case study..... | A-9 |
| Appendix E | Process of urban land use classification in Hanoi for UCM | A-11 |
| Appendix F | Process of urban land use classification in JB for UCM..... | A-17 |
| Appendix G | Validation results of WRF simulation at all weather stations in JB | A-21 |
| Appendix H | Effects of monsoon winds on UHI in JB | A-25 |
| Appendix I | Creation process of the LULC datasets for WRF simulation with four domains configuration..... | A-27 |
| Appendix J | Surface parameters used in the WRF simulations | A-33 |
| Appendix K | URBPARAM.TBL | A-35 |
| Appendix L | TAOYAKA Onsite team project in Kita-Hiroshima | A-37 |

Abstract

The aim of this doctoral thesis is to investigate the impact of urban warming on the future challenges of urban climates in the growing cities of Southeast Asia. Major cities of Southeast Asia are suspected of experiencing further urban warming attributed to the urban heat islands and global warming effects.

The review in Chapter 2 focused on the existing studies on UHIs. The review revealed a research gap in the assessment of the effect of global warming on the urban climates under the future master plans via direct dynamical downscaling with an RCM. Further, the studies on UHI mitigation through a plausible scenario of anthropogenic heat emission is still lacking.

Chapter 3 discussed the methodology used in this study. A numerical simulation model, Weather Research and Forecasting (WRF), was mainly used in for urban climate simulations while a building simulation program, TRNSYS, was used to investigate the impacts of warmed urban temperature on thermal comfort and cooling load in buildings.

Chapter 4 investigated the impact of land use changes on urban climate. Two case studies cities were selected, which are Hanoi City in Vietnam and Johor Bahru City in Malaysia. The urban climate simulation were conducted under two land use conditions, i.e. current condition and master plan condition for each case study. It is estimated that the peak air temperature will increase particularly in the night-time.

Chapter 5 included the future weather conditions in 2030s into the urban climate simulation of Hanoi case study. The future weather were produced via direct dynamical downscaling with WRF under RCP4.5 and RCP8.5 scenarios. The simulation results with

global warming effects illustrated that the urban air temperature was expected to increase along with global warming. Global warming contributed, at most, 71% of the temperature increase in existing urban areas of Hanoi City in the 2030s.

Chapter 6 compared various configurations of green spaces in Hanoi through urban climate simulations. The resulting cooling impact were then discussed. The results show that the proposed green spaces are not necessarily effective to cool the entire urban areas. On the other hand, when the same amount of the proposed green spaces were distributed equally in the city, this strategy resulted in a better reduction of urban air temperature, especially at night.

Chapter 7 investigated the impact of the Low Carbon Society Blueprint on the reduction of air temperature in Johor Bahru City. It is found that the added heat from anthropogenic activities to the urban environment largely increases the air temperature particularly during the night-time. A significant reduction of air temperature under the master plan condition was achievable when the antropogenic emission scenario of the blueprint was implemented.

Chapter 8 compared the impact of various energy saving techniques and ventilation conditions on the thermal comfort and cooling load in an urban row house in Hanoi. Furthermore, the methodology consists in evaluating each energy saving technique at different four levels of modification intensity, respectively, under the current and future weather conditions. The results show that among the energy-saving techniques considered in this study, improvment of the glazing for windows and insulation layers ware the most influential techniques to reduce the cooling load under the future weather conditions.

Chapter 9 provides the recommendation to counter the urban warming for the the growing cities of Southeast Asia. Considering that 71% of the increased temperature in the future is attributed to global warming, the growing cities of Southeast Asia should pay serious attention to the global warming countermeasures. One of the recommended measures is to reduce the anthropogenic heat emission in the city. This measure has co-benefits since it can reduce the GHG emissions to the atmosphere and also lower the nocturnal air temperature in the city.

For the final conclusions, Chapter 10 summarized the main findings of this study and recommended areas for the future studies based on the limitations and findings of this thesis.

Acknowledgement

This thesis would not have been made possible without the great assistance, support, and guidance from many people and organizations. Therefore, please allow me to dedicate my acknowledgement of gratitude toward the following significant advisors and contributors:

To my main supervisor, Associate Prof. **Tetsu Kubota**, I would like to express my deepest gratitude for his excellence guidance, caring, patience, and providing me with an excellent atmosphere for doing research. He patiently turned me from an arrogant and poseur Indonesian into an arrogant and poseur Indonesian who might actually know something about building and urban environmental science. His constant enthusiasm for research fueled me during my time at Hiroshima University. I remember he used to say that I should “break the wall” to encourage me to enjoy and improve my research work further. He has supported me not only by providing a research assistantship over almost five years, but also academically and emotionally through the rough road to finish this thesis.

My doctoral examination committee has guided me through all these years. Thank you to Prof. **Junyi Zhang**, Prof. **Yukihiko Matsumura**, Assoc. Prof. **Han Soo Lee**, and Assoc. Prof. **Takahiro Tanaka** for being my major advisors. Prof. Zhang and Prof. Matsumura always give me constructive suggestions and comments; Assoc. Prof. Lee and Assoc. Prof. Tanaka guided me on climate modelling and have given enormous support on the numerical simulation. They have been very supportive since the days I began working on my research as a Master’s student. Also thank you to Assoc. Prof. **Satoru Iizuka** for giving me an opportunity to learn the Urban Canopy Model at his fine laboratory in Nagoya University. I would also like to deliver my gratitude to Professor Emeritus **Takao Yamashita** for always being so helpful and supportive on my research.

A very special gratitude goes out to the **TAOYAKA Program** for providing the scholarship, study opportunity, research grants and various kinds of support that enabled me to fully focus pursuing this doctoral degree. In particular, I would like to thank all of the academic and non-academic staffs at the program who have supported me along the way. I would also like to thank all of the people involved in the Onsite Team Project of TAOYAKA Program, particularly to the members of **NPO INE OASA**: Mr. **Takahiro Hotta**, Mr. **Yuji Makura**, and Ms. **Asuka Toya** for their kind cooperation and support during the implementation of the project in Kita-Hiroshima town.

And talking about the Onsite Team Project, I have to thank these extraordinary team members: Ms. **Mattana Tunchai**, Ms. **Nattacha Paksung**, and Mr. **David Perez Barbosa**, whom I consider the best partners not only in the project but also in the daily life. I wish to acknowledge a friendship that began right after our welcoming ceremony in the GELs program and became ripe throughout my years at Hiroshima University.

Dozens of people have helped and taught me immensely at Hiroshima University. I thank all my beloved friends in BUESA, especially to the current and past members of the urban heat island team: Mr. **Kento Sumida**, Mr. **Nguyen Huy Tung**, and Mr. **Tran Hoang Hai Nam** because their excellent works on the building simulation had become an important and inseparable part of this thesis. I also thank Ms. **Tran Thi Thu Phuong**. Ms. Phuong started this research before me and she had passed such an excellent work that had helped me a lot to understand this topic at the beginning of my study.

I would also like to thank the **Vietnam Institute of Urban and Rural Planning (VIUP)** and the **Vietnam Institute of Architecture (VIAR)** for always being cooperative to provide data and information for my research.

I am grateful to my parents and siblings, who have provided me through moral and emotional support. They have been the most basic energy source of my life. I am also grateful to my other family members and friends. Their support has been unconditional all these years, they have cherished with me every great moment and supported me whenever I needed it.

I thank to Allah, the almighty, for this life.

List of Figures

| | | |
|-----|---|----|
| 1.1 | Factors influencing urban heat islands: (1) complex urban canyon geometry, (2) high thermal capacity building materials, (3) the greenhouse effect, (4) increase of anthropogenic heat releases, (5) reduction of evaporative cooling source, (6) obstructed wind pattern..... | 5 |
| 1.2 | Location of Hanoi in the northern region of Vietnam. Source: VIAP, 2011..... | 9 |
| 1.3 | Air temperature records in Hanoi City from 1980 to 2010 exhibit the gradual increments. Plain lines indicate annual mean temperatures and dashed lines are linear trends for available periods. The data are obtained from the weather station located in Lang which represents urban area and from the suburban and rural stations located in Bavi and Hadong, respectively. For the locations of each station, see Fig. 1.4. Weather data are provided by National Centre for Hydro-Meteorological Forecasting (NCHMF)..... | 10 |
| 1.4 | Land use map of Hanoi for (a) current condition in 2010 and (b) Hanoi Master Plan 2030. Source: VIAP, 2011. | 11 |
| 1.5 | Map showing the location of Johor Bahru. The inset shows the location of Johor Bahru at the tip of Malaysian peninsula. Source: Google Earth. | 12 |
| 1.6 | Map of (a) existing land use and (b) the CDP of Iskandar Malaysia by 2025. Source: Khazanah Nasional, 2006. | 14 |
| 2.1 | Schematic depiction of terms involved in the radiation and energy fluxes over an urban and a rural area on a clear day. The width of the arrows approximates the size of the flux..... | 24 |
| 2.2 | Köppen-Geiger climate type map of Southeast Asia. Source: Peel et al. (2007)... | 26 |
| 3.1 | Methodological framework..... | 50 |
| 3.2 | WRF system components..... | 51 |
| 3.3 | ARW η coordinate. | 52 |
| 3.4 | (a) Horizontal and (b) vertical grids of the ARW. | 55 |
| 3.5 | WRF-ARW modeling system flow chart. The red-dashed line indicates the program flow used in this study. Source: (Skamarock et al., 2008) | 57 |

| | | |
|------|---|----|
| 3.6 | Schematic diagram showing the flow of data processing and program components in WPS and how the WPS feeds initial data to the ARW. Source: (Skamarock et al., 2008) | 58 |
| 3.7 | (a) Schematic of the single-layer urban canopy model. T_a is the air temperature at reference height Z_a , T_R is the building roof temperature, T_W is the building wall temperature, T_G is the road temperature, T_S is the temperature defined at $Z_T + d$, H is the sensible heat exchange at the reference height, H_a is the sensible heat flux from the canyon space to the atmosphere, H_W is that from wall to the canyon space, H_G is that from road to the canyon space, and H_R is that from roof to the atmosphere. Source: Kusaka & Kimura, 2004. | 63 |
| 3.8 | (a) Radiative Forcing of the Representative Concentration Pathways. From van Vuuren et al. (2011). (b) Global temperature change (mean and one standard deviation as shading) relative to 1986-2005 for the RCP scenarios run by CMIP5. The number of models is given in brackets. From Knutti & Sedláček (2012)..... | 67 |
| 3.9 | (a) CMIP5 38-models ensemble mean surface temperature over Hanoi region (102° – 107° E and 18° – 23° N) from 2015 to 2100 (the target period of assessment is shaded in grey), and (b) surface temperature over the same region for 10 years from 2026 to 2035 from five GCMs including MIROC5 together with the ensemble mean of 38 CMIP5 models for RCP8.5 and RCP4.5, respectively. | 68 |
| 3.10 | The computational domains for WRF simulations for Hanoi. | 70 |
| 3.11 | The computational domains for WRF simulations for JB. | 71 |
| 3.12 | The configuration of components in TRNSYS Simulation Studio. | 73 |
| 3.13 | Heat balance on the zone air node. | 74 |
| 3.14 | Types of air mass flows between zones. | 75 |
| 3.15 | Surface heat fluxes and temperatures. $S_{s,i}$ is radiation heat flux absorbed at the inside surface, $S_{s,o}$ is the radiation heat flux absorbed at the outside surface, $q_{r,s,i}$ net radiative heat transfer with all other surfaces within the zone, $q_{r,s,o}$ is net radiative heat transfer with all surfaces in view of the outside surface, $q_{w,g,i}$ is user defined heat flux to the wall or window surface, $q_{s,i}$ is the conduction heat flux from the wall at the inside surface, $q_{s,o}$ is the conduction heat flux into the wall at the outside surface, $q_{c,s,i}$ is the convective heat flux from the inside surface to the zone air, $q_{c,s,o}$ is the convective heat flux to the outside surface from the boundary/ambient, $T_{s,i}$ is the inside surface temperature, and $T_{s,o}$ is the outside surface temperature. | 76 |
| 3.16 | Flowchart of input weather data preparation. The illustrative figures describe the characteristics of data between the WRF output and the input data for TRNSYS. | 77 |
| 4.1 | (a) Land use and land cover (LULC) of current condition in 2010 for domain 3 and (b) LULC of the Hanoi Master Plan 2030. Since the land use data from VIUP were available only within the administrative boundary of Hanoi City, the surrounding areas of Hanoi City in domain 3 were covered by the Landsat 8 | 82 |

| | |
|--|----|
| imagery (acquired in 2013) and assumed to be unchanged even in the master plan condition. | |
| 4.2 Land use proportions in (a) existing and (b) new urban areas in the current and master plan conditions. | 83 |
| 4.3 LULC used in domain 3 for (a) case 1 (i.e. current condition) and (b) case 2 (i.e. the CDP). | 84 |
| 4.4 Land use proportions in (a) existing and (b) new urban areas of JB. | 85 |
| 4.5 Comparisons between observed (blank dots) and simulated air temperature (red line), wind speed (red line) and direction (red dots) at Noibai weather station, 21.22 °N and 105.8072 °E (see location in Fig. 1.4). Current land use and land cover data for domain 3 are used for the model validation purpose. | 87 |
| 4.6 Comparisons between observed (blank dots) and simulated air temperature (red line), wind speed (red line) and direction (red dots) at Senai weather station (see location in Fig. 1.5). Current land use and land cover data for domain 3 are used for the model validation purpose. The WRF simulation considered the anthropogenic heating. | 90 |
| 4.7 Spatial distribution of average air temperature at 2m and wind directions at 10 m above the surface at 1:00 for (a) case 1 and (b) case 2-1. The black line highlights the boundary of Hanoi City. | 91 |
| 4.8 Same as Fig. 4.7 but at 14:00. | 92 |
| 4.9 Frequency distributions of air temperatures area by land use category at 14:00 in the existing urban for (a) case 1 and (b) case 2-1. The air temperatures are the temporal-averaged air temperatures calculated from the days with prevailing south-easterly winds. | 93 |
| 4.10 Same as Fig. 4.9 but at 1:00. | 93 |
| 4.11 Frequency distributions of air temperatures area by land use category at 14:00 in new urban for (a) case 1 and (b) case 2-1. The air temperatures are the temporal-average air temperatures calculated from the days with prevailing south-easterly winds. | 94 |
| 4.12 Same as Fig. 4.11 but at 1:00. | 94 |
| 4.13 Spatial distribution of air temperature difference between case 1 and case 2-1 at (a) 1:00 and (b) 14:00. The positive values indicate the increase of air temperature, while the negative values indicate the reduction of air temperature due to the master plan. The black line is the boundary of Hanoi, while the dashed black lines are the boundaries of existing and new urban areas as also shown in Fig.4.1. | 96 |
| 4.14 Diurnal variation of temporal average air temperature at 2 m above the ground during in (a) existing urban area and (b) new urban area. | 97 |
| 4.15 Spatial distribution of average air temperature at 2 m and wind directions at 10 m above the surface at 1:00 for (a) case 1 and (b) case 2-1. The black line highlights the boundary of JB. | 98 |
| 4.16 Spatial distribution of average air temperature at 2 m and wind directions at 10 m above the surface at 16:00 for (a) case 1 and (b) case 2-1. The black line highlights the boundary of JB. | 99 |

| | | |
|------|---|-----|
| 4.17 | Temporal average air temperature distribution in the existing urban areas by land use categories at 1:00 for (a) case 1 and (b) case 2; and at 16:00 for (c) case 1 and (d) case 2. | 100 |
| 4.18 | Temporal average air temperature distribution in the new urban areas by land use categories at 1:00 for (a) case 1 and (b) case 2; and at 16:00 for (c) case 1 and (d) case 2. | 101 |
| 4.19 | Air temperature difference between case 1 and case 2 at (a) 1:00 and (b) 16:00. The positive values indicate the increase of air temperature, while the negative values indicate the reduction of air temperature due to the master plan. | 102 |
| 4.20 | Diurnal variations of average air temperatures at 2 m above the surface during the clear days in (a) existing and (b) new urban areas. | 103 |
| 4.21 | Sensible, latent, and conductive heat fluxes before and after the implementation of the master plan. The left-hand side panels show the heat fluxes in the existing urban areas while the right-hand side panels describe the heat fluxes in the new urban areas, respectively. | 104 |
| 4.22 | The left panels are the sensible heat flux in (a) existing urban areas and (c) new urban areas of JB under the land use condition of the current and master plan. The right panels are the latent heat flux in (b) existing urban areas and (d) new urban areas. The influence of anthropogenic emissions are not taken into account. | 105 |
| 5.1 | Spatial distribution of average air temperature at 2m and wind directions at 10m above the surface at 1:00 for (a) case 2-1, (b) case 2-2, and (c) case 2-3. The black line highlights the boundary of Hanoi City. | 111 |
| 5.2 | Same as Fig. 5.1 but at 14:00. | 111 |
| 5.3 | Spatial distribution of average air temperature differences at 1:00 for (a) cases 2-1 and 2-2, (b) cases 2-1 and 2-3; and at 16:00 for (c) cases 2-1 and 2-2, (d) cases 2-1 and 2-3. | 112 |
| 5.4 | Statistical summary (maximum, minimum, 25 th percentiles, 75 th percentiles, and median) of average air temperature in the existing urban area for (a) RCP4.5, (b) RCP8.5, and at the new urban area for (c) RCP4.5 and (d) RCP8.5. In order to see the climate variations over the 2030s, the results from 10 simulated months from 2026 to 2035 are shown. The box-plot at the far right of each graph is the mean value from 10 simulated months. The results from cases 1 and 2-1 are also shown for comparison. | 113 |
| 5.5 | Frequency of occurrence for spatial-average air temperatures in urban areas (both in existing and new urban areas) over the simulation periods of cases 2-1, 2-2, and 2-3, respectively. The result is represented as the per-day frequency for each future scenario. | 114 |
| 5.6 | Diurnal variations of spatial- and temporal-average air temperature in (a) existing urban area and (b) new urban area for all cases. The results are calculated from the days with prevailing south-easterly winds and only the values from the built-up land use types are taken into account. The shaded areas (blue and red shaded) indicate 5 th to 95 th percentile. The increasing temperatures due to the land use change are shown from the gap between the black line (case | 115 |

1) and red line (case 2-1), while the impacts of global warming and land use change are represented with the blue line (case 2-2) and dashed red line (case 2-3). The maps show the location of existing and new urban areas under current and master plan situations.

| | | |
|------|---|-----|
| 6.1 | Four computational domains for WRF modelling. The smallest domain, Domain 4, covers the entire Hanoi City with 1 km spatial grid resolution (indicated with red line square). | 120 |
| 6.2 | Spatial distribution of green belts (green color) and green buffers (red color) in the Hanoi Master Plan 2030. Blue color indicates the water bodies. The dashed lines indicate the location of for north-south and west-east cross sections for the analysis in Figs. 6.12 and 6.13. | 121 |
| 6.3 | LULC used for domain 4 in numerical experiments. (a) Scenario 1 (master plan condition), (b) scenario 2, (c) scenario 3, and (d) scenario 4. In the scenarios 2-4, the spatial distribution of green belts and green buffers are changed into built-up lands to assess their effects on urban heat island. The surrounding areas of Hanoi City remain unchanged. | 122 |
| 6.4 | Comparison between observed and simulated air temperature, wind speed and direction at Lang station (21.02° N and 105.8° E) in Hanoi urban center. Land use and land cover data of current status in domain 4 are used for the validation purpose. | 123 |
| 6.5 | LULC used for domain 4 in numerical experiments. (a) Scenario 5, (b) scenario 6, and (c) scenario 7. | 124 |
| 6.6 | (a) WRF 3 domains configuration. LULC of domain 3 for (b) case 2-1. The resulted LULC maps based on GCRs and vegetation types in (c) case 2-4, (d) case 2-5, and (e) case 2-6. | 126 |
| 6.7 | Spatial distribution of simulated air temperature and winds at 4:00 10:00, 16:00, and 22:00 on 17 June 2010. | 127 |
| 6.8 | Temporal variations of the simulated air temperatures in different scenarios at Lang Station (see Fig. 1.4 for the location). As shown, the temporal variations of scenarios 2 and 4 are similar, the same for scenarios 1 and 3. | 129 |
| 6.9 | Differences of air temperature between the current status and scenario 4 (master plan condition without green strategies) at (a) 1:00 and (b) 16:00. | 130 |
| 6.10 | Air temperature distribution by land use categories at 1:00 for (a) scenario 1 (master plan condition), (b) scenario 2, (c) scenario 3, and (d) scenario 4 on 17 June 2010. | 131 |
| 6.11 | Air temperature distribution by land use categories at 16:00 for (a) scenario 1 (master plan condition), (b) scenario 2, (c) scenario 3, and (d) scenario 4 on 17 June 2010. | 131 |
| 6.12 | Variations of the simulated air temperature and wind speed from scenario 1 (SC1) and from scenario 4 (SC4) along the west-east cross-section of the zonal line at 21.04° N at (a) 1:00, (b) 10:00, (c) 13:00, (d) 16:00, and (e) 20:00. The horizontal color bar indicates the land use types. | 133 |
| 6.13 | Variations of the simulated air temperature and wind speed from scenario 1 (SC1) and from scenario 4 (SC4) along the south-north cross-section of the zonal | 134 |

| | | |
|------|--|-----|
| | line at 105.81° E at (a) 1:00, (b) 10:00, (c) 13:00, (d) 16:00, and (e) 20:00. The horizontal color bar indicates the land use types. | |
| 6.14 | Spatial distributions of air temperatures and winds at 1:00 on 17 th June for (a) scenario 1 (b) scenario 5, (c) scenario 6, and (d) scenario 7. | 136 |
| 6.15 | Spatial distributions of air temperatures and winds at 16:00 on 17 th June for (a) scenario 1 (b) scenario 5, (c) scenario 6, and (d) scenario 7. | 137 |
| 6.16 | Spatial distributions of air temperature differences between scenario 1 and (a) scenarios 5, (b) scenario 6, and (c) scenario 7 at 1:00 on 17 June. | 138 |
| 6.17 | Spatial distributions of air temperature differences between scenario 1 and (a) scenarios 5, (b) scenario 6, and (c) scenario 7 at 16:00 on 17 June. | 138 |
| 6.18 | Air temperature distribution over the built-up areas on 17 th June at (a) 1:00 and (b) 16:00. The y-axis represent the percentage of built-up area to the total areas in domain 4. | 139 |
| 6.19 | Spatial distributions of average air temperatures at 1:00 (night-time) for (a) Case 2-1,(b) Case 2-4, (c) Case 2-5, and (d) Case 2-6. | 140 |
| 6.20 | Spatial distributions of average air temperatures at 14:00 (daytime) for (a) Case 2-1,(b) Case 2-4, (c) Case 2-5, and (d) Case 2-6. | 141 |
| 6.21 | Distribution of average air temperatures by different land use categories in existing urban areas at 1:00 for (a) case 2-1, (b) case 2-4, (c) case 2-5, and (d) case 2-6. | 142 |
| 6.22 | Distribution of average air temperatures by different land use categories in existing urban areas at 14:00 for (a) case 2-1, (b) case 2-4, (c) case 2-5, and (d) case 2-6. | 143 |
| 6.23 | Distribution of average air temperatures by different land use categories in new urban areas at 1:00 for (a) case 2-1, (b) case 2-4, (c) case 2-5, and (d) case 2-6.... | 144 |
| 6.24 | Distribution of average air temperatures by different land use categories in new urban areas at 14:00 for (a) case 2-1, (b) case 2-4, (c) case 2-5, and (d) case 2-6.. | 145 |
| 6.25 | Spatial distributions of air temperature differences. The above panels illustrated the spatial distribution of air temperature difference at 1:00 between (a) cases 2-1 and 2-4, (b) cases 2-1 and 2-5, (c) cases 2-1 and 2-6. The below panels are the spatial distributions at 16:00 between (d) cases 2-1 and 2-4, (e) cases 2-1 and 2-5, (f) cases 2-1 and 2-6. | 146 |
| 6.26 | The upper panels shows the diurnal variations of (a) air temperature, (b) wind speed, and (c) relative humidity in existing urban areas while the lower panels are for those in new urban areas. | 147 |
| 6.27 | The sensible, latent, and conductive heat fluxes in different land use conditions in existing (left panels) and new urban areas (right panels) of Hanoi case study ... | 148 |
| 7.1 | Map showing the location of the survey stations listed in Table 7.1 and land use categories in JB. | 153 |
| 7.2 | Average traffic volume by vehicle type in (a) commercial, (b) residential, and (c) industrial. The period from 22:00-6:00 use the minimum counts of each vehicle type. | 155 |
| 7.3 | Ensemble average of diurnal variation of Q_v at commercial, residential, and industrial urban category. | 156 |

| | | |
|------|--|-----|
| 7.4 | Histogram showing the distribution of total floor areas at (a) townhouses, (b) Flats, (c) Apartments, and (d) single-story terraced house. | 158 |
| 7.5 | Histogram showing the distribution of total floor areas at (a) semi-detached factories, (b) detached factories, and (c) industrial complex..... | 159 |
| 7.6 | Ensemble average of diurnal variation of Q_B at commercial, residential, and industrial buildings. | 161 |
| 7.7 | Ensemble average of diurnal variation of Q_m at commercial, residential, and industrial buildings. | 163 |
| 7.8 | Ensemble average of diurnal variation of Q_v at commercial, residential, and industrial buildings for (a) BaU scenario and (b) CM scenario..... | 165 |
| 7.9 | Ensemble average of diurnal variation of Q_B at commercial, residential, and industrial buildings for (a) BaU scenario and (b) CM scenario..... | 166 |
| 7.10 | Ensemble average of diurnal variation of Q_M at commercial, residential, and industrial buildings used in both BaU and CM scenarios..... | 167 |
| 7.11 | Q_F in commercial for (a) current, (b) BaU, and (c) CM scenarios..... | 167 |
| 7.12 | Q_F in residential for (a) current, (b) BaU, and (c) CM scenarios..... | 168 |
| 7.13 | Q_F in industrial for (a) current, (b) BaU, and (c) CM scenarios..... | 168 |
| 7.14 | Comparison of air temperature at 2m and wind conditions at 10 m above the ground between WRF simulations with/without UCM and the observed values at (a) Senai airport in Johor Bahru and (b) Changi airport in Singapore..... | 169 |
| 7.15 | Spatial distribution of average air temperature in (a) case 1, (b) case 2-1, and (c) case 2-2 at 1:00. | 170 |
| 7.16 | Spatial distribution of average air temperature in (a) case 1, (b) case 2-1, and (c) case 2-2 at 16:00. | 170 |
| 7.17 | Diurnal variation of average air temperature in built-up area for case 1 (current status), case 2-1 (BaU scenario), and case 2-2 (CM scenario) at (a) existing and (b) new urban areas. | 171 |
| 7.18 | Diurnal variation of average air temperatures in new urban areas for case 2 (master plan without anthropogenic heating), case 2-1 (BaU scenario), and case 2-2 (CM scenario). The shaded area indicates the air temperature increase due to the added heat from anthropogenic heat emissions. | 172 |
| 8.1 | The residential buildings in Hanoi. (a) Row house, (b) villa and (c) apartments. Source: Author's documentation. | 176 |
| 8.2 | Floor plan and cross section of the case study house..... | 178 |
| 8.3 | Comparisons between the simulated and measured temperatures in the master bedroom. The measured outdoor temperature is also included..... | 181 |
| 8.4 | Outdoor and indoor operative temperatures for each floor for existing urban area in current condition and existing urban area and new urban area in future condition (A: Day time ventilation B: Night time ventilation C: Full day ventilation). | 182 |
| 8.5 | Outdoor temperature and indoor temperature for each floor with energy saving techniques in the case of level 4 under night ventilation condition for existing urban area in future condition. | 184 |

| | | |
|-----|--|-----|
| 8.6 | Thermal comfort evaluation of simulated indoor operative temperatures with energy saving techniques under night ventilation conditions for existing urban area in future condition at (a) GF, (b) 1F, (c) 2F and (d) 3F..... | 185 |
| 8.7 | Cooling load of base and each level for single energy saving techniques in master bedroom for (a) night-time ventilation and (b) full day ventilation..... | 186 |
| 9.1 | (a) The large and centralized “Central Park” in New York, US and (b) the garden city concept in Savannah, Georgia, US. | 192 |

List of Tables

| | | |
|-----|---|-----|
| 1.1 | Urban population and percentage of population residing in urban areas in the Southeast Asian countries in 2005, 2010, 2030, and 2050..... | 2 |
| 1.2 | Urban development plans in Southeast Asian cities..... | 3 |
| 1.3 | Carbon reduction contribution of 12 mitigation actions for low carbon Iskandar Malaysia. | 15 |
| 1.4 | Distribution of specific research objectives in each case study. | 17 |
| 2.1 | Summary of the existing UHI countermeasures. | 32 |
| 2.2 | Summary of the impact of cool roof on indoor environment of buildings..... | 35 |
| 2.3 | Summary of the impact of cool roof on outdoor environment of buildings..... | 36 |
| 2.4 | Summary of the cooling impact of cool roof, roof insulation, and other techniques. | 37 |
| 3.1 | Weather stations and available parameters deployed in and outside of Hanoi City. | 60 |
| 3.2 | Weather stations and available parameters deployed in and outside of JB..... | 60 |
| 3.3 | WRF configuration for each model parameterisation in the sensitivity analysis. | 61 |
| 3.4 | WRF configuration for sensitivity analysis. | 62 |
| 3.5 | Domain configuration for the direct dynamical downscaling using WRF..... | 63 |
| 3.6 | The set-up values for geogrid section in the WPS of Hanoi case study. | 71 |
| 3.7 | The set-up values for geogrid section in WPS of JB case study. | 72 |
| 3.8 | Descriptions of components used in the study..... | 74 |
| 4.1 | WRF model configuration of Hanoi case study..... | 86 |
| 4.2 | WRF model configuration of JB case study..... | 88 |
| 4.3 | The urban parameter table for Single layer UCM. | 89 |
| 5.1 | Summary of scenarios for numerical experiments. | 110 |

| | | |
|------|---|-----|
| 6.1 | WRF model configuration of Hanoi case study with four domains..... | 120 |
| 6.2 | LULC data sources for each domain and numerical experiments..... | 122 |
| 6.3 | Summary of simulation cases..... | 125 |
| 7.1 | Summary of data collection at all traffic survey stations in JB..... | 153 |
| 7.2 | Percentage of fuel type by vehicle type..... | 154 |
| 7.3 | Percentage of vehicle by types from 2008 to 2013..... | 154 |
| 7.4 | Net heat combustion and fuel density of fuel type..... | 154 |
| 7.5 | Supply of residential units by municipalities in Iskandar Malaysia..... | 157 |
| 7.6 | Floor area of residential unit by type in Iskandar Malaysia..... | 158 |
| 7.7 | Supply of industrial units by type in Iskandar Malaysia..... | 159 |
| 7.8 | Floor area of industrial units by type in Iskandar Malaysia..... | 159 |
| 7.9 | Annual energy consumptions and daily energy consumptions by urban category and scenarios for numerical experiments..... | 160 |
| 7.10 | Energy consumption per m ² by urban category..... | 160 |
| 7.11 | Hourly energy consumptions by urban category..... | 161 |
| 7.12 | Metabolic heat production values of activity types..... | 162 |
| 7.13 | Number of workers by sector in Iskandar Malaysia..... | 163 |
| 7.14 | Estimated weekend and weekdays population at sleep and active periods..... | 163 |
| 7.15 | Summary of daily energy consumptions for traffic..... | 164 |
| 7.16 | Summary of the daily energy consumption, total floor area, and energy consumption per m ² for all scenarios and land use categories..... | 166 |
| 8.1 | Summary of energy saving techniques for residential buildings in Hanoi..... | 177 |
| 8.2 | Schedule of the window “open” and “closed” mode in all ventilation techniques..... | 179 |
| 8.3 | Levels distributed to each energy saving techniques..... | 180 |
| 8.4 | AC setting in simulation..... | 186 |
| 9.1 | Summary of the cooling effect of the UHI mitigation measures..... | 191 |

List of Acronyms

| | |
|--------------|---|
| ARW | Advanced Research WRF |
| BaU | Business as Usual |
| CDO | Climate Data Online |
| CM | Counter Measure |
| CMIP5 | Coupled Model Intercomparison Project Phase 5 |
| DDD | Direct Dynamical Downscaling |
| GCM | Global Climate Model |
| GCR | Green Coverage Ratio |
| GIS | Geographic Information System |
| GrADS | Grid Analysis and Display System |
| HMS | Hydro-Meteorological Service |
| JB | Johor Bahru |
| LCS | Low Carbon Society |
| LULC | Land Use/Land Cover |

| | |
|-----------------|--|
| MIROC | Model for Interdisciplinary Research on Climate |
| NCAR | National Center for Atmospheric Research |
| NCEI | National Centre for Environmental Information |
| NCEP-FNL | National Centers for Environmental Prediction (Final) |
| NCL | NCAR Command Language |
| NetCDF | Network Common Data Form |
| PBL | Planetary Boundary Layer |
| PGW | Pseudo Global Warming |
| RCM | Regional Climate Model |
| RCP | Representative Concentration Pathway |
| RIP4 | Read/Interpolate/Plot version 4.0 |
| SUHI | Surface Urban Heat Island |
| TRNSYS | Transient Systems Simulation Program |
| UCM | Urban-Canopy Model |
| UHI | Urban Heat Island |
| USGS | United States Geological Survey |
| VIAP | Vietnam Institute of Architecture, Urban, and Rural Planning |
| VIUP | Vietnam Institute of Urban and Rural Planning |
| WRF | Weather Research and Forecasting |
| WPS | WRF Pre-Processing System |

List of Publications and Awards

Refereed Journal Papers

- Kubota, T., Lee, H.S., **Trihamdani, A.R.**, Phuong, T.T.T., Tanaka, T., Matsuo, K. (2017) Impacts of land use changes from the Hanoi Master Plan 2030 on urban heat islands: Part 1. Cooling effects of proposed green strategies. *Sustainable Cities and Society*, 32, pp. 295-317.
- Lee, H.S., **Trihamdani, A.R.**, Kubota, T., Iizuka, S., Phuong, T.T.T. (2017) Impacts of land use changes from the Hanoi Master Plan 2030 on urban heat islands: Part 2. Influence of global warming. *Sustainable Cities and Society*, 31, pp.95-108.
- Trihamdani, A.R.**, Kubota, T., Lee, H.S., Sumida, K., Phuong, T.T.T. (2017) Impacts of land use changes on urban heat islands in Hanoi, Vietnam: Scenario analysis. *Procedia Engineering*. (Accepted for publication).
- Trihamdani, A.R.**, Lee, H.S., Kubota, T., Phuong, T.T.T. (2015) Configuration of green spaces for urban heat island mitigation and future building energy conservation in Hanoi Master Plan 2030, *Buildings*, 5(3), pp.933-947.
- Nam, T.H.H., Kubota, T., **Trihamdani, A.R.** (2015) Impact of urban heat island under the Hanoi Master Plan 2030 on cooling loads in residential buildings, *International Journal of Built Environment and Sustainability*, 2(1), pp.48-61.

Refereed Conference Papers

- Ida, M., Kubota, T., **Trihamdani, A.R.**, Sumida, K. (2017) Factors affecting occurrence of dengue fever in major cities of Southeast Asia, *Proceedings of the 17th Conference of the Science Council of Asia*, Pasay City, Philippines, 14-16 June.
- Trihamdani, A.R.**, Sumida, K., Kubota, T., Lee, H.S., Phuong, T.T.T. (2016) Urban greening for urban heat island mitigation in the future Hanoi City, *Proceedings of the International Symposium on Architectural Interchanges in Asia (ISAIA) 2016*, Sendai, Japan, 20-23 Sep.
- Trihamdani, A.R.**, Kubota, T., Lee, H.S., Sumida, K., Phuong, T.T.T. (2016) Impacts of land use changes on urban heat islands in Hanoi, Vietnam: Scenario Analysis, *Proceedings of Urban Transitions Global Summit 2016*, Shanghai, China, 5-9 Sep.
- Trihamdani, A.R.**, Kraus, J., Kubota, T., Lee, H.S. (2015) Influence of existing open spaces and vacant lands on mitigation of urban heat island in Johor Bahru City, Malaysia, *Proceedings of the International Joint-Conference, SENVAR-iNTA-AVAN 2015*, Johor Bahru, Malaysia, 24-26 Nov.
- Tung, N.H., **Trihamdani, A.R.**, Kubota, T. (2015) Field investigation of indoor thermal environments in urban row houses in Hanoi: Impact of urban heat island on indoor thermal comfort, *Proceedings of 7th International Conference on Sustainable Development in Building and Environment (SuDBE)*, Reading, UK, 27-29 July.

-
- Trihamdani, A.R.**, Lee, H.S., Kubota, T., Phuong, T.T.T. (2015) Configuration of green spaces for urban heat island mitigation in Hanoi Master Plan 2030, Proceedings of 2015 TAU Conference: Mitigating and Adapting Built Environments for Climate Change in the Tropics, Jakarta, Indonesia, 30-31 Mar.
- Trihamdani, A.R.**, Lee, H.S., Phuong, T.T.T., Kubota, T., Tanaka, T., Matsuo, K. (2014) The cooling effect of green strategies proposed in the Hanoi Master Plan for mitigation of urban heat island, Proceedings of 30th PLEA International Conference, Ahmedabad, India, 16-18 Dec.
- Trihamdani, A.R.**, Lee, H.S., Phuong, T.T.T., Kubota, T., Tanaka, T., Matsuo, K. (2013) Impact of the green strategy proposed in the Hanoi master plan on urban heat island effects, Proceedings of the 14th International Conference on Sustainable Environmental and Architecture (SENVAR), Aceh, Indonesia, 7-9 Nov.

Non-Refereed Conference Papers

- Trihamdani, A.R.**, Sumida, K., Kubota, T. (2017) Effects of Anthropogenic heat reduction from Iskandar Malaysia on Urban Heat Islands in Johor Bahru, Malaysia, Annual Meeting, AIJ, Hiroshima.
- Trihamdani, A.R.**, Kubota, T., Iizuka, S. (2016) Impact of land use changes on urban heat islands in Hanoi under influence of global warming, Annual Meeting, AIJ, Kyushu, Japan, 24-26 Aug.
- Trihamdani, A.R.**, Kubota, T. (2015) Impacts of land use changes on urban heat island during the monsoon seasons in Johor Bahru, Malaysia, Annual Meeting, AIJ, Kanagawa, Japan, 4-6 Sep.
- Trihamdani, A.R.**, Tung, N.H., Kubota, T., Lee, H.S., Phuong, T.T.T. (2015) Urban heat islands in the future Hanoi City: Impacts on indoor thermal comfort and cooling load in residential buildings, Proceedings of 9th International Conference on Urban Climate, Toulouse, France, 20-24 July.
- Kraus, J., **Trihamdani, A.R.**, Kubota, T., Lee, H.S., Kawamura, K. (2015) Comparison of land cover and land use data for urban climate modelling in Southeast Asian cities: A case study of Johor Bahru, Proceedings of 9th International Conference on Urban Climate, Toulouse, France, 20-24 July.
- Trihamdani, A.R.**, Lee, H.S., Phuong, T.T.T., Kubota, T., Tanaka, T., Matsuo, K. (2014) Effect of green strategy proposed in the Hanoi Master Plan on its urban climate, Proceedings of Grand Renewable Energy 2014, Tokyo, 27-31 July.

Awards

- 2016 Hiroshima University Excellent Student Scholarship**, 2016: Trihamdani, A.R., *Graduate School for International Development and Cooperation, Division of Development Science*, December 16, Hiroshima University, Japan.
- Best Presentation Awards**, 2015: Trihamdani, A.R., Kraus, J., Kubota, T., Lee, H.S., Influence of existing open spaces and vacant lands on mitigation of urban heat island in Johor Bahru City, Malaysia. *SENVAR-iNTA-AVAN 2015*, Johor Bahru, Malaysia, 24-26 Nov.

1 Introduction

1.1 Research background

1.1.1 The growing cities in Southeast Asia

Major cities in Southeast Asia have been experiencing rapid urbanisation, coincident with rapid industrialisation and economic growth. In 2011, cities in this region contributed up to 86% of the national GDP, and are projected to have a promising economic growth in the next decades (Ostojic et al., 2013). Along with the positive economic growth, estimation indicates that more than half of the Southeast Asian population will live in the cities, with the percentage of urban population is projected to increase from 47.9% in 2010 to 65.6% in 2050 (see Table 1.1).

According to Bhatta (2010), developing countries are currently passing through the process of industrialisation. At this transition time, many new commercial enterprises create new jobs in cities. Industrialisation also transforms the traditional farming to be more mechanised, leaving many labours in agricultural sector out of work and inducing migration to the cities. As a result, the growth rate of urban population in these developing countries is higher than the industrialised countries. In industrialised countries, the future growth of urban populations will be comparatively moderate because of the current low growth rates and over 80% of their population already live in urban areas. In contrast, developing countries in Southeast Asia are in the middle of the transition process from a pre-industrial society to an industrial one, resulting in a very high urban population growth rates.

In Southeast Asia, the explosive urbanisations take place in the form of mega-cities. Cities are spreading out, followed by the increase of density in the fringe of urban areas (Murakami et al., 2005; Schneider et al., 2015). Moreover, cities were merged together to create urban settlements on a scale never seen before. In 2007, there is only one megacity with more than 10 million people in this region, which is Metro Manila, the capital of the Philippines. Then,

Table 1.1 Urban population and percentage of population residing in urban areas in the Southeast Asian countries in 2005, 2010, 2030, and 2050.

| Countries | Urban population (millions) | | | | Percentage of population residing in urban areas (%) | | | |
|-------------------|-----------------------------|-------|-------|-------|--|-------|-------|-------|
| | 2005 | 2010 | 2030 | 2050 | 2005 | 2010 | 2030 | 2050 |
| Brunei Darussalam | 0.3 | 0.3 | 0.4 | 0.5 | 73.5 | 75.5 | 80.7 | 84.0 |
| Cambodia | 2.6 | 2.8 | 4.9 | 8.2 | 19.2 | 19.8 | 25.6 | 36.2 |
| Indonesia | 103.1 | 120.2 | 184.9 | 227.8 | 45.9 | 49.9 | 63.0 | 70.9 |
| Lao PDR | 1.6 | 2.1 | 4.5 | 6.4 | 27.4 | 33.1 | 50.9 | 60.8 |
| Malaysia | 17.2 | 20.1 | 30.2 | 36.2 | 66.6 | 70.9 | 81.9 | 85.9 |
| Myanmar | 14.5 | 16.3 | 25.1 | 32.2 | 28.9 | 31.4 | 42.8 | 54.9 |
| Philippines | 40 | 42.3 | 59.2 | 88.4 | 46.6 | 45.3 | 46.3 | 56.3 |
| Singapore | 4.5 | 5.1 | 6.6 | 7.1 | 100.0 | 100.0 | 100.0 | 100.0 |
| Thailand | 24.6 | 29.3 | 43.1 | 44.3 | 37.5 | 44.1 | 63.9 | 71.8 |
| Timor-Leste | 0.3 | 0.3 | 0.6 | 1 | 26.3 | 29.5 | 41.0 | 48.3 |
| Viet Nam | 23.2 | 27.1 | 43.7 | 55.7 | 27.3 | 30.4 | 43.0 | 53.8 |

Source: (United Nations (UN), 2014).

Jakarta, the capital of Indonesia, joined in 2010 after the surrounding urban agglomerations, namely Jabodetabek (Jakarta, Bogor, Depok, Tangerang and Bekasi) are taken into account. This ranks Jabodetabek among the other mega-cities in the world with its 28 million inhabitants. The Bangkok Metropolitan Area in Thailand followed with its 14 million population.

The growth of major cities is not the whole story. Cities in all sizes are growing, with higher rates of population growth for small cities than the established large agglomerations during the last decades (Birkmann et al., 2016; Schneider et al., 2015). Meanwhile, studies on urbanisation have tended to overstate the role of very large cities and have underemphasized the importance of small- and medium-sized cities (Montgomery, 2008). UN (2014) defines small- and medium-sized cities as the cities of 500,000 to 1 million inhabitants and 1 to 5 million inhabitants, respectively. These emerging towns, cities, and urban agglomerations of the coming decades, primarily in Africa and Asia, will have a critical impact on energy use and carbon emissions in the future (Seto et al., 2014).

Currently, the small- and medium-sized cities in Southeast Asia have been growing rapidly and they plan to increase their population further. For instance, in Johor Bahru City, Malaysia, the Malaysian government launched the Comprehensive Development Plan (CDP) 2006-2025 for the South Johor Economic Region (SJER), also known as Iskandar Malaysia. In the master plan, the population is projected to increase from 1.5 million to 3 million by 2025 (Khazanah Nasional, 2006). Bandung City in Indonesia launched the urban land use plan, namely Rencana Tata Ruang dan Wilayah (RTRW) Kota Bandung 2011-2031. With the projection of population increase from 2.3 million in 2008 to 4.1 million people in 2031, the city plans to distribute its population to the new urban areas located in the eastern part of the city (RTRW Bandung, 2011). In Hanoi, Vietnam, a long-term urban development plan, namely the Hanoi Master Plan 2030, was established in 2011. In the master plan, the population of Hanoi is projected to increase from 6.7 million in 2010 to 9 to 9.2 million by 2030. Consequently, the constructed land will sharply increase to almost three times the existing amount, from 46,340 ha (14%) to more than 129,500 ha (39%). As shown in Table 1.2, most cities will undergo the

transitions from small- to medium-sized cities or from medium-sized to large cities in the near future. The growth of these cities would result in a dramatic change in land use as the most direct environmental impact.

Table 1.2 Urban development plans in the Southeast Asian cities.

| Countries | Cities | Name of the master plan | Development year | Target year | Population in 2010 (millions) | Population in target year (millions) |
|-------------|--|---|------------------|-------------|-------------------------------|--------------------------------------|
| Indonesia | Bandung ¹ | RTRW Kota Bandung 2011-2031 | 2011 | 2031 | 2.4 | 4.1 |
| | Jakarta ² | Regional Spatial Plan Jakarta 2030 (RTRW Jakarta 2030) | 2014 | 2030 | 9.6 | 12.5 |
| Malaysia | Johor Bahru ³ | Iskandar Malaysia | 2005 | 2025 | 1.5 | 3 |
| | Kuala Lumpur ⁴ | Kuala Lumpur Structure Plan 2020 | 2000 | 2020 | 1.5 | 2.2 |
| Philippines | Manila ⁵ | Metro Manila Green Print 2030 | 2012 | 2030 | 11.64 | 16.9 |
| Singapore | Singapore ⁶ | Master Plan 2014 | 2014 | 2019 | 5 | - |
| Thailand | Bangkok Metropolitan Region ⁷ | Bangkok Metropolitan Region Land Use Conceptual Plan 2057 | 2007 | 2057 | 15.4 | 15.9 |
| Vietnam | Hanoi ⁸ | The Hanoi Master Plan 2030 | 2009 | 2030 | 6.4 | 9.2 |
| Myanmar | Yangon ⁹ | Development Plan for Greater Yangon | 2013 | 2040 | 5.0 | 11.73 |
| Cambodia | Phnom Penh ¹⁰ | Phnom Penh Strategic Orientation 2035 | 2015 | 2035 | 1.5 | 2.87 |

Sources: ¹RTRW Bandung, 2011; ²Jakarta Capital City Government, 2012; ³Khazanah Nasional, 2006; ⁴Dewan Bandaraya Kuala Lumpur, 2000; ⁵Metropolitan Manila Development Authority, 2015; ⁶Urban Redevelopment Authority, 2014; ⁷The Department of Public Works and Town Planning, 2004; ⁸Vietnam Institute of Architecture Urban and Rural Planning, 2011; ⁹Japan International Cooperation Agency, 2013; ¹⁰Municipality of Phnom Penh, 2007.

1.1.2 Urbanisation and its environmental impact

Consequences of urbanisation may have positive and negative impacts. However, the negative impacts are generally more highlighted because the growth of a city is often uncontrolled or uncoordinated and therefore the negative impacts override the positive sides (B. Bhatta, 2010). Furthermore, the impact of urbanisation can go beyond the urban areas themselves. The urban development can place additional burdens on rural economic such as forestry and farming. For instance, in Japan, migration of young people to urban areas largely give disadvantages to the rural areas. With little prospect of the younger generations taking over the farming or remaining businesses in the rural region, the number of abandoned agricultural lands and vacant houses have been increasing. This condition also leads to the increasing demand on the social services for resident, such as medical and nursing care. Rural

revitalisation is what the rural areas need these days. An example of the rural revitalisation through bio-mass based eco-tourism was conducted by the Onsite Team Project of the TAOYAKA Program, Hiroshima University Japan, as highlighted in Appendix L.

Meanwhile in the urban areas, urban dwellers alter their environment through their consumption of resources: food, energy, water, and land. And the increasing urbanisation in the future is likely to aggravate the exploitation of resources, which is deleterious to the environment. Grimm et al. (2008) mapped five major types of environmental change that affect and are affected by urbanisation, which are changes in land use and land cover, biodiversity, biogeochemical cycles, hydro systems, and climate.

Land use/land cover change is one of the most direct impacts of urbanisation. Associated with this change is the transformation of native vegetation to impervious surfaces and other land covers, not only within the urban areas but also beyond the urban areas themselves. For instance, the demand for beef from big cities has transformed the tropical rainforests into grazing land. This results in the habitat loss and species extinction (Aronson et al., 2014; Hahs et al., 2009). In many developing countries, especially in Asia, urban expansions are taking places in agricultural lands (Seto, Kaufmann, & Woodcock, 2000). The agricultural lands vanish as the urban areas spread outward (Murakami et al., 2005), inducing changes in soil, built-structures, markets, and informal human settlements (Grimm et al., 2008).

Urbanisation contributes to the changes in biogeochemical cycles. As a city expands, the emission from traffic increases following the increased driving distance and fuel consumption (Kahn, 2000). Wastes produced from urban areas are likely in a tremendous growth along with the increased consumption of materials (e.g. food, plastics, papers, and building materials) (Khajuria, Yamamoto, & Morioka, 2008). Those wastes affect biogeochemical cycles from local to global scales (Grimm et al., 2008).

Humans have modified the hydro systems to meet a large number goals, such as disaster protection (e.g. flood and tsunami), water reservoir, waterways, buildings and foundations, etc. Among the most important modifications is the increased impervious surfaces due to the constructions of buildings and infrastructures, which in turn induces more total runoff volume. The urban areas located in flood-prone areas are exposed to increased flood hazard. Moreover, most ongoing urbanisations are happening in delta areas, especially in coastal cities, which is in subsidence-prone areas. The excessive groundwater extraction for domestic and industrial water supply would cause land subsidence. Without proper action, parts of coastal cities will sink below sea level, e.g. in Bangkok (Phienweij et al., 2006) and Jakarta (Bakr, 2015).

Although cities cover less than 3% of the earth's surface, they are the point of sources of CO₂ and other greenhouse gas emissions which affect the local and global climate. Cities, as aggregates of human activities, require energy in a variety of forms. Much of the primary energy sources transformed to be available to most of the cities around the world are still fossil-based, resulting in global climate change. Yet, the global climate change influence on cities may be aggravated by the local climate changes that resulted from urbanisation, known as the urban heat island (UHI) effect. In other words, cities are encountering particular problems related to urban climate, which is the urban warming due to the global warming and UHI effects.

1.1.3 UHI effect

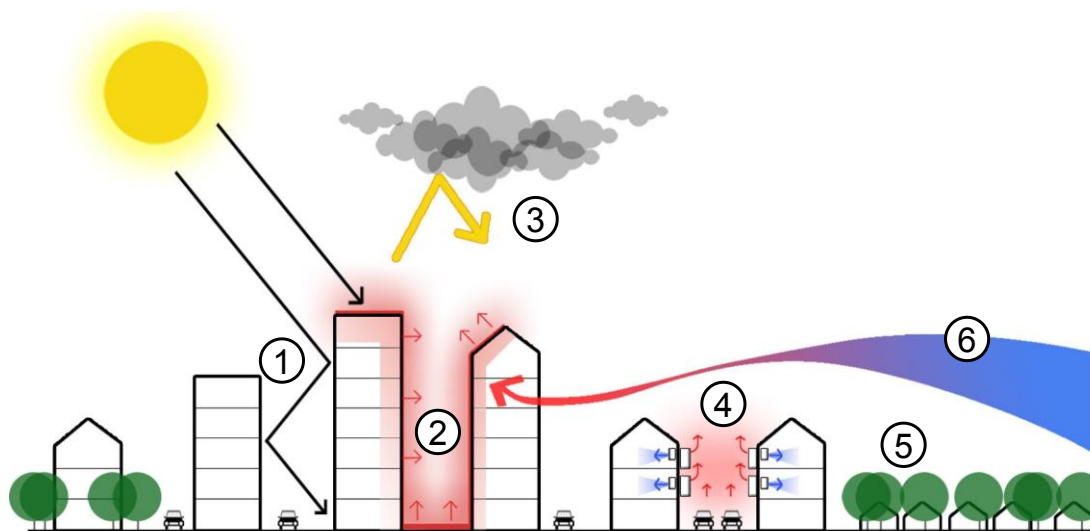


Fig. 1.1 Factors influencing urban heat islands: (1) complex urban canyon geometry, (2) high thermal capacity building materials, (3) the greenhouse effect, (4) the increases in anthropogenic heat emissions, (5) reduction of evaporative cooling source (i.e. green spaces, water bodies, etc.), (6) obstructed wind pattern.

The UHI effect is one of the well-known urban environmental issues characterised by higher air temperature in the urban area than that of the surrounding rural area (Oke, 1987), especially at night. It is a result of urban-rural energy balance differences (Roth, 2013). The effect was first observed by Luke Howard in 1833 in London (Gartland, 2008). Nowadays, the UHI effect has been discovered in cities throughout the world (Santamouris, 2015a). It is expected that major cities in Southeast Asia with high urbanisation rates have been experiencing this phenomenon.

Heat islands form in urban areas because many common materials absorb and retain more of the sun's heat than in rural areas (Gartland, 2008). In the late afternoon and early evening, air temperature begins to decrease in both urban and rural areas. However, with the considerable stored heat in urban areas, the heat release in the rural area takes place faster. This creates a large difference in air temperature between rural and urban at night. The formation of UHI is attributed to these following causes (Gartland, 2008; Kleerekoper, van Esch, & Salcedo, 2012; Oke, 1987; Wong & Chen, 2008) (illustrated in Fig.1.1):

1. *Canyon geometry.* The short-wave radiation from the sun is absorbed by low albedo materials and trapped by multiple reflections and absorption within the urban canyon. The incident radiation and longwave radiation emitted from streets and buildings will move into indoor spaces or re-emit back to the surroundings after sunset;
2. *Building materials.* The direct radiation and trapped heat within the urban canyon are stored by building materials with low albedo and high thermal capacities, such as brick,

- concrete, and asphalt. The stored heat will be released at night which results in high temperature during the night-time;
3. *Greenhouse effect*. Long-wave radiation is absorbed by the polluted urban atmosphere and re-emit to the urban environment;
 4. *Anthropogenic heat*. –or human produced heat is released from industrial combustion, vehicles, air-conditioners, and even people themselves. This aggravates the UHI effect;
 5. *Evaporative cooling source*. As the results of the expansion of urban areas, the number of impervious surfaces increases while the number of evaporative surfaces decreases. As a consequence, more energy is turned into sensible heat and less into latent heat.
 6. *Wind pattern*. The heat loss from urban areas can be reduced when the wind is obstructed by the urban settings (i.e. building height, urban layout, etc.). Lower wind speeds tend to increase heat storage during the day and slow the release of heat at night.

UHI may be observed both at the surface (surface urban heat islands (SUHIs)) and in the atmosphere in and above the city (atmospheric urban heat islands (AUHIs)). Furthermore, the AUHIs may be classified into the urban canopy layer (UCL) and urban boundary layer (UBL), respectively (Oke, 1976). The AUHIs for UCL is micro scale concept where the climate is dominated by the nature of immediate urban setting (e.g. materials and geometry) with the limit to lie at, or just below, roof level. Meanwhile, the UBL is a local or mesoscale concept referring to the layer above UCL influenced by the presence of an urban area at its lower boundary. This study deals with the AUHIs for UCL and focuses on the changes in the near-surface temperature within UCL (although the term ‘UHI’ is generally used in hereafter).

The UHI is a local phenomenon with negligible effect on global climate. This is due to the fact that urban areas cover less than 3% of the global land surface. Thus, direct urban heat is considered to be essentially a negligible factor in producing global warming (Trenberth et al., 2007). Nevertheless, many indirect effects of UHI and further trend of urbanisation may represent harbingers of the future warming climate (Forman, 2014; Grimm et al., 2008; Oleson, Bonan, Feddema, & Jackson, 2011). At the same time, cities are heavily vulnerable to the impacts of global warming.

1.1.4 Global warming

Global warming refers to the recent and ongoing rise in global average temperature. It is caused mostly by increasing concentration of greenhouse gases in the atmosphere. Global warming is causing climate patterns to change. In other words, global warming itself represents only one aspect of climate change (US EPA, 2017). Climate change includes major changes in temperature, precipitation, or wind patterns, among other effects, that occur over several decades or longer.

The effects of global warming vary according to geographical locations (Hartmann et al., 2013). At the ocean, when the sea temperature gets warmer, storms get stronger. Warmer water increases the moisture content of storms, forming a big, one-time rainfalls and increasing the percentage of annual precipitation which causing flood events in many places on Earth. The precipitation also decreased in some regions, causing drought, dramatic water shortages,

and the risk of wildfires. Moreover, Antarctica has been losing a massive amount of ice since 2002 which causing sea levels to rise several meters over the next 50 to 150 years.

In the Southeast Asian region, the future precipitation will be generally affected by any change in tropical cyclone characteristics. Moreover, the projected seasonal changes vary strongly within the region (Christensen et al., 2007). For instance, Hulme & Sheard (1999a, 1999b) found a pattern of rainfall increases across northern Indonesia and the Philippines, and decrease over the southern Indonesia archipelago. Since most of the tropical cyclones form along the monsoon trough and are also influenced by ENSO (El Niño–Southern Oscillation), changes in the occurrence, intensity and characteristics of tropical cyclones and their inter-annual variability will be affected by changes in ENSO (Christensen et al., 2007).

Apart from the uncertainties and variabilities of climate change projections, urban dwellers has been affected by the rising sea levels, increased precipitation, inland floods, more frequent and stronger cyclones and storms, and periods of more extreme hot and cold. Moreover, they are also vulnerable to the associated health impacts of global warming such as heat-stress and new infectious diseases. The UHI and global warming effects result in a greater increase of hot nights for cities than neighbouring rural areas, increasing the thermal stress and vulnerability to heat waves of urban dwellers in a warmer urban setting compared to their rural counterparts (McCarthy, Best, & Betts, 2010).

1.1.5 The impact of urban warming

Urban warming strongly influences the quality of life or urban dwellers. Higher urban temperatures affect the energy consumption of buildings, increase the concentration of pollutants and deteriorate the environmental quality in the city, decrease the indoor and outdoor comfort levels, and affect human health; as will be discussed below.

Impact of the urban warming on energy

High urban temperature increases the energy needs for cooling and decreases the needs for heating. While the urban warming can reduce the heating penalty in cities in temperate climate, its effect is certainly unwelcome in the cooling dominated region (i.e. tropics). The increased urban air temperature induces more energy consumption for space cooling and affects the peak electricity demand. The increase in peak electricity demand is an important matter for the authorities since they should anticipate the sudden increase in electricity demand by building additional power plants. Santamouris et al. (2015) found that the increase of the peak electricity demand per degree of temperature rise varies between 0.45% to 4.6%. Moreover, they also found that the increase of the hourly, daily, or monthly electricity consumption ranges between 0.5% and 8.5% per degree of temperature rise. The difference of energy consumptions among cities attributed to urban warming depends on the characteristic of the building stock, the climate zone, the type of provided energy services, and the strength of the UHI phenomenon.

Impact of the urban warming on the environment, thermal comfort, and health

Many natural rhythms are altered by the warmed urban spaces. The growing season for plants becomes longer (Gilbert, 1991). The phenology of plants, including the flower blooming or leaf drop, is changed (Zipper et al., 2016). Bird nesting and migration differ in timing and location (Tryjanowski, Sparks, Kuźniak, Czechowski, & Jerzak, 2013).

The urban warming may result in some negative impacts on urban air quality. The elevated temperature can increase the rate of the formation of ground level ozone, which is the principal component of the harmful photochemical smog. Moreover, the concentration level of pollutants (e.g. NO_x, CO₂, and CO) increase significantly with the high ambient temperatures (Agarwal & Tandon, 2010; Lai & Cheng, 2009). The dispersion of pollutants in urban areas becomes limited since UHIs are found to slow down the penetration of sea breeze in cities, resulting in a high concentration of pollutants in the city centre (Yoshikado & Tsuchida, 1996).

The urban warming strongly deteriorates the indoor and outdoor comfort condition of the urban dwellers. Studies have found the increases of overheating hours under the future climate, particularly in naturally ventilated buildings (Jentsch, Bahaj, & James, 2008; Lomas & Ji, 2009). Santamouris (2015b) concluded that urban zones suffering from UHI show lower outdoor thermal comfort level. Moreover, due to the global warming, the outdoor thermal discomfort conditions may increase in both duration and frequency in the near future.

The urban warming also involves the hazard of heat-stress related injuries which can threaten the health of urban dwellers (Flynn, McGreevy, & Mulkerrin, 2005). Moreover, it increases human vulnerability to new and unfamiliar diseases. For instance, cities with high land surface temperature, low humidity, and poor vegetation are considered to favour the transmission of the mosquito-borne dengue fever (Araujo et al., 2015; Xu et al., 2016).

1.2 The case study cities

The following are two case study cities that demonstrate the growing cities in Southeast Asia. Both cities are projected to experience rapid urbanisations and massive land use changes in the near future (i.e. 2025-2030). They are Hanoi City in Vietnam and Johor Bahru City in Malaysia.

Hanoi and Johor Bahru are selected as the case study because of their characteristics in terms of the geographical location and urban planning scheme. Hanoi, for instance, is a city located inland. This city aims to be a sustainable urban region by proposing a series of green space network in the master plan. On the other hand, Johor Bahru City is located in the coastal area. This city plans for a low carbon society in the future through a series of carbon emission reduction strategies in its master plan.

The environmental assessments in the master plans of both cities have discussed several environmental issues, such as air pollution and water pollution. However, the impact of the

master plan on the thermal environment has not been addressed. The thermal/heat-related issue will be an important aspect in the near future (i.e. 2025-2030), especially when considering that the effect of global warming is getting more apparent and intense.

1.2.1 Hanoi, Vietnam

Location, geographic, population and climatic features

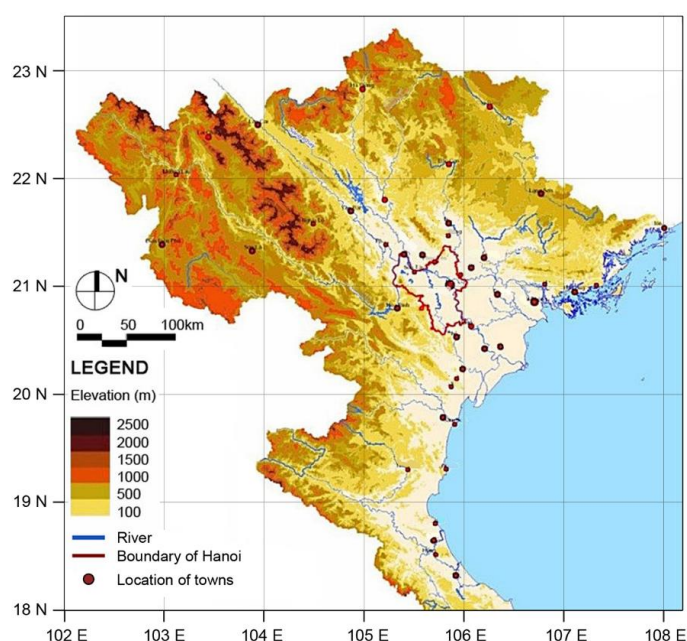


Fig. 1.2 Location of Hanoi in the northern region of Vietnam. Source: VIAP, 2011.

Hanoi is located in the northern region of Vietnam ($21^{\circ}1'12''$ N $105^{\circ}48'$ E), situated in the area along the Vietnam's Red River Delta, nearly 90 km away from the coastal area (Fig. 1.2). The delta area is surrounded by mountain ranges located at its northern and western sides. The terrain elevation gradually decreases from the North to the South and from the West to the East, with an average height ranging from 5 to 20 m above the sea level. The western border of the Hanoi Region stretches around the foot of a mountain range that has an altitude of up to 1300 m.

During the first decade of the 21st century, Vietnam experienced a stable 7-8% annual economic growth. Foreign investment increased rapidly leading to the increase of demands for houses and offices. As the results, many constructions project emerged rapidly in new urban areas. In 2008, due to the urban sprawl, Hanoi and its neighbouring province Ha Tay were merged together. This made up an area of area of 3,324.5 km² which includes one town, 10 urban districts and 18 outskirt districts. The city is neighbouring with the provinces of Thai Nguyen and Vinh Phuc to the north, Bac Ninh and Hung Yen to the east, Ha Nam to the south, and Phu Tho and Hoa Binh to the west.

The city has a total population of approximately 6,688,600 in 2010. The urban population in Hanoi has been increasing from 1.6 million in 2001 to 3.5 million in 2015, while the rural population experiences a steady decrease over the last five years, from 3.8 million in 2010 to 3.6 million in 2015. Currently, the capital city is ranked second in terms of population and the first in terms of total area in Vietnam.

According to the Köppen-Geiger climate classification, Hanoi has a humid subtropical climate (Cwa) (Peel, Finlayson, & McMahon, 2007). The city experiences a hot-humid season (April to October) and a cool and relatively dry season (November to March). The southeasterly wind prevails during the hot season, while the northeast is the prevailing wind direction during the cool season (Vietnam Institute of Architecture Urban and Rural Planning (VIAP), 2011). The maximum monthly average air temperature is observed in June, which is approximately 30.3 °C, whereas the minimum average value is recorded in February (approximately 17.5 °C).

Meanwhile, Hanoi experienced an upward trend in the annual air temperature over an extended time period. Fig. 1.3 presents the annual average temperature recorded at three weather stations in Hanoi from 1980 to 2010. Based on the location of each station, climatic records derived from Lang, Ha Dong and Ba Vi Station can be considered as the representatives of urban, suburban and rural stations in Hanoi, respectively. As shown in Fig. 1.3, during the 30-year period, there is an unsteady and even sporadic rise in the average temperatures at all stations, which is mostly due to the El Nino and La Nina phenomenon. However, the historical climatic data clearly show that the urban-rural air temperature difference increased steadily from approximately 0.3°C in 1980 to more than 0.8°C in 2010, showing that the UHI has occurred in this city.

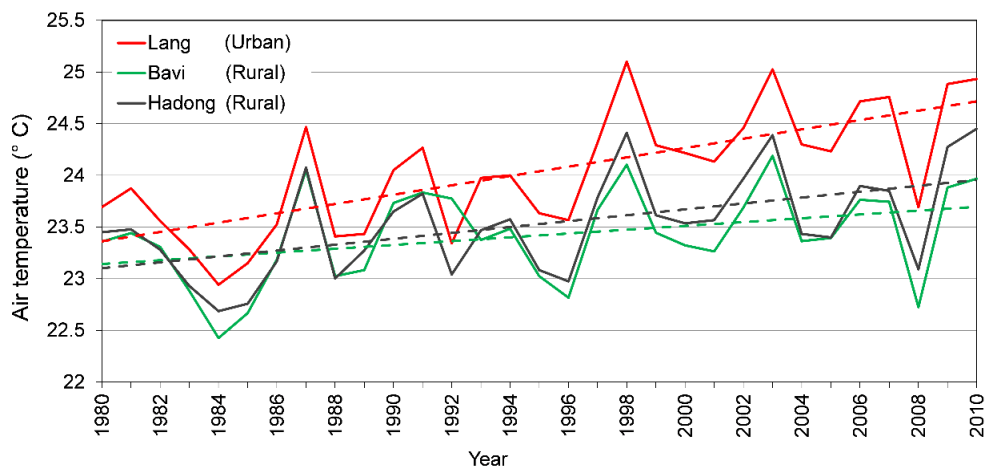


Fig. 1.3 Air temperature records in Hanoi City from 1980 to 2010 exhibit the gradual increments. Plain lines indicate annual mean temperatures and dashed lines are linear trends for available periods. The data are obtained from the weather station located in Lang which represents urban area and from the suburban and rural stations located in Bavi and Hadong, respectively. For the locations of each station, see Fig. 1.4. Weather data are provided by National Centre for Hydro-Meteorological Forecasting (NCHMF).

The Hanoi Master Plan 2030

In the context of rapid urbanisation causing massive pressures on resources and the environment, the government of Vietnam officially presented the Hanoi Master Plan 2030 in July 2011. In the master plan, the population of Hanoi is projected to reach 7.3 to 7.9 million by 2020, 9 to 9.2 million by 2030 and approximately 10.8 million by 2050. The major target of the master plan is to develop Hanoi as a green-cultured and civilised modern city. In order to achieve the above target, the master plan proposes a series of spatial development strategies for the city. One of these strategies is the network of green spaces in the capital consisting of the established green corridor, green belts, green buffers and other green spaces. The green belts are large green spaces located inside the urban development areas, while the green buffer is the boundary space between the existing urban areas and expanded urban clusters. As a result, the green coverage in the master plan would account for approximately 52% of the total land of the city.

Fig. 1.4 shows the land use changes due to the implementation of the master plan. To meet the demand of expanding urban development, 28% of the city's natural land will be allocated for urban construction land by 2030. In total, the constructed land will sharply increase to almost three times the existing amount, from 46,340 ha (14%) to more than 129,500 ha (39%). As shown in Fig. 1.4, the largest transition will take place with regard to agricultural land, as approximately 52,280 ha will be converted to other land use types, reducing the agricultural land contribution from approximately 50% in 2009 to approximately 34% of the total city land by 2030. In addition, nearly 4,470 ha of water bodies, 2,250 ha of forest and 5,230 ha of unused land will be converted to other functional land use types. In contrast, the green spaces will increase remarkably, from only 745 ha (0.2%) in 2009 to 15,770 ha (5%) in 2030.

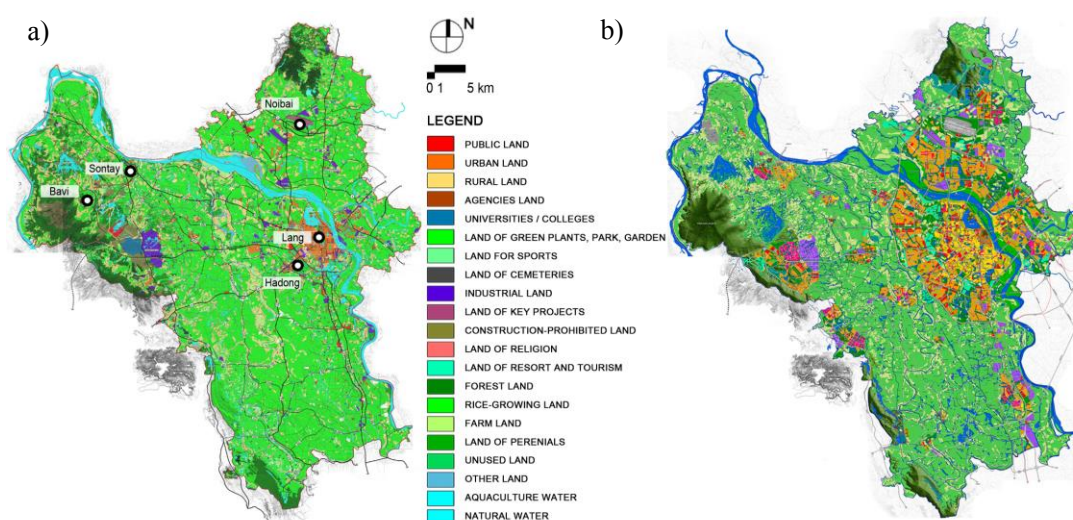


Fig. 1.4 Land use map of Hanoi for (a) current condition in 2010 and (b) Hanoi Master Plan 2030. This map shows the administrative boundary for the metropolitan area of Hanoi. Source: VIAP, 2011.

1.2.2 Johor Bahru, Malaysia

Location, geography, population and climatic features

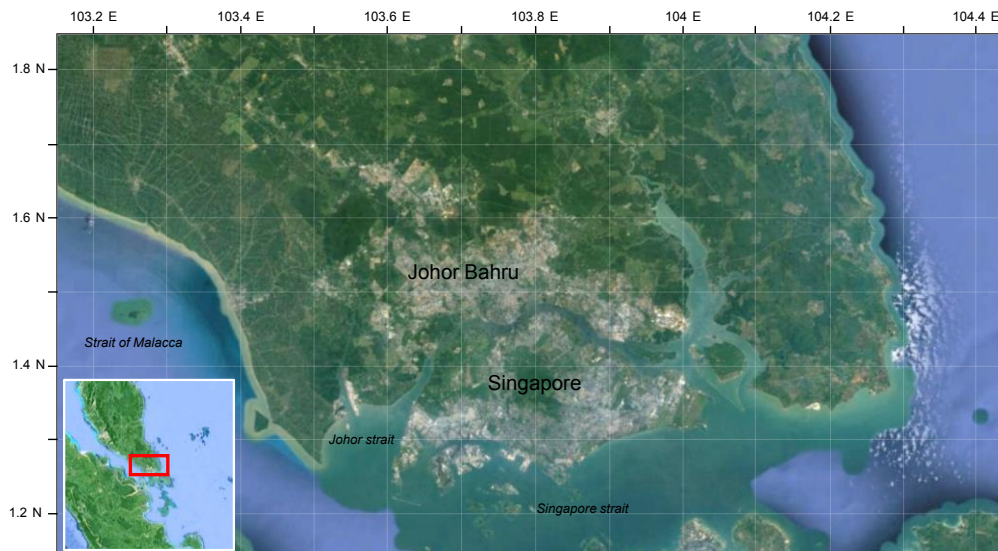


Fig. 1.5 Map showing the location of Johor Bahru. The inset shows the location of Johor Bahru at the tip of Malaysian peninsula. Source: Google Earth.

Johor Bahru (hereinafter referred to as JB), the capital of Johor State, Malaysia, is a city located at the southern tip of the Malay Peninsula ($1^{\circ}29' N$ $103^{\circ}44' E$). The metropolitan area had a population of about 1.3 million in 2010. It is the second largest city in Malaysia (after Kuala Lumpur, the capital city of Malaysia). The metropolitan region covers 220,000 ha, of which only 15% is urbanised, while the remaining areas are for agricultural use, forest, and river basins (Khazanah Nasional, 2006). JB is neighbouring with Singapore. The two cities are separated by 1.6 to 4.8-km wide sea channel called The Johor Strait and linked by two bridges namely The Causeway and The Second Link. The terrain of JB is relatively flat. The only major high point is at Gunung Pulai (654 m AMSL), located 19 km away from the city centre.

The population of JB has been increased from 988,291 in 2000 to 1.3 million in 2010. In line with the increased population, massive speculative developments of medium-rise buildings and two to three storeys shophouses have emerged uncontrollably (Rizzo & Glasson, 2012). JB is one of the fastest-growing cities in Malaysia after Kuala Lumpur. It is the main commercial centre for Johor and is located in the triangle of Indonesia-Malaysia-Singapore. This makes JB as the centre for industrial and commercial activities in the region. The heavy industry is located in the eastern part of urban area in Pasir Gudang area, the main harbour for various factories are located around Senai, the airport, and Port of Tanjung Pelepas (PTP) cargo harbour, while small and medium enterprises are scattered all over the city.

According to the Köppen-Geiger climate classification, JB has a tropical rainforest climate (Af) (Peel et al., 2007). The climate is described with consistent temperatures, a considerable

amount of rain, and high humidity throughout the year. According to the weather data from 2000 to 2013, the mean temperature is 27.26°C. On average, the warmest and coolest month are May and January, respectively, while June is the driest month with less number of precipitation.

Although the temperatures are generally consistent, it can change through the monsoon seasons with variations of wind speeds and direction, cloudiness, and wet and dry seasons throughout the year. Though the wind over the country is generally light and variable, there are some uniform periodic changes in the wind flow patterns. Based on these changes, four seasons can be distinguished, which are the south-west monsoon, northeast monsoon and two shorter periods of inter-monsoon seasons. The south-west monsoon season is usually established in June and ends in August. The prevailing wind flow is generally southwesterly and light, below 7.7 m/s. The northeast monsoon season usually commences between December and February. During this season, steady easterly or northeasterly winds of 5 to 10 m/s prevail. The two inter-monsoon seasons are from March to May and September to November, respectively, which are relatively calm with less rain and weaker winds.

Meanwhile, UHI effect had been observed in JB. Kubota and Ossen (2009) found that the nocturnal temperature difference between urban-rural reached 4°C during the sunny day, while it was 2°C in the rainy day. The maximum nocturnal air temperatures were observed in the built-up areas such as in commercial district, housing estates, and industrial areas.

Iskandar Malaysia

In 2006, JB and its metropolitan region (the SJER) was chosen to be the second economic corridor, after Kuala Lumpur. The SJER was later renamed as 'Iskandar Malaysia', honouring the late Sultan of Johor. Accordingly, a Comprehensive Development Plan (CDP) was produced and the regional development authority, called Iskandar Malaysia Development Authority (IRDA), was also formed. The development aims to strengthen the Malaysian economy and also to modernise the JB's urban and economic infrastructures.

The CDP is planned to accommodate population growth from 1.3 million in 2008 to 3 million by 2025. The urban development focuses on five flagship zones within Iskandar Malaysia:

1. Johor Bahru, the core of the development as the financial centre of the region.
2. Nusajaya, to be developed as residential, retail and shopping, educational facilities, health and medical facilities, light-industry, and tertiary uses;
3. Western Gate Development, to strengthen the surrounding area of the PTP cargo harbour than has been growing rapidly;
4. Eater Gate Development, to redevelop the area around Pasir Gudang Port and its heavy industries. This area focuses on heavy industry and cargo port activities;
5. Senai-Skudai, two districts located in the northern part of JB, as the location for the quaternary facilities and infrastructure, such as universities, airport, warehouses, high tech industry, etc.

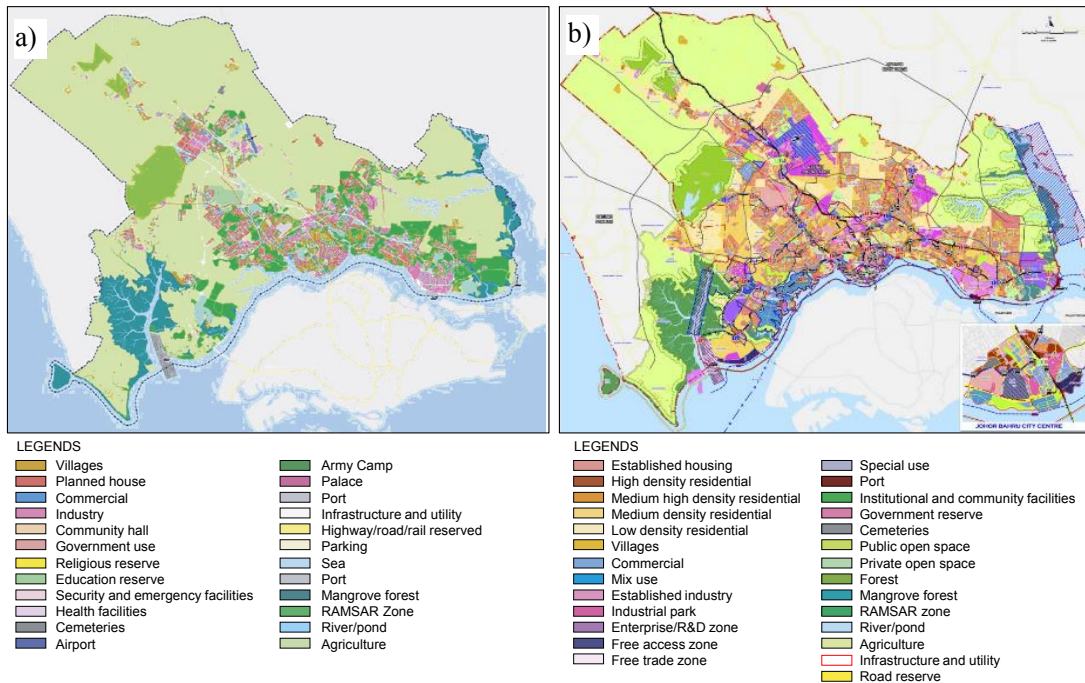


Fig. 1.6 Map of (a) existing land use and (b) the CDP of Iskandar Malaysia by 2025. This map shows the administrative boundary of Iskandar Malaysia.

Source: Khazanah Nasional, 2006.

The five flagship zones are designated as the priority areas for major investment and developments. Within each zone, the commercial, industrial, and other associated amenities are provided to reduce travelling demand and to bring the workplace closer to residential areas.

According to the CDP, the residential land is projected to cover approximately 26.7% of the total land, from only 4.7% in existing condition (Khazanah Nasional, 2006). Moreover, the land for commercial is projected to increase from 1,213 ha to 3,752 ha by 2025. Most of the development projects will take place in the former lands for agriculture and forest. Around 46,000 ha of agricultural land and 600 ha of forest area are turned into the built-up land (see Fig. 1.6).

Low Carbon Society Blueprint for Iskandar Malaysia 2025

In line with the Malaysia Government's aspiration to reduce carbon intensity by 40% by 2020 as compared to its level in 2005 and transforming Iskandar Malaysia into a sustainable metropolis with international standing, the Low Carbon Society (LCS) Blueprint for Iskandar Malaysia was launched in 2012. The blueprint for Iskandar Malaysia 2025 is a comprehensive climate change mitigation, focusing on carbon emission reduction, and detailed strategies towards a strong and sustainable metropolis by 2025 (UTM Low Carbon Asia Research Center, 2013). It incorporates various national policies, including the CDP for South Johor Economic

Table 1.3 Carbon reduction contribution of 12 mitigation actions for low carbon Iskandar Malaysia.

| Mitigation options | Reduction (ktCO ₂ eq) | Percentage (%) |
|--|----------------------------------|----------------|
| Green Economy | 6,937 | 54 |
| Action 1- Integrated Green Transportation | 1,916 | 15 |
| Action 2- Green Industry | 1,094 | 9 |
| Action 3- Low Carbon Urban Governance | - | - |
| Action 4- Green Building and Construction | 1,203 | 9 |
| Action 5- Green Energy System and Renewable Energy | 2,725 | 21 |
| Green Community | 2,727 | 21 |
| Action 6- Low Carbon Lifestyle | 2,727 | 21 |
| Action 7- Community Engagement and Consensus Building | - | - |
| Green Environment | 3,094 | 25 |
| Action 8- Walkable, Safe, and Livable City Design | 263 | 2 |
| Action 9- Smart Urban Growth | 1,214 | 10 |
| Action 10- Green and Blue Infrastructure and Rural Resources | 392 | 3 |
| Action 11- Sustainable Waste Management | 1,224 | 10 |
| Action 12- Clean Air Environment | - | - |

Source: (UTM Low Carbon Asia Research Center, 2013).

Region 2006-2025. The main function of the CDP and the blueprints is to provide a cooperation framework for all stakeholders within Iskandar Malaysia to legally abide.

According to the Kyoto Protocol, the low carbon society is described as a new society that consumes relatively low amount of resources (e.g. raw material, energy, and water) in minimising GHGs emission to avoid the adverse effect of climate change. The performance of the blueprint is assessed by comparing these following three scenarios: (1) 2005- base year; (2) 2025 business as usual (BaU), which is the upcoming year with the development according to CDP without any carbon mitigation measures; and (3) 2025 countermeasure (CM), the scenario in which is the development according to CDP adopts carbon mitigation options proposed in the LCS blueprint. In order to transform Iskandar Malaysia into a low carbon society, twelve mitigation actions are proposed. They were formed under three themes, namely Green Economy, Green Community, and Green Environment (Table 1.3). If all actions are taken place, they are able to provide 41% emission cut back from 2025 BaU to 2025 CM scenario. Green Economy contributes the most with 54% reduction, followed by Green Environment (25%), and Green Community (21%).

As the biggest contributor in the emission reduction, the Green Economy covers the transportation, industry, building and construction, and energy sectors, respectively. In the transportation sector, the strategy includes the promotion of a more integrated transportation system, rail-based and water-based public transportation modes, intercity high-speed rail transit system, and low-carbon vehicles.

Meanwhile, the promotions of green industries and decarbonisation of industries are the fundamental strategy in the industrial sector. The strategy includes a long-term focus to continuously improve the environmental performance regardless of sector, size, or location of the industry. It also includes commitment to and action on improving the production efficiency and reducing the generation of wastes and emissions. Some techniques are proposed, such as the automated energy management systems and the use of high-efficiency motors (HEMs).

In the building and construction sector, five strategies were proposed, which are: promoting green building standards in the new development project, energy efficiency improvement of existing buildings, green construction, green building design technology, and green buildings in the rural areas. Several techniques are proposed. For instance, the adoption of Industrialized Building System (IBS). IBS is defined as a construction technique in which components are manufactured in a controlled environment (on or off site). IBS promotes minimization of waste generation, extensive usage of energy efficient building material, effective logistics, and long term economic stability.

Meanwhile, almost all of the existing building stock is not designed according to the 'green standards'. As a result, these buildings consume a large amount of electricity and are not energy efficient. Retrofitting is the key strategy for this kind of buildings. Subsidies and tax reduction are provided to help the building owners retrofit their buildings.

Three key strategies were proposed in the energy sector, which are the promotion of renewable and alternative energy utilisation such as solar energy, biomass, biogas, etc.; the establishment of advance energy system such as smart grid and decentralised electricity generation; and the provision of incentives and subsidies and derivation of tariff rate to promote the utilisation renewable and alternative energy.

1.3 Research objectives

The main goal of this thesis is to investigate the impact of urban warming on the future challenges of urban climates as well as to assess the relevant countermeasures for the growing cities of Southeast Asia. Growing cities in Southeast Asia are expected to see further population growth in their already crowded cities over the next few decades that will exacerbate urban environmental conditions such as UHIs. This study focuses on Hanoi and JB in particular, but the results of this study would provide useful insights for policy making in urban planning for other Southeast Asian cities in achieving climate-sensitive urban design due to the similarities in the climatic and socio-demographic conditions. The specific objectives of this thesis are as follows:

1. To investigate the temporal and spatial characteristics of UHIs in growing cities of Southeast Asia.
2. To assess the impacts of land use changes brought by the urban master plans on urban climates in growing cities of Southeast Asia.

3. To examine the influences of global warming on the urban climates in growing cities of Southeast Asia (for the 2030s).
4. To assess the cooling effect of urban greening on UHIs.
5. To investigate the influence of anthropogenic heat release on UHIs.
6. To investigate the impacts of urban warming on the indoor thermal comfort and cooling load of residential buildings.
7. To propose the countermeasures to urban warming for growing cities of Southeast Asia.

The specific objectives are distributed into each case study as listed in Table 1.4. The assessment of the impact of master plan on urban climate is conducted for both case study. In particular, the Hanoi case study discusses the impact of global warming on urban climate and the cooling effect of the green spaces. Furthermore, the impact of the increased outdoor temperature on the indoor thermal comfort and cooling load in residential building will also be discussed in the Hanoi case study. Meanwhile, the JB case study assesses the influence of anthropogenic heat releases on urban climate based on the scenarios proposed in the LCS Blueprint for Iskandar Malaysia.

Table 1.4 Distribution of specific research objectives in each case study.

| Point of assessment | Case study | |
|---|------------|-------------|
| | Hanoi | Johor Bahru |
| Impact of the master plan on urban climate | ✓ | ✓ |
| Impact of global warming in 2030s on urban climate | ✓ | - |
| Cooling effect of the green spaces | ✓ | - |
| Influence of anthropogenic heat release on urban climate | - | ✓ |
| Thermal comfort and cooling load assessment in residential building | ✓ | - |

1.4 Structure of thesis

In this dissertation, a literature review on the study of UHIs is given in Chapter 2. Chapter 3 describes the data and method used for this study, including the descriptions of the WRF and TRNSYS models. The results of analysis on the impact of land use changes on urban climate in Hanoi and JB case studies are described in Chapter 4. The impact of global warming on the future urban climate is discussed in Chapter 5, focusing particularly on the Hanoi case study. Chapter 6 discusses the cooling effect of various configurations of the green spaces on the thermal environment in the master plan condition of Hanoi City. Meanwhile, the influence of anthropogenic heat releases on the urban climate is discussed in Chapter 7. The impact of the increased urban temperature on the indoor thermal comfort and cooling load of a residential building in Hanoi is described in Chapter 8. Chapter 9 contains a recommendation for the countermeasures to urban warming for the growing cities of Southeast Asia. The conclusions are presented in Chapter 10.

References

- Agarwal, M., & Tandon, A. (2010). Modeling of the urban heat island in the form of mesoscale wind and of its effect on air pollution dispersal. *Applied Mathematical Modelling*, 34(9), 2520–2530.
- Araujo, R. V., Albertini, M. R., Costa-da-Silva, A. L., Suesdek, L., Franceschi, N. C. S., Bastos, N. M., ... Allegro, V. L. A. C. (2015). São Paulo urban heat islands have a higher incidence of dengue than other urban areas. *The Brazilian Journal of Infectious Diseases*, 19(2), 146–155.
- Aronson, M. F. J., La Sorte, F. A., Nilon, C. H., Katti, M., Goddard, M. A., Lepczyk, C. A., ... Winter, M. (2014). A global analysis of the impacts of urbanization on bird and plant diversity reveals key anthropogenic drivers. *Proceedings of the Royal Society B*, 281(1780), 20133330.
- Bakr, M. (2015). Influence of Groundwater Management on Land Subsidence in Deltas-A Case Study of Jakarta (Indonesia). *Water Resource Management*, 29, 1541–1555.
- Bhatta, B. (2010). Causes and Consequences of Urban Growth and Sprawl. In B. Bhatta (Ed.), *Analysis of Urban Growth and Sprawl from Remote Sensing Data, Advances in Geographic Information Science* (p. 171). Berlin Heidelberg: Springer-Verlag.
- Birkmann, J., Welle, T., Solecki, W., Lwasa, S., & Garschagen, M. (2016). Boost resilience of small and mid-sized cities. *Nature*, 537(7622), 605–608.
- Christensen, J. H., Hewitson, B., Busuoiu, A., Chen, A., Gao, X., Held, I., ... Whetton, P. (2007). Regional Climate Projections. In S. Solomon, D. Qin, M. Manning, Z. Chen, M. Marquis, K. B. Averyt, ... H. L. Miller (Eds.), *Climate Change 2007: The Physical Science Basis. Contribution of Working Group I to the Fourth Assessment Report of the Intergovernmental Panel on Climate Change* (p. 2007). Cambridge, United Kingdom and New York, NY, USA: Cambridge University Press.
- Dewan Bandaraya Kuala Lumpur. (2000). *Kuala Lumpur Structure Plan 2020*. Kuala Lumpur.
- Flynn, A., McGreevy, C., & Mulkerrin, E. C. (2005). Why do older patients die in a heatwave? [Commentary] *QJM - Monthly Journal of the Association of Physicians*, 98(3), 227–229.
- Forman, R. T. T. (2014). *Urban ecology : science of cities*. Cambridge, United Kingdom: Cambridge University Press.
- Gartland, L. (2008). *Heat Islands: Understanding and Mitigating Heat in Urban Areas*. London: Earthscan.
- Gilbert, O. L. (1991). The Urban Climate and Air Pollution. In *The Ecology of Urban Habitats* (pp. 25–40). Dordrecht: Springer Netherlands.
- Grimm, N. B., Faeth, S. H., Golubiewski, N. E., Redman, C. L., Wu, J., Bai, X., & Briggs, J. M. (2008). Global Change and the Ecology of Cities. *SCIENCE*, 319(5864), 756–760.
- Hahs, A. K., McDonnell, M. J., McCarthy, M. A., Vesk, P. A., Corlett, R. T., Norton, B. A., ... Williams, N. S. G. (2009). A global synthesis of plant extinction rates in urban areas. *Ecology Letters*, 12(11), 1165–1173.

- Hartmann, D. J., Klein Tank, A. M. G., Rusticucci, M., Alexander, L. V., Brönnimann, S., Charabi, Y. A.-R., ... Zhai, P. (2013). Observations: Atmosphere and Surface. In *Climate Change 2013: The Physical Science Basis. Contribution of Working Group I to the Fifth Assessment Report of the Intergovernmental Panel on Climate Change* (pp. 159–254). Cambridge, United Kingdom and New York, USA.
- Hulme, M., & Sheard, N. (1999a). *Climate Change Scenarios for Indonesia*. Norwich, UK.
- Hulme, M., & Sheard, N. (1999b). *Climate Change Scenarios for the Philippines*. Norwich, UK.
- Jakarta Capital City Government. (2012). *Regional Spatial Plan Jakarta 2030*. Jakarta.
- Japan International Cooperation Agency. (2013). *A Strategic Urban Development Plan of Greater Yangon*.
- Jentsch, M. F., Bahaj, A. S., & James, P. A. B. (2008). Climate change future proofing of buildings- Generation and assessment of building simulation weather files. *Energy and Buildings*, 40(12), 2148–2168.
- Kahn, M. E. (2000). The environmental impact of suburbanization. *Journal of Policy Analysis and Management*, 19(4), 569–586.
- Khajuria, A., Yamamoto, Y., & Morioka, T. (2008). Solid waste management in Asian countries: problems and issues. *WIT Transactions on Ecology and the Environment*, 109, 643–653.
- Khazanah Nasional. (2006). *Comprehensive Development Plan for South Johor Economic Region 2006-2025*. Kuala Lumpur.
- Kleerekoper, L., van Esch, M., & Salcedo, T. B. (2012). How to make a city climate-proof, addressing the urban heat island effect. *Resources, Conservation and Recycling*, 64, 30–38.
- Kubota, T., & Ossen, D. R. (2009). Spatial characteristics of Urban Heat Island in Johor Bahru City, Malaysia. *Proceedings of The 3rd Symposium of South East Asian Technical University Consortium (SEATUC)*, 39–44.
- Lai, L.-W., & Cheng, W.-L. (2009). Air quality influenced by urban heat island coupled with synoptic weather patterns. *Science of The Total Environment* (Vol. 407).
<https://doi.org/10.1016/j.scitotenv.2008.12.002>
- Lomas, K. J., & Ji, Y. (2009). Resilience of naturally ventilated buildings to climate change: Advanced natural ventilation and hospital wards. *Energy and Buildings*, 41(6), 629–653.
- McCarthy, M. P., Best, M. J., & Betts, R. A. (2010). Climate change in cities due to global warming and urban effects. *Geophysical Research Letters*, 37(9), 1–5.
- Metropolitan Manila Development Authority. (2015). *The Metro Manila greenprint 2030 : building a vision*.
- Montgomery, M. R. (2008). The Urban Transformation of the Developing World. *Science*, 319(February), 761–765.

- Municipality of Phnom Penh. (2007). *Phnom Penh Strategic Orientation 2035*. Phnom Penh.
- Murakami, A., Medrial Zain, A., Takeuchi, K., Tsunekawa, A., & Yokota, S. (2005). Trends in urbanization and patterns of land use in the Asian mega cities Jakarta, Bangkok, and Metro Manila. *Landscape and Urban Planning*, 70(3–4 SPEC. ISS.), 251–259.
- Oke, T. R. (1976). The distinction between canopy and boundary layer urban heat islands. *Atmosphere*, 14(July 2015), 268–277.
- Oke, T. R. (1987). *Boundary Layer Climates* (2nd ed.). New York, USA: Routledge.
- Oleson, K. W., Bonan, G. B., Feddema, J., & Jackson, T. (2011). An examination of urban heat island characteristics in a global climate model. *International Journal of Climatology*, 31(12), 1848–1865.
- Ostojic, D. R., Bose, R. K., Krambeck, H., Lim, J., & Zhang, Y. (2013). *Energizing Green Cities in Southeast Asia*. The World Bank.
- Peel, M. C., Finlayson, B. L., & McMahon, T. A. (2007). Updated world map of the Köppen-Geiger climate classification. *Hydrology and Earth System Sciences*, 11(3), 1633–1644.
- Phienweij, N., Giao, P., & Nutalaya, P. (2006). Land subsidence in Bangkok, Thailand. *Engineering Geology*, 82(4), 187–201.
- Rizzo, A., & Glasson, J. (2012). Iskandar Malaysia. *Cities*, 29(6), 417–427.
- Roth, M. (2013). Urban Heat Islands. In *Handbook of Environmental Fluid Dynamics, Volume Two* (pp. 143–159). CRC Press.
- RTRW Bandung. (2011). Rencana Tata Ruang Wilayah Kota Bandung 2011-2031.
- Santamouris, M. (2015a). Analyzing the heat island magnitude and characteristics in one hundred Asian and Australian cities and regions. *Science of the Total Environment*, 512–513, 582–598.
- Santamouris, M. (2015b). Regulating the damaged thermostat of the cities—Status, impacts and mitigation challenges. *Energy and Buildings*, 91, 43–56.
- Santamouris, M., Cartalis, C., Synnefa, A., & Kolokotsa, D. (2015). On the impact of urban heat island and global warming on the power demand and electricity consumption of buildings—A review. *Energy and Buildings*, 98, 119–124.
- Schneider, A., Mertes, C. M., Tatem, A. J., Tan, B., Sulla-Menashe, D., Graves, S. J., ... Dastur, A. (2015). A new urban landscape in East–Southeast Asia, 2000–2010. *Environmental Research Letters*, 10(3), 34002.
- Seto, K. C., Dhakal, S., Bigio, A., Blanco, H., Delgado, G. C., Dewar, D., ... Ramaswami, A. (2014). *Human Settlements, Infrastructure, and Spatial Planning*. In: *Climate change 2014: Mitigation of climate change. Contribution of Working Group III to the Fifth Assessment Report of the Intergovernmental Panel on Climate Change. Climate change 2014: Mitigation of climate change. Contribution of Working Group III to the Fifth Assessment Report of the*

- Intergovernmental Panel on Climate Change*. Cambridge, United Kingdom and New York, USA. <https://doi.org/10.1017/CBO9781107415416.018>
- Seto, K. C., Kaufmann, R. K., & Woodcock, C. E. (2000). Landsat reveals China's farmland reserves, but they're vanishing fast. *Nature*, *406*(6792), 121–121.
- The Department of Public Works and Town Planning. (2004). *Bangkok and Vicinities Regional Plan*. Bangkok.
- Trenberth, K. E., Jones, P. D., Ambenje, P., Bojariu, R., Easterling, D., Tank, A. K., ... Zhai, P. (2007). Observations: Surface and Atmospheric Climate Change. In *Climate Change 2007: The Physical Science Basis. Contribution of Working Group I to the Fourth Assessment Report of the Intergovernmental Panel on Climate Change* (Vol. 164, pp. 235–336). Cambridge, United Kingdom and New York, NY, USA.: Cambridge University Press.
- Tryjanowski, P., Sparks, T. H., Kuźniak, S., Czechowski, P., & Jerzak, L. (2013). Bird Migration Advances More Strongly in Urban Environments. *PLoS ONE*, *8*(5), 1–6.
- United Nations. (2014). *World Urbanization Prospects: The 2014 Revision*.
- Urban Redevelopment Authority. (2014). *Master Plan 2014*. Singapore: Urban Regional.
- US EPA. (2017). *Climate Change: Basic Information*.
- UTM Low Carbon Asia Research Center. (2013). *Low Carbon Society Blueprint for Iskandar Malaysia 2015*. UTM-Low Carbon Asia Research Center. Johor Bahru. <https://doi.org/10.1017/CBO9781107415324.004>
- Vietnam Institute of Architecture Urban and Rural Planning (VIAP). (2011). *The Hanoi Capital Construction Master Plan 2030 and Vision to 2050, Comprehensive Report*. Hanoi, Vietnam: VIAP.
- Wong, N. H., & Chen, Y. (2008). *Tropical Urban Heat Islands: Climate, Buildings and Greenery*. New York, USA: Taylor & Francis.
- Xu, L., Stige, L. C., Chan, K.-S., Zhou, J., Yang, J., Sang, S., ... Stenseth, N. C. (2016). Climate variation drives dengue dynamics. *Proceedings of the National Academy of Sciences of the United States of America*, *114*(1), 113–118.
- Yoshikado, H., & Tsuchida, M. (1996). High Levels of Winter Air Pollution under the Influence of the Urban Heat Island along the Shore of Tokyo Bay. *Journal of Applied Meteorology*, *35*(10), 1804–1813.
- Zipper, S. C., Schatz, J., Singh, A., Kucharik, C. J., Townsend, P. a, & Loheide, S. P. (2016). Urban heat island impacts on plant phenology: intra-urban variability and response to land cover. *Environmental Research Letters*, *11*(5), 54023.

2

Literature Review

2.1 UHI in general

UHI is the phenomenon whereby urban regions experience warmer temperature than rural surroundings. The formation of UHI is related to the energy balance of the urban area. The energy balance is affected by the urban structures and materials, land cover change, and human activities. The UHI is, therefore, the result of energy balance differences between urban and rural (Roth, 2013). The energy balance in urban areas is defined as (Oke, 1988)

$$Q^* + Q_F = Q_H + Q_E + Q_S + \Delta Q_A \quad (\text{W m}^{-2}) \quad (2.1)$$

where Q^* is the net all-wave radiation flux; and Q_H and Q_E are the turbulent sensible and latent heat fluxes, respectively; Q_S is the net uptake or release of energy by sensible heat changes in the urban ground-canopy-air volume; ΔQ_A is the net horizontal advective heat flux; Q_F is the anthropogenic heat flux from heat released by combustion fuels (e.g. traffic, building HVAC systems).

The available energy at any location to heat the air or ground or evaporate water depends on the radiation balance

$$Q^* = K^* + L^* = K \downarrow - K \uparrow + L \downarrow - L \uparrow \quad (\text{W m}^{-2}) \quad (2.2)$$

where K and L are the shortwave (from the sun radiation) and longwave radiation flux, respectively. The arrows indicate whether the flow of energy is toward (\downarrow) or away (\uparrow) from the surface.

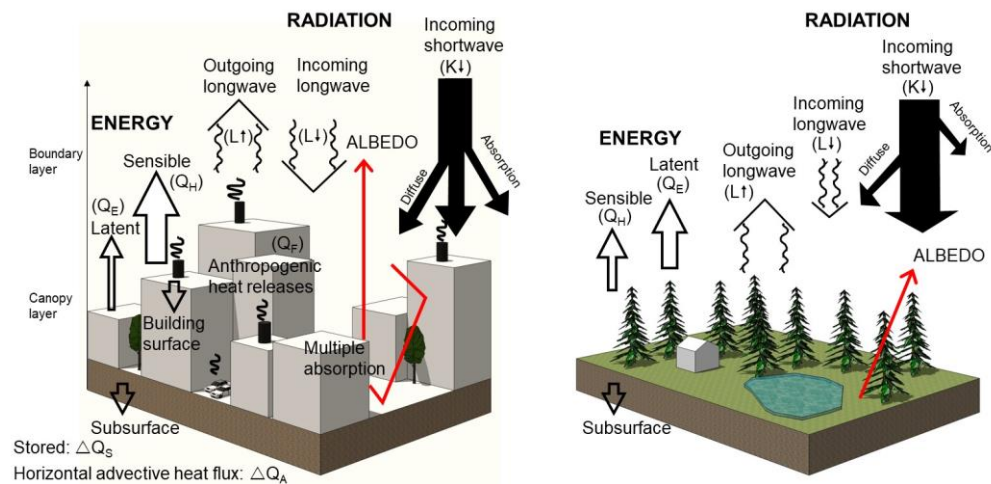


Fig. 2.1 Schematic depiction of terms involved in the radiation and energy fluxes over an urban and a rural area on a clear day. The width of the arrows approximates the size of the flux (adapted from Oke (1988)).

The existence of the city alters all elements in (2.1) and (2.2). The surface morphology results in lower albedo because of multiple reflections of the incoming solar radiation. Street canyons trap longwave radiation resulting in a lower net longwave loss (L^*) at street level. The surface materials influence the albedo, surface temperature and emissivity, and therefore the outgoing short- and longwave radiation and respective net fluxes. The warmed and polluted urban atmosphere also affects the net long-wave radiation balance (M Roth, 2013). Fig. 2.1 illustrates the schematic depiction of the radiation and energy balance in urban and rural areas.

The warm and rough nature of the urban surface promotes turbulent mixing, and unstable conditions prevail during daytime and mildly unstable or neutral conditions at night, especially in summertime and in densely built-up areas (M Roth, 2013). The convective fluxes are therefore usually driven away from the surface at most hours of the day. Reduction of Q_E in the city is common during daytime but evapotranspiration process is still an important energy (or heat) sink in the built-up areas. The evapotranspiration process depends on the amount of greenspaces, surface wetness, precipitation, or irrigation. Because of lower Q_E in the city, heat during the daytime is preferentially channelled into sensible forms (Q_H and Q_S), which results in a warming of the environment. Key characteristics that influence the magnitude of Q_S are the surface materials and the urban structure. The materials in urban areas commonly have a good ability to absorb, conduct, and diffuse heat. Therefore, Q_S is significantly and consistently larger in an urban area than its rural surroundings. Q_S is usually transported into the building volume in the morning, transferred back into the surface by mid to late afternoon, and then released to the atmosphere. This helps to maintain a positive Q_S flux in cities in the evening and at night, resulting in the heat island in the air. At night, the urban-rural air temperature difference is more apparent because of the radiative heat from the extra heat stored in the urban fabric during the daytime.

Heat islands may be measured as either surface or atmospheric phenomena, and a further distinction is sometimes introduced according to the observation method (Roth, 2013). Most of the earlier UHI studies generally used data from fixed weather stations or mobile transverse for subsequent analysis. Data archived from these methods of UHI measurement were commonly used for calculating the air temperature difference between urban and rural areas, identifying regional two-dimensional impacts or evaluating UHI trends over time as a region develops. Thus, the calculated results were highly associated with the location, and the surrounding land cover information for the meteorological stations could not be used to determine temperatures and other characteristics of the surfaces (Mirzaei & Haghghat, 2010). Remote Sensing, conversely, has been employed in determining the surface temperature (LST) and surface energy balance. Remote sensing technology also enables researchers to visualize LST over large areas but only provides a birds-eye view of the surface temperature and excludes the temperatures of walls, vegetation and under trees (Gartland, 2008).

Although the above UHI measurement methods are useful, these methods are difficult to use for predicting future scenarios of urban climate or assessing how well the UHI mitigation measures can ameliorate the urban temperatures, energy use, and air pollution. Numerical modelling is an important and useful method for understanding how the heat island functions and estimating the effectiveness of different UHI mitigation measures. In addition to various local- and micro-scale models that focus on UHI effect on individual buildings, a single street, or neighbourhood, regional climate models (RCMs) can be used to evaluate UHI effect on entire urban regions (Ching, 2013; Gartland, 2008; Santamouris & Kolokotsa, 2016). For example, the WRF (Skamarock et al., 2008), one of the most well-known and advanced meso-scale meteorological models, has been applied to urban climate (Gsella et al., 2014; Meng et al., 2011; Tewari et al., 2007) and extreme weather studies (Kusaka et al., 2005; Lee et al., 2013). Various research have also applied WRF to UHI case studies for evaluating the impact of land use changes on urban climates from past to present (Q.-V. Doan & Kusaka, 2015; Morris, Chan, Salleh, et al., 2016) and also under the future climate (Jiang et al., 2008). A precise prediction of atmospheric conditions in an urban environment using a meteorological model requires a LULC data set that accurately represents the environmental conditions. Several studies demonstrated the importance of high-resolution LULC data for improving surface boundary mixing and local wind patterns (Cheng & Byun 2008; Chng et al. 2010).

2.2 UHI studies in the tropics

To date, numerous studies on UHIs have been conducted in various regions (Santamouris, 2015a). However, most of the past research focused on the mid-latitude climates in the Northern hemisphere (Roth, 2007). Roth (2007) argued that the research on urban climate in the equatorial or subtropical context is still lacking though the UHI effect is certainly unwelcome in a tropical climate (Wong & Chen, 2008). Nevertheless, studies on urban heat islands in tropical climates have rapidly increased in the last decade (Qaid et al., 2016).

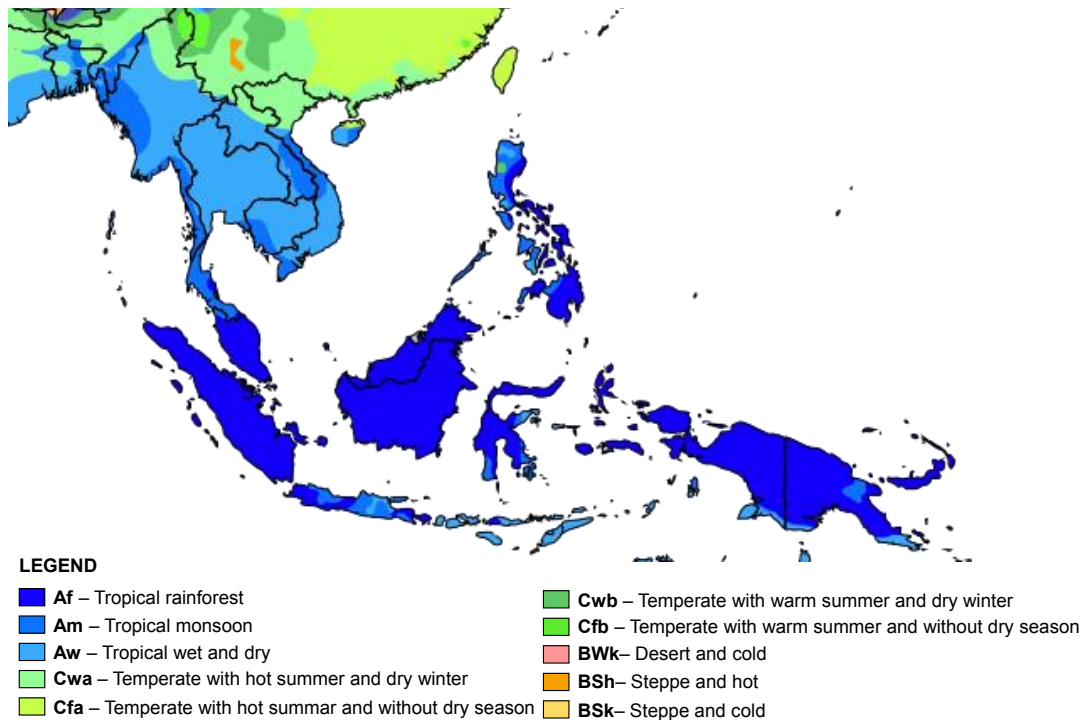


Fig. 2.2 Köppen-Geiger climate type map of Southeast Asia. Source: Peel et al. (2007)

According to Köppen classification (Peel et al., 2007), the tropics near the equator can be further classified into a tropical wet climate (Köppen classification: *Af*) with abundant rainfall throughout the year; e.g. Singapore, tropical wet/dry (*Aw*; pronounced dry season; e.g. Mumbai), tropical monsoonal climate (*Am*; relative dryness for 1-3 months; e.g. Jakarta), and a tropical highland climate (*H* or *Cwb*; high altitude without the climate would be tropical wet/dry; e.g. Bogota and Mexico City). Some cities of Southeast Asia also experience humid subtropical climates (*Cfa*, *Cfb*, and *Cwa*), e.g. Hanoi. The subtropical climates have very warm to hot summers and the winter is relatively cold but not go below freezing and little rainfall. Fig. 2.2 shows the climate type map in Southeast Asia region.

Singapore was most likely the first city in a tropical climate to be the subject of UHI study (Nieuwolt, 1966). This led to the subsequent local urban climate research conducted by Sani (1972) in Kuala Lumpur, Malaysia. The studies in other locations include the tropical wet/dry in Chennai, India (Amirtham, 2016); the tropical monsoon climate, such as in Rio de Janeiro, Brazil (Lucena et al., 2013) and in Jakarta, Indonesia (Tokairin et al., 2010); and the subtropical highland climates, such as in Johannesburg, South Africa (Goldreich, 1992), Shanghai (Longxun et al., 2003), Hong Kong (Giridharan et al., 2005), and Buenos Aires (Figueroa & Mazzeo, 1998). A review of UHI studies in the (sub)tropics by Roth (2007) concluded that the morphology of UHI in the tropics, for example, is sensitive to building density or land use, similar with the studies in the temperate cities.

UHIs in the tropics also show a strong seasonal variability. Despite being characterized with fairly uniform weather condition throughout the year, UHIs are clearly associated with the relatively drier southwest and wetter north-easterly monsoon (Chow & Roth, 2006; Sani, 1990). Furthermore, in the observational study in JB, Kubota & Ossen (2009) found that the nocturnal UHI intensity reached 4°C in the sunny day, and can reach 2°C in the rainy day, showing that UHI still exists due to the effect of anthropogenic heat even in a rainy day.

Cities are often located in complex geographical locations (e.g. coastal, bottom of valley, confluence of rivers, etc.) that generate advection and thermal wind systems at scales larger than the city, which interact with urban atmosphere and have potential to modulate the UHI (Fernando, 2010). The effect of sea breeze on the reduction of air temperature is significant in the coastal cities (Boonjawat et al., 2006), where the air temperatures tend to decrease with the proximity of such area to the sea. The effect of UHI results in a change of the wind system and causes a delay of sea breezes to reach inland areas (Kusaka et al., 2000; Yoshikado, 1992). In the study in six largest cities of South Korea, Kim & Baik (2004) found that, in average, the UHI intensity tends to be smaller in coastal cities than in inland cities. Meanwhile, in Hanoi, the hot and dry Fohn wind generated from the mountainous region in the western part of the city may occur during summer months and strongly contributed to the increasing temperature in the urban areas (Nguyen & Reiter, 2014).

2.3 Impacts of land use changes on UHIs

The relationship between land use/land cover (LULC) and urban climate has been established in a number of studies (Chen et al., 2014; Guo et al., 2015; Jusuf et al., 2007; Zhou et al., 2016). In most cases, SUHIs were observed in built-up areas such as industrial or commercial areas, while cool islands were discovered in vegetated areas such as parks and forests.

In regards to the rapidly growing cities in tropical climates of Asia, such as Hanoi and JB, it is important to project the impacts of land use changes brought by the master plans on urban climates. There are a number of studies that analysed the effect of land use changes on urban climate by using observation data (Cui & Shi, 2012; He et al., 2007; Nonomura et al., 2009), satellite remote sensing data (Chen et al., 2017; Hu & Jia, 2010; Polydoros & Cartalis, 2015; Radhi, Fikry, & Sharples, 2013; Van Nguyen et al., 2015; Zhang et al., 2013), or meso-scale models such as WRF (Doan et al., 2016; Kusaka et al., 2000; Miao et al., 2009; Morris et al., 2016; Wang et al., 2009).

Most of the studies investigating the UHI effect were based on the historical land use changes from the past to the present. For example, Tokairin et al. (2010) compared the observation and numerical simulation results in the 1970s and 2000s in Jakarta; Chen et al. (2006) analysed the LANDSAT 5 images between 1990 and 2000 and measured the land surface temperature and UHI intensity over 19 counties and cities along the Pearl River Delta. Li et al. (2012) analysed the spatiotemporal pattern of the UHI in Shanghai by comparing the Landsat TM/ETM+

images from 1997 to 2008; Zhang et al. (2013) and Feng et al. (2014) analysed the Landsat TM/ETM+ images over the city of Xiamen, China between 1987 to 2007. In general, those studies agree that the changes of land use strongly affect the urban climate attributed to the urban sprawl and conversion of cropland/farmland into built-up area.

There are relatively few studies investigating the UHI effect based on the future land use changes and compare the results with the current situation. Several relevant studies include Velazquez-Lozada et al. (2006) in San Juan, Puerto Rico; Coutts et al. (2008) in Melbourne, Australia; Marshall Shepherd et al. (2010) in Houston, US; and Shin & Baigorria (2012) in Florida. Regardless the geographical location of each case study, in general, the above studies concluded that the increasing non-vegetated/built-up land due to urban growth has significant impact on urban climate, characterized by the increases of sensible heat and number of areas with high temperatures. In addition to the future land use changes, several studies also considered the effect of future climate (i.e. under global warming condition) into the analysis, such as Kikumoto et al. (2015) and Adachi et al. (2012) in Tokyo, Iizuka, Xuan, et al. (2015) in Nagoya, and Argüeso et al. (2014) in Sydney.

As explained before, many cities in Southeast Asia are likely to experience dramatic land use changes associated with the implementation of their large-scale master plans in the near future. However, almost none of the studies on UHI was conducted in the developing countries to project the urban climates after the implementation of the proposed master plans. A very rare exception is the recent study conducted by Doan et al. (2016). They examined the impact of future urbanization on UHI in the rapidly growing city of Ho Chi Minh, Vietnam.

2.4 Influences of global warming on urban climate

The effects of global warming vary according to geographical locations and are highly anticipated in urban areas even in the future as near as 2030 (Hartmann et al., 2013). Thus, the urban climates of rapidly growing cities such as Hanoi and JB are predicted to change not only owing to land use changes but also global warming.

To investigate the urban climate under global warming condition, most of the studies have relied on outputs of the Global Climate Models (GCMs) (Bhuvandas et al., 2014; UNFCC, 2004). However, the typical outputs of GCMs are too coarse (approx. 50-100km) for urban-scale climate simulation. Nevertheless, the utilisation of GCM outputs as the input for WRF has been made possible by employing a downscaling method. There are two downscaling techniques: statistical and dynamical methods (Bhuvandas et al., 2014). Statistical downscaling incorporates observational data at the regional climate and large-scale climate projected by the GCMs. This method strongly relies on the quality of past observations. Therefore, the method is unsuitable when past observational data are lacking (Kikumoto et al., 2015). On the other hand, dynamical downscaling directly incorporates the future climate into a regional climate model (RCM) and relies less on past observational data (Conry et al., 2015). An attempt by Arima et al. (2015) employed this method to achieve 2-km horizontal grid

spacing of a simulated future urban climate in the summers of the 2030s in Tokyo for estimating cooling loads in residential buildings. A finer horizontal grid spacing of 0.333 km was employed by Conry et al. (2015) for assessing UHI and climate change in Chicago in the 2080s. A high spatial resolution of RCMs is ideal for assessing the effects of land use changes on a regional climate at different scales (Wang et al., 2004). In addition to the direct dynamical downscaling method Kimura & Kitoh (2007) developed a new downscaling method called the pseudo global warming (PGW) method. Instead of directly downscaling GCM outputs, the initial and boundary conditions for the regional climate projections in PGW method are given by the summation of present weather conditions and global warming increment estimated from GCMs. Thus, the influences of biases from GCM are much reduced in the PGW method. This approach has been applied to the WRF model with 1-km horizontal grid spacing for assessing impacts of urban forms on the future thermal environment in Beijing (Yang et al., 2016) and in Nagoya for investigating the impacts of disaster prevention scenarios on the future thermal environment (Iizuka et al., 2015). Nevertheless, this method assumes there is no change in synoptic and climate variability in the future climate projections (Wakazuki & Rasmussen, 2015). To overcome this limitation, Kusaka et al. (2012) suggested to use a direct dynamical downscaling method.

As described above, several studies have analysed UHIs under the influence of future global warming, but there have been few studies considering the effects of future urbanisation of rapidly growing cities, such as those in Asia or Africa. Two relevant studies are those by Yang et al. (2016) and Doan et al. (2016). In their study of UHIs in Beijing, Yang et al. (2016) estimate the total increase in air temperature to be up to 2.98 °C by the 2050s. Climate and land use change are responsible for up to 2.44°C and 0.4°C, respectively, of this temperature change. Doan et al. (2016) employed the dynamical downscaling method to examine the impact of future urbanisation on UHIs in the growing city of Ho Chi Minh City, Vietnam. However, the boundary condition was fixed at the current time in the simulations to investigate only the impact of further urbanisation, without considering the effects of future global warming. The study conducted by Iizuka, Ito, et al. (2015) projected the possible future thermal and wind environments in Vinh City, Vietnam, by the 2030s by employing the PGW method. Still, as has been mentioned earlier, the climate variability could not be represented by this method. To the author's knowledge, studies have not been conducted in growing cities to project the effect of global warming on UHIs under their future master plans via direct dynamical downscaling with an RCM.

2.5 Studies on the impacts of urban warming

2.5.1 Impact on building energy consumption

High urban temperatures increase the energy needs for cooling, decrease the needs for heating and affect the peak electricity demand during the summer period. Numerous studies have been performed to investigate the impact of urban warming on the energy demand and consumption in cities. It is found that the average increase of the peak electricity varies between 0.45% to 4.6% per degree of temperature rise (Santamouris et al., 2015). Moreover, the increase of the hourly, daily or monthly electricity consumption ranges between 0.5% to 8.5 % per degree of temperature rise (Santamouris et al., 2015). In Bangkok, the monthly electricity consumption rise by up to 7.49% if the average ambient temperature increase by 1°C (Wangpattarapong & Maneewan, 2008). Meanwhile in Singapore, a 1°C rise in average temperature would raise the electricity consumption between 0.5% and 2.75% (Doshi et al., 2013).

The studies on the energy impact of urban warming were commonly performed by using two methods: the energy assessment of typical buildings and/or the energy assessment based on the total building stock. The former method is the most frequent method used in the energy studies related to urban warming. In this method, a reference or more typical buildings are selected and their energy loads are investigated. In fact, a single reference building may not represent the whole building stock in a city. Therefore, several studies have been conducted to investigate the energy impact of urban warming of the total building stock in a city (Hirano & Fujita, 2012; Li et al., 2014; Santamouris et al., 2001). In Tokyo, Hirano & Fujita (2012) found that the effects of the UHI decrease the total energy consumption, particularly due to a larger energy saving in space-heating and water-heating in winter than the increase in cooling energy consumption in summer. Nevertheless, in case of cities in the tropics, it is quite possible that the UHIs might increase the urban energy consumption, especially for cooling.

2.5.2 Impacts on indoor and outdoor thermal comfort

The increased urban temperatures increase discomfort conditions and have serious impact on the physiological conditions of human beings both indoor and outdoor. Several studies have attempted to evaluate the specific impact of urban warming on outdoor thermal comfort and concluded that the outdoor thermal discomfort conditions may increase in both duration and frequency in the near future (Santamouris, 2015b).

Changes in outdoor temperature have impact on the indoor environment. Buildings located in the urban areas will suffer more than the rural counterparts due to the UHI effect. The implications of urban warming on buildings involve the impact on indoor thermal comfort and air quality through the risk of summertime overheating, changes in the need for space heating, the occurrence of the need for comfort cooling and the performance of the mechanical air conditioning systems (Aries & Bluysen, 2009).

2.5.3 Impact on health

There is a very strong relationship between ambient temperature and mortality. Existing studies show that the heat related mortality increases rapidly for temperatures above 22-30 °C. However, the threshold rapidly changes as a function of the climate of each zone, other specific local parameters, age of the people and the physiological characteristics of the population (Conti et al., 2005; Vandentorren & Empereur-Bissonnet, 2005). Excess mortality reported in several Asian cities showed that above 29 C the additional mortality increase range between 4.1 and 7.5% per degree of temperature rise (Chan et al., 2012; Goggins et al., 2012). Moreover, the increased urban temperature may affect human vulnerability to new and unfamiliar diseases. For instance, cities with high land surface temperature, low humidity, and poor vegetation are considered to favour the transmission of the mosquito-borne dengue fever (Araujo et al., 2015; Xu et al., 2016).

The implication of urban warming is also affecting the indoor health risk in terms of occupational heat stress (Spengler, 2012). The warmer atmosphere with increased outdoor air pollution, dust, excessive rainfall, droughts, floods, and other impacts of urban warming can penetrate indoors and would influence the occupant health.

2.6 Countermeasures to UHI

To counter the negative impacts of UHI, mitigation and adaptation technologies are proposed. In general, four major clusters of countermeasures are as follows (Santamouris & Kolokotsa, 2016):

1. Mitigation technologies aiming to decrease absorption of the solar radiation in the urban environment. This is mainly achieved through the application of high reflective and thermal emissivity materials, which is known as cool materials.
2. Techniques aiming to improve the evapotranspiration processes in the urban environment. This may be achieved by the intensive of urban greenery, and also through the use of water-retentive pavements and sprayed water mist.
3. Techniques aiming to dissipate the excess heat into a sink of much lower temperature like the ground and/or by enhancing urban ventilation.
4. Techniques aiming to decrease the release of anthropogenic heat releases in the urban atmosphere. This may be achieved through introduction of sustainable transportation system and low-carbon lifestyle in the city.

Furthermore, Moriyama & Tanaka (2012) suggested to consider the scale of the horizontal space over a city, i.e. either a regional, district, or building scales when designing the countermeasures to the UHIs. Table 2.1 outlines the existing UHI countermeasure techniques in different clusters and scales.

Table 2.1 Summary of the existing UHI countermeasures.

| Scales | Measures | | | |
|--------------------------|--|---|--|--|
| | Highly reflective materials (cool materials) | Improvement of evapotranspiration processes | Dissipating excess heat through heat sink and urban ventilation | Reduction of anthropogenic heat releases |
| Regional Scale (1:25000) | <ul style="list-style-type: none"> • Use cool materials for roads, pavements, etc. • Use of light coloured paint. | <ul style="list-style-type: none"> • Increase the vegetative surfaces (e.g. parks, roof garden, green wall). • Well distributed green spaces in the city. | <ul style="list-style-type: none"> • Utilizing sea breeze for cooling. • Maximation street orientation as the wind path. • Utilizing river as the wind path and urban heat sink. | <ul style="list-style-type: none"> • Energy saving guideline. • Use public transportation. • District heating and cooling system using renewable energy. |
| District scale (1:2500) | <ul style="list-style-type: none"> • Use of cool materials for pavements in the public spaces. | <ul style="list-style-type: none"> • Create shade by planting trees and shrubs or erecting pilotis, canopies, etc. • Use water-retentive or permeable materials for paving. | <ul style="list-style-type: none"> • Use void deck to improve the air circulation in pedestrian level. • Use water as a large-scale urban heat sink (e.g. ponds with or without fountains). | <ul style="list-style-type: none"> • Improve the heat release method from buildings and cars and their location and place. |
| Building scale (1:250) | <ul style="list-style-type: none"> • Reduce the heat input into the building by using highly reflective roofing materials. • Use of cool materials for facades, roofs, pavements in buildings. | <ul style="list-style-type: none"> • Minimize the area of pavement in the vicinity. • Greenify the rooftops and the exterior walls as much as possible. | <ul style="list-style-type: none"> • Create an open and airy space by planting turf, grass and shrub or by constructing walkways. • Design the building by considering the prevailing winds. | <ul style="list-style-type: none"> • Release the heat from the high-rise portion of the building. • Minimize any rise in atmospheric temperature by reducing the exhaust heat temperature. |

Sources: Moriyama & Tanaka, (2012); Santamouris & Kolokotsa, (2016); Wong & Chen, (2008); Yamamoto, (2005).

2.6.1 Cooling effect of greenery on urban climate

Urban green spaces play important roles in cooling urban thermal environment and mitigating the UHIs. Urban green spaces, such as parks, urban forests, and sidewalk trees, have cooler temperature than their surrounding environment, and therefore have a cooling effect like an oasis (Taha et al., 1991) or cool island effect (Chang et al., 2007; Spronken-

Smith & Oke, 2010), attributed to the evaporative cooling, shading effects, and their thermal properties (Feyisa et al., 2014; Wong & Chen, 2008). A key process of the cooling effect is evapotranspiration, which describes the movement of water within plant and the subsequent loss of water from the plant and soil as a vapour into the atmosphere. Evapotranspiration increases the latent heat rather than the sensible heat, and in turn leads to lower ambient temperatures (Taha, 1997).

Most of the relevant studies focused on the cooling extents of vegetation such as green parks on microclimate in towns/cities were based on the results of field measurements (Chang & Li, 2014; Doick et al., 2014; Oliveira et al., 2011; Skoulika et al., 2014; Wong & Yu, 2005), remote sensing (Cao et al., 2010; Cheng, Wei et al., 2014), or numerical simulations (Honjo & Takakura, 1990; Papangelis et al., 2012). Nevertheless, there are relatively few studies that investigate the ameliorating effect of large-scale green spaces on the whole urban climate. A relevant study was conducted by Morris et al. (2016) in Putrajaya, Malaysia. Their study revealed that the established greenery and water bodies contributed to the reduction of average air temperature over the whole city by up to 0.14 and 0.39°C, respectively. As has been mentioned earlier, the study on the cooling effect of large-scale green spaces is still lacking, especially focusing on the planned green spaces in the growing cities, such as those proposed in the Hanoi Master Plan 2030.

The relationship between the cooling effect and the size of the green spaces have been investigated extensively. A study in Berlin compared 42 green spaces of different sizes with the resulting temperatures at their surroundings (von Stulpnagel et al., 1990). The study showed that the air temperature within a larger park is much lower than the smaller ones. Based on this study, Forman (2014) assumed that the large park provides noticeable cooling effect to the surrounding areas than the smaller parks of the same total area.

In contrast, Cheng et al., (2014) argued that there are nonlinear relationships between park sizes and their cooling effect. In their study on 39 parks in Shanghai, they found that although the maximum cooling distance increases with park size, the cooling distance of most parks were limited within 600 m and the cooling area of most of the parks were less than 150 ha. They also suggested that the small parks should be preferred when considering the cooling efficiency in the urban area with pricy space (Cheng et al., 2014). This finding is in line with the study conducted by Honjo & Takakura (1990). Based on the numerical models, they concluded that the effective cooling of surrounding areas can be achieved by arranging smaller green areas with sufficient intervals. This doesn't mean that large urban parks are not effective in terms of improving urban climate, but they are considered as a luxury, especially in the cities undergoing rapid urbanization (Wong & Chen, 2008).

Another important aspect influencing the cooling effect of the green spaces is the characteristic of the tree. The ability of tree to reduce air temperature is likely to due to number of factors, such as tree species, tree size and tree canopy characteristics, which affect the penetration of solar radiation (Bueno-bartholomei & Labaki, 2003; Georgi & Zafiriadis, 2006; Lin & Lin, 2010). Two studies compared the cooling effects between single tree and a cluster of trees. One study found that the tree cluster is cooler than single tree (Streiling & Matzarakis, 2003)

but the second study found no difference between either types (Souch & Souch, 1993). Related to the latter finding, Chang et al. (2007) argued that there is a possibility for trees to create warmer parks at night due to the buffer effect of the trees that hinders the heat exchange between the interior of a park and the cooler air mass above it. Replacing vegetation in a park (14x14 m) with trees of different kind with higher evapotranspiration rate, does not seem to have a big effect (less than 0.5K) (Dimoudi & Nikolopoulou, 2003). In contrast, on a larger scale, Luley & Bond (2001) reported that an up to 1 K reduction in air temperature is expected over Manhattan, New York City, when all urban grass are replaced by trees. Ng et al. (2012) suggested a proper greening in urban area should be investigated more methodologically to produce the greatest benefits to urban dwellers. Moreover, the variability of the results shows that the question still remain about the effect of planting different species, in different spatial arrangements (centralized or distributed), or in different location within a city (e.g. streets, gardens, parks).

2.6.2 Cooling effect of cool materials on urban climate

Cool materials are characterized with high albedo (i.e. lower absorption of the solar radiation) and high thermal emissivity. The cool materials limit the stored heat and minimize the release of sensible heat to the atmosphere. This technique can be applied in building's façade, roof, and pavement. The mitigation potentials of reflective roof have been extensively investigated. Further than their cooling effect, cool roof is capable to improve the indoor thermal comfort and reduce the energy consumption in buildings. The previous studies on cool roofs can be classified into two categories which are: the impacts of cool roof on the indoor environment and the impacts on the surrounding environment of the buildings. The former category mainly focused on the potential of temperature reduction and energy saving by the reflective materials. Meanwhile, the latter category discussed the environmental impacts of reflective roof on a larger area particularly when this technique was applied in a single building, group of buildings, as well as a large-scale deployment of reflective roof in urban areas. Tables 2.2 and 2.3 summarize the characteristics and cooling impacts from of the first and second categories, respectively.

Comparison between cool roof, roof insulation and other techniques on the thermal comfort and cooling load reduction.

The comparative analysis of thermal performance between the reflective roof and thermal insulation has been conducted by Brito Filho & Santos (2014). Their study shows that the performances of reflective roof, thermal insulation, and the combination of both techniques depends on the geographical location. Moreover, the roof with thermal insulation layer would increase the surface temperature of the roof and would potentially contribute to form UHI.

A similar study by Romeo & Zinzi (2013) found that the cooling load reduction after applying the cool roof was up to 54%. Table 2.4 summarise the studies that compare the performance of cool roof and other passive cooling techniques.

Table 2.2 Summary of the impact of cool roof on indoor environment of buildings.

| Source | Methodology | Albedo | Indoor temperature reduction | Cooling load reduction |
|------------------------|---|---------------------|---|---|
| (Romeo & Zinzi, 2013) | Experiment in a single-story school building using white double layer paint with gloss emulsion coating on the roof. | 0.859 | up to 3.5 °C of mean temperature (in a west facing room). | up to 54%. |
| (Synnefa et al., 2008) | Reflective materials in a single story building simulated using TRNSYS. | 0.2 to 0.6 and 0.85 | - | 13-29 kWh/m ² for albedo 0.6 up to 21-48 kWh/m ² for albedo 0.85 |
| (Synnefa et al., 2007) | TRNSYS simulation in a single story building using cool coatings in 27 cities with various climatic conditions. | 0.2 to 0.6 and 0.85 | up to 56% of discomfort hours if the threshold temperature is 27 °C. | up to 35% in the cooling dominated cities. |
| (Synnefa et al., 2012) | TRNSYS model validated with measurement in a double-story school building using white elastomeric waterproof coating. | 0.2 to 0.89 | up to 3°C in the zone adjacent to the roof (in uninsulated building). | up to 40% (in uninsulated building) |
| (Pisello et al., 2014) | Cool coating on clay tiles in 3-story residential building simulated using EnergyPlus. | 0.36 to 0.77 | up to 18% of operative Temperature more than 26 °C. | - |
| (Zinzi & Agnoli, 2012) | EnergyPlus simulation in a row house and a detached house. | 0.25 to 0.8 | up to 2°C | up to 30%. |

Nevertheless, most of the studies were conducted in a single story building. Moreover, if the study was conducted on the multi-story buildings, the thermal comfort and cooling load were investigated in the room underneath/adjacent to the roof. The residential building in Hanoi, especially the urban row houses, are 4-5 story building. The master bedroom, where the AC is installed, is mostly located at 2nd or 3rd floor. In other words, the target room where the AC is installed may be not affected directly by the cooling benefits of cool roof or roof insulation.

2.6.3 Influences of anthropogenic heat emission on urban climate

Urban areas are the sources of anthropogenic heat emission from the burning of fossil fuels for heating and cooling, from industrial processes, transportation of people and goods, etc. The increase in anthropogenic heat emission results in worsening atmospheric condition. Nevertheless, heat emission associated with energy consumption in cities has been largely ignored or overly simplified in many studies of urban climate (Sailor, 2011).

Table 2.3 Summary of the impact of cool roof on outdoor environment of buildings.

| Source | Methodology | Albedo | Surface temperature reduction | Ambient temperature reduction |
|------------------------------|---|-----------------------|---|--|
| (Romeo & Zinzi, 2013) | Experiment in a single-story school building using white double layer paint with gloss emulsion coating on the roof. | 0.859 | Reduction up to 20 °C of roof surface temperature from the original roof (grey concrete). | Change of outdoor air temperature is insignificant. |
| (Brito Filho & Santos, 2014) | Numerical simulation using mathematical model. | 0.3 to 0.9 | Reduction up to 17.74% of roof surface temperature. | |
| (Synnefa et al., 2012) | TRNSYS model validated with measurement in a double-story school building using white elastomeric waterproof coating. | 0.2 to 0.89 | | |
| (Synnefa et al., 2008) | MM5 v3.6.1 and MRF over Athens. | 0.18 to 0.63 and 0.85 | | Reduction of up to 1.5 and 2.2 °C for albedo 0.63 and 0.85, respectively. |
| (Y. Zhou & Shepherd, 2010) | WRF simulation over Atlanta, US. | 0.15 to 0.3 and 0.45 | | Negligible reduction when albedo is doubled. Reduction of up to 2.5 °C. |
| (Li et al., 2014) | WRF simulation over Baltimore/Washington | 0.3 to 0.7 | Reduction of up to 1 °C if the cool roof fraction is 30% at minimum. | Reduction of up to 0.5 °C if the cool roof fraction is 95%. |

The anthropogenic heat influence the urban climate in a complex manner. To understand and simplify the complexity, Oke (1988) suggested an equation called the urban (surface) energy balance (UEB) which is expressed in (2.1). Most of the estimations of Q_F use either the inventory based approach or energy balance closure approach (Quah & Roth, 2012). The former approach has been used frequently by most studies to estimate more realistic anthropogenic heat emission values (e.g. Grimmond, 1992; Klyzik, 1996; Pigeon et al., 2007; Sailor & Lu, 2004). Meanwhile, the latter approach was used by few studies because of the inherent problem of accumulating errors arising during the measurement of Q_H and Q_E and modelling of ΔQ_S and ΔQ_A (which cannot be directly measured) in the residual Q_F .

The magnitudes of anthropogenic heat emission depend on climate, population density and intensity of industrial and commercial activities (Sailor, 2011). According to Oke (1988) the mean annual magnitude of Q_F for large cities ranges from 20 to 160 W m⁻². For US cities, the values between 20 to 40 W m⁻² in summer and 70-210 W m⁻² in winter have been reported

Table 2.4 Summary of the cooling impact of cool roof, roof insulation, and other techniques

| Source | Methodology | Cool roof | Roof insulation | Other techniques |
|------------------------------|---|---|--------------------------------------|---|
| (Zinzi & Agnoli, 2012) | EnergyPus simulation in a two-story row house and a detached house. | Energy savings of up to 42% in non-insulated row house in cooling dominated city. | - | Green roof could reduce energy consumption up to 13% in non-insulated row house in cooling dominated city. |
| (Brito Filho & Santos, 2014) | Numerical simulation using mathematical model. | Reduction up to 18% of roof surface temperature (without thermal insulation). | Reduce the average heat flux by 47%. | Reduction up to 2.95% of roof surface temperature with combination of thermal insulation layer and white roof. |
| (Li et al., 2014) | TRNSYS simulation in a single story school building. | Cooling savings up to 54%. | Cooling savings up to 44%. | Cooling savings of: - Night ventilation: 22% - External shading: 39% - Cool roof and insulation: 61% - Night ventilation and cool roof: 61% - Cool roof and external shading: 78%. |

(Taha, 1997). In regards to the seasonal and diurnal variation, the estimations of Q_F from cities in northern hemisphere indicate a larger value in winter compared to those estimated for the summer (Allen et al., 2011; Quah & Roth, 2012) and a typical diurnal variation with a daytime peak slightly larger than that during night-time (Sailor & Lu, 2004). Q_F values were found to be larger in megacities with compact form, wealthy economies, and continental or temperate climates, while values are smallest in megacities with low population density or with low-middle income economies in (sub) tropical climates (Stewart & Kennedy, 2015).

The influence of anthropogenic heat emission on the urban climate has been explored in numerical simulations (Y. Chen, Jiang, Zhang, He, & Zhou, 2009; Ichinose, Shimodozono, & Hanaki, 1999; Kimura & Takahashi, 1991). Chen et al (2009) estimated the daily mean contribution ratios of anthropogenic heat emission to UHI were 54.5% and 43.6% in winter and summer, respectively, while it was up to 75% as reported by Zhang et al. (2016). In Tokyo, Kimura & Takahashi (1991) found that the contribution of anthropogenic heat is much larger at night, in spite of lower energy consumption as compared to the daytime. Numerical simulation in winter suggested that anthropogenic heating contributes 2-3C to the nocturnal UHI (Fan & Sailor, 2005).

Although many studies have focused on the impact of anthropogenic heat on the urban thermal environment of the current conditions, few works were carried out for the future possible changes in the anthropogenic heat emission derived from plausible scenarios of energy saving or low-carbon scenarios.

2.7 Summary

Many cities in Southeast Asia are likely to experience dramatic land use changes associated with the implementation of their large-scale master plans in the near future. However, very few studies on UHI was conducted in the developing countries to project the urban climates after the implementation of the proposed master plans. Moreover, studies have not been conducted in growing cities to project the effect of global warming on the urban climates under the future master plans via direct dynamical downscaling with an RCM.

The above review also shows that UHI mitigation measures have been widely studied and developed. Nevertheless, given the fact that the anthropogenic heat emissions have an important role in deteriorating or ameliorating the urban climates, few works were carried out to investigate the impacts of the future possible changes in the anthropogenic heat emission derived from plausible scenarios on mitigating the UHIs. Further studies on the countermeasures of UHI, particularly in the urban green spaces as well as adaptation technique in the building scale will be useful to help designing the UHI mitigation measures that produce the greatest benefits to urban dwellers.

In general, urban development in these developing countries is still at an early stage, and therefore opportunities exist for climate-sensitive urban design, for which it is necessary to better understand the climates of these cities. Nevertheless, it is also apparent that the relevant studies in growing cities of Asian region, particularly in the tropical cities are still lacking given the size of the problem and potential concern.

References

- Adachi, S. A., Kimura, F., Kusaka, H., Inoue, T., & Ueda, H. (2012). Comparison of the impact of global climate changes and urbanization on summertime future climate in the Tokyo metropolitan area. *Journal of Applied Meteorology and Climatology*, *51*(8), 1441–1454.
- Allen, L., Lindberg, F., & Grimmond, C. S. B. (2011). Global to city scale urban anthropogenic heat flux: Model and variability. *International Journal of Climatology*, *31*(13), 1990–2005.
- Amirtham, L. R. (2016). Urbanization and its impact on urban heat Island intensity in Chennai Metropolitan Area, India. *Indian Journal of Science and Technology*, *9*(5), 1–8.
- Araujo, R. V., Albertini, M. R., Costa-da-Silva, A. L., Suesdek, L., Franceschi, N. C. S., Bastos, N. M., ... Allegro, V. L. A. C. (2015). São Paulo urban heat islands have a higher incidence of dengue than other urban areas. *The Brazilian Journal of Infectious Diseases*, *19*(2), 146–155.
- Argüeso, D., Evans, J. P., Fita, L., & Bormann, K. J. (2014). Temperature response to future urbanization and climate change. *Climate Dynamics*, *42*(7–8), 2183–2199.
- Aries, M. B. C., & Bluysen, P. M. (2009). Climate change consequences for the indoor environment. *Heron*, *54*(1), 49–70.
- Arima, Y., Ooka, R., Kikumoto, H., & Yamanaka, T. (2015). Effect of climate change on building cooling loads in Tokyo in the summers of the 2030s using dynamically downscaled GCM data. *Energy and Buildings*, *114*, 123–129.
- Bhuvandas, N., Timbadiya, P. V., Patel, P. L., & Porey, P. D. (2014). Review of downscaling methods in climate change and their role in hydrological studies. *International Journal of Environmental, Chemical, Ecological, Geological and Geophysical Engineering*, *8*(10), 648–653.
- Boonjawat, J., Niitsu, K., & Kubo, S. (2000). Urban Heat Island : Thermal Pollution and Climate Change in Bangkok. *Journal of Health Science*, *9*(1).
- Brito Filho, J. P., & Santos, T. V. O. (2014). Thermal analysis of roofs with thermal insulation layer and reflective coatings in subtropical and equatorial climate regions in Brazil. *Energy and Buildings*, *84*, 466–474.
- Bueno-bartholomei, C. L., & Labaki, L. C. (2003). How much does the change of species of trees affect their solar radiation attenuation. *Proceeding of the Fifth International Conference on Urban Climate*, *5*, 267–270.
- Cao, X., Onishi, A., Chen, J., & Imura, H. (2010). Quantifying the cool island intensity of urban parks using ASTER and IKONOS data. *Landscape and Urban Planning*, *96*(4), 224–231.
- Chan, E. Y. Y., Goggins, W. B., Kim, J. J., & Griffiths, S. M. (2012). A study of intracity variation of temperature-related mortality and socioeconomic status among the Chinese population in Hong Kong. *Journal of Epidemiology and Community Health*, *66*(4), 322–327.

- Chang, C. R., & Li, M. H. (2014). Effects of urban parks on the local urban thermal environment. *Urban Forestry and Urban Greening*, 13(4), 672–681.
- Chang, C. R., Li, M. H., & Chang, S. D. (2007). A preliminary study on the local cool-island intensity of Taipei city parks. *Landscape and Urban Planning*, 80(4), 386–395.
- Chen, X. L., Zhao, H. M., Li, P. X., & Yin, Z. Y. (2006). Remote sensing image-based analysis of the relationship between urban heat island and land use/cover changes. *Remote Sensing of Environment*, 104(2), 133–146.
- Chen, Y. C., Chiu, H. W., Su, Y. F., Wu, Y. C., & Cheng, K. S. (2017). Does urbanization increase diurnal land surface temperature variation? Evidence and implications. *Landscape and Urban Planning*, 157, 247–258.
- Chen, Y., Jiang, W. M., Zhang, N., He, X. F., & Zhou, R. W. (2009). Numerical simulation of the anthropogenic heat effect on urban boundary layer structure. *Theoretical and Applied Climatology*, 97(1–2), 123–134.
- Cheng, F.-Y., & Byun, D. W. (2008). Application of high resolution land use and land cover data for atmospheric modeling in the Houston–Galveston metropolitan area, Part I: Meteorological simulation results. *Atmospheric Environment*, 42(33), 7795–7811.
- Cheng, X., Wei, B., Chen, G., Li, J., & Song, C. (2014). Influence of Park Size and Its Surrounding Urban Landscape Patterns on the Park Cooling Effect. *Journal of Urban Planning and Development*, 141(3), A4014002.
- Ching, J. K. S. (2013). A perspective on urban canopy layer modeling for weather, climate and air quality applications. *Urban Climate*, 3, 13–39.
- Chng, L. K., Abdullah, A. M., Sulaiman, W. N. A., & Ramli, M. F. (2010). The effects of improved land use on the meteorological modeling in Klang Valley region Malaysia. *EnvironmentAsia*, 3(Special Issue), 117–123.
- Chow, W. T. L., & Roth, M. (2006). Temporal Dynamics of the Urban Heat Island of Singapore. *International Journal of Climatology*, 26, 2243–2260.
- Conry, P., Sharma, A., Potosnak, M. J., Leo, L. S., Bensman, E., Hellmann, J. J., & Fernando, H. J. S. (2015). Chicago's heat island and climate change: Bridging the scales via dynamical downscaling. *Journal of Applied Meteorology and Climatology*, 54(7), 1430–1448.
- Conti, S., Meli, P., Minelli, G., Solimini, R., Toccaceli, V., Vichi, M., ... Perini, L. (2005). Epidemiologic study of mortality during the Summer 2003 heat wave in Italy. *Environmental Research*, 98(3), 390–399.
- Coutts, A. M., Beringer, J., & Tapper, N. J. (2008). Investigating the climatic impact of urban planning strategies through the use of regional climate modelling: a case study for Melbourne, Australia. *International Journal of Climatology*, 28(March 2008), 1943–1957.
- Cui, L., & Shi, J. (2012). Urbanization and its environmental effects in Shanghai, China. *Urban*

Climate, 2, 1–15.

- Dimoudi, A., & Nikolopoulou, M. (2003). Vegetation in the urban environment: Microclimatic analysis and benefits. *Energy and Buildings*, 35(1), 69–76.
- Doan, Q.-V., & Kusaka, H. (2015). Numerical study on regional climate change due to the rapid urbanization of greater Ho Chi Minh City's metropolitan area over the past 20 years. *International Journal of Climatology*, 3650(December 2015), n/a-n/a.
- Doan, Q. Van, Kusaka, H., & Ho, Q. B. (2016). Impact of future urbanization on temperature and thermal comfort index in a developing tropical city: Ho Chi Minh City. *Urban Climate*, 17.
- Doick, K. J., Peace, A., & Hutchings, T. R. (2014). The role of one large greenspace in mitigating London's nocturnal urban heat island. *Science of the Total Environment*, 493, 662–671.
- Doshi, T. K., Rohatgi, A., Zahur, N. Bin, & Hung, Y. K. (2013). Impact of climate change on electricity demand of singapore. In *Proceedings of the Singapore Economic Review Conference 2013* (pp. 1–15). Singapore.
- Emmanuel, R., & Johansson, E. (2006). Influence of urban morphology and sea breeze on hot humid microclimate: The case of Colombo, Sri Lanka. *Climate Research*, 30(3), 189–200.
- Fan, H., & Sailor, D. J. (2005). Modeling the impacts of anthropogenic heating on the urban climate of Philadelphia: A comparison of implementations in two PBL schemes. *Atmospheric Environment*, 39(1), 73–84.
- Feng, H., Zhao, X., Chen, F., & Wu, L. (2014). Using land use change trajectories to quantify the effects of urbanization on urban heat island. *Advances in Space Research*, 53(3), 463–473.
- Fernando, H. J. S. (2010). Fluid dynamics of urban atmospheres in complex terrain. *Annual Review of Fluid Mechanics*, 42, 365–389.
- Feyisa, G. L., Dons, K., & Meilby, H. (2014). Efficiency of parks in mitigating urban heat island effect: An example from Addis Ababa. *Landscape and Urban Planning*, 123, 87–95.
- Figuerola, P. I., & Mazzeo, N. A. (1998). Urban-rural temperature differences in Buenos Aires. *International Journal of Climatology*, 18(15), 1709–1723.
- Forman, R. T. T. (2014). *Urban ecology : science of cities*. Cambridge, United Kingdom: Cambridge University Press.
- Gartland, L. (2008). *Heat Islands: Understanding and Mitigating Heat in Urban Areas*. London: Earthscan.
- Georgi, N. J., & Zafiriadis, K. (2006). The impact of park trees on microclimate in urban areas. *Urban Ecosystems*, 9(3), 195–209.
- Giridharan, R., Lau, S. S. Y., & Ganesan, S. (2005). Nocturnal heat island effect in urban residential developments of Hong Kong. *Energy and Buildings*, 37(9), 964–971.

- Goggins, W. B., Chan, E. Y. Y., Ng, E., Ren, C., & Chen, L. (2012). Effect modification of the association between short-term meteorological factors and mortality by urban heat islands in Hong Kong. *PLoS ONE*, 7(6), 9–14.
- Goldreich, Y. (1992). Urban climate studies in Johannesburg, A sub-tropical city located on a ridge-A review. *Atmospheric Environment*, 26B(3), 407–420.
- Grimmond, C. S. B. (1992). The Suburban Energy-Balance: Methodological Considerations and Results for a Mid-latitude West Coast City Under Winter and Spring Conditions. *International Journal of Climatology*, 12, 481–497.
- Gsella, A., De Meij, A., Kerschbaumer, A., Reimer, E., Thunis, P., & Cuvelier, C. (2014). Evaluation of MM5, WRF and TRAMPER meteorology over the complex terrain of the Po Valley, Italy. *Atmospheric Environment*, 89, 797–806.
- Guo, G., Wu, Z., Xiao, R., Chen, Y., Liu, X., & Zhang, X. (2015). Impacts of urban biophysical composition on land surface temperature in urban heat island clusters. *Landscape and Urban Planning*, 135, 1–10.
- Hartmann, D. J., Klein Tank, A. M. G., Rusticucci, M., Alexander, L. V, Brönnimann, S., Charabi, Y. A.-R., ... Zhai, P. (2013). Observations: Atmosphere and Surface. In *Climate Change 2013: The Physical Science Basis. Contribution of Working Group I to the Fifth Assessment Report of the Intergovernmental Panel on Climate Change* (pp. 159–254). Cambridge, United Kingdom and New York, USA.
- He, J. F., Liu, J. Y., Zhuang, D. F., Zhang, W., & Liu, M. L. (2007). Assessing the effect of land use/land cover change on the change of urban heat island intensity. *Theoretical and Applied Climatology*, 90(3–4), 217–226.
- Hirano, Y., & Fujita, T. (2012). Evaluation of the impact of the urban heat island on residential and commercial energy consumption in Tokyo. *Energy*, 37(1), 371–383.
- Honjo, T., & Takakura, T. (1990). Simulation of Thermal Effects of Urban ree Areas on Their Surrounding Areas. *Energy and Buildings*, 16, 443–446.
- Hu, Y., & Jia, G. (2010). Influence of land use change on urban heat island derived from multi-sensor data. *International Journal of Climatology*, 30(9), 1382–1395.
- Ichinose, T., Shimodozono, K., & Hanaki, K. (1999). Impact of anthropogenic heat on urban climate in Tokyo. *Atmospheric Environment*, 33(24–25), 3897–3909.
- Iizuka, S., Ito, T., & Miyata, M. (2015). Impacts of a future city master plan on thermal and wind environments in Vinh city, Vietnam. In *ICUC9 - 9th International Conference on Urban Climate jointly with 12th Symposium on the Urban Environment* (pp. 1–4).
- Iizuka, S., Xuan, Y., & Kondo, Y. (2015). Impacts of disaster mitigation/prevention urban structure models on future urban thermal environment. *Sustainable Cities and Society*, 19, 414–420.
- Kardinal Jusuf, S., Wong, N. H., Hagen, E., Anggoro, R., & Hong, Y. (2007). The influence of land

- use on the urban heat island in Singapore. *Habitat International*, 31(2), 232–242.
- Kikumoto, H., Ooka, R., & Arima, Y. (2015). A study of urban thermal environment in Tokyo in summer of the 2030s under influence of global warming. *Energy and Buildings*, 114, 54–61.
- Kim, Y. H., & Baik, J. J. (2004). Daily maximum urban heat island intensity in large cities of Korea. *Theoretical and Applied Climatology*, 79(3–4), 151–164.
- Kimura, F., & Kitoh, A. (2007). *Downscaling by Pseudo Global Warming Method. The Final Report of ICCAP*. Kyoto, Japan.
- Kimura, F., & Takahashi, S. (1991). The effects of land-use and anthropogenic heating on the surface temperature in the Tokyo Metropolitan area: A numerical experiment. *Atmospheric Environment. Part B. Urban Atmosphere*, 25(2), 155–164.
- Klysiak, K. (1996). Spatial and seasonal distribution of anthropogenic heat emissions in Lodz, Poland. *Atmospheric Environment*, 30(20), 3397–3404.
- Kubota, T., & Ossen, D. R. (2009). Spatial characteristics of Urban Heat Island in Johor Bahru City, Malaysia. *Proceedings of The 3rd Symposium of South East Asian Technical University Consortium (SEATUC)*, 39–44.
- Kusaka, H., Crook, A., Dudhia, J., & Wada, K. (2005). Comparison of the WRF and MM5 models for simulation of heavy rainfall along the Baiu Front. *SOLA*, 1, 197–200.
- Kusaka, H., Hara, M., & Takane, Y. (2012). Urban Climate Projection by the WRF Model at 3-km Horizontal Grid Increment: Dynamical Downscaling and Predicting Heat Stress in the 2070's August for Tokyo, Osaka, and Nagoya Metropolises. *Journal of the Met. Soc. of Japan*, 90B.
- Kusaka, H., Kimura, F., Hirakuchi, H., & Mizutori, M. (2000). The Effects of Land-Use Alteration on the Sea Breeze and Daytime Heat Island in the Tokyo Metropolitan Area. *Journal of the Meteorological Society of Japan*, 78(4), 405–420.
- Lee, H. S., Yamashita, T., Hsu, J. R. C., & Ding, F. (2013). Integrated modeling of the dynamic meteorological and sea surface conditions during the passage of Typhoon Morakot. *Dynamics of Atmospheres and Oceans*, 59, 1–23.
- Li, C., Zhou, J., Cao, Y., Zhong, J., Liu, Y., Kang, C., & Tan, Y. (2014). Interaction between urban microclimate and electric air-conditioning energy consumption during high temperature season. *Applied Energy*, 117, 149–156.
- Li, D., Bou-Zeid, E., & Oppenheimer, M. (2014). The effectiveness of cool and green roofs as urban heat island mitigation strategies. *Environmental Research Letters*, 9(5), 55002.
- Li, Y. Y., Zhang, H., & Kainz, W. (2012). Monitoring patterns of urban heat islands of the fast-growing Shanghai metropolis, China: Using time-series of Landsat TM/ETM+ data. *International Journal of Applied Earth Observation and Geoinformation*, 19(1), 127–138.
- Lin, B. S., & Lin, Y. J. (2010). Cooling effect of shade trees with different characteristics in a

- subtropical urban park. *HortScience*, 45(1), 83–86.
- Longxun, C., Wenqin, Z., Xiuji, Z., & Zijiang, Z. (2003). Characteristics of the Heat Island Effect in Shanghai and Its Possible Mechanism. *Advances in Atmospheric Sciences*, 20(6), 991–1001.
- Lucena, A. J. de, Rotunno Filho, O. C., Fran??a, J. R. de A., Peres, L. de F., & Xavier, L. N. R. (2013). Urban climate and clues of heat island events in the metropolitan area of Rio de Janeiro. *Theoretical and Applied Climatology*, 111(3–4), 497–511.
- Luley, C. J., & Bond, J. (2001). A Report to North East State Foresters Association A Plan to Integrate Management of Urban Trees into Air Quality Planning. *Davey Resource Group*.
- Marshall Shepherd, J., Carter, M., Manyin, M., Messen, D., & Burian, S. (2010). The impact of urbanization on current and future coastal precipitation: A case study for houston. *Environment and Planning B: Planning and Design*, 37(2), 284–304.
- Meng, W., Zhang, Y., Li, J., Lin, W., Dai, G., & Li, H. (2011). Application of WRF / UCM in the Simulation of a Heat Wave Event and Urban Heat Island around Guangzhou. *Journal of Tropical Meteorology*, 17(3), 257–267.
- Miao, S., Chen, F., LeMone, M. A., Tewari, M., Li, Q., & Wang, Y. (2009). An observational and modeling study of characteristics of urban heat island and boundary layer structures in Beijing. *Journal of Applied Meteorology and Climatology*, 48(3), 484–501.
- Mirzaei, P. a., & Haghighat, F. (2010). Approaches to study Urban Heat Island – Abilities and limitations. *Building and Environment*, 45(10), 2192–2201.
- Moriyama, M., & Tanaka, T. (2012). The Mitigation of UHI Intensity through an Improved Land-Use Plan in the Urban Central Area : Application to Osaka City , Japan. *Journal of Heat Island Institute International*, 7, 65–71.
- Morris, K. I., Chan, A., Ooi, M. C., Oozeer, M. Y., Abakr, Y. A., & Morris, K. J. K. (2016). Effect of vegetation and waterbody on the garden city concept: An evaluation study using a newly developed city, Putrajaya, Malaysia. *Computers, Environment and Urban Systems*, 58, 39–51.
- Morris, K. I., Chan, A., Salleh, S. A., Ooi, M. C. G., Oozeer, M. Y., & Abakr, Y. A. (2016). Numerical study on the urbanisation of Putrajaya and its interaction with the local climate, over a decade. *Urban Climate*, 16, 1–24.
- Ng, E., Chen, L., Wang, Y., & Yuan, C. (2012). A study on the cooling effects of greening in a high-density city: An experience from Hong Kong. *Building and Environment*, 47(1), 256–271.
- Nguyen, A.-T., & Reiter, S. (2014). A climate analysis tool for passive heating and cooling strategies in hot humid climate based on Typical Meteorological Year data sets. *Energy and Buildings*, 68.
- Nieuwolt, S. (1966). The urban microclimate of Singapore. *Journal of Tropical Geography*, 22.
- Nonomura, A., Kitahara, M., & Masuda, T. (2009). Impact of land use and land cover changes on the ambient temperature in a middle scale city, Takamatsu, in Southwest Japan. *Journal of*

- Environmental Management*, 90(11), 3297–3304.
- Oke, T. R. (1988). The urban energy balance. *Progress in Physical Geography*, 12(4), 471–508.
- Oliveira, S., Andrade, H., & Vaz, T. (2011). The cooling effect of green spaces as a contribution to the mitigation of urban heat : A case study in Lisbon. *Building and Environment*, 46(11), 2186–2194.
- Papangelis, G., Tombrou, M., Dandou, A., & Kontos, T. (2012). An urban “green planning” approach utilizing the Weather Research and Forecasting (WRF) modeling system. A case study of Athens, Greece. *Landscape and Urban Planning*, 105(1–2), 174–183.
- Peel, M. C., Finlayson, B. L., & McMahon, T. A. (2007). Updated world map of the Köppen-Geiger climate classification. *Hydrology and Earth System Sciences*, 11(3), 1633–1644.
- Pigeon, G., Legain, D., Durand, P., & Masson, V. (2007). Anthropogenic heat release in an old European agglomeration (Toulouse, France). *International Journal of Climatology*, 27(September 2007), 1969–1981.
- Pisello, A. L., Cotana, F., & Brinchi, L. (2014). On a cool coating for roof clay tiles: Development of the prototype and thermal-energy assessment. *Energy Procedia*, 45, 453–462.
- Polydoros, A., & Cartalis, C. (2015). Assessing the impact of urban expansion to the state of thermal environment of peri-urban areas using indices. *Urban Climate*, 14, 166–175.
- Qaid, A., Bin Lamit, H., Ossen, D. R., & Raja Shahminan, R. N. (2016). Urban heat island and thermal comfort conditions at micro-climate scale in a tropical planned city. *Energy and Buildings*, 133, 577–595.
- Quah, A. K. L., & Roth, M. (2012). Diurnal and weekly variation of anthropogenic heat emissions in a tropical city, Singapore. *Atmospheric Environment*, 46, 92–103.
- Radhi, H., Fikry, F., & Sharples, S. (2013). Impacts of urbanisation on the thermal behaviour of new built up environments: A scoping study of the urban heat island in Bahrain. *Landscape and Urban Planning*, 113, 47–61.
- Romeo, C., & Zinzi, M. (2013). Impact of a cool roof application on the energy and comfort performance in an existing non-residential building. A Sicilian case study. *Energy and Buildings*, 67, 647–657.
- Roth, M. (2007). Review of urban climate research in (sub) tropical regions. *International Journal of Climatology*, 1873(August), 1859–1873.
- Roth, M. (2013). Urban Heat Islands. In *Handbook of Environmental Fluid Dynamics, Volume Two* (pp. 143–159). CRC Press.
- Sailor, D. J. (2011). A review of methods for estimating anthropogenic heat and moisture emissions in the urban environment. *International Journal of Climatology*, 31(2), 189–199.
- Sailor, D. J., & Lu, L. (2004). A top-down methodology for developing diurnal and seasonal

- anthropogenic heating profiles for urban areas. *Atmospheric Environment*, 38(17), 2737–2748.
- Sani, S. (1972). Some aspects of urban micro-climate in Kuala Lumpur West Malaysia. *Akademika*, 1.
- Sani, S. (1990). Urban climatology in Malaysia : An overview. *Energy and Buildings*, 15–16, 105–117.
- Santamouris, M. (2015a). Analyzing the heat island magnitude and characteristics in one hundred Asian and Australian cities and regions. *Science of the Total Environment*, 512–513, 582–598.
- Santamouris, M. (2015b). Regulating the damaged thermostat of the cities—Status, impacts and mitigation challenges. *Energy and Buildings*, 91, 43–56.
- Santamouris, M., Cartalis, C., Synnefa, A., & Kolokotsa, D. (2015). On the impact of urban heat island and global warming on the power demand and electricity consumption of buildings—A review. *Energy and Buildings*, 98, 119–124.
- Santamouris, M., & Kolokotsa, D. (2016). *Urban Climate Mitigation Techniques*. Routledge.
- Santamouris, M., Papanikolaou, N., Livada, I., Koronakis, I., Georgakis, C., Argiriou, A., & Assimakopoulos, D. . (2001). On the impact of urban climate on the energy consumption of buildings. *Solar Energy*, 70(3), 201–216.
- Shin, D. W., & Baigorria, G. A. (2012). Potential influence of land development patterns on regional climate: A summer case study in the Central Florida. *Natural Hazards*, 62(3), 877–885.
- Skamarock, W. C., Klemp, J. B., Dudhi, J., Gill, D. O., Barker, D. M., Duda, M. G., ... Powers, J. G. (2008). A Description of the Advanced Research WRF Version 3. *Technical Report*, (June), 113.
- Skoulika, F., Santamouris, M., Kolokotsa, D., & Boemi, N. (2014). On the thermal characteristics and the mitigation potential of a medium size urban park in Athens, Greece. *Landscape and Urban Planning*, 123, 73–86.
- Souch, C. A., & Souch, C. (1993). The effect of trees on summertime below canopy urban climates: a case study Bloomington, Indiana. *Journal of Arboriculture*, 19(5), 303–312.
- Spengler, J. D. (2012). Climate change, indoor environments, and health. *Indoor Air*, 22(2), 89–95.
- Spronken-Smith, R. A., & Oke, T. R. (2010). The thermal regime of urban parks in two cities with different summer climates. *International Journal of Remote Sensing*, 19(11), 2085–2104.
- Stewart, I., & Kennedy, C. (2015). Estimating anthropogenic heat release from megacities. In *Proceedings of 9th International Conference on Urban Climate* (pp. 1–6). Toulouse.
- Streiling, S., & Matzarakis, A. (2003). Influence of single and small clusters of trees on the bioclimatic of a city: A case study. *Journal of Arboriculture*, 29(6), 309–316.
- Syneffa, A., Dandou, A., Santamouris, M., Tombrou, M., & Soulakellis, N. (2008). On the use of cool materials as a heat island mitigation strategy. *Journal of Applied Meteorology and Climatology*,

- 47(11), 2846–2856.
- Synnefa, A., Saliari, M., & Santamouris, M. (2012). Experimental and numerical assessment of the impact of increased roof reflectance on a school building in Athens. *Energy and Buildings*, 55.
- Synnefa, A., Santamouris, M., & Akbari, H. (2007). Estimating the effect of using cool coatings on energy loads and thermal comfort in residential buildings in various climatic conditions. *Energy and Buildings*, 39(11), 1167–1174.
- Synnefa, A., Santamouris, M., Kolokotsa, D., & Dimitriou, V. (2008). Passive cooling of the built environment – use of innovative reflective materials to fight heat islands and decrease cooling needs. *International Journal of Low Carbon Technologies*, 3(2), 71–82.
- Taha, H. (1997). Urban climates and heat islands: albedo, evapotranspiration, and anthropogenic heat. *Energy and Buildings*, 25(2), 99–103.
- Taha, H., Akbari, H., & Rosenfeld, A. (1991). Heat island and oasis effects of vegetative canopies: Micro-meteorological field-measurements. *Theoretical and Applied Climatology*, 44(2), 123–138.
- Tewari, M., Chen, F., Kusaka, H., & Miao, S. (2007). *Coupled WRF/Unified Noah/urban-canopy modeling system. NCAR WRF Documentation.*
- Tokairin, T., Sofyan, A., & Kitada, T. (2010). Effect of land use changes on local meteorological conditions in Jakarta, Indonesia: Toward the evaluation of the thermal environment of megacities in Asia. *International Journal of Climatology*, 30(13), 1931–1941.
- UNFCC. (2004). *Compendium on methods and tools to evaluate impacts of, and vulnerability and adaptation to, climate change. Strategies.* <https://doi.org/10.1029/2008GB003339.2>
- Van Nguyen, O., Kawamura, K., Trong, D. P., Gong, Z., & Suwandana, E. (2015). Temporal change and its spatial variety on land surface temperature and land use changes in the Red River Delta, Vietnam, using MODIS time-series imagery. *Environmental Monitoring and Assessment*, 187(7).
- Vandentorren, S., & Empeur-Bissonnet, P. (2005). Health impact of the 2003 Heat-Wave in France. *Extreme Weather Events and Public Health Responses*, (August 2003), 81–87.
- Velazquez-Lozada, A., Gonzalez, J. E., & Winter, A. (2006). Urban heat island effect analysis for San Juan, Puerto Rico. *Atmospheric Environment*, 40(9), 1731–1741.
- von Stulpnagel, A., Horbert, M., & Sukopp, H. (1990). The importance of vegetation for the urban climate. In H. Sukopp, S. Hejny, & I. Kowarik (Eds.), *Urban ecology* (pp. 175–193). The Hague, Netherlands: SPB Academic Publishing.
- Wakazuki, Y., & Rasmussen, R. (2015). Incremental dynamical downscaling for probabilistic analysis based on multiple GCM projections. *Geophysical Research Letters*, 42(24), 10847–10855.
- Wang, X., Chen, F., Wu, Z., Zhang, M., Tewari, M., Guenther, A., & Wiedinmyer, C. (2009). Impacts of weather conditions modified by urban expansion on surface ozone: Comparison between the Pearl River Delta and Yangtze River Delta regions. *Advances in Atmospheric Sciences*, 26(5).

- Wang, Y. Q., Leung, L. R., McGregor, J. L., Lee, D.-K. K., Wang, W.-C. C., Ding, Y. H., & Kimura, F. (2004). Regional climate modeling: Progress, challenges, and prospects. *Journal of the Meteorological Society of Japan*, 82(6), 1599–1628.
- Wangpattarapong, K., & Maneewan, S. (2008). The impacts of climatic and economic factors on residential electricity consumption of Bangkok Metropolis, 40, 1419–1425.
- Wong, N. H., & Chen, Y. (2008). *Tropical Urban Heat Islands: Climate, Buildings and Greenery*. New York, USA: Taylor & Francis.
- Wong, N. H., & Yu, C. (2005). Study of green areas and urban heat island in a tropical city. *Habitat International*, 29, 547–558.
- Xiaoyan Jiang, Wiedinmyer, C., Fei Chen, Zong-Liang Yang, & Lo, J. c.-F. (2008). Predicted impacts of climate and land use change on surface ozone in the Houston, Texas, area. *Journal of Geophysical Research - Part D - Atmospheres*, 113(D20), (16 pp.).
- Xu, L., Stige, L. C., Chan, K.-S., Zhou, J., Yang, J., Sang, S., ... Stenseth, N. C. (2016). Climate variation drives dengue dynamics. *Proceedings of the National Academy of Sciences of the United States of America*, 114(1), 113–118.
- Yamamoto, Y. (2005). Measures to Mitigate Urban Heat Islands. *Quarterly Review No.18*, 65–83.
- Yang, L., Niyogi, D., Tewari, M., Aliaga, D., Chen, F., Tian, F., & Ni, G. (2016). Contrasting impacts of urban forms on the future thermal environment : example of Beijing metropolitan area. *Environmental Research Letters*, 11, 1–10.
- Yoshikado, H. (1992). Numerical Study of the Daytime Urban Effect and Its Interaction with the Sea Breeze. *Journal of Applied Meteorology*.
- Zhang, H., Qi, Z., Ye, X., Cai, Y., Ma, W.-C., & Chen, M. (2013). Analysis of land use/land cover change, population shift, and their effects on spatiotemporal patterns of urban heat islands in metropolitan Shanghai, China. *Applied Geography*, 44, 121–133.
- Zhang, N., Wang, X., Chen, Y., Dai, W., & Wang, X. (2016). Numerical simulations on influence of urban land cover expansion and anthropogenic heat release on urban meteorological environment in Pearl River Delta. *Theoretical and Applied Climatology*, 126(3–4), 469–479.
- Zhou, D., Zhang, L., Hao, L., Sun, G., Liu, Y., & Zhu, C. (2016). Spatiotemporal trends of urban heat island effect along the urban development intensity gradient in China. *Science of the Total Environment*, 544(219), 617–626.
- Zhou, Y., & Shepherd, J. M. (2010). Atlanta’s urban heat island under extreme heat conditions and potential mitigation strategies. *Natural Hazards*, 52(3), 639–668.
- Zinzi, M., & Agnoli, S. (2012). Cool and green roofs. An energy and comfort comparison between passive cooling and mitigation urban heat island techniques for residential buildings in the Mediterranean region. *Energy and Buildings*, 55, 66–76.

3

Methodology

3.1 Overall research approach

This thesis mainly deals with modelling and simulation studies. The modelling study aims to develop a representation of an actual condition/process or a situation we are attempting to describe/explain while the simulation study aims to take the models, expressed as a computer program, and run them to obtain the results that can be compared.

As has been introduced, this thesis aims to investigate the impacts of the land use changes brought by the proposed master plan and the global warming effect on the urban climates. Further, this study also aims to investigate the thermal comfort and cooling load in residential buildings under the current and future land use as well as weather conditions. To deal with the scales of the study, firstly, a meso-scale numerical simulation was employed, mainly to assess the impact of land use changes and global warming effect on the urban climates. Then, the simulated weather data resulted from the urban climate simulations were used to assess the thermal comfort and cooling load by using a building simulation program. Fig. 3.1 shows the methodological framework of this thesis. As shown in Fig. 3.1, the simulated weather data from the current condition and future conditions projected for 2030s are used in the building simulation.

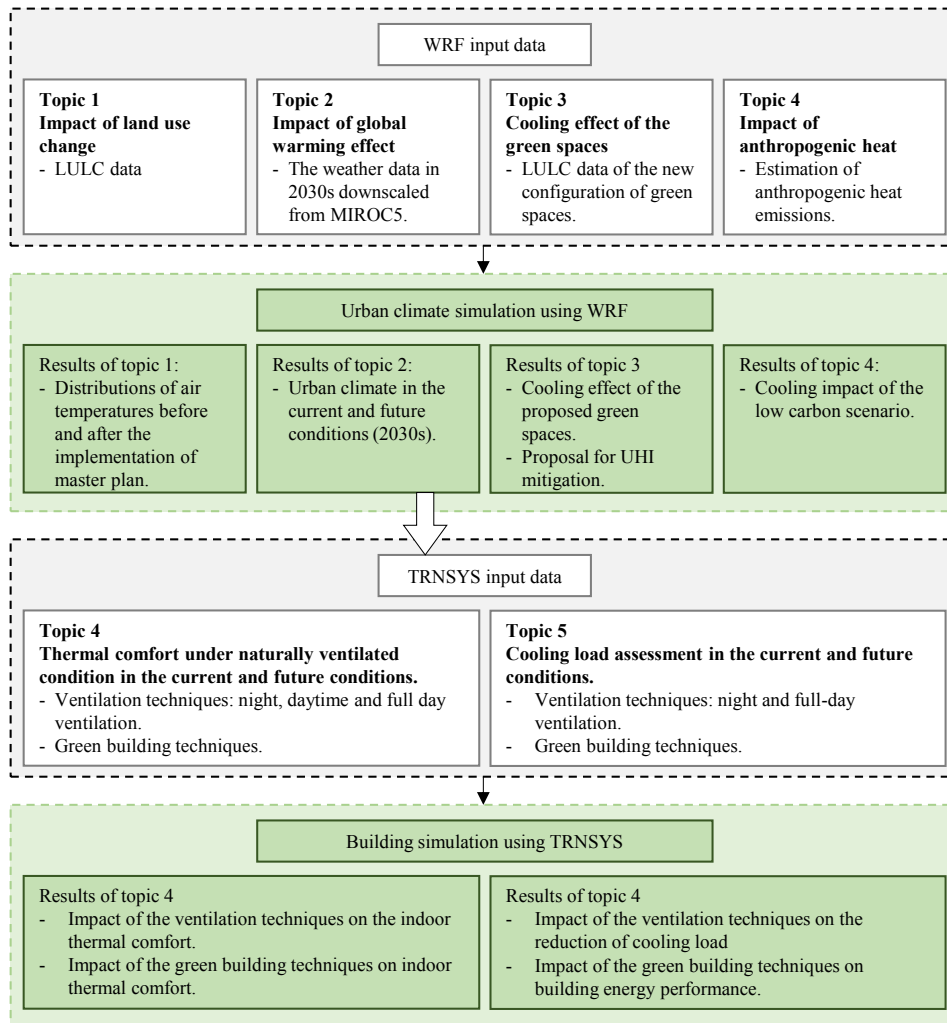


Fig. 3.1 Methodological framework.

3.2 Numerical simulation using WRF

3.2.1 Overview

Meteorological modelling and simulations were performed to obtain basic weather elements such as air temperature, humidity, surface winds and pressure using the Advanced Research WRF (ARW) model (Skamarock et al., 2008). The WRF is a three-dimensional non-hydrostatic meso-scale meteorological model developed at the National Center for Atmospheric Research (NCAR) based on the non-hydrostatic compressible form of the governing equations in spherical and sigma coordinates with physical processes, such as

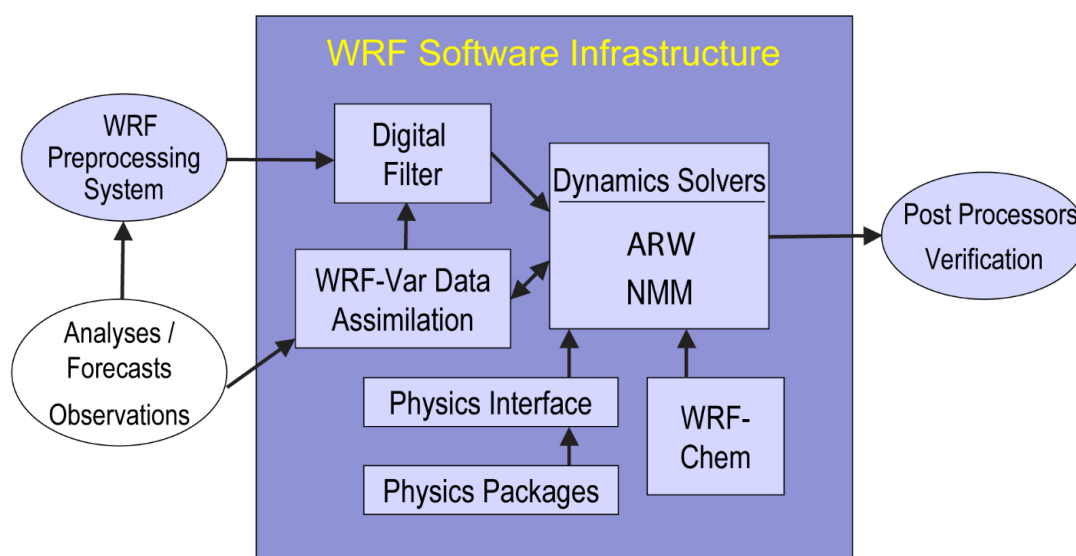


Fig. 3.2 WRF system components.

cumulus clouds, microphysics, planetary boundary layer (PBL) processes and atmospheric radiation processes, incorporated into a number of physics parameterisations.

The WRF is designed to be flexible, state-of-the-art atmospheric simulation system that is portable on available parallel computing platforms. This model has been widely used in a wide span of applications across scales ranging from large-eddy to global modelling (Ching, 2013). Such applications include real-time weather forecasts, regional climate modelling, air quality modelling, downscaling climate simulations, atmosphere-ocean interaction, data assimilation studies, parameterized-physics research, monitoring of urban climate, extreme weather and idealized simulations. The WRF Software Framework (WSF) (Fig. 3.2) provides the infrastructure that accommodates multiple dynamic solvers: the Advanced Research WRF (ARW) solver and NMM (Non-hydrostatic Mesoscale Model). For the present study, we used ARW solver.

A meso-scale model implies the spatial resolution to be in magnitude of a few kilometers, so a particular meso-scale zone is assumed as a homogeneous area and the surface properties are estimated with bulk values (e.g., albedo, emissivity, and roughness) (Mirzaei & Haghightat, 2010). This causes a limitation to observe detailed interactions between buildings and their environments. Increasing the domain and spatial resolution is not preferable due to the expensive computational cost. Regardless of the limitation, the meso-scale model is an appropriate tool to investigate a large-scale UHI variation of a city broadly. Furthermore, investigating the impacts of urban-scale policies to mitigate UHIs (e.g. urban greening) is mostly analysed using a meso-scale model (Mirzaei, 2015).

3.2.2 The governing equations

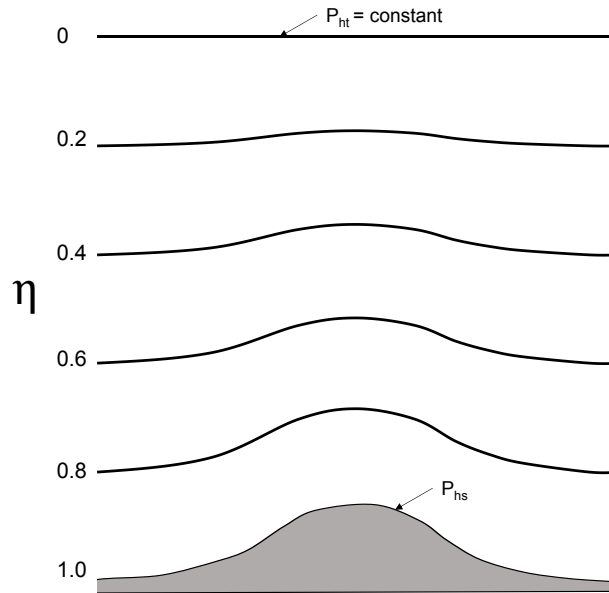


Fig. 3.3 ARW η coordinate.

The equations for numerical weather prediction models are based on the following physical laws: (1) Newton's second law of motion, (2) conservation of mass, and (3) the first law of thermodynamics. These laws are represented by the set of primitive equations that consist of the horizontal and vertical momentum equations, the continuity equation, and the thermodynamic energy equation.

Vertical coordinate and variables

The ARW dynamic solver integrates the compressible, non-hydrostatic Euler equation. The term non-hydrostatic means that the models use altitude or sigma altitude for their vertical coordinates, while the hydrostatic models use either pressure or sigma-pressure vertical coordinates which is not able to deal with complex topography. The non-hydrostatic equations are formulated using a terrain-following mass vertical coordinate, with vertical grid stretching is permitted. Top of model is a constant pressure surface. Therefore, unlike the hydrostatic models, this feature allows non-hydrostatic models to be used for complex terrain with the horizontal scales of the order of 100 m, resolving small-scale mesoscale circulations such as cumulus convection and sea-breeze circulations.

The vertical coordinate denote by η and defined as

$$\eta = (p_h - p_{ht})/\mu \quad \text{where } \mu = p_{hs} - p_{ht} \quad (3.1)$$

p_h is the hydrostatic component of the pressure, and p_{hs} and p_{ht} refer to values along the surface and top boundaries, respectively. The coordinate definition (3.1), proposed by Laprise (1992), is the traditional σ coordinate used in many hydrostatic atmospheric models. η varies from a value of 1 at the surface to 0 at the upper boundary of the model domain (Fig. 3.3). This vertical coordinate is also called a mass vertical coordinate. Since $\mu(x, y)$ represents the mass per unit area within the column in the model domain at (x, y) , the appropriate flux form variables are

$$V = \mu v = (U, V, W), \quad \Omega = \mu \eta', \quad \Theta = \mu \theta \quad (3.2)$$

where $V = (U, V, W)$ are the covariant velocities in the two horizontal and vertical directions, respectively, while $\omega = \eta'$ is the contravariant 'vertical' velocity. θ is the potential temperature. Also appearing in the governing equations of the ARW are the non-conserved variables $\varphi = gz$ (the geopotential), p (pressure), and $\alpha = 1/\rho$ (the inverse density).

Flux-form Euler equations

Using the variables defined above, the flux-form Euler equations can be written as:

for momentum

$$\partial_t U + (\nabla \cdot Vu) - \partial_x(p\varphi_\eta) + \partial_\eta(p\varphi_x) = F_U \quad (3.3)$$

$$\partial_t V + (\nabla \cdot Vv) - \partial_y(p\varphi_\eta) + \partial_\eta(p\varphi_y) = F_V \quad (3.4)$$

$$\partial_t W + (\nabla \cdot Vw) - g(\partial_\eta p - \mu) = F_W \quad (3.5)$$

for potential temperature

$$\partial_t \Theta + (\nabla \cdot V\theta) = F_\Theta \quad (3.6)$$

for continuity

$$\partial_t \mu + (\nabla \cdot V) = 0 \quad (3.7)$$

for geopotential height

$$\partial_t \varphi + \mu^{-1}[(V \cdot \nabla_\varphi) - gW] = 0 \quad (3.8)$$

along with the diagnostic relation for the inverse density

$$\partial_\eta \varphi = -\alpha \mu \quad (3.9)$$

and the equation of state

$$p = p_0(R_a \theta / p_0 \alpha)^{\gamma} \quad (3.10)$$

in the above equations, the subscripts x , y and η denote differentiation,

$$\nabla \cdot Va = \partial_x(Ua) + \partial_y(Va) + \partial_\eta(\Omega a),$$

and

$$V \cdot \nabla a = U\partial_x a + V\partial_y a + \Omega\partial_\eta a,$$

where a represents a generic variable. $\gamma = c_p/c_v = 1.4$ is the ratio of the heat capacities for dry air, R_d is the gas constant for dry air, and p_0 is a reference pressure (typically 105 Pascals). The right-hand-side terms F_U, F_V, F_W and F_θ represent forcing terms arising from model physics, turbulent mixing, spherical projections, and the earth's rotation. The prognostic equations are cast in conservative form except for the last one, which is the material derivative of the definition of the geopotential. It could be cast in flux form but there is no advantage in doing so since $\mu\phi$ is not a conserved quantity. It should be noted that the relation for the hydrostatic balance does not represent a constraint on the solution; rather it is a diagnostic relation that formally is part of the coordinate definition.

The equations are conservative for the scalar variables. The prognostic variables are velocity components u and v in Cartesian coordinate, vertical velocity w , perturbation potential temperature, perturbation geopotential, and perturbation surface pressure of dry air. Optionally, turbulent kinetic energy and any number of scalars such as water vapour mixing ratio, rain/snow mixing ratio, cloud water/ice mixing, and chemical species and tracers.

3.2.3 Numerical methods

The WRF uses the dynamical techniques by numerically solving the governing equations. The numerical methods converts the spatial and temporal derivatives into algebraic equations that a computer can solve. The WRF model uses finite difference method (FDM), meaning that the method solves differential equations by approximating them with difference equations, in which finite differences approximate the derivatives.

3.2.4 Horizontal and vertical grid

The ARW solver uses the Arakawa C-grid staggering for the variables where the normal velocities are staggered one-half grid length from the thermodynamic variables in the horizontal and vertical planes (Fig. 3.4). The diagnostic variables used in the model, the pressure p and inverse density α , are computed at mass points. The grid lengths dx and dy are constants in the model formulation; changes in the physical grid lengths associated with the various projections to the sphere are accounted for using the map factors.

The vertical grid length is not a fixed constant; it is specified in the initialization. The user is free to specify the values of the model levels. Subject to the constraint that $\eta = 1$ at the surface, $\eta = 0$ at the model top, and η decreases monotonically between the surface and model top.

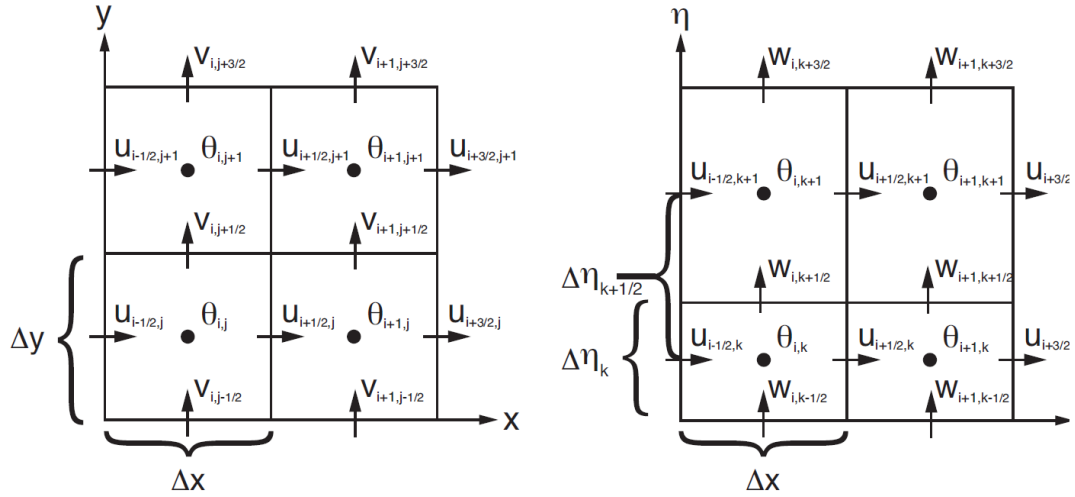


Fig. 3.4 (a) Horizontal and (b) vertical grids of the ARW.

Using these grid and variable definitions, we can define the spatial discretization for the ARW solver.

3.2.5 Time integration

The model has time-split integration that uses a 3rd order Runge-Kutta scheme with smaller time step for acoustic and gravity-wave modes. Spatial discretization has 2nd to 6th order advection options in horizontal and vertical. Full Coriolis terms are included in the dynamics. Three map projections are supported for real-data simulation in which the Curvature terms are included, they are polar stereographic, Lambert-conformal and Mercator.

3.2.6 Initial conditions

The ARW may be run with initial conditions that are defined analytically for idealized simulations, or it may be run using interpolated data from either a large-scale analysis or forecast for real-data cases. Both 2D and 3D tests cases for idealized simulations are provided. The ARW's pre-processor generates the specific initial conditions for the selected idealized or real data case function similarly.

The pre-processor takes a user's definition of a domain (or domains for a nested run), together with various terrestrial datasets for terrain, land use, soil type, annual deep soil temperature, monthly vegetation fraction, maximum snow albedo, monthly albedo, slope data, and meteorological data from another model (in GriB format) to create mesoscale domains, and interpolate the above data to those domains, respectively.

3.2.7 Boundary conditions

Several lateral boundary condition options exist for the ARW that are suitable for idealized flows, and a specified lateral boundary condition for real-data simulations is available. The coarsest grid of any single simulation is eligible for any of the lateral boundary selections. Real-data cases could use combinations of periodic, symmetric, or open lateral boundary conditions instead of the more traditional time-dependent conditions provided by an external boundary file. The ARW supports rectangular horizontal grid refinement with integer ratios of the parent and child grid distances and time steps. Gravity wave absorbing (diffusion or Rayleigh damping) $w = 0$ is the top boundary condition at constant pressure level. Bottom boundary conditions are physical.

3.2.8 Nesting

The ARW supports horizontal nesting that allows resolution to be focused over a region of interest by introducing an additional grid (or grids) into the simulation. Only horizontal refinement is available, there is no vertical nesting option. The nested grids are rectangular and are aligned with the parent (coarser) grid within which they are nested. Additionally, the nested grids allow any integer spatial and temporal refinements of the parent grid. Nested grid simulations can be produced using one-way, two-way, and moving nests (Skamarock et al., 2008).

3.2.9 Parameterisations

The parameterisation is the key feature of WRF modelling. Parameterisation is necessary because computers are not yet powerful enough to treat many physical processes explicitly, either due to too small or too complex to be resolved. Some physical processes also cannot be explicitly modelled because they are not sufficiently understood to be represented in equation format or there are no appropriate data.

The major improvements in the WRF model are derived from multiple parameterisations in each release. This allows users to select parameterisation schemes best suited for their use. The parameterisations include the physics options such as: cumulus parameterisation; microphysics; shortwave and longwave radiations; planetary boundary layer (PBL); surface layer; and land-surface model. Specifically, a notable impact on rainfall events and air temperature occurs from changes in the cumulus scheme, microphysics and PBL (Jankov et al., 2005). The PBL is responsible for vertical sub-grid-scale fluxes due to eddy transport in the whole atmospheric column, not just in the boundary layer. The microphysics schemes include explicitly resolved water vapour, cloud and precipitation processes. While cumulus parameterization deals with the sub-grid-scale effects of convective and/or shallow clouds.

3.2.10 WRF program workflows

The principal components of the WRF system are illustrated in Fig. 3.5. As shown, the WRF modelling system consists of three major programs, which are: (1) WRF Pre-processing System (WPS), (2) WRF-ARW model and (3) Post-processing and visualization tools.

It should be noted that the usage of each program depends on the purpose of the study. In general, the workflow can be classified as follows:

1. In case of running idealized cases (i.e. without modification/default case), the program flow only requires the WRF ARW Model with Post-processing tools.
2. For the real cases with variational analysis (e.g. external observational data), the program flow requires WPS, WRF-Var, WRF ARW Model and Post-processing tools.
3. In the real-case simulation, the program flow requires WPS, WRF ARW Model and Post-processing tools. This program flow is used in this study (see red-dashed line in Fig. 3.5).

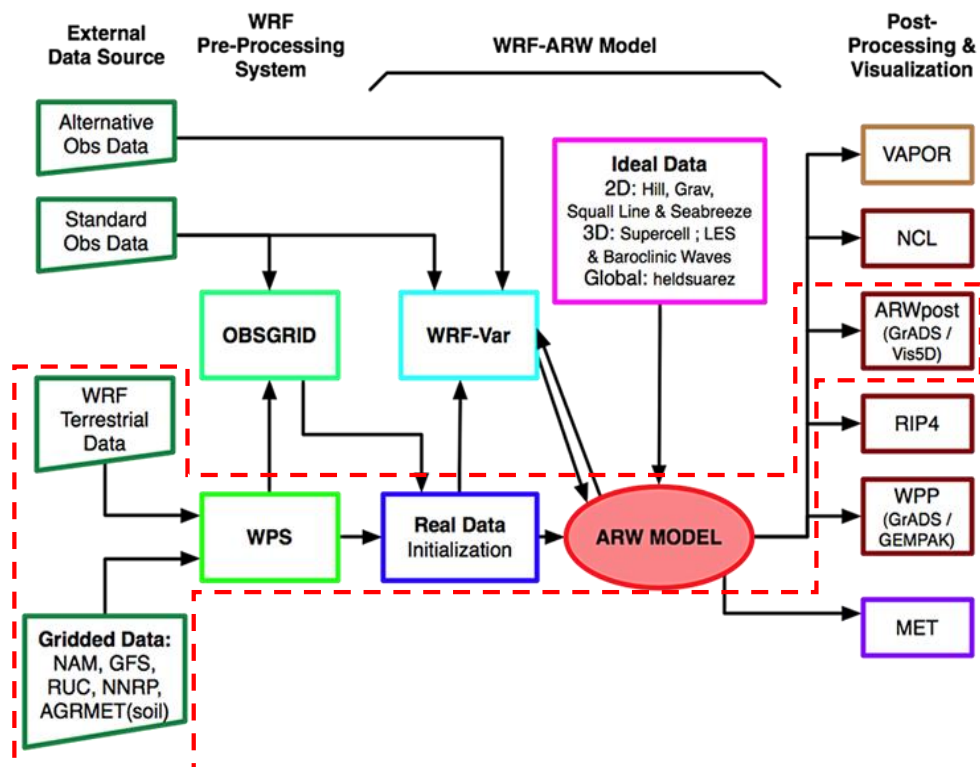


Fig. 3.5 WRF-ARW modeling system flow chart. The red-dashed line indicates the program flow used in this study. Source: (Skamarock et al., 2008)

WPS

As described in Fig. 3.5, the WRF process relies on the input produced by the WPS. The WPS defines the simulation domains, interpolates terrestrial data (e.g., terrain height, soil, and land use type) to simulation grid, and interpolates time-varying meteorological fields (e.g., soil moisture, winds, temperature, and precipitation) onto simulation domains. The input data processed in WPS are based on the external data sources, such as the reanalyses data, forecasted data, or observation-based data.

In this study, the terrestrial data were composed from the USGS data for the terrain height and the own-processed data for the land use and land cover. Further, we employed two types of initial and boundary conditions for current and future weather conditions. For current condition, the NCEP FNL (Final) Operational Global Analysis data with $1^\circ \times 1^\circ$ resolution (<http://rda.ucar.edu/datasets/ds083.2/>) were used, while the data from CMIP5 projected by the MIROC were utilised (Taylor et al., 2012) for the future weather conditions. The input data produced by the WPS were used for the initial and boundary conditions for WRF simulations. The Advanced Research WRF (ARW) solver was used for all simulations.

Fig. 3.6 shows the flow of data processing and program components of WPS. The first step for WPS is to configure the model domain and create static files of terrestrial data such as elevations, location of study area and model resolution (indicated as GEOGRID in Fig. 3.6). Independent from the domain configuration, an external process is conducted to reformat the GriB (binary data format for storing historical and forecast weather data) into a format suitable for ARW solver data processing (i.e. UNGRIB in Fig. 3.6). With a specific domain and meteorological data input have been prepared (i.e. outputs from GEOGRID and UNGRIB), WPS interpolates the meteorological data into each specific domains (indicated as METGRID in Fig. 3.6).

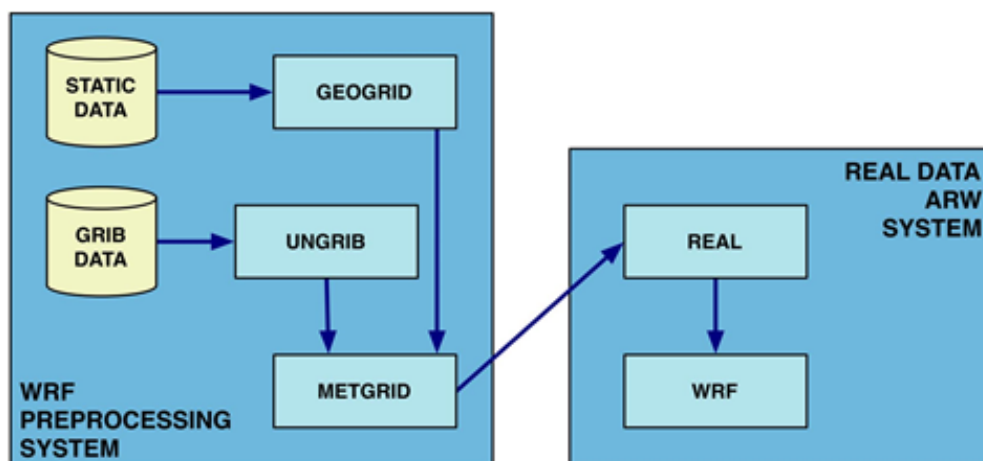


Fig. 3.6 Schematic diagram showing the flow of data processing and program components in WPS and how the WPS feeds initial data to the ARW. Source: (Skamarock et al., 2008)

ARW Solver

The ARW Solver is the key component of the WRF modelling system. As has been previously discussed, it is fully compressible, non-hydrostatic model (with a hydrostatic option). Its vertical coordinate is a terrain-following hydrostatic pressure coordinate. The grid staggering is the Arakawa C-grid. The ARW solver encompasses a number of governing equations used in producing a simulation. Some major basic equations in the model consist of momentum equations such as the mass conservation equation, conservation equation for potential temperature and the geopotential equation.

Post-processing and visualization tools

There are a number of visualization tools available to process the WRF-ARW model output. The output is in NetCDF (Network Common Data Format). It is developed by Unidata as a means for data transfer between Unidata applications. The concept is implemented as a library of computer 'functions' that can be assembled by a user to access or can be readily interchanged between users without the need for supplementary materials. The files can contain data of different types, multiple variables as well as ancillary data or descriptive text (McGuffie & Henderson-Sellers, 2005). It can be essentially displayed using any tool capable of displaying this data format. Currently, the following post-processing tools are supported: NCL, RIP4, ARWPost, WPP and VAPOR. Since this study deals with real data, ARWPost was employed.

The ARWPost processes the output data from ARW solver. This process generates a set of file which can be processed by the visualization program, e.g. GrADS (Grid Analysis and Display System). GrADS is an interactive desktop tool that is used for easy access, manipulation, and visualization of earth science data. GrADS has two data models for handling gridded and station data. It supports many data file formats and freely available on the internet. It can produce a variety of graphical techniques such as line and bar graphs, scatter plots, smoothed contours, shaded contours, streamlines, wind vectors, grid boxes, shaded grid boxes, and station model plots.

3.3 Observational weather records

The observed weather records are used to validate the results of WRF simulations. They are also used for determining the simulation periods (e.g. simulation in hot summer days, simulation in an average weather condition, simulation in the days with prevailing wind direction, etc.). The data were collected from the weather stations in JB and Hanoi, respectively. Most of the observed weather data used in this study were retrieved from the Climate Data Online (CDO) of National Centre for Environmental Information (NCEI) (<https://www.ncdc.noaa.gov/cdo-web/>). Some data were also obtained from the meteorological agency in each city, such as the National Hydro-Meteorological Service (HMS) in Hanoi and the Malaysian Meteorological Department (METMalaysia) in JB.

Table 3.1 Weather stations and available parameters deployed in and outside of Hanoi City.

| Stations | Latitude | Longitude | Available parameters | Interval | Source |
|----------|-----------|------------|--|----------|----------|
| Noibai | 21.2211°N | 105.8072°E | Air temperature, Wind speed and direction | Hourly | CDO NCEI |
| Lang | 21.02°N | 105.8 °E | Air temperature, wind speed and direction | Hourly | CDO NCEI |
| Ha Dong | 20.95°N | 105.75°E | Air temperature, Wind speed and direction | 3-hourly | HMS |
| Ba Vi | 21.1°N | 105.43°E | Air temperature, Wind speed and direction | 3-hourly | HMS |
| Son Tay | 21.032°N | 105.832°E | Air temperature, Wind speed and direction | 3-hourly | HMS |

Note: Data were collected between 2000 and 2015.

Table 3.2 Weather stations and available parameters deployed in and outside of JB.

| Stations (City) | Latitude | Longitude | Available parameters | Interval | Source |
|---------------------------|------------|--------------|--|----------|----------|
| Senai (JB) | 1.6413°N | 103.6696°E | Air temperature, Wind speed and direction | Hourly | CDO NCEI |
| Changi (Singapore) | 1.3677°N | 103.9833°E | Air temperature, wind speed and direction | Hourly | CDO NCEI |
| Paya Lebar (Singapore) | 1.360417°N | 103.90953°E | Air temperature, Wind speed and direction | Hourly | CDO NCEI |
| Seletar (Singapore) | 1.41695°N | 103.867653°E | Air temperature, Wind speed and direction | Hourly | CDO NCEI |
| NUS (Singapore) | 1.3°N | 103.766667°E | Air temperature, Wind speed and direction | Hourly | NUS |

Note: Data were collected between 2000 and 2015.

However, the weather data from the national agencies are restricted and must be purchased. Moreover, we also collected the weather data at the same stations from other open data sources to confirm the validity of the data from NCEI. In general, there are no significant differences between NCEI's data and data from other sources. A slight difference is mainly due to the variabilities of the unit and format, for instance, degree Fahrenheit (°F) is used in NCEI, while others use degree Celcius (°C).

Table 3.1 shows information of the weather stations in and outside Hanoi while Table 3.2 lists the weather stations in JB and Singapore. The locations of the weather stations are shown in Fig. 1.4 and Fig. 1.5 for Hanoi and JB, respectively. As shown, there is only one weather station in JB. Meanwhile, there are four weather stations located in the neighbouring city Singapore. It is necessary to include the weather stations in Singapore since they are also located within the simulation domain of JB case study.

3.4 Experiments for validation and sensitivity testing of the parameterisations

The WRF model have different sets of physical parameterisation configuration options. Currently, as the model becomes more sophisticated, greater number of physical processes can be incorporated into it, and there is a range of physical schemes that can be used in the simulation. Nevertheless, some problems or error in the WRF simulation are associated with the use of parameterisations. It can be resulted from interactions between parameterization schemes, where each schemes contains its own set of errors and assumption. For instance, a soil model and radiation scheme passing back and forth the information about heating at the boundary layer. The error may also be resulted from the increasing complexity and interconnectedness of parameterisations, which result in forecast errors that are more difficult to trace back to specific processes. These problems and impacts require users to have physical reasoning and interpretation on a case by case basis.

As previously mentioned, the WRF model includes a number of physical schemes that affect the modelling results (Jankov et al., 2005). Therefore, the sensitivity of air temperature in a hot and humid urban climate to physics changes has to be identified for improving the modelling. Among the physical processes described, the PBL processes, microphysics, and cumulus schemes were evaluated with five different combinations as shown in Table 3.3 since those three physical schemes are shown to be the most influential on rainfall events and air temperature (Jankov et al., 2005). Then, the chosen parameter configuration for the WRF simulation was determined by choosing the model with relatively reasonable values in terms of the root mean square error (RMSE) and the coefficient of determination (R^2). They are calculated as follows:

$$R^2 = 1 - \frac{\sum_i (y_i - f_i)^2}{\sum_i (y_i - \bar{y}_i)^2}, \text{ where } \bar{y}_i = \frac{1}{N} \sum_{i=1}^N y_i \quad (3.11)$$

$$RMSE = \sqrt{\frac{1}{N} \sum_{i=1}^N (y_i - f_i)^2} \quad (3.12)$$

Table 3.3 WRF configuration for each model parameterisation in the sensitivity analysis.

| | Run 1 | Run 2 | Run 3 | Run 4 | Run 5 |
|----------------|-----------------------|------------------------------------|---------------------------|---------------------------|------------------------------------|
| PBL Type | YSU Scheme | Mellor-Yamada-Janjic ETA Scheme | YSU Scheme | YSU Scheme | Mellor-Yamada-Janjic ETA Scheme |
| Microphysics | WRF SM 3-class scheme | WRF SM 3-class scheme | WRF SM 3-class scheme | Ferrier | Ferrier |
| Cumulus Scheme | Kain-Fritsch scheme | Kain-Fritsch scheme | Bett-Miller-Janjic Scheme | Bett-Miller-Janjic Scheme | Kain-Fritsch scheme |
| R^2 | 0.876 | 0.907 | 0.757 | 0.443 | 0.914 |
| RMSE | 1.056 | 1.916 | 2.033 | 3.633 | 1.720 |

In the equations (3.11) and (3.12), y_i is the observation value, while f_i is the simulated value.

The R^2 indicates the proportion of the variance in the dependent variable that is predictable from the independent variable(s). In the model validation, the R^2 value can be interpreted as the goodness of fit of a model. Its value ranges from 0 to 1. An R^2 of 1 indicates that the modeled values perfectly fits the observed data. Similar with R^2 , the RMSE is also used to see how effectively the model predicts the actual condition. Its values represent the differences between values predicted by a model and the values actually observed.

The simulation period for sensitivity tests is 14 days, from 00:00 UTC 7 to 00:00 UTC 20 June 2010. The simulations adopt four domains that have horizontal resolutions of 27, 9, 3 and 1 km, respectively (see Fig. 6.1 in Chapter 6). The initial and boundary conditions use NCEP FNL Operational Global Analysis data with $1^\circ \times 1^\circ$ latitude–longitude resolution. The model topographies for the domains 1 to 4 use the US Geological Survey (USGS) data, which are the default LULC dataset for WRF. Table 3.4 displays the model configurations, such as domain size and other physical schemes except the three physics for sensitivity tests.

The results of sensitivity tests in Table 3.3 indicate that the Run 1 is the most reasonable combination of physical schemes because of the lowest RMSE value, even though the squared correlation coefficient is slightly lower than Runs 2 and 5. Therefore, the physical schemes used in Run 1 is applied for further numerical experiments in this study. It should be kept in mind, however, that no one parameterization or combination are obviously best at all times and thresholds (Jankov et al., 2005).

Table 3.4 WRF configuration for sensitivity analysis.

| Physics/Parameterizations | Domain 1 | Domain 2 | Domain 3 | Domain 4 |
|-------------------------------|----------|---------------------------------|----------|----------|
| Horizontal resolution (km) | 27 | 9 | 3 | 1 |
| Longwave radiation | | RRTM scheme | | |
| Shortwave radiation | | Dudhia scheme | | |
| Surface-layer | | Monin-Obukhov similarity scheme | | |
| Land-surface parameterization | | Noah LSM | | |

3.5 Coupling WRF with Urban-Canopy Model (UCM)

In order to better represent the physical processes involved in the exchange of heat, momentum and water vapour in urban environment in mesoscale model, an UCM is coupled to the WRF model (Tewari et al., 2007). The UCM is a single layer model which simplifies the urban geometry. Fig. 3.7a shows the schematic of the single layer UCM which consist of 2-dimensional, symmetrical street canyons with infinite length, meaning and simplified building geometry. The radiation treatment is 3-dimensional because it includes the canyon orientation and the diurnal variation of azimuth angle. The model estimates the surface temperature of roof, wall and road surfaces as well as the fluxes from these surfaces. Fig 3.7b shows the radiation trapping between the walls of the buildings.

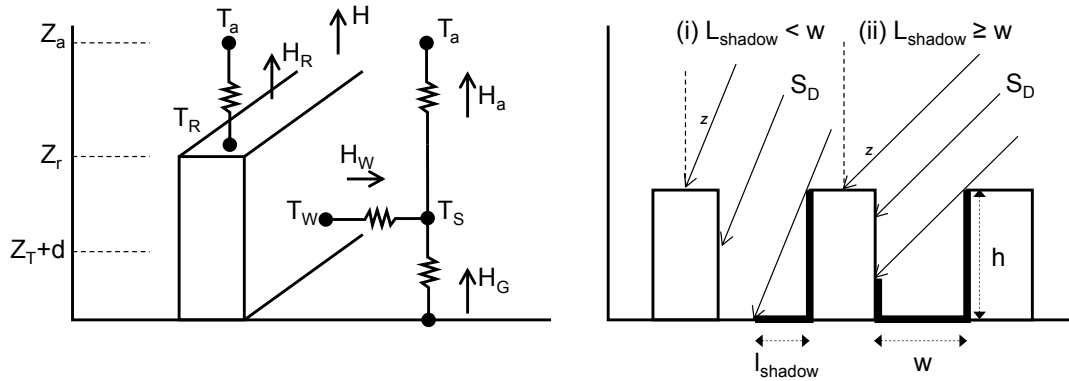


Fig. 3.7 (a) Schematic of the single-layer urban canopy model. T_a is the air temperature at reference height Z_a , T_R is the building roof temperature, T_W is the building wall temperature, T_G is the road temperature, T_S is the temperature defined at $Z_T + d$, H is the sensible heat exchange at the reference height, H_a is the sensible heat flux from the canyon space to the atmosphere, H_w is that from wall to the canyon space, H_G is that from road to the canyon space, and H_R is that from roof to the atmosphere. Source: Kusaka & Kimura, 2004.

(b) Radiation of the single-layer urban canopy model. S_D is the direct solar radiation incident on a horizontal surface, w is the normalized road width, h is the normalized building height ($l_{roof} + w = 1$), and l_{shadow} is the normalized shadow length on the road. Source: Kusaka & Kimura, 2004.

The UCM aims to estimate the surface temperature of roof, wall, and road from the surface energy balance (3.13) as well as the individual fluxes from various surfaces.

$$R_{n,i} = H_i + lE_i + G_i \quad (3.13)$$

Here, $R_{n,i}$, H_i , lE_i , and G_i are the net radiative flux density to the surface, the sensible and latent heat fluxes, and the heat into the ground, which is interpreted as the ground heat flux at the surface. The subscript i indicates the type of surface, which can be roof, wall, or road. The model has a very thin bucket scheme, i.e., roof and road surfaces are covered with an impermeable layer and the city has a very adequate drainage system. Latent heat flux from street trees along the road and grass in the open spaces are calculated from a single-layer vegetation model. Total latent heat flux from the urban surface is obtained by the average of fluxes on each model (Kimura, 1989).

3.5.1 Solar fluxes

Building heights has a significant effect on surface temperature, owing to the effects of the shadows and the reflected solar and longwave radiation. The model is assumed to be a Lambertian surface. The normalized shadow length l_{shadow} on the road is defined as:

$$l_{shadow} = \begin{cases} h \tan \theta_z \sin \theta_n & (l_{shadow} \leq w) \\ w & (l_{shadow} \geq w) \end{cases} \quad (3.14)$$

Here, h and w are normalized building height and road width between two buildings ($r+w=1$), respectively; θ_z is the solar zenith angle.

The net amount that is absorbed by the roof, wall, and road are calculated from (refer to Fig. 3.7b):

$$S_R = S_D(1 - \alpha_R) + S_Q(1 - \alpha_R) \quad (3.15)$$

$$S_{W,1} = S_D \frac{l_{shadow}}{2h} (1 - \alpha_W) + S_Q F_{W \rightarrow S} (1 - \alpha_W) \quad (3.16)$$

$$S_{W,2} = S_D \frac{(w-l_{shadow})}{w} \alpha_G F_{W \rightarrow G} (1 - \alpha_W) + S_Q F_{W \rightarrow G} (1 - \alpha_W) + S_D \frac{l_{shadow}}{2h} \alpha_W F_{W \rightarrow W} (1 - \alpha_W) + S_Q F_{W \rightarrow S} \alpha_W F_{W \rightarrow W} (1 - \alpha_W) \quad (3.17)$$

$$S_{G,1} = S_D \frac{(w-l_{shadow})}{w} (1 - \alpha_G) + S_Q F_{G \rightarrow S} (1 - \alpha_G) \quad (3.18)$$

$$S_{G,2} = S_D \frac{l_{shadow}}{2h} \alpha_W F_{G \rightarrow W} (1 - \alpha_G) + S_Q F_{W \rightarrow S} \alpha_W F_{G \rightarrow W} (1 - \alpha_G) \quad (3.19)$$

The solar radiation is positive when directed towards the surface. S_D and S_Q are the direct solar radiation and the diffuse solar radiation received by a horizontal surface, respectively; the subscripts 1 and 2 refer to the absorption of the direct and reflected radiation, respectively; the subscripts W , G , and S denote wall, ground, and sky, respectively; α_R , α_W , and α_S are albedo at roof, wall, and road surface, respectively. The sky view factor F_P of an arbitrary point P on a wall, a distance z_P from the roof level, as well as the road view factor for the wall, the wall view factor for the road, the wall view factor for the wall and sky view factor for the road are described in Kusaka et al. (2001). The canyon orientation in a real city is usually heterogeneous over the grid size of a mesoscale meteorological model. Therefore, in practice, some canyon types should be set up that are based on a survey or an identical model city for a simulation. The total direct solar radiation to a grid element is evaluated by the weighted average according to the relative area of different canyons. Diffuse solar and downward longwave radiation are assumed to be emitted from the entire sky; i.e., it is assumed isotropic.

3.5.2 Longwave fluxes

The net longwave fluxes absorbed by the roof, wall, and road surfaces are calculated from:

$$L_R = \epsilon_R (L \downarrow - \sigma T_R^4) \quad (3.20)$$

$$L_{W,1} = \epsilon_W(L \downarrow F_{W \rightarrow S} + \epsilon_G \sigma T_G^4 F_{W \rightarrow G} + \epsilon_W \sigma T_W^4 F_{W \rightarrow W}) \quad (3.21)$$

$$L_{W,2} = \epsilon_W[(1 - \epsilon_G)L \downarrow F_{G \rightarrow S} F_{W \rightarrow G} + (1 - \epsilon_G)\epsilon_W \sigma T_W^4 F_{G \rightarrow W} F_{W \rightarrow G} + (1 - \epsilon_W)L \downarrow F_{W \rightarrow S} F_{W \rightarrow W} + (1 - \epsilon_W)\epsilon_G \sigma T_G^4 F_{W \rightarrow G} F_{W \rightarrow W} + (1 - \epsilon_W)\sigma T_W^4 F_{W \rightarrow W} F_{W \rightarrow W}] \quad (3.22)$$

$$L_{G,1} = \epsilon_G[L \downarrow F_{G \rightarrow S} + \epsilon_W \sigma T_W^4 F_{G \rightarrow W} - \sigma T_G^4] \quad (3.23)$$

$$L_{G,2} = \epsilon_G[(1 - \epsilon_W)L \downarrow F_{W \rightarrow S} F_{G \rightarrow W} + (1 - \epsilon_W)\epsilon_G \sigma T_G^4 F_{W \rightarrow G} F_{G \rightarrow W} + \epsilon_W(1 - \epsilon_W)\sigma T_W^4 F_{W \rightarrow W} F_{G \rightarrow W}] \quad (3.24)$$

Here, $L \downarrow$ is the downward atmospheric longwave radiation. ϵ_R , ϵ_W , and ϵ_G are emissivities of the roof, wall, and road surfaces, respectively. T_R , T_W , and T_G are surface temperatures of the roof, wall, and road, respectively. The subscripts 1 and 2 refer to the absorption of the direct and reflected radiation, respectively.

3.5.3 Sensible heat flux

Sensible heat flux from the building roof, building wall, and road was estimated at each surface separately. The sensible heat fluxes from the wall H_W and road H_G are calculated by this formula (i.e. Jurge's formula):

$$H_W = C_W(T_W - T_S) \quad (3.25)$$

$$H_G = C_G(T_G - T_S) \quad (3.26)$$

$$C_W = C_G = \begin{cases} 7.51U_S^{0.78} & (U_S > 5 \text{ m s}^{-1}) \\ 6.15 + 4.18U_S & (U_S \leq 5 \text{ m s}^{-1}) \end{cases} \quad (3.27)$$

Here, T_W and T_S are surface temperatures at the wall and road, respectively. The equations to determine the sensible heat exchange between canyon space and the overlaying atmosphere is described in Kusaka et al. (2001).

3.5.4 Wind speed in the canyon

The mean wind speed in the canyon was used as a reference to calculate H_G and H_W . Although this approximates actual field conditions, the model can clearly distinguish energy balances

between above roof level and within canyon. The calculation of wind speeds at the roof level and within the canyon are described in more detail in Kusaka et al. (2001).

3.5.5 Surface temperature

The roof, wall, and road surface temperatures were determined as the temperatures that balance the energy budgets on the individual canyon surfaces through their effect on the heat fluxes. The one-dimensional energy conservation equation was solved numerically with a variable grid interval to calculate the roof, wall, and road interior temperatures for the layers. The boundary condition is zero heat flux or constant temperature at the bottom layer. The ground heat flux $G_{Z,i}$ and interior temperature $T_{Z,i}$ at depth z to the i surface are calculated by the following equations:

$$G_{Z,i} = -\lambda_i \frac{\partial T_{Z,i}}{\partial z} \quad (3.28)$$

and

$$\frac{\partial T_{Z,i}}{\partial t} = -\frac{1}{\rho_i c_i} \frac{\partial G_{Z,i}}{\partial z} \quad (3.29)$$

where λ_i is the interior thermal conductivity and $\rho_i c_i$ is volumetric heat capacity that are specific to surface i . The subscript i indicates roof, wall, or road.

3.6 Input weather data for global warming condition

3.6.1 IPCC AR5 RCP Scenario

The Intergovernmental Panel on Climate Change (IPCC) has used emissions and climate scenarios as a central component of its work of assessing climate change research. Previous IPCC scenarios include the IPCC Scenario A (SA90) for the First Assessment Report (FAR) in 1990. IPCC Scenarios (IS92) used on the Third Assessment Report (TAR) in 1992 and the Special Report on Emission Scenarios (SRES) in TAR and the Fourth Assessment Report (AR4). In the latest assessment report (i.e. AR5) released in 2014, the IPCC decided to rely on new scenarios developed by the research community.

In the new process, the emissions and socioeconomic scenarios are developed in parallel, resulting in different trajectories of radiative forcing over time. These radiative forcing trajectories were named Representative Concentration Pathways (RCPs) (Fig. 3.8). They are the representative of the future emission scenario and resulting greenhouse gas concentration.

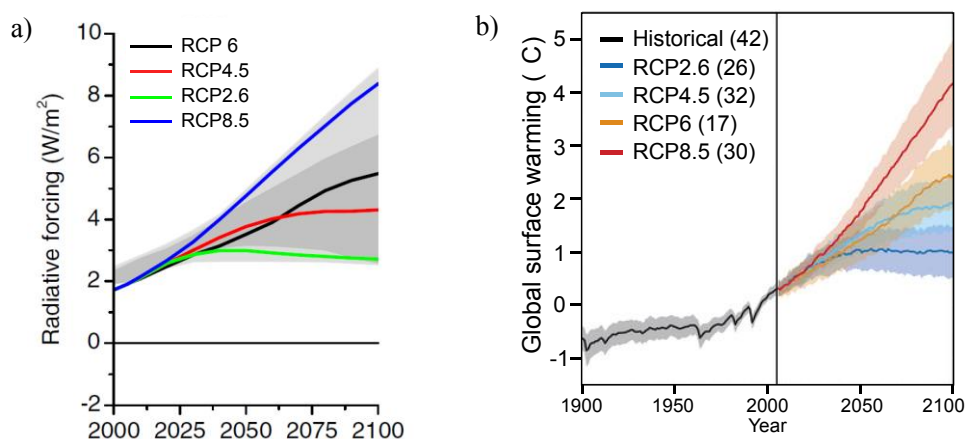


Fig. 3.8 (a) Radiative Forcing of the Representative Concentration Pathways. From van Vuuren et al. (2011). (b) Global temperature change (mean and one standard deviation as shading) relative to 1986-2005 for the RCP scenarios run by CMIP5. The number of models is given in brackets. From Knutti & Sedláček (2012).

There are four pathways, known as RCP8.5, RCP6.0, RCP4.5, and RCP2.6 (van Vuuren et al., 2011). They are named after a possible range of radiative forcing values in the year 2100 relative to pre-industrial values (i.e. 2.6, 4.5, 6, and 8.5 W/m², respectively) (see Fig. 3.8a).

In this study, we focused on RCP4.5 and RCP8.5, which are considered as moderate and extreme scenarios, respectively. RCP4.5 is defined as a typical global warming mitigation scenario, which includes explicit steps for combating greenhouse gas emissions (Thomson et al., 2011). In contrast, RCP8.5 is considered a business-as-usual scenario that does not include any specific climate mitigation measures (Riahi et al., 2011).

3.6.2 GCMs

General Circulation Models or the GCMs represents physical processes in the atmosphere, ocean, cryosphere and land surface. GCMs are the most advance tools for simulating the response of the global climate system to increasing greenhouse gas concentrations. They depict the climate using a three dimensional grid over the globe, typically having a horizontal resolution of between 250 and 600 km, 10 to 20 vertical layers in the atmosphere and sometimes as many as 30 layers in the oceans.

Since the AR4, the IPCC used the materials from the experiments conducted by climate modelling groups from around the world. These experiments comprise the fifth phase of the Coupled Model Intercomparison Project (CMIP5). Among CMIP5 datasets from various GCMs, the Model for Interdisciplinary Research on Climate Version 5 (MIROC5) was employed in this study. MIROC5 was developed jointly by the Center for Climate System Research (CCSR), the University of Tokyo, and a number of institutes (Watanabe et al., 2010).

In general, the consideration of more ensembles is desirable for reducing uncertainty in the projection of future climatic conditions, in particular, by utilizing more GCM outputs from CMIP5 for RCM downscaling. However, in this study, we adopt only the MIROC5 output for future climatic conditions. Fig. 3.9 illustrates the mean surface temperature from 2015 to 2100 for RCP4.5 and RCP8.5 from 38 GCM outputs over the Hanoi region (102°–107°E and 18°–

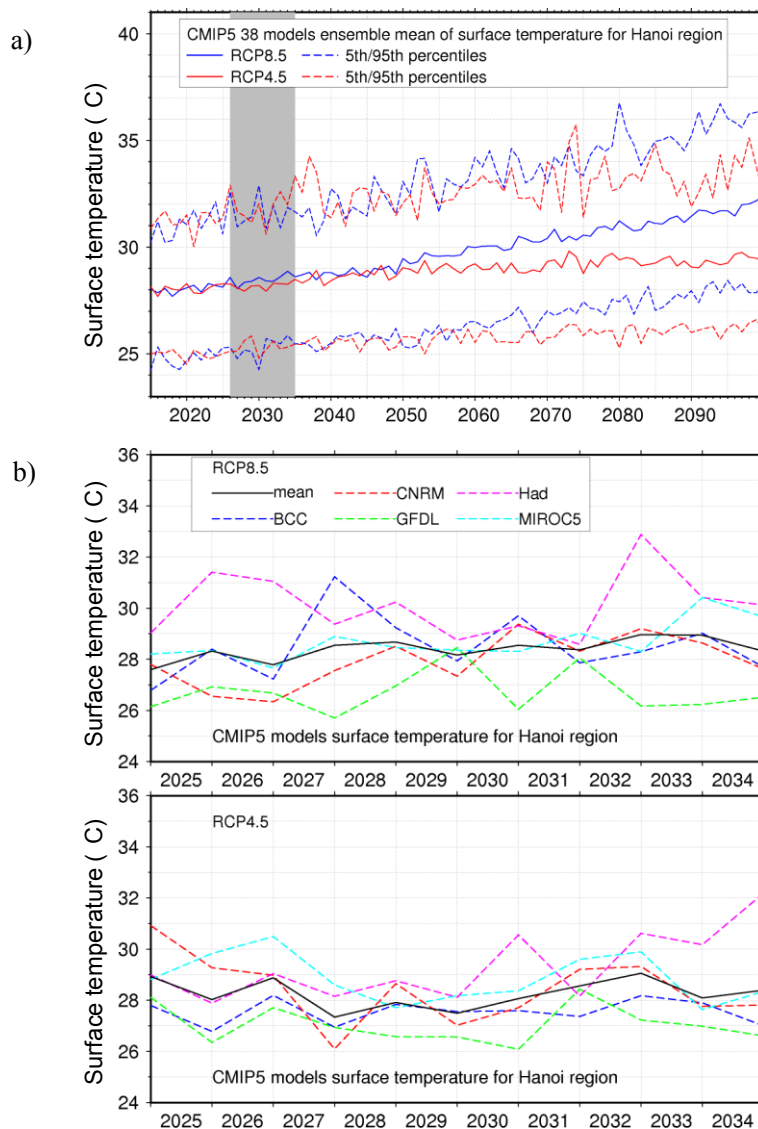


Fig. 3.9 (a) CMIP5 38-models ensemble mean surface temperature over Hanoi region (102°–107° E and 18°–23° N) from 2015 to 2100 (the target period of assessment is shaded in grey), and (b) surface temperature over the same region for 10 years from 2026 to 2035 from five GCMs including MIROC5 together with the ensemble mean of 38 CMIP5 models for RCP8.5 and RCP4.5, respectively.

23°N) and the surface temperature over the same region for 10 years from 2026 to 2035 from five GCMs, including the MIROC5. In the Hanoi region in Fig. 3.9a, the difference in surface temperature between RCP4.5 and RCP8.5 is not significant until approximately 2050, after which it becomes considerable. For the period from 2026 to 2035 with the Hanoi Master Plan, the 38-ensemble mean surface temperature of RCP8.5 is higher than that of RCP4.5, which might be partly due to stronger inter-annual variability than the background long-term trend. Among the five GCM outputs considered, the MIROC5 represents the 5-ensemble mean well (Fig. 3.9b). Therefore, it is reasonable to use the MIROC5 output for RCM downscaling for obtaining a general climate trend in the Hanoi region. Furthermore, in order to consider climate variability and uncertainty from the inter-annual variability in climate projection, we conducted a WRF simulation of each June between 2026 and 2035. We then obtained the mean and variation from the 10 simulation results of each future climate scenario (i.e., cases 2–2 and 2–3) to take into account the inter-annual variability of the MIROC5. This 10-year repetitive simulations of each June will also provide the upper and lower bounds from the dominant inter-annual variability, and further insight for a multi-model ensemble mean and variation over the Hanoi region.

3.6.3 Direct dynamical downscaling (DDD) method

The GCMs perform at coarse resolutions (typically with 0.5° or 1° in spatial resolution) and cannot resolve important sub-grid scale characteristics such as clouds, topography and urban features. Therefore, the GCM outputs are not appropriate for local impact studies. Downscaling methods have been developed to overcome this problem and to obtain local-scale weather and climatic features, particularly at the surface level, from global- and regional-scale atmospheric GCM output variables. The dynamical downscaling uses a high-resolution regional climate model (i.e., WRF in this study) driven by initial and boundary conditions from a GCM to derive smaller-scale features of the local climate. Domains configuration in the dynamical downscaling are shown in Table 3.5.

Dynamical downscaling processes with WRF driven by the MIROC5 dataset were performed for RCP4.5 and RCP8.5 for moderate and extreme cases, respectively. The weather components of MIROC5 used as initial and boundary conditions in WRF simulations include air temperature (ta), near-surface air temperature (tas), specific humidity (hus), near-surface

Table 3.5. Domain configuration for the direct dynamical downscaling using WRF.

| Parameterization | Domain 1 | Domain 2 | Domain 3 |
|----------------------------|------------------|----------|----------|
| Horizontal resolution (km) | 4.5 | 1.5 | 0.5 |
| Domain size (km) | 990x990 | 312x312 | 98x98 |
| Vertical layer | 30 | 30 | 30 |
| e_we and e_sn | 220 | 208 | 196 |
| geog_data_res | 5m | 2m | 30s |
| ref_lat and ref_lon | 20.98 and 105.65 | | |
| truelat1 and truelat2 | 20.98 | | |
| stand_lon | 105.65 | | |

specific humidity (huss), eastward wind (ua), northward wind (va), eastward near-surface wind (uas), northward near-surface wind (vas), sea level pressure (psl), surface temperature (tlsi), water content of soil layer (msls), soil temperature (tsl), and sea surface temperature (tso).

3.7 WRF domain set-ups

The WRF simulations in this dissertation were performed under two different domain set-ups. The first set-up is with four domains, while the latter set-up is with three domains configurations. In this dissertation, the WRF model with four domains were only used in the assessment of the cooling effect of the proposed green spaces in Hanoi (see Section 6.2), while the rest of simulation studies were conducted using the WRF model with three domains.

The WRF model with three domains were set-up with horizontal resolutions of 4.5, 1.5, and 0.5 km for domains 1, 2, and 3, respectively. In both case studies, the domain 3 covers the whole administrative boundary of each city. The LULC for domains 1 to 2 employed the USGS data. Meanwhile, for domain 3, we adopted the LULC datasets which were created from the combination between satellite images and digital land use data of each case study.

3.7.1 WRF domain set-up of Hanoi case study

The WRF domain for Hanoi case study was set with the domain sizes of 990x990 km, 312x312 km, and 98x98 km for domains 1, 2, and 3 are, respectively (Fig.3.10). As shown in Fig. 3.10, the red square indicates the domain 3 that covers the whole administrative area of

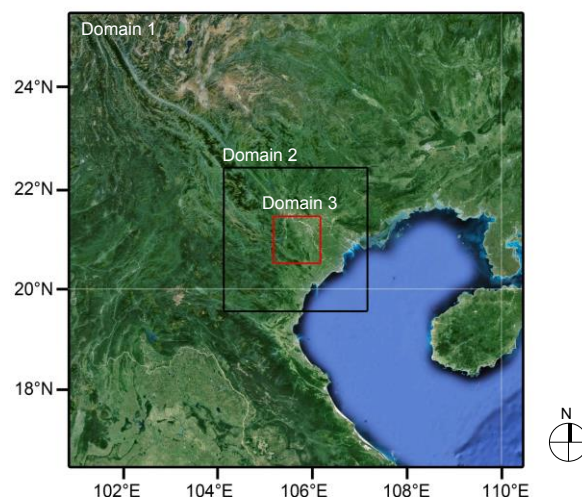


Fig. 3.10 The computational domains for WRF simulations for Hanoi.

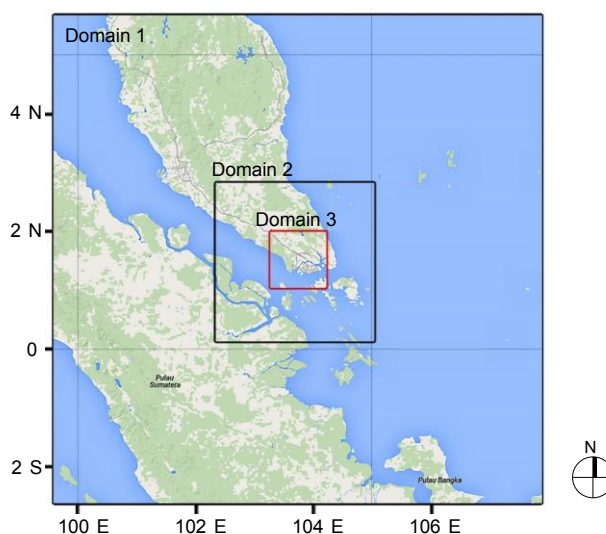
Table 3.6 The set-up values for geogrid section in the WPS of Hanoi case study.

| Parameter's name | Domain 1 | Domain 2 | Domain 3 |
|-------------------|----------|----------|----------|
| parent_id | 1 | 1 | 2 |
| parent_grid_ratio | 1 | 3 | 3 |
| i parent start | 1 | 76 | 72 |
| j parent start | 1 | 76 | 72 |
| e_we | 220 | 208 | 196 |
| e_sn | 220 | 208 | 196 |
| geog_data_res | 5m | 2m | 30s |
| dx and dy | 4500 | | |
| map_projection | Lambert | | |
| ref_lat | 20.98 | | |
| ref_lon | 105.65 | | |
| truelat1 | 20.98 | | |
| truelat2 | 20.98 | | |
| stand_lon | 105.65 | | |

Hanoi City. The vertical layer was set up to 30 sigma levels. The set-up values for geogrid in WPS (i.e. in namelist.wps) are listed in Table 3.6.

3.7.2 WRF domain set-up of JB case study

The WRF domain sizes for JB case study were 918x918 km, 298.5x298.5 km, and 102x102 km for domains 1, 2, and 3 are, respectively. The vertical layer was set up to 30 sigma levels (Fig. 3.11). The domain 3 covers the entire Iskandar Malaysia development area and

**Fig. 3.11** The computational domains for WRF simulations for JB.

also the whole area of Singapore. Although the urban areas of Singapore are also within domain 3, the land use data of Singapore is not included in the LULC data for WRF simulation, and assumed to remain unchanged even in the future condition. The set-up values for geogrid in WPS are listed in Table 3.7.

Table 3.7 The set-up values for geogrid section in WPS of JB case study.

| Parameter's name | Domain 1 | Domain 2 | Domain 3 |
|-------------------|------------|----------|----------|
| parent_id | 1 | 1 | 2 |
| parent_grid_ratio | 1 | 3 | 3 |
| i parent start | 1 | 69 | 69 |
| j parent start | 1 | 69 | 69 |
| e_we | 205 | 199 | 205 |
| e_sn | 205 | 199 | 205 |
| geog_data_res | 5m | 2m | 30s |
| dx and dy | 4500 | | |
| map_projection | Lambert | | |
| ref_lat | 1.527785 | | |
| ref_lon | 103.749997 | | |
| truelat1 | 1.527785 | | |
| truelat2 | 1.527785 | | |
| stand_lon | 103.749997 | | |

3.8 Building simulation using TRNSYS

3.8.1 Overview

Building energy simulation programs are increasingly used to analyse the energy performance of buildings. Among various programs, the TRNSYS 17 was selected as the building energy simulation tool due to its modular nature of the simulation software, and well-documented programming interface. TRNSYS is a complete and extensible simulation environment for the transient simulation of thermal systems, including multi-zone buildings (Klein et al., 2009). Its application is wide – ranging from small systems such as domestic hot water systems to whole building simulations that may include passive cooling strategies, HVAC equipment, occupants and renewable energy systems. The software was developed by Solar Energy Laboratory (SEL) at University of Wisconsin-Madison and made available since 1975. A current release, i.e. TRNSYS Version 17.01.0025, was used in this work.

TRNSYS has a modular program package. It consists of two parts, which are the TRNSYS simulation engine and TRNSYS Simulation Studio. The former is an engine that reads and processes the input file, iterates the mathematical models until convergence was reached within the specified tolerances. The second part is an extensive library of components, each of which models the performance of one part of the system. It includes a variety of models such

as multi-zone buildings, weather data processors, economics routines, and basic air-conditioning equipment. The Simulation Studio generates a text input file for the TRNSYS simulation engine.

A TRNSYS project is typically setup by connecting components graphically in the Simulation Studio. Each Type of component is described by a mathematical model in the TRNSYS simulation engine and has a set of matching inputs, outputs, parameters, etc. in the Simulation Studio. TRNSYS components are referred to as ‘Type’. This study use the Multizone building model which is known as Type 56 to model the thermal zones of a row house. The building model was defined in TRNSYS 3D Plug-In in Google SketchUp. This data were processed in TRNBUILD of TRNSYS.

3.8.2 The numerical solver and components used

The components that were used for the simulation in this study are shown in Fig. 3.12. Further, the general descriptions of the components are listed in Table 3.8. As shown in Fig. 3.12, the weather data reading and processing uses Types 9e, 16c, 33e, and 69b. Meanwhile, the building thermal zones were modelled using Type 56. The outputs are plotted by Type 65d and printed into text file by using Type 25a. The source code of the TRNSYS simulation engine is described in detail in the user manual (Klein et al., 2009). The following sections describe some of the key points.

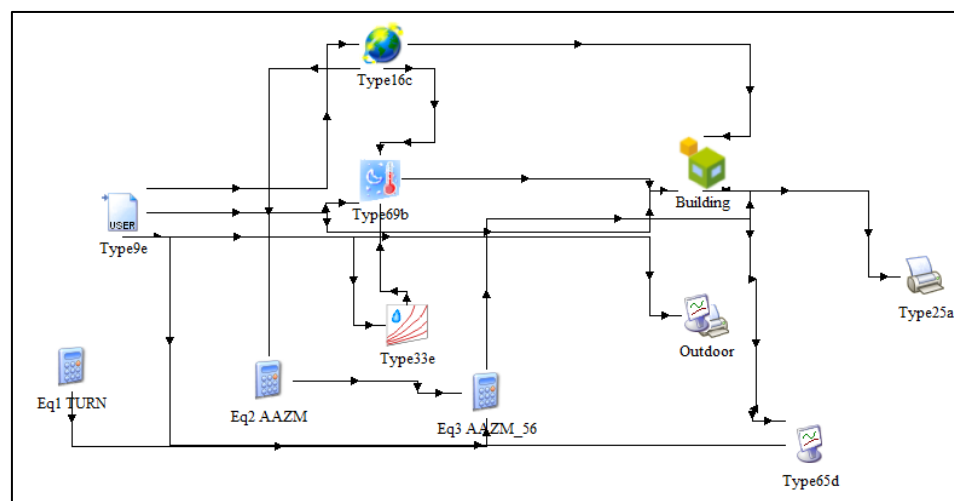


Fig. 3.12 The configuration of components in TRNSYS Simulation Studio.

The TRNSYS Solver

The TRNSYS simulation engine simultaneously solves a set of algebraic and differential equations in the system model at each simulation step based on the parameter and

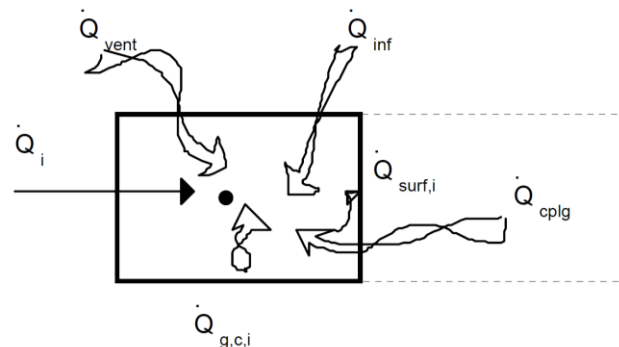
Table 3.8 Descriptions of components used in the study

| Components | Description |
|------------|--|
| Type 9e | The data reader. To read any free format or formatted text file. It can interpolate data or not and has several operation modes to handle initial values |
| Type 16c | The radiation processors. A powerful component that handles all operations that are necessary to calculate the incident radiation on a tilted surface from the available solar radiation in a typical data file. |
| Type 33e | Psychrometrics. A flexible component that can be used to calculate different properties of humid air from two independent variables. |
| Type 69b | .Effective Sky Temperature. It calculates an effective sky temperature used to take into account long-wave radiation between walls, roofs, collectors, etc. and the sky. |
| Type 65d | The online plotter. The online graphics component is used to display selected system variables at specified intervals of time while the simulation is progressing. |
| Type 25 a | A generic printer that can generate text files in different formats. It can print with a time step that is different from the simulation time step. |
| TURN | The equation used to rotate the building. |
| AAZM | Solar azimuth angle |

input values at the beginning of the time step. Results are returned as average values for every time step. The Modified-Euler method was selected for solving differential equations used in the components (Klein et al., 2009). Furthermore, the successive solution method which is recommended for buildings and systems with a thermal capacity, as in this study, was applied. All the simulation attained convergence within a tolerance of 0.0, which is changing less than 1% of the iteration value.

The thermal model of Type 56 Multi-zone building

Type 56 describes a building with multiple thermal zones, i.e. rooms. The building model in Type 56 is a non-geometrical balance model with one air node per zone, representing the thermal capacity of the zone air volume and capacities which are closely connected with the air node. Therefore, each room has a homogenous temperature, and radiation heat between the rooms is based on the room area. The model uses data from wall and window materials and thicknesses. Heat addition from solar direct and diffuse radiation is calculated for each room depending on window and heat transfer properties. The heat balance on the air node of

**Fig. 3.13** Heat balance on the zone air node.

each zone is illustrated in Fig. 3.13. In general, the heat balance model for the whole model are based on: (1) convective heat flux to the air node; (2) short-wave and long-wave radiation, conduction and convection heat fluxes to the walls and windows; and (3) thermal history of high thermal walls (Klein et al., 2007).

Convective heat flux to the air node

As shown in Fig. 3.13 the heat balance on the air node is affected by convective heat flux to the air node. The convective heat gains are the infiltration gains $Q_{inf,i}$ (i.e. air flow from outside only), ventilation gains $Q_{vent,i}$ (i.e. air flow from a user-defined source, e.g. HVAC), internal convective gains $Q_{g,c,i}$ (e.g. people, equipment, radiators, etc.), and the gains due to connective air flow from zones or boundary condition $Q_{cplg,i}$. The convective heat flux to the air node is expressed as follows:

$$Q_i = Q_{surf,i} + Q_{inf,i} + Q_{vent} + Q_{g,c,i} + Q_{cplg,i} \quad (3.30)$$

Coupling

The coupling statement allows the air mass flow between zones, considered as a heat flow from or to the air node. The statement does not automatically define the air flow back to the adjacent zone as would occur in an inter-zonal air exchange (Klein et al., 2007). To consider this return flow, the corresponding coupling must be defined in the adjacent zone to receive the same air flow in return. The reason for this convention is to allow the user to describe cross ventilation or a ventilation circle within 3 or more zones (see Fig. 3.14).

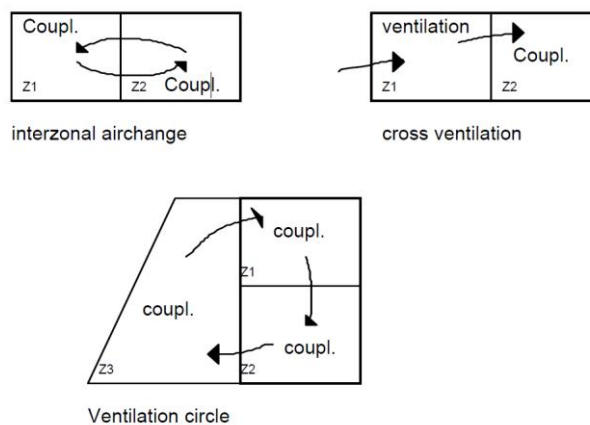


Fig. 3.14 Types of air mass flows between zones.

Radiative heat flows to the walls and windows

The radiative energy flows to the walls is expressed by the following equation:

$$Q_{r,w_i} = Q_{g,r,i,w_i} + Q_{sol,w_i} + Q_{long,w_i} + Q_{wall-gain} \quad (3.31)$$

where Q_{r,w_i} is the radiative gains for the wall surface temperature node, Q_{g,r,i,w_i} is the radiative zone internal gains received by wall, Q_{sol,w_i} is the solar gains through zone windows received by walls, Q_{long,w_i} is the long-wave radiation exchange between the wall and all other walls and windows ($\varepsilon_i=1$), and $Q_{wall-gain}$ is the user-specified heat flow to the wall or window surface. All of these quantities are given in kJ/h.

Furthermore, the heat fluxes and temperatures that characterize the thermal behavior of any wall or window are illustrated in Fig. 3.15. A window on a wall is thermally considered as an external wall with no thermal mass, partially transparent to solar, but opaque to long-wave and internal gains. Long-wave absorption is considered to occur only at the surfaces.

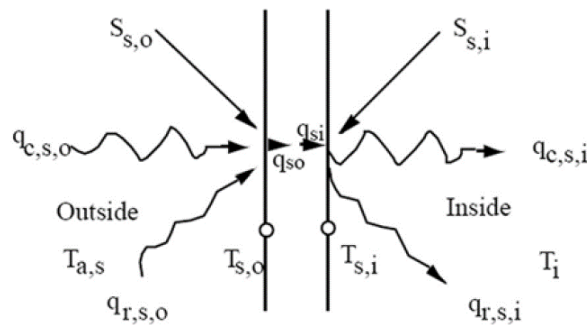


Fig. 3.15 Surface heat fluxes and temperatures. $S_{s,i}$ is radiation heat flux absorbed at the inside surface, $S_{s,o}$ is the radiation heat flux absorbed at the outside surface, $q_{r,s,i}$ net radiative heat transfer with all other surfaces within the zone, $q_{r,s,o}$ is net radiative heat transfer with all surfaces in view of the outside surface, $q_{w,g,i}$ is user defined heat flux to the wall or window surface, $q_{s,i}$ is the conduction heat flux from the wall at the inside surface, $q_{s,o}$ is the conduction heat flux into the wall at the outside surface, $q_{c,s,i}$ is the convective heat flux from the inside surface to the zone air, $q_{c,s,o}$ is the convective heat flux to the outside surface from the boundary/ambient, $T_{s,i}$ is the inside surface temperature, and $T_{s,o}$ is the outside surface temperature.

3.8.3 Input weather data for TRNSYS simulation

TRNSYS is capable of accepting many forms of input weather data. In this study, we mainly use two types of weather data. The first type is based on the field measurement. This data were used to validate the TRNSYS model. The second type is the weather data resulted from WRF simulations. The WRF simulations in this study were conducted for the current and future weather conditions. Therefore, the resulted weather data from WRF can be used as the input weather data in TRNSYS to assess the indoor thermal environment and energy performance of a residential building under the current and future weather conditions.

In this study, five weather variables were used as input weather data of TRNSYS simulation. They are air temperature, relative humidity, wind speed and direction, air pressure, and solar radiation. Each of the weather variable was prepared in the format of daily average which were spatially (i.e. for existing and new urban areas) and temporally (i.e. hourly and days with prevailing wind direction) averaged (Fig. 3.16). This final result is a one diurnal average weather condition which was then multiplied by seven to fourteen times to create the weekly variation of weather data. This weather data were used in the TRNSYS simulation.

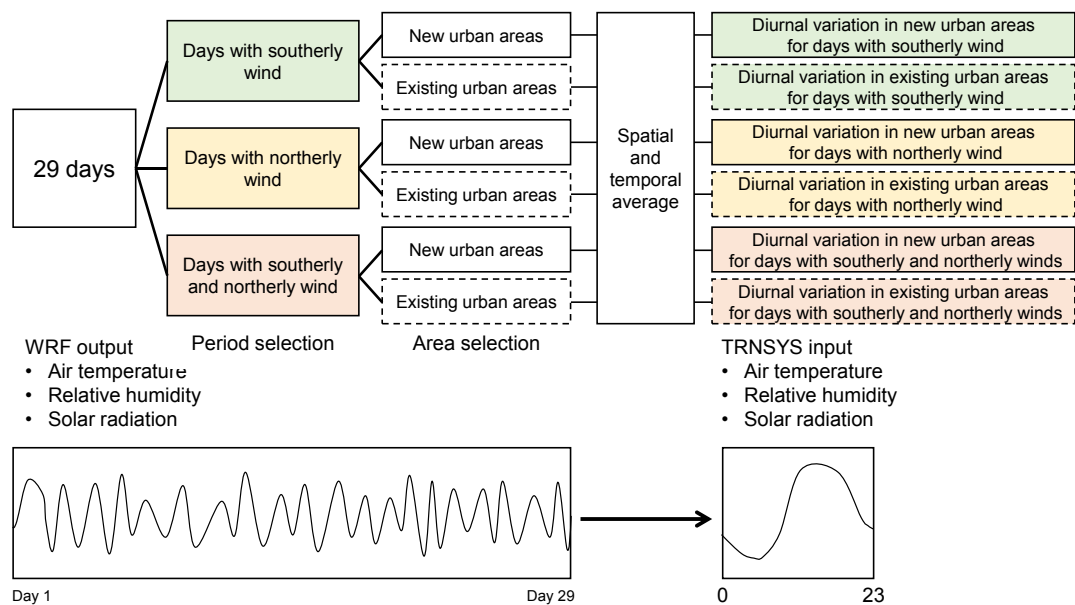


Fig. 3.16 Flowchart of input weather data preparation. The illustrative figures describe the characteristics of data between the WRF output and the input data for TRNSYS.

References

- Ching, J. K. S. (2013). A perspective on urban canopy layer modeling for weather, climate and air quality applications. *Urban Climate*, 3, 13–39.
- Jankov, I., Gallus, W. a., Segal, M., Shaw, B., & Koch, S. E. (2005). The Impact of Different WRF Model Physical Parameterizations and Their Interactions on Warm Season MCS Rainfall. *Weather and Forecasting*, 20(2001), 1048–1060.
- Jankov, I., Gallus Jr., W. A., Segal, M., Shaw, B., & Koch, S. E. (2005). The impact of different WRF model physical parameterizations and their interactions on warm season MCS rainfall. *Weather and Forecasting*, 20, 1048–1060.
- Kimura, F. (1989). Heat-Flux on Mixtures of Different Land-Use Surface-Test of a New Parameterization Scheme. *Journal of the Meteorological Society of Japan*, 67(June), 401–409.
- Klein, S. A., Duffie, J. A., Mitchell, J. C., Kummer, J. P., Thornton, J. W., Bradley, D. E., ... Kummert, M. (2007). Multizone Building Modelling with Type 56 and TRNBuild. In *Trnsys 16-a Transient System Simulation Program* (Vol. 6, pp. 1–11). Madison, USA.
- Klein, S. A., Duffie, J. A., Mitchell, J. C., Kummer, J. P., Thornton, J. W., Bradley, D. E., ... Kummert, M. (2009). Getting Started. In *TRNSYS 17: A Transient System Simulation Program* (Vol. 1, pp. 1–79). Madison, USA.
- Knutti, R., & Sedláček, J. (2012). Robustness and uncertainties in the new CMIP5 climate model projections. *Nature Climate Change*, 3(October), 1–5.
- Kusaka, H., & Kimura, F. (2004). Coupling a Single-Layer Urban Canopy Model with a Simple Atmospheric Model: Impact on Urban Heat Island Simulation for an Idealized Case. *Journal of the Meteorological Society of Japan*, 82(1), 67–80.
- Kusaka, H., Kondo, H., Kikegawa, Y., & Kimura, F. (2001). A simple single-layer urban canopy model for atmospheric models: Comparison with multi-layer and slab models. *Boundary-Layer Meteorology*, 101(3), 329–358.
- Laprise, R. (1992). The Euler Equations of Motion with Hydrostatic Pressure as an Independent Variable. *Monthly Weather Review*.
- McGuffie, K., & Henderson-Sellers, A. (2005). *A Climate Modelling Primer* (Third Edit). Chichester, West Sussex, England: John Wiley & Sons, Ltd.
- Mirzaei, P. A. (2015). Recent challenges in modeling of urban heat island. *Sustainable Cities and Society*, 19, 200–206.

- Mirzaei, P. a., & Haghghat, F. (2010). Approaches to study Urban Heat Island – Abilities and limitations. *Building and Environment*, 45(10), 2192–2201.
- Riahi, K., Rao, S., Krey, V., Cho, C., Chirkov, V., Fischer, G., ... Rafaj, P. (2011). RCP 8.5- A scenario of comparatively high greenhouse gas emissions. *Climatic Change*, 109(1), 33–57.
- Skamarock, W. C., Klemp, J. B., Dudhi, J., Gill, D. O., Barker, D. M., Duda, M. G., ... Powers, J. G. (2008). A Description of the Advanced Research WRF Version 3. *Technical Report*, (June), 113.
- Taylor, K. E., Stouffer, R. J., & Meehl, G. A. (2012). An overview of CMIP5 and the experiment design. *Bulletin of the American Meteorological Society*, 93(4), 485–498.
- Tewari, M., Chen, F., Kusaka, H., & Miao, S. (2007). *Coupled WRF/Unified Noah/urban-canopy modeling system. NCAR WRF Documentation.*
- Thomson, A. M., Calvin, K. V., Smith, S. J., Kyle, G. P., Volke, A., Patel, P., ... Edmonds, J. A. (2011). RCP4.5: A pathway for stabilization of radiative forcing by 2100. *Climatic Change*, 109(1), 77–94.
- van Vuuren, D. P., Edmonds, J., Kainuma, M., Riahi, K., Thomson, A., Hibbard, K., ... Rose, S. K. (2011). The representative concentration pathways: An overview. *Climatic Change*, 109(1), 5–31.
- Watanabe, M., Suzuki, T., O’Ishi, R., Komuro, Y., Watanabe, S., Emori, S., ... Kimoto, M. (2010). Improved climate simulation by MIROC5: Mean states, variability, and climate sensitivity. *Journal of Climate*, 23(23), 6312–6335.

4

Impacts of land use changes on urban climate: Case studies of Hanoi and Johor Bahru

4.1 Objectives

The main interest of this chapter is to evaluate the urban climate before and after the implementation of the master plans in Hanoi and JB, respectively. In general, the WRF simulations were conducted under two land use conditions. The former depicts the LULC of current status while the latter scenario represents the LULC of the master plan. The simulations for the current status and master plan scenarios were conducted under the same weather condition so that the impacts of land use changes to the urban warming can be observed.

4.2 Scenarios for numerical experiments

4.2.1 Simulation scenarios for Hanoi case study

In order to investigate the influence of the land use change proposed in the master plan to the urban thermal environment in Hanoi, two land use conditions were assessed, namely

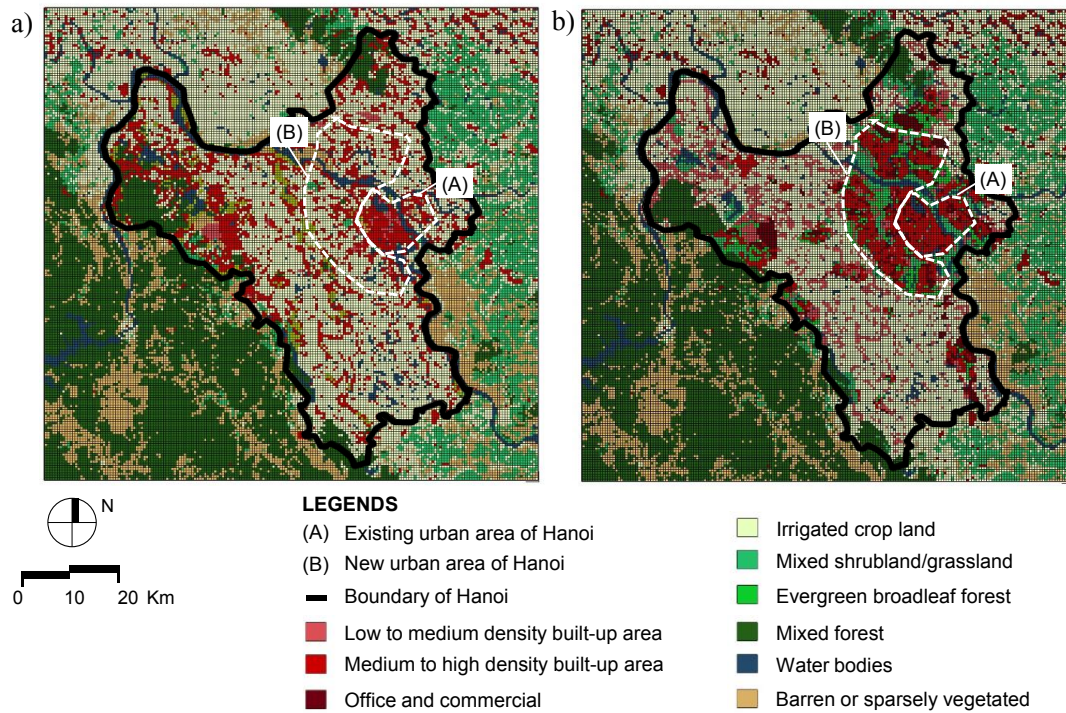


Fig. 4.1 (a) Land use and land cover (LULC) of current condition in 2010 for domain 3 and (b) LULC of the Hanoi Master Plan 2030. Since the land use data from VIUP were available only within the administrative boundary of Hanoi City, the surrounding areas of Hanoi City in domain 3 were covered by the Landsat 8 imagery (acquired in 2013) and assumed to be unchanged even in the master plan condition.

case 1 and case 2-1, respectively. The simulations for both cases were conducted under the same weather condition, which was in June 2013. The monthly average air temperature in June 2013 was 33.6 °C, relatively close to the average air temperature in June over the 15-year period from 2000 to 2015 of 33.71 °C (see Appendix B). Therefore, June 2013 can represent the average summer condition in Hanoi.

Case 1 depicts the current land use condition of Hanoi City. The LULC data within Hanoi's administrative boundary for case 1 were produced using the digital land use data of 2010 obtained from VIUP (in Geographic Information System (GIS) format). Meanwhile, case 2-1 represents the proposed land use plan in the Hanoi Master Plan 2030. The LULC maps of domain 3 for both cases are shown in Fig. 4.1. The land use data for both cases were available only within the administrative boundary of Hanoi City. Therefore, the surrounding areas of Hanoi City in domain 3 were covered by the Landsat 8 satellite images (acquired in 2013) and assumed to be unchanged even in the master plan condition. The process of combining the digital land use data with Landsat 8 imagery is outlined in Appendix A.

4.2.2 Land use proportion in current and master plan conditions of Hanoi

Fig. 4.2 shows the proportion of all land use categories within the existing and new urban areas in cases 1 and 2-1, respectively. The proportions shown in Fig.4.2 were based on the number of meshes for each land use category within the areas defined as new and existing urban areas in domain 3, respectively (see Fig. 4.1). In existing urban areas, the proportion of built-up land increases by 19%, from 51% in current condition to 70% in the master plan condition, respectively. Most of the land use conversions take place in the irrigated cropland, barren or sparsely vegetated land, and water bodies. Moreover, the proportion of mixed shrubland/grassland increases from 3% to 12% mostly due to the green belts proposed in the master plan. Meanwhile, in the new urban areas, the proportion of built-up land increases by 28%. In contrast, the proportion of irrigated cropland decreases dramatically from 60% to 11%. Most of the irrigated cropland in new urban areas are converted not only into built-up land but also for the proposed green spaces (i.e. green belt and green buffer). In both new and existing urban areas, the evergreen broadleaf forest emerges as the new land use category. This newly emerged land use category is the part of the proposed green spaces in the master plan.

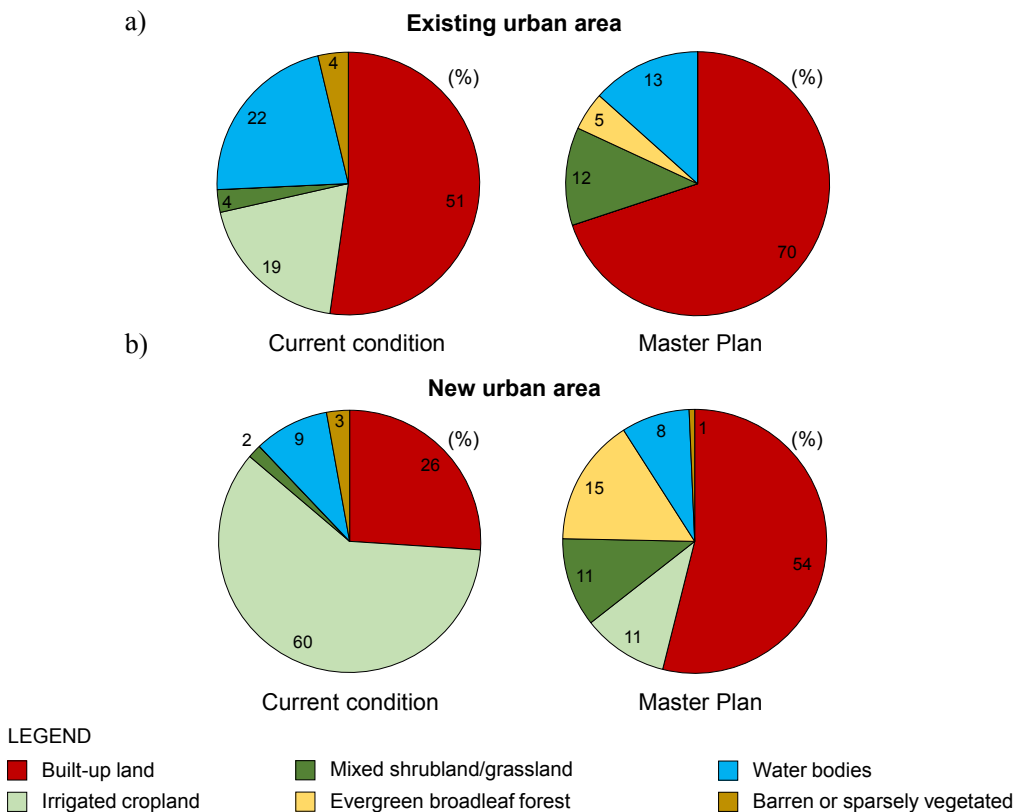


Fig. 4.2 Land use proportions in (a) existing and (b) new urban areas in the current and master plan conditions of JB.

4.2.3 Simulation scenarios for JB case study

Similar to Hanoi case study, the JB case study also proposed two scenarios, namely case 1 and case 2 which represent the LULC of current and master plan conditions, respectively. The land use plan in 2008 was used in case 1 while case 2 employed the land use plan for 2025 proposed by the CDP. The land use maps of domain 3 are shown in Fig. 4.3. Both land use datasets were in GIS format and were obtained from IRDA. The digital land use data only cover the area within the administrative boundary of Iskandar Malaysia. Therefore, Landsat 8 imagery (acquired in 2013) was used for the area outside Iskandar Malaysia and remained unchanged even in the master plan condition. The process of combining digital land use data and satellite images is given in Appendix C.

The simulations for both cases were conducted in June 2009. Based on the analysis of the weather records from 2000 to 2013, the year 2009 has the average annual temperature of 27.35 °C, relatively close to the average air temperature over 13 years, which was 27.26 °C. Therefore, the year 2009 could represent the average weather condition in JB. Then, the month of June was chosen to represent the southwest monsoon month. The analysis of wind directions in JB is shown in Appendix D.

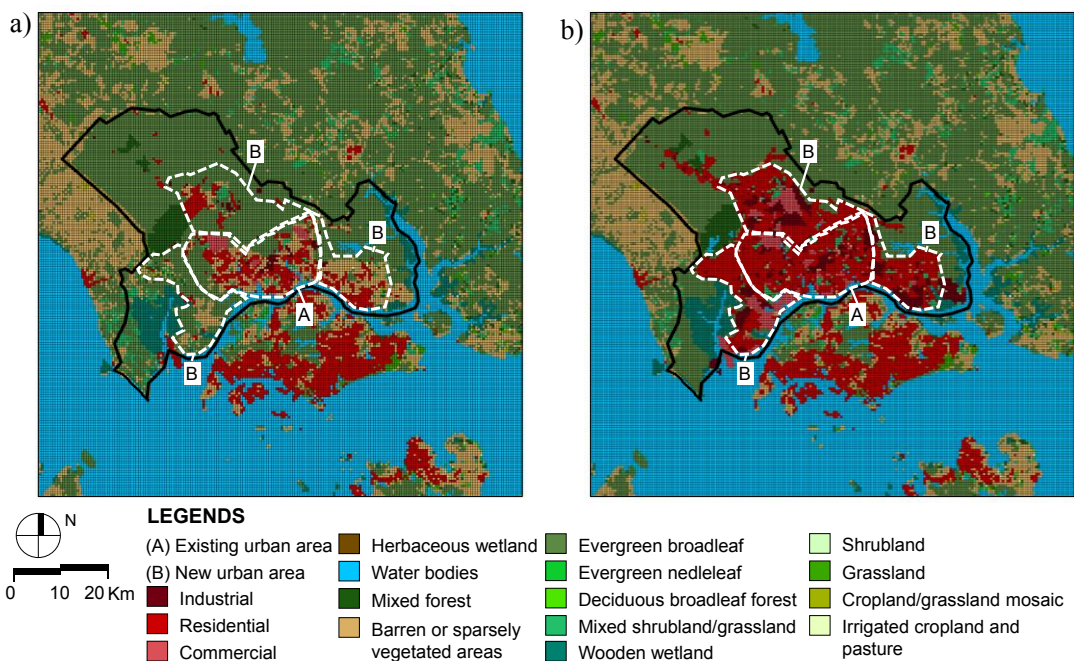


Fig. 4.3 LULC used in domain 3 for (a) case 1 (i.e. current condition) and (b) case 2 (i.e. the CDP). Since the land use data were available only within the administrative boundary of Iskandar Malaysia, the surrounding areas of Iskandar Malaysia in domain 3 were covered by the Landsat 8 imagery (acquired in 2013) and assumed to be unchanged even in the master plan condition. The existing urban areas also represent the existing city center of Johor Bahru City.

4.2.4 Land use proportions in current and master plan conditions of JB

Fig. 4.4 shows the proportions of land use categories within the existing and new urban areas in cases 1 and 2, respectively. In general, the proportions of built-up land increases dramatically after the implementation of the master plan by up to 54.6% and 32.9% in existing and new urban areas, respectively. The increase of built-up land in existing urban areas is higher than in new urban areas because JB is relatively a sprawled city, which has plenty of vacant lands even within the area of the urban core. Many land use conversions into built-up land take place in those vacant lands (i.e. barren or sparsely vegetated land). This land use category accounts for the second largest proportion of non-built-up lands in existing and new urban areas of case 1. Moreover, in both existing and new urban areas, most of the land conversion into built-up land take place in the evergreen broadleaf forest. The evergreen broadleaf forest is the land use category to represent the palm oil plantation which abundantly exists in the non-urbanized areas of JB.

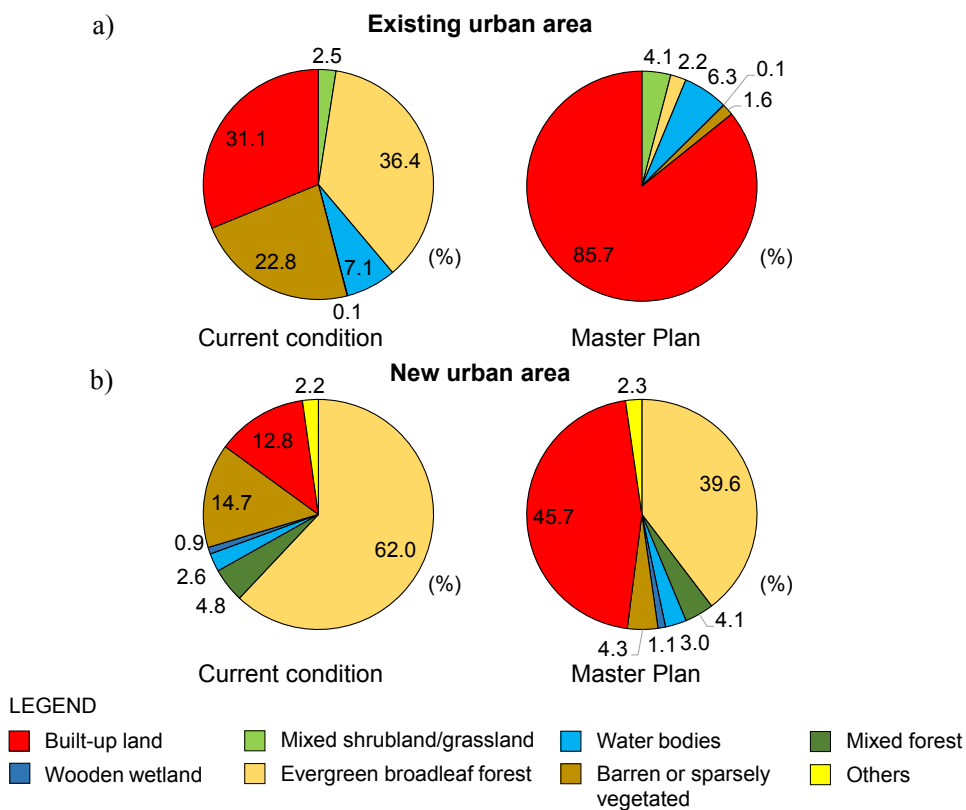


Fig. 4.4 Land use proportions in (a) existing and (b) new urban areas of JB.

4.3 WRF model configuration and validation

4.3.1 WRF model configuration and validation of Hanoi case study

The WRF model of case 1 was simulated from 00:00 UTC 12 to 00:00 24 June 2013. The urban canopy model (UCM) was set up with default parameterisation (see Chen et al. (2011) for simulation of the effect of urban geometries on urban climate (Kusaka et al. 2001). In order to run WRF with UCM, the urban areas of JB need to be classified into three categories, which were named as follows: (1) low- to medium-density built-up area, (2) medium- to high-density built-up area, and (3) office and commercial. The process of urban land use classification for UCM is outlined in Appendix E. The model configurations and physics schemes used in numerical experiments are listed in Table 4.1.

The initial and boundary conditions for WRF simulation were imposed by the NCEP FNL data from June 2013. The simulation results were compared with the observational data from the weather station located in Noibai International Airport in Hanoi (see the location in Fig. 1.4).

The validation results are shown in Fig. 4.5. The observed wind speeds were adjusted to the 10-m winds above the ground, according to the power law for vertical wind profiles. The calculated wind direction was not adjusted. Overall, the simulated air temperature at 2 m above the surface is in agreement with the observed values, with a coefficient of determination of 0.789. Moreover, the calculated wind speed and direction at Nobai are fairly in accordance with the observed values with the coefficient of determination for wind speed of 0.30 unlike the modelled winds at coastal and offshore sites with high correlation coefficient compared to observed data (Lee 2015).

Table 4.1 WRF model configuration of Hanoi case study

| Physics/parameterization | Domain 1 | Domain 2 | Domain 3 |
|----------------------------|---|----------------|---|
| Horizontal resolution (km) | 4.5 | 1.5 | 0.5 |
| Domain size (km) | 990 x 990 | 312 x 312 | 98 x 98 |
| Land use and land cover | USGS (default) | USGS (default) | Landsat 8 imagery combined with digital land use data |
| Vertical layers | 30 | | |
| Microphysics | WRF single-moment 3-class scheme | | |
| Longwave radiation | Rapid Radiative Transfer Model (RRTM) scheme | | |
| Shortwave radiation | Dudhia scheme | | |
| Surface-layer | MM5 similarity based on Monin-Obukhov scheme | | |
| Land surface model | Noah Land Surface Model (LSM) and Single layer UCM with default urban parameterisations | | |
| Planetary boundary layer | Yonsei University (YSU) Scheme | | |
| Simulation period | 00:00 UTC 12 to 00:00 UTC 24 June 2013 (for validation purpose) | | |

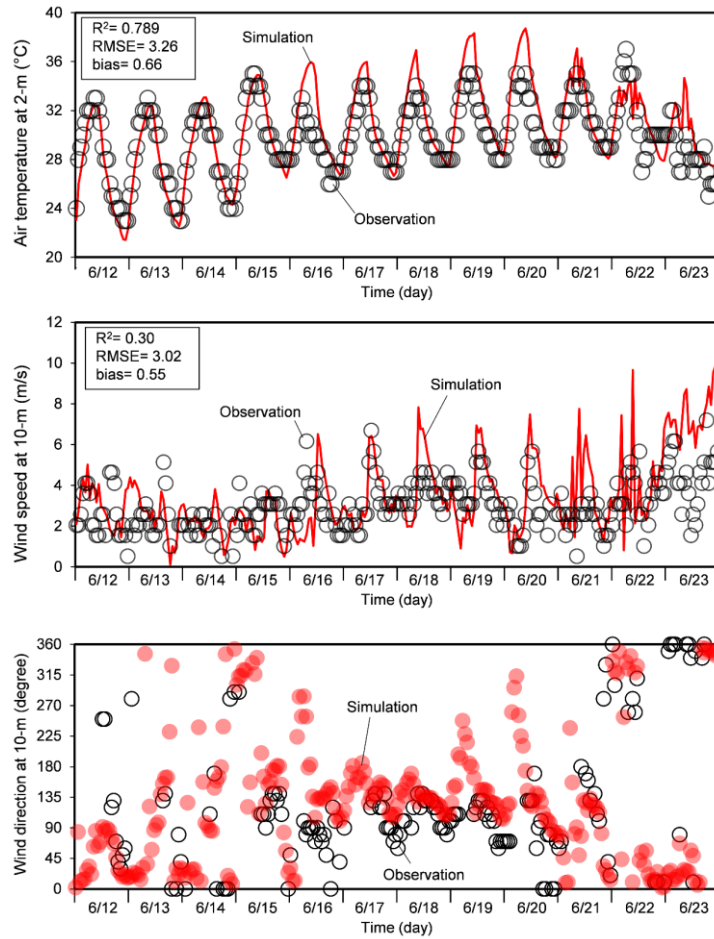


Fig. 4.5 Comparisons between observed (blank dots) and simulated air temperature (red line), wind speed (red line) and direction (red dots) at Noibai weather station, 21.22 °N and 105.8072 °E (see location in Fig. 1.4). Current land use and land cover data for domain 3 are used for the model validation purpose.

4.3.2 WRF model configuration and validation of JB case study

For the model validation purpose, the WRF model of case 1 was simulated from 00:00 UTC 12 June 2013 to 00:00 18 June 2013. The simulation period for model validation was chosen following the acquisition of the Landsat-8 imagery that was used in this study. Table 4.2 shows the WRF model configuration and parameterization for three domains.

UCM option with three urban categories was employed. Unlike in Hanoi case study, in JB case study, we analyzed the average building coverage ratio, average building height, and thermal properties of average building materials for each urban category. The results were used in the urban parameterization for UCM. Further, UCM requires three urban categories, however, the digital land use data of current condition has 21 categories for urban land use. For example, the land use for residential is divided into low-, medium- and high-density residential; the land use for the industry has three categories; and so on. Hence, we classified/simplified the urban land uses in the digital datasets into only three categories. The process of urban classification are outlined in Appendix F. As the results of urban classification, we obtained three urban categories which were described as (1) commercial, (2) residential, and (3) industrial, respectively.

In this chapter, the additional heat from anthropogenic heat emission is not considered. This topic is discussed separately in Chapter 7 (i.e. Influence of anthropogenic heat emission on urban climate: A case study of JB). Nevertheless, the AH releases were considered for the model validation. We assumed that the urban parameterization of UCM remains unchanged even in the master plan condition. The urban parameterisations for each urban category are listed in Table 4.3. Other parameters that are not listed in the table use the default values which have been set in URBPARAM.TBL (i.e. default input data table for UCM in the WRF).

Table 4.2 WRF model configuration of JB case study

| Physics/parameterization | Domain 1 | Domain 2 | Domain 3 |
|----------------------------|---|----------------|---|
| Horizontal resolution (km) | 4.5 | 1.5 | 0.5 |
| Domain size (km) | 922.5 x 922.5 | 298.5 x 298.5 | 102.5 x 102.5 |
| Land use and land cover | USGS (default) | USGS (default) | Landsat 8 imagery combined with digital land use data |
| Vertical layers | 30 | | |
| Microphysics | WRF single-moment 3-class scheme | | |
| Longwave radiation | Rapid Radiative Transfer Model (RRTM) scheme | | |
| Shortwave radiation | Dudhia scheme | | |
| Surface-layer | MM5 similarity based on Monin-Obukhov scheme | | |
| Land surface model | Noah Land Surface Model (LSM) and Single layer UCM | | |
| Planetary boundary layer | Yonsei University (YSU) Scheme | | |
| Simulation period | 00:00 UTC 12 to 00:00 UTC 18 June 2013 (for validation purpose) | | |

Table 4.3 The urban parameter table for Single layer UCM.

| Parameters | Description (unit) | Industrial | Residential | Commercial |
|------------|--|--------------------|-------------------|--------------------|
| ZR | Roof level/building height (m) | 8 | 8 | 10 |
| SIGMA_ZED | Standard deviation of roof height (m) | 1 | 1 | 2 |
| ROOF_WIDTH | Roof (i.e. building) width (m) | 10 | 10 | 10 |
| ROAD_WIDTH | Road width | 10 | 10 | 10 |
| AHOPTION | 0: no anthropogenic heating, 1: anthropogenic heating will be added to sensible heat flux term | 1 | 1 | 1 |
| AH | Anthropogenic heat ($W m^{-2}$) | 180 | 31 | 116 |
| FRC_URB | Fraction of the urban landscape which does not have natural vegetation | 0.5 | 0.3 | 0.4 |
| CAPR | Heat capacity of roof ($J m^{-3} K^{-1}$) | 3.5×10^6 | 1.5×10^6 | 1.75×10^6 |
| CAPB | Heat capacity of building wall ($J m^{-3} K^{-1}$) | 1.75×10^6 | 1.5×10^6 | 1.75×10^6 |
| CAPG | Heat capacity of ground/road ($J m^{-3} K^{-1}$) | 1.6×10^6 | 1.6×10^6 | 1.6×10^6 |
| AKSR | Thermal conductivity of roof ($J m^{-2} s^{-1} K^{-1}$) | 30 | 1 | 1.3 |
| AKSB | Thermal conductivity of building wall ($J m^{-2} s^{-1} K^{-1}$) | 1.3 | 0.8 | 1.3 |
| AKSR | Thermal conductivity of ground/road ($J m^{-2} s^{-1} K^{-1}$) | 0.7 | 0.7 | 0.7 |
| ALBR | Surface albedo of roof (fraction) | 0.8 | 0.3 | 0.65 |
| ALBB | Surface albedo of building wall (fraction) | 0.6 | 0.6 | 0.6 |
| ALBG | Surface albedo of ground/road (fraction) | 0.2 | 0.2 | 0.2 |
| EPSR | Surface emissivity of roof | 0.3 | 0.9 | 0.9 |
| EPSB | Surface emissivity of building wall | 0.9 | 0.6 | 0.9 |
| EPSG | Surface emissivity of ground/road | 0.95 | 0.95 | 0.95 |

Note: Other parameters that are not listed in this table use the default values.

The simulated results of case 1 were compared with the observed data from four weather stations located in Johor Bahru and Singapore. The results of the model validation for air temperature at 2 m above ground and wind speed and direction at 10 m height at Senai weather station are shown in Fig. 4.6. The validation results at other stations can be seen in Appendix G. In general, the simulation results for air temperature and wind conditions show a good agreement with the observed data.

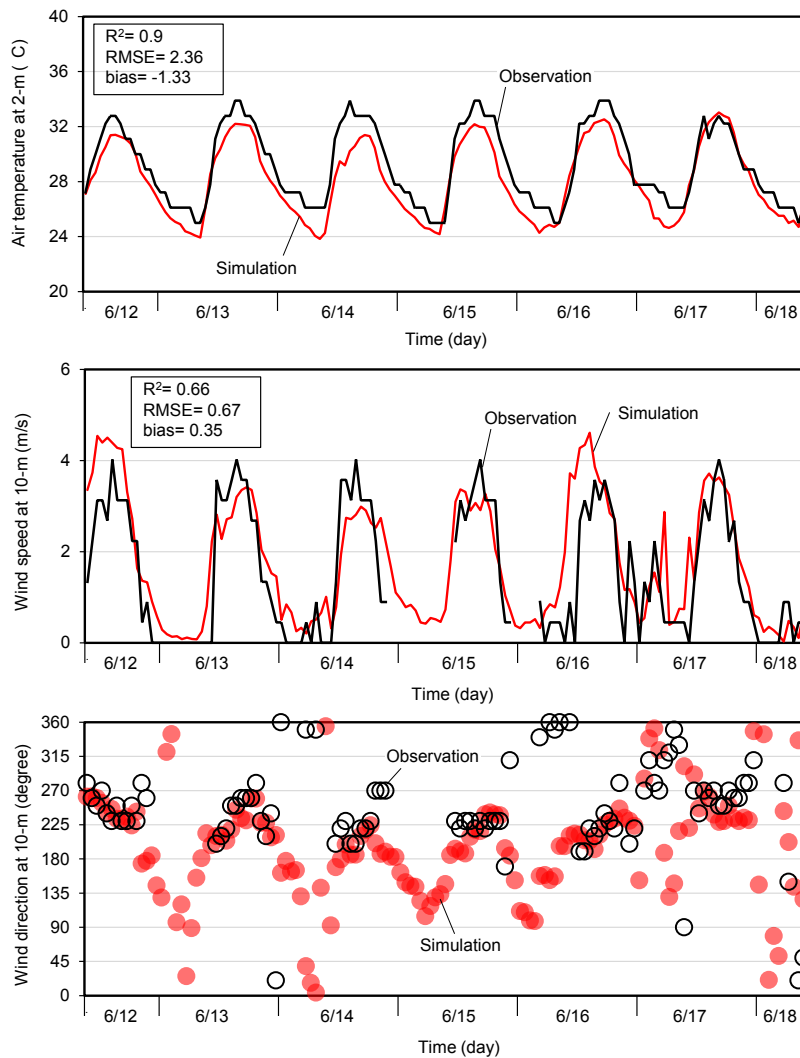


Fig. 4.6 Comparisons between observed (blank dots) and simulated air temperature (red line), wind speed (red line) and direction (red dots) at Senai weather station (see location in Fig. 1.5). Current land use and land cover data for domain 3 are used for the model validation purpose. The WRF simulation considered the anthropogenic heating.

4.4 Results and discussion

4.4.1 Hanoi case study

Air temperature distribution of current status and master plan

This section discusses the results from cases 1 and 2–1. The WRF simulations for the two cases were conducted under the same climatic condition that represents the average summer weather in Hanoi; therefore, the impacts of land use changes on UHIs can be determined. The analysis in this section shows the temporally averaged results from the days with prevailing south-easterly winds (winds coming from directions between 90° and 180°).

Figs. 4.5 and 4.6 illustrate the average air temperature distributions at 2 m above the surface and the wind directions at 10 m above the surface for all cases at 1:00 and 14:00, respectively. In general, the average air temperatures in urban areas during the daytime are up to 1 °C higher than those over surrounding agricultural fields (i.e., rural areas). The discrepancy in average air temperature between urban and rural areas becomes more significant at night than that of the daytime when the air temperature difference reaches 2 °C.

In the current conditions (case 1), the maximum nocturnal average air temperatures are approximately 30–31 °C. The peak average air temperature of 31 °C is generally observed in urban areas (Fig. 4.7a). At night, due primarily to the implementation of the master plan, hotspots expand widely following the spread of new urban areas in case 2–1 (Fig. 4.7b).

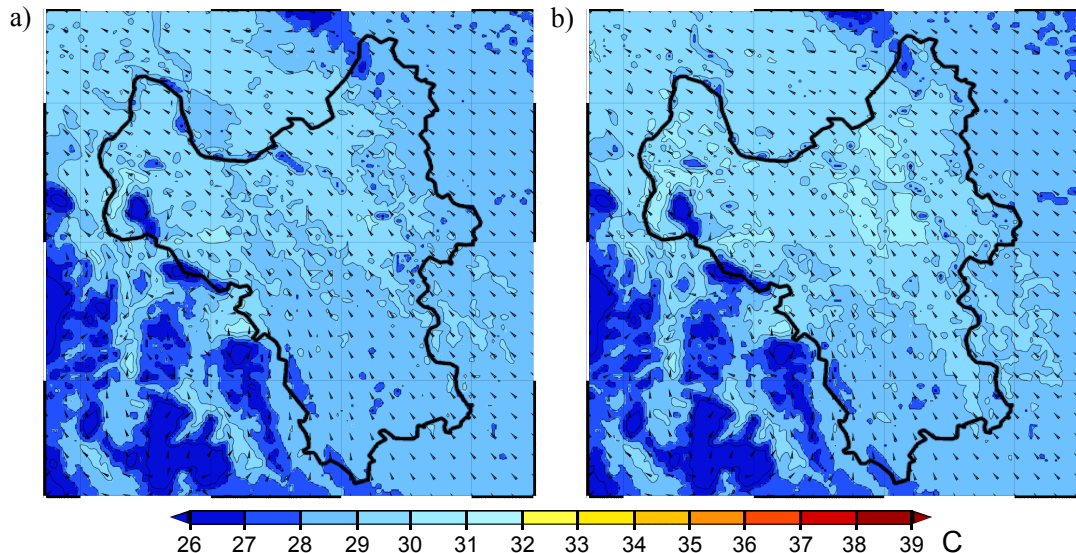


Fig. 4.7 Spatial distribution of average air temperature at 2m and wind directions at 10 m above the surface at 1:00 for (a) case 1 and (b) case 2–1. The black line highlights the boundary of Hanoi City.

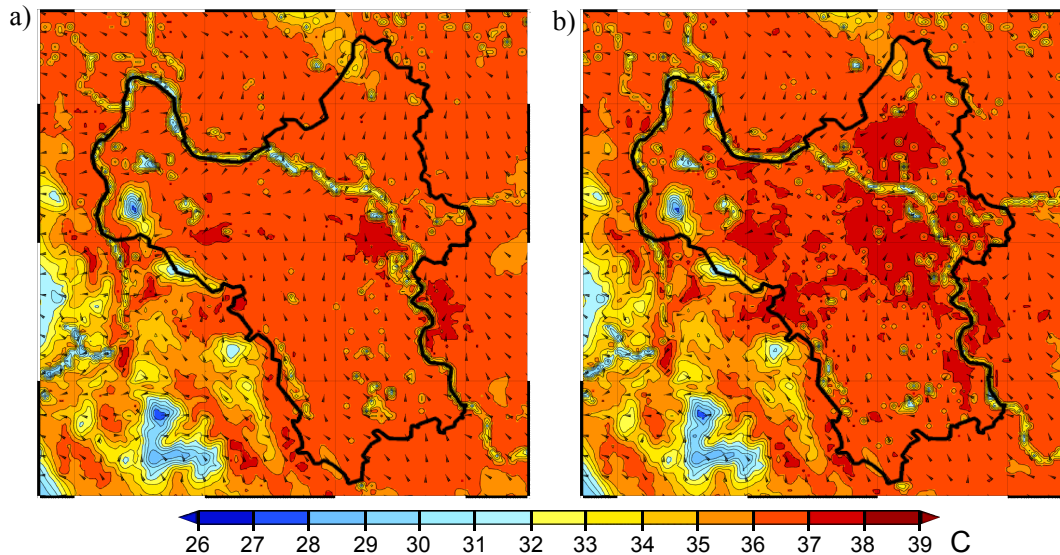


Fig. 4.8 Same as Fig. 4.7 but at 14:00

Moreover, the number of hotspots with the average temperature of 31 °C increases significantly both in existing and new urban areas (see the location of urban areas in Fig. 4.1). The average air temperature in the newly emerged hotspots increases by up to 2 °C over that of the same areas in case 1.

During the daytime, peak average air temperatures are observed in most parts of the urban areas in both cases (Fig. 4.8a and b). Although the peak average air temperatures remain almost at the same level even after the implementation of the master plan, the new hotspots with temperatures between 37 and 38 °C expand over the newly developed urban areas in case 2–1 (Fig. 4.8b). The average air temperature in those newly emerged hotspots increases by up to 1 °C over that of the same areas in case 1.

Distribution of air temperature in existing and new urban areas by land use category

Figs. 4.9 and 4.10 show the distributions of average air temperatures at 2 m above the surface for different land use categories in existing urban areas of cases 1 and 2–1 at 14:00 and 1:00, respectively. At 14:00, in case 1, the average air temperatures of built-up lands in existing urban areas range between 37 and 38 °C, with the mode value of 37.5 °C. Furthermore, the area with the peak air temperature of 38 °C accounts for 18.5% of the total area in existing urban. The irrigated cropland accounts for the largest proportion of vegetative land use in existing urban areas, with the average air temperature ranges between 36.5 and 37.5 °C. Most of the irrigated cropland experience the air temperature of 37 °C, which is 0.5 to 1 °C lower than that of built-up lands. Water bodies, which are abundant in Hanoi in the form of rivers, lakes, and small ponds, experience the average air temperatures of 37 and 37.5 °C in most of their areas (Fig. 4.9a).

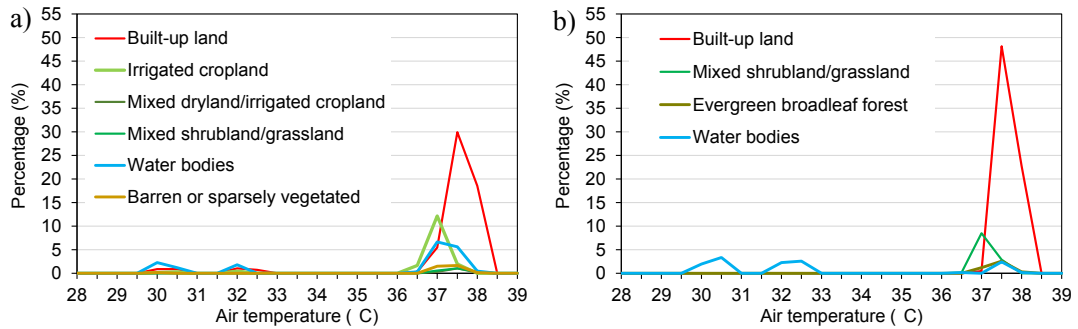


Fig. 4.9 Frequency distributions of air temperatures area by land use category at 14:00 in the existing urban for (a) case 1 and (b) case 2-1. The air temperatures are the temporal-averaged air temperatures calculated from the days with prevailing south-easterly winds.

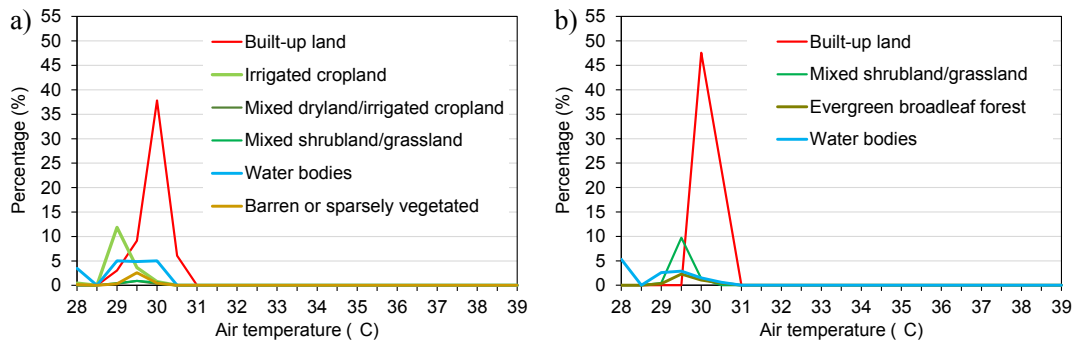


Fig. 4.10 Same as Fig. 4.9 but at 1:00.

After the implementation of the master plan (i.e. case 2–1), the amount of built-up land significantly increases while the irrigated cropland decreases (Fig. 4.9b). The air temperature range in the built-up land remains the same with that of case 1. Nevertheless, if compared with case 1, the number of built-up areas with relatively low air temperature zones (i.e. 36.5 and 37 °C) decrease and likely shift to higher air temperature zones (i.e. 37.5 and 38 °C). This results in the increases of the percentages of built-up lands with average air temperatures of 37.5 and 38 °C by up to 18% and 4%, respectively. This shows that the master plan will likely increase the average air temperature by 0.5 °C in existing urban areas during the daytime. Meanwhile, mixed shrubland/grassland accounts for the largest proportion of vegetative land cover, with the air temperature range between 36.5 and 37.5 °C, and with the mode value of 37 °C (Fig. 4.9b).

At night, in case 1, the average air temperatures of the built-up land in existing urban areas range between 29 and 30.5 °C with the mode value of 30 °C (Fig. 4.10a). Approximately only 6% of the built-up land experience the peak average air temperature of 30.5 °C. The average air temperatures in the irrigated cropland range between 29 and 30 °C, with the mode value of 29 °C, which is 1°C lower than that of the built-up land. On the other hand, water bodies experience relatively high air temperature zones of 29 to 30 °C in most of their areas at night.

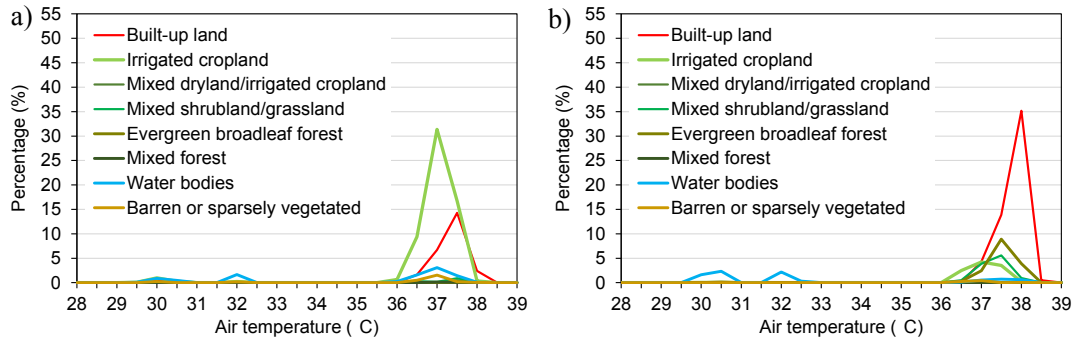


Fig. 4.11 Frequency distributions of air temperatures area by land use category at 14:00 in new urban for (a) case 1 and (b) case 2-1. The air temperatures are the temporal-average air temperatures calculated from the days with prevailing south-easterly winds.

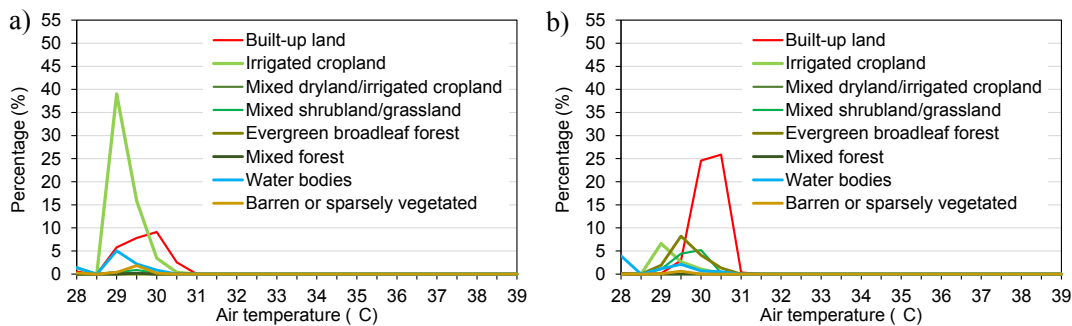


Fig. 4.12 Same as Fig. 4.11 but at 1:00.

In case 2-1, the average air temperature range of the built-up lands is between 30 and 30.5 °C with the mode value of 30 °C (Fig. 4.10b). The amount of built-up land with the average air temperature of 30 °C increases by up to 10% after the implementation of the master plan. This increase was mainly caused by the expansion of the city, inducing greater warming in existing urban areas, especially in the vicinity of existing urban areas where most of the land use changes occur. Moreover, the percentage of built-up lands with the peak air temperature of 30.5°C increases by up to 18% after the implementation of the master plan (see Fig. 4.10b). Meanwhile, the relatively low-temperature zone of 29.5°C occurs in most of the areas for the green buffer at night (i.e. mixed shrubland/grassland in Fig. 4.10b).

Figs. 4.11 and 4.12 show the distributions of average air temperatures by land use categories in new urban areas of cases 1 and 2-1 at 14:00 and 1:00, respectively. At 14:00, in case 1, the irrigated cropland accounts for the largest proportion of land use with the average air temperatures range between 36.5 and 38 °C. The built-up land accounts for the second largest proportion of land use in new urban areas with the average air temperatures range between 36.5 and 38 °C. Within the built-up land itself, most of the areas experience the average air temperatures of 37 and 37.5 °C (i.e. 7% and 14%, respectively) while the areas with the peak average air temperature of 38 °C peaking at less than 3%. However, the implementation of the master plan dramatically increases the number of areas with the peak air temperatures of 38 °C

by 33% (Fig. 4.11b). Moreover, the simulation results also show that some areas experience a higher average air temperature zone of 38.5 °C, but the proportion is less than 1% of the total built-up land. Meanwhile, the air temperature range in the proposed green spaces is between 36.5 and 38 °C with the mode value of 37.5 °C (i.e. the air temperature ranges of mixed shrubland/grassland and evergreen broadleaf forest in Fig. 4.11b).

At night, in case 1, the average air temperatures of built-up lands in new urban areas range between 29 to 30.5 °C, with the mode value of 30 °C (Fig. 4.12a). In case 2-1, the proportions of relatively low air temperature zones (i.e. 29 and 29.5 °C) decrease, while the proportions of areas with the average air temperatures of 30 and 30.5 °C increase by up to 15% and 23%, respectively. Furthermore, some areas also experience a higher temperature zone of 31°C, which does not exist in case 1. However, the proportion is very small compared to the total built-up land, which is only 0.6%. Nevertheless, the results show that the implementation of the master plan will likely lead to the increase of peak daytime and nocturnal air temperatures by up to 0.5°C particularly in new urban areas.

Meanwhile, the air temperature ranges within the proposed green spaces are generally lower than that of built-up lands. As has been mentioned, the land use category of the proposed green spaces is represented by evergreen broadleaf forest and mixed shrubland/grassland. The average air temperatures in those land use categories range between 29 and 30.5 °C, with the mode values of 29.5 and 30 °C for evergreen broadleaf forest and mixed shrubland/grassland, respectively.

Spatial distributions of air temperature differences between cases 1 and 2-1

Fig. 4.13 shows the spatial distribution of average air temperature differences between cases 1 and 2-1 at 14:00 and 1:00, respectively. Based on the figures, the specific areas that experience air temperature changes (i.e. decreased or increased) due to the implementation of the master plan can be observed. The positive values (i.e. red shaded areas) in Fig. 4.13 indicate the increase of air temperature, while the negative values (i.e. blue shaded areas) indicate the reduction of air temperature from current to master plan conditions.

In general, at night, the average air temperature increases by up to 1.5 °C (Fig.4.13a). Meanwhile during the daytime, the increases of the average air temperatures due to the implementation of the master plan range between 0.5 and 1 °C (Fig. 4.13b). The discrepancy of air temperatures between case 1 and case 2-1 is apparent particularly over the newly expanded urban areas.

In contrast, existing urban areas generally do not experience any significant temperature changes. The exception is in the eastern part of existing urban areas where many development projects are proposed in the master plan and thus lead to significant land use changes (Fig. 4.13). The average air temperature increase in that area is up to 0.5 °C in the daytime and could reach 1 °C at night. Furthermore, the thermal environment in existing urban areas is not affected by the increased air temperatures that occur in new urban areas.

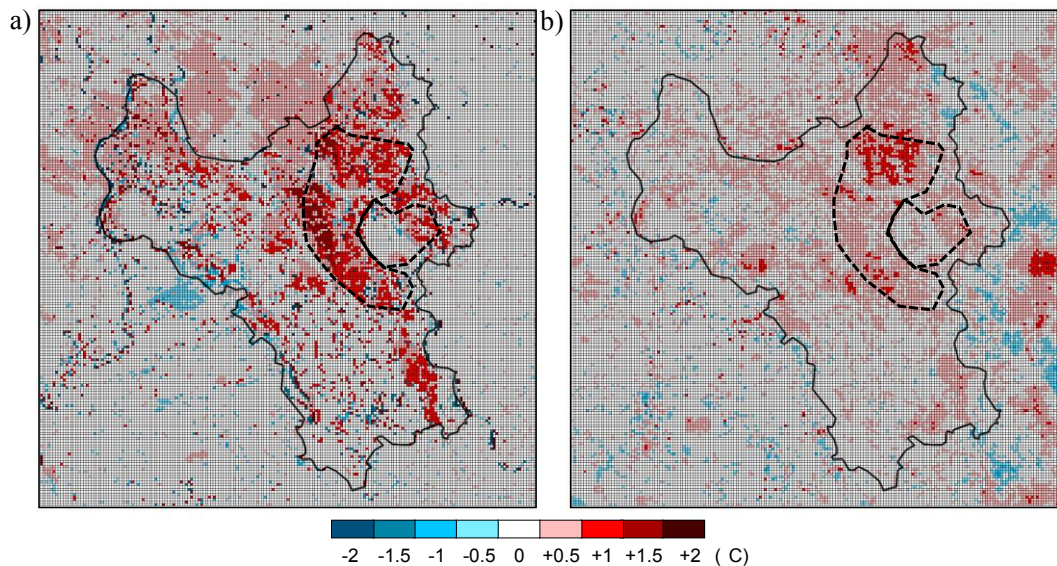


Fig. 4.13 Spatial distribution of air temperature difference between case 1 and case 2-1 at (a) 1:00 and (b) 14:00. The positive values indicate the increase of air temperature, while the negative values indicate the reduction of air temperature due to the master plan. The black line is the boundary of Hanoi, while the dashed black lines are the boundaries of existing and new urban areas as also shown in Fig.4.1.

Diurnal variation of air temperature in existing and new urban areas

Fig. 4.14 shows the diurnal variation of average air temperature of cases 1 and 2-1 in existing and new urban areas, respectively. The results shown in this figure are the temporal average of the days with prevailing southerly winds during the simulation period. As shown in Fig. 4.14a, the implementation of master plan slightly increases the average air temperature in existing urban areas both in the daytime (06:00-17:00) and night-time (00:00-05:00, 18:00-00:00). The increases in air temperature due to the land use change in those areas are by up to 0.5 °C and 0.6 °C in the daytime and night-time, respectively. In new urban areas (Fig. 4.14b), the massive land use change brought by the master plan results in a higher increase of average air temperatures than in the existing urban area, by up to 0.9°C and 1°C in the daytime and night-time, respectively.

The results are primarily in agreement with those of previous studies. For example, in the future urban climate projection for Ho Chi Ming City, Doan et al. (2016) presented that the increase in surface air temperature due to the future land use changes would be merely 0.22 °C in existing urban areas and approximately 0.41°C in the newly urbanized areas. Similarly, in Melbourne, Australia, the climatic impacts of the future master plan in the city was investigated, showing that the resultant impact was not seen to increase the peak daytime temperature due to increased storage limiting the amount of sensible heating of the atmosphere

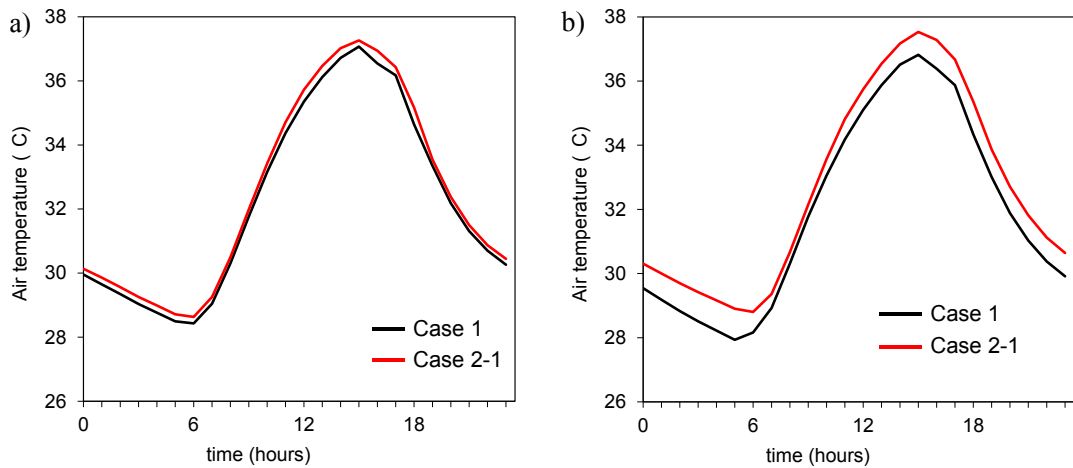


Fig. 4.14 Diurnal variation of temporal average air temperature at 2 m above the ground during in (a) existing urban area and (b) new urban area.

(Coutts et al. 2008). The case study of Sydney (Argüeso et al. 2014) obtained the similar results, concluding that urban expansion footprint was discernible in the future climate projections of all variables, except for maximum temperature and the related extremes indices that were little, or not at all, affected by urbanization. In particular, the projected land use changes were found to have a strong effect on future minimum temperature.

4.4.2 JB case study

Air temperature distribution of current status and master plan during southwest monsoon

Figs. 4.15 and 4.16 illustrate the spatial distributions of the average air temperatures at 2 m above the surface and the winds at 10 m above the surface in case 1 (current status) and case 2 (master plan) at 1:00 and 16:00, respectively. The air temperatures shown in the graphs as well as in the overall analysis of this section were the temporal average values calculated from the non-rainy days during the simulation period in June 2009 (i.e. southwest monsoon). The numbers of non-rainy days for case 1 and case 2 are 12 days and 18 days, out of 30 days, respectively.

At 1:00, in case 1, the peak nocturnal average air temperature of 28.5 °C is generally observed over the built-up lands of JB. The high air temperature zone is also observed over the rural areas of JB, particularly in those consist of barren and sparsely vegetated land (Fig. 4.15a). In case 2, the peak average air temperature of built-up land remains at the same levels with that of case 1. However, the hot temperature areas of 25-26 °C expanded over the newly developed built-up land of case 2 (Fig. 4.15b).

At night, the average air temperature of the sea ranges between 27 and 28 °C, which is as warm as those of built-up areas. The temperature of the sea remains constant for the whole day thus the sea surface temperature during the daytime is significantly lower than that of built-up areas by up to 2-3 °C. Hence, the prevailing southwesterly winds bring relatively cool sea breeze into the land. Under this condition, the built-up areas located along the seashore experience

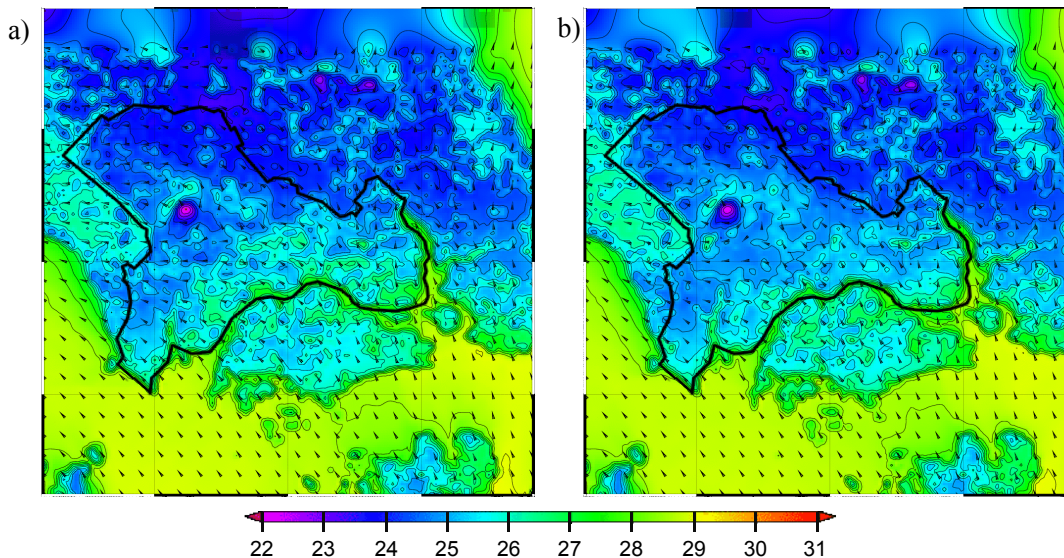


Fig. 4.15 Spatial distribution of average air temperature at 2 m and wind directions at 10 m above the surface at 1:00 for (a) case 1 and (b) case 2–1. The black line highlights the boundary of Iskandar Malaysia.

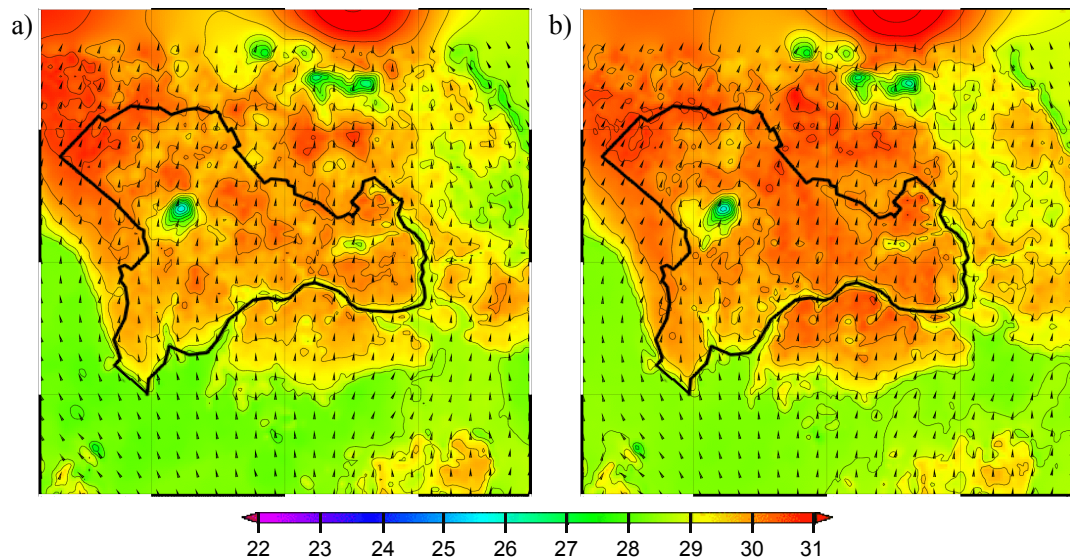


Fig. 4.16 Spatial distribution of average air temperature at 2 m and wind directions at 10 m above the surface at 16:00 for (a) case 1 and (b) case 2-1.

relatively lower average air temperatures than those in inland areas by up to 1-2 °C (Fig. 4.16). Nevertheless, JB is located approximately 20 km away from the southern sea shore of Singapore, and therefore the sea breeze is not expected to cool the urban areas in JB sufficiently.

During the daytime, in case 1, the peak air temperature observed in the built-up land is up to 30.5 °C (Fig. 4.16a). After the implementation of the master plan, the peak temperature increases by up to 0.5 °C, but it is only observed in a small portion of the area in case 2 (Fig. 4.16b). Moreover, the hot spots with air temperatures of 30-31 °C expand widely over the newly constructed areas in case 2. The average air temperature difference between built-up areas and non-built-up areas in the daytime is up to 1 °C.

Distribution of air temperature in existing and new urban areas by land use category

Fig. 4.17 shows the distribution of temporal average air temperatures in the existing urban areas by different land use categories for all cases at 1:00 and 16:00, respectively. At 1:00, in case 1, the air temperatures of built-up areas (i.e. residential, commercial and industrial) range from 24.5 to 27 °C with the mode value of 25.5 °C in commercial and residential areas. The highest temperature in the built-up area is observed in the residential land with the air temperature up to 27 °C (Fig. 4.17a). Residential land accounts for the largest proportion of built-up land in existing urban areas. Meanwhile, the barren or sparsely vegetated land is the largest proportion of non-built-up land in existing urban area. The air temperature range in this area is similar with those in residential land. Furthermore, most of the area in this land use category experience high-air temperature zones of 25.5 and 26 °C.

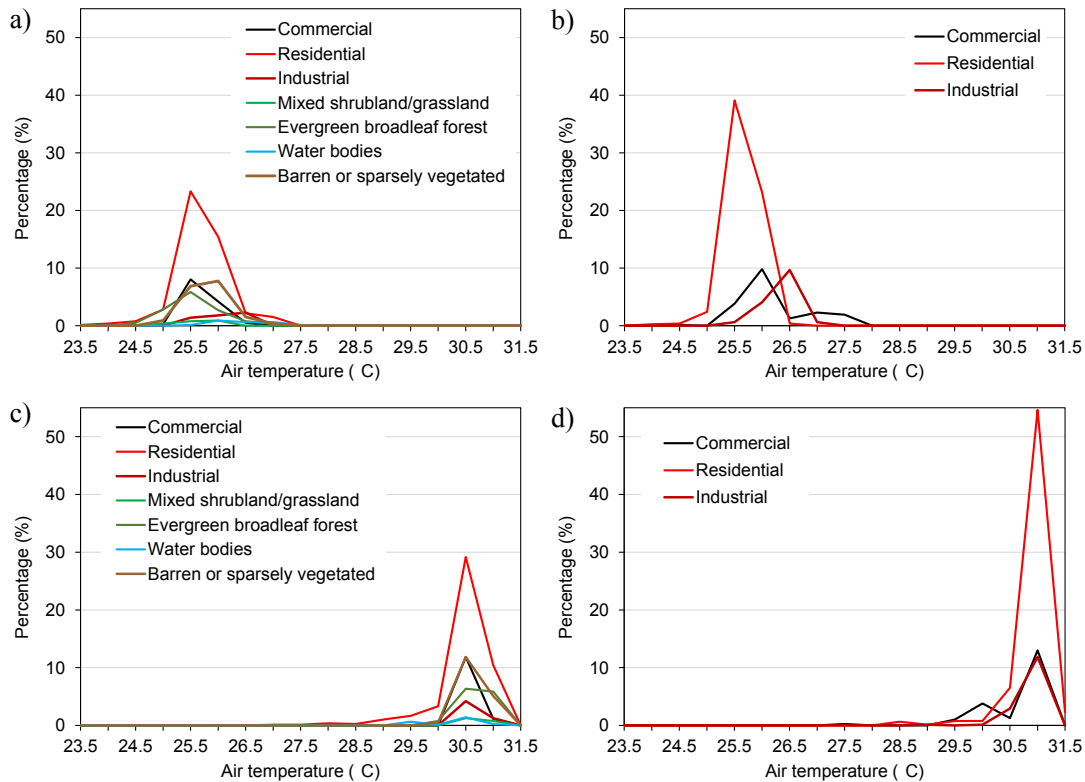


Fig. 4.17 Temporal average air temperature distribution in the existing urban areas by land use categories at 1:00 for (a) case 1 and (b) case 2; and at 16:00 for (c) case 1 and (d) case 2.

In case 2, most of the non-built-up lands in case 1 are turned into the built-up land (i.e. commercial, residential, and industrial). Hence, the proportions of the built-up lands increase significantly compared with those in case 1 (Fig. 4.17b). For instance, the residential areas with the average air temperatures of 25.5 and 26 °C increase by 16% and 8%, respectively. The peak nocturnal air temperature in the built-up area is observed in the commercial land, by up to 27.5 °C, which is 0.5 °C higher than that recorded in case 1.

In the daytime, both the temperatures of built-up and non-built-up in case 1 range between 28.5 and 31.5 °C, with the mode values of 30.5 °C in all land use categories (Fig. 4.17c). The mode values of built-up lands shift to 31°C in case 2 (Fig. 4.17d), indicating that the urban air temperature in existing areas is expected to increase by 0.5 °C due to the massive land use change proposed in the master plan.

Fig. 4.18 shows the distributions of the average air temperatures in new urban areas by different land use categories for all cases at 1:00 and 16:00, respectively. In case 1, the evergreen broadleaf forest and barren or sparsely vegetated land account for the largest proportion of land use in new urban areas (Fig. 4.18ac). At night, the average air temperatures of the evergreen broadleaf forest range from 24.5 to 27.5 °C, with the mode value of 25.5 °C.

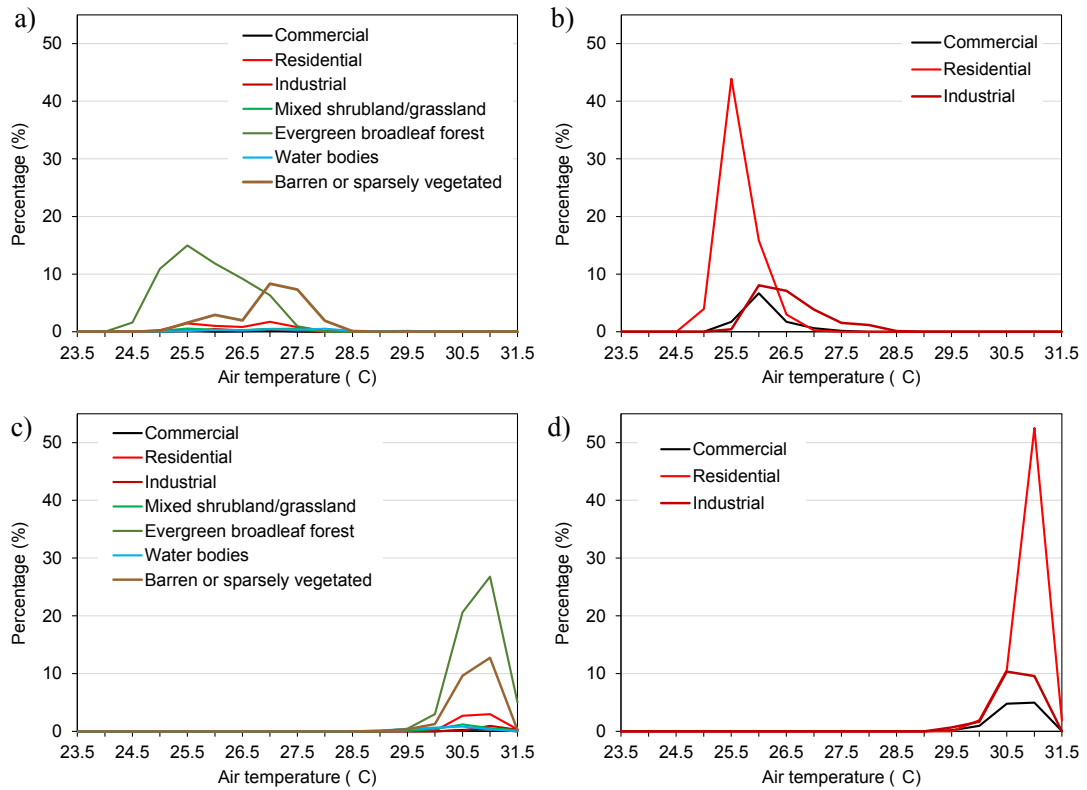


Fig. 4.18 Temporal average air temperature distribution in the new urban areas by land use categories at 1:00 for (a) case 1 and (b) case 2; and at 16:00 for (c) case 1 and (d) case 2.

In contrast, the proportion of average air temperatures in the barren or sparsely vegetated areas peaked at 27 °C and 27.5 °C, respectively. This temperature range is even higher than those of the residential land in case 2 (Fig. 4.18b). This indicates that instead of causing the temperature increases at night, the master plan might lead to the reductions in air temperature in particular areas, especially in the land use conversion within the barren or sparsely vegetated lands.

During the daytime, in case 1, the average air temperatures in the non-built-up land range between 30 and 31.5 °C, with the mode values of 30 °C. Unlike in the night-time, the air temperature range and the mode value of the non-built-up land are similar with those of the built-up lands in case 2.

Spatial distributions of air temperature differences between cases 1 and 2

Fig. 4.19 shows the spatial distributions of air temperature differences between cases 1 and 2 at 1:00 and 16:00, respectively. The positive values (i.e. red shaded areas) in Fig. 4.19

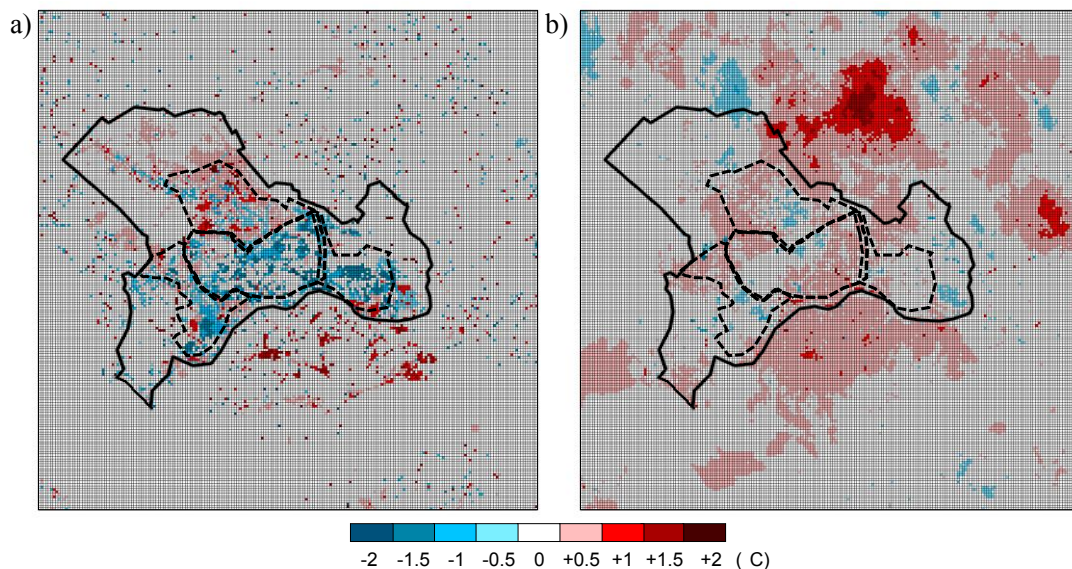


Fig. 4.19 Air temperature difference between case 1 and case 2 at (a) 1:00 and (b) 16:00. The positive values indicate the increase of air temperature, while the negative values indicate the reduction of air temperature due to the master plan. The dashed lines are the boundaries of the existing and new urban areas (see Fig. 4.3).

indicate the increase of air temperature, while the negative values (i.e. blue shaded areas) indicate the reduction of air temperature from current to master plan conditions.

At night, instead of causing the temperature increase, the land use change results in the reductions in air temperatures in some particular areas by up to 1.5 °C (Fig. 4.19a). Those particular areas strongly correspond with the locations of the barren or sparsely vegetated land in existing and new urban areas of case 1 (Fig. 4.19a). As has been shown in the previous section, the air temperature of the barren or sparsely vegetated land in case 1 is higher than the air temperature of the same area in case 2. The number of cooled regions is less in the northern part of new urban areas because the land use category in that area is dominated by the evergreen broadleaf forest (see Fig. 4.3). The average air temperature increase in the northern urban areas is up to 1 °C at night.

Furthermore, the established built-up lands in existing urban areas of case 1 generally do not experience any significant changes in average air temperature after the implementation of the master plan at night (Fig. 4.19a). Nevertheless, the air temperatures in some of those areas increase by up to 0.5°C in the daytime (Fig. 4.19b), attributed to the land use change from vegetative land use to built-up land and also from residential lands to commercial or industrial lands. Meanwhile, in new urban areas, the increased average air temperatures reach 0.5 °C during the daytime.

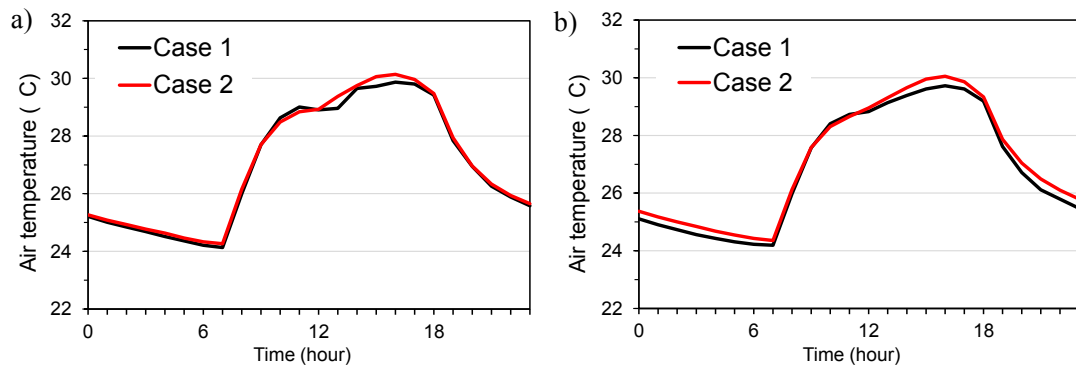


Fig. 4.20 Diurnal variations of average air temperatures at 2 m above the surface during the clear days in (a) existing and (b) new urban areas.

Diurnal variation of air temperature in existing and new urban areas

Fig. 4.20 shows the diurnal variations of average air temperatures in existing and new urban areas in JB for cases 1 and 2, respectively. The average air temperatures in Fig. 4.20 were the average air temperatures calculated from the non-rainy days in June 2013. Furthermore, they were also spatially averaged from the air temperatures over the built-up lands in existing and new urban areas, respectively. The air temperatures in other land use categories are not taken into account in the calculation.

In existing urban area, the diurnal variation of air temperature of case 2 is slightly higher than that in case 1, with the difference of air temperature up to 0.1 and 0.4 °C in the night-time and daytime, respectively (Fig. 4.18a). The discrepancy of average air temperature between cases 1 and 2 is more apparent in new urban areas than in existing urban areas. The implementation of the master plan in case 2 generally raises the urban air temperature throughout the day. The maximum average air temperature differences between cases 1 and 2 reach 0.4 °C in during the daytime and night-time, respectively (Fig. 4.20b).

4.4.3 Energy balance analysis of Hanoi and JB case studies

Fig. 4.21 shows the sensible, latent, and conductive heat fluxes before and after the implementation of the master plan in the existing and new urban areas of Hanoi, respectively. As shown in the left hand-side panels of Fig. 4.21, the land use change proposed in the master plan does not significantly affect the energy balance in the existing urban areas. The sensible and latent heat fluxes remain almost at the same level although there is a considerable increase in the conductive heat flux after the implementation of the master plan in the existing urban area. On the other hand, in new urban area, the land use change significantly increase the sensible and conductive heat fluxes, respectively. Moreover, the increased built-up land and the lack of vegetative surfaces in the new urban areas of master plan condition (i.e. case 2-1)

result in the significant reduction of latent heat (Fig. 4.21d). As a result, the number of hotspots in the master plan condition increases because more energy are transformed into sensible heat and less into latent heat.

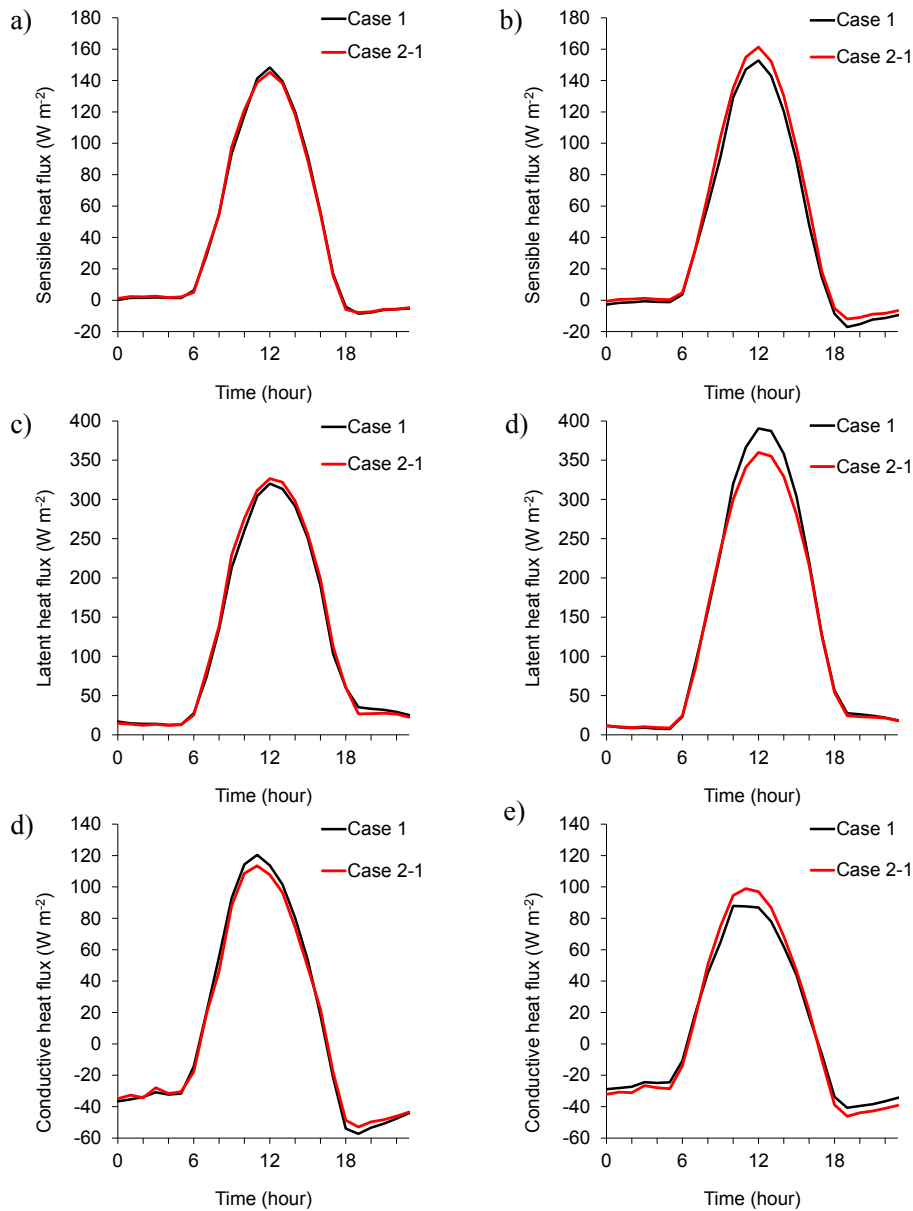


Fig. 4.21 Sensible, latent, and conductive heat fluxes before and after the implementation of the master plan. The left-hand side panels show the heat fluxes in the existing urban areas while the right-hand side panels describe the heat fluxes in the new urban areas, respectively.

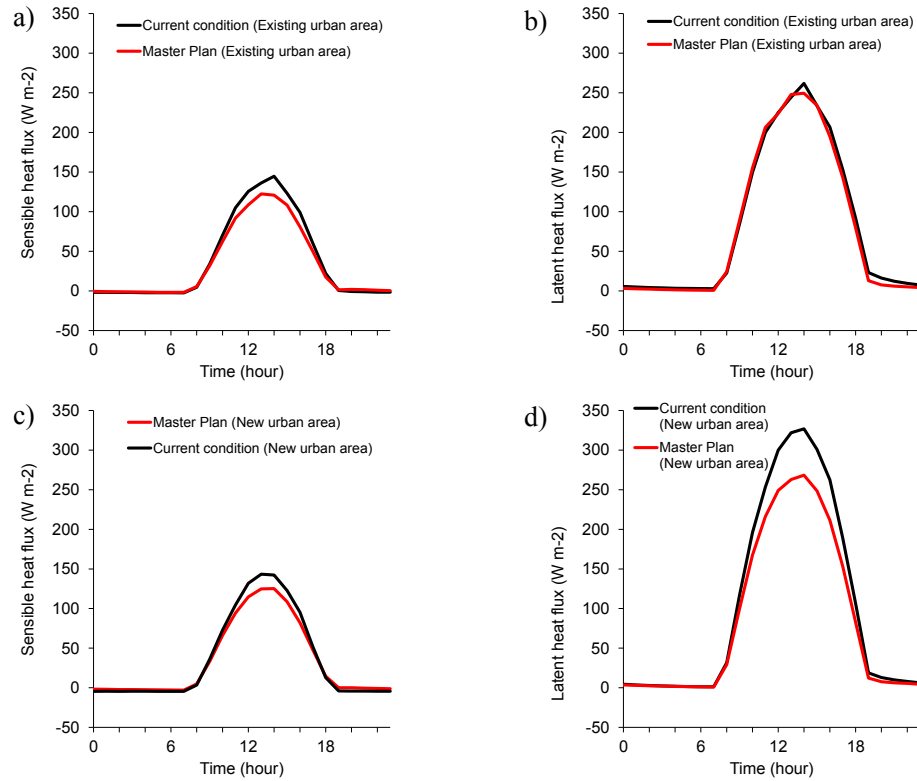


Fig. 4.22 The left panels are the sensible heat flux in (a) existing urban areas and (c) new urban areas of JB under the land use condition of the current and master plan. The right panels are the latent heat flux in (b) existing urban areas and (d) new urban areas. The influence of anthropogenic emissions are not taken into account.

Fig. 4.22 depicts the surface energy fluxes in the existing and new urban area under the current and master plan condition in JB. The implementation of the master plan results in the significant reduction of sensible heat in both existing and new urban areas. This is mostly due to abundant barren and sparsely vegetated lands both in the existing and new urban areas of JB. Meanwhile, the latent heat is just slightly reduced in existing urban areas, meaning that the barren and sparsely vegetated land has less effect on transforming energy into the latent heat flux. On the other hand, the latent heat in new urban areas is significantly decreased because many vegetative covers in those areas are transformed into built-up lands.

Summary

The main findings of this chapter are summarized as follows:

1. The daytime peak air temperature is projected to remain at almost the same level as the current condition (approximately 0.5 to 1°C higher at maximum) even after the implementation of the master plan in Hanoi and JB. However, the high air temperature areas would expand widely over the planned built-up areas.
2. It is important to consider the potential cooling effect of vacant lands. Vacant lands are normally left barren and sparsely vegetated. The result of the study in JB found that the barren and sparsely vegetated lands surrounding and within the urban areas have relatively warm air temperatures and can affect the thermal environment in the urban areas.

References

- Argüeso, D. et al., 2014. Temperature response to future urbanization and climate change. *Climate Dynamics*, 42(7–8), pp.2183–2199.
- Chen, F. et al., 2011. The integrated WRF/urban modelling system: Development, evaluation, and applications to urban environmental problems. *International Journal of Climatology*, 31(2), pp.273–288.
- Coutts, A.M., Beringer, J. & Tapper, N.J., 2008. Investigating the climatic impact of urban planning strategies through the use of regional climate modelling: a case study for Melbourne, Australia. *International Journal of Climatology*, 28(March 2008), pp.1943–1957. Available at: http://cdiac.esd.ornl.gov/oceans/GLODAP/glodap_pdfs/Thermohaline.web.pdf.
- Doan, Q., Kusaka, H. & Ho, Q.-B., 2016. Urban climate impact of future urbanization on temperature and thermal comfort index in a developing tropical city : Ho Chi Minh City. *Urban Climate*, 17, pp.20–31. Available at: <http://dx.doi.org/10.1016/j.uclim.2016.04.003>.
- Kusaka, H. et al., 2001. A simple single-layer urban canopy model for atmospheric models: Comparison with multi-layer and slab models. *Boundary-Layer Meteorology*, 101(3), pp.329–358.
- Lee, H.S., 2015. Evaluation of WAVEWATCH III performance with wind input and dissipation source terms using wave buoy measurements for October 2006 along the east Korean coast in the East Sea. *Ocean Engineering*, 100, pp.67–82.

5

Influence of global warming on urban climate: A case study of Hanoi

5.1 Objectives

The main objective of this chapter is to investigate the contributions of land use change and global warming to the future increase of air temperature in Hanoi in the 2030s. Accordingly, WRF simulations were conducted for the land use condition of the master plan under the influence of global warming in the 2030s utilising the climate data projected by a Global Climate Model (GCM), Model for Interdisciplinary Research on Climate Version 5 (MIROC5), via a direct dynamical downscaling method. Then, we compared the results of the global warming simulations with the results in Chapter 4. Through the comparison, the contribution of land use change and global warming to the urban warming in Hanoi in the 2030s can be observed, respectively.

5.2 Scenarios for numerical experiments

To investigate the contribution of land use changes and global warming to the future increase in urban temperature in Hanoi, this study assesses four scenarios. The first two scenarios (i.e. case 1 and 2-1) investigate the impacts of land use changes to the urban warming

Table 5.1 Summary of scenarios for numerical experiments.

| | Land use and land cover conditions | Global warming effects | Initial and boundary weather conditions |
|--------------------|------------------------------------|------------------------|---|
| Case 1 (base case) | Current (2010) | × | Current (June 2013) |
| Case 2-1 | Future master plan (2030) | × | Current (June 2013) |
| Case 2-2 | Future master plan (2030) | ○ (RCP4.5) | 2030s (June 2026-2035) |
| Case 2-3 | Future master plan (2030) | ○ (RCP8.5) | 2030s (June 2026-2035) |

and have been discussed in Chapter 4. This chapter assesses the latter two scenarios, namely case 2-2 and case 2-3, respectively. The initial and boundary conditions for cases 2-2 and 2-3 utilise the RCP4.5 and RCP8.5 datasets of MIROC5, respectively, for moderate and extreme climate changes.

Furthermore, in order to consider climate variability and uncertainty from the inter-annual variability in climate projection, we conducted a WRF simulation of each June between 2026 and 2035. We then obtained the mean and variation from the 10 simulation results of each future climate scenario (i.e., cases 2-2 and 2-3) to take into account the inter-annual variability of the MIROC5. This ten-year repetitive simulations of each June will also provide the upper and lower bounds from the dominant inter-annual variability, and further insight for a multi-model ensemble mean and variation over the Hanoi region. Table 5.1 summarises the scenarios for numerical experiments.

5.3 Results and discussion

5.3.1 Urban climate conditions in the 2030s

In this section, the impacts of global warming are discussed based on the temporal average air temperature at 2 m above the ground every June, the typical summer month, from 2026 to 2035. The wind directions resulting from the global warming simulations show significant discrepancies in every simulated months. These discrepancies largely affect the distribution of air temperatures. Therefore, for a fair comparison of the results of cases 1 and 2-1, only the days with prevailing wind direction are taken into account in the analysis. As previously described herein, the prevailing winds in Hanoi in June are the south-easterly winds ranging from 90° to 180° (VIAP 2011). In addition, the analysis in this section is generally divided into two types of urban areas: existing and new urban areas (see Fig. 4.1). Although there are various land use types within each urban area, the results in this section are calculated only from the values taken from the built-up lands (i.e., low- to high-density built-up areas, as well as offices and commercial areas).

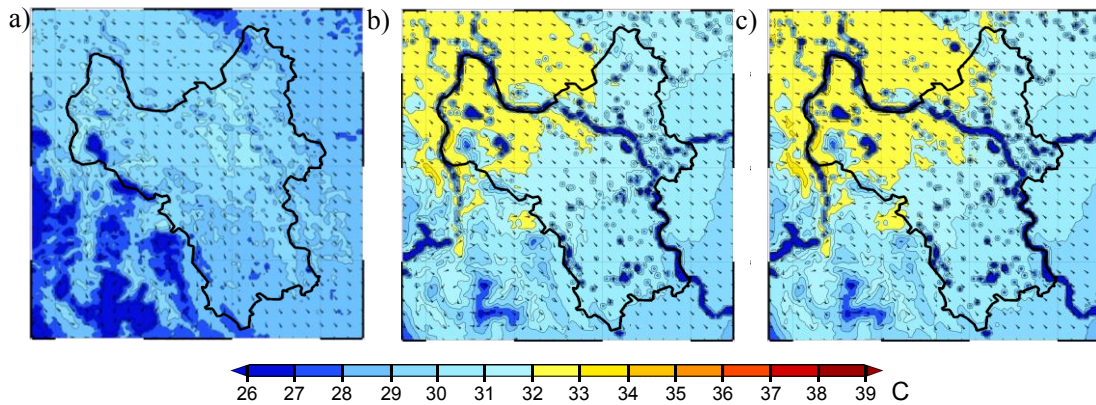


Fig. 5.1 Spatial distribution of average air temperature at 2m and wind directions at 10m above the surface at 1:00 for (a) case 2-1, (b) case 2-2, and (c) case 2-3. The black line highlights the boundary of Hanoi City.

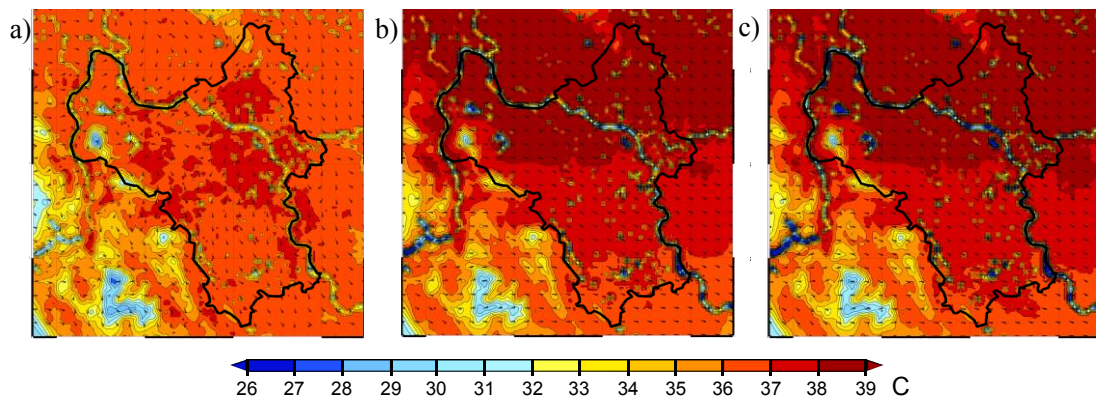


Fig. 5.2 Same as Fig. 5.1 but at 14:00.

Figs. 5.1 and 5.2 illustrate the spatial distributions of the average air temperature at 2 m above the surface and the wind directions at 10 m above the surface for cases 2-1, 2-2, and 2-3, respectively. The results are included in the figures for comparison. In general, the global warming significantly alter the urban climate in Hanoi City. Under global warming conditions, temperature increases are observed in the whole region (Figs. 5.1 and 5.2).

Figs. 5.3 shows the spatial distributions of average air temperature differences at 1:00 and 14:00 between cases 2-1 and 2-2; and between cases 2-1 and 2-3, respectively. As has been discussed, the global warming rises the air temperature over the simulated domain. At night, the air temperature increase recorded over the urban areas is up to 2.5 °C in both RCP scenarios. Meanwhile during the daytime the maximum temperature increase in urban areas is up to 1.5°C also for both RCP scenarios. There is no significant difference between cases 2-2 and 2-3 on the increased temperatures in Hanoi City.

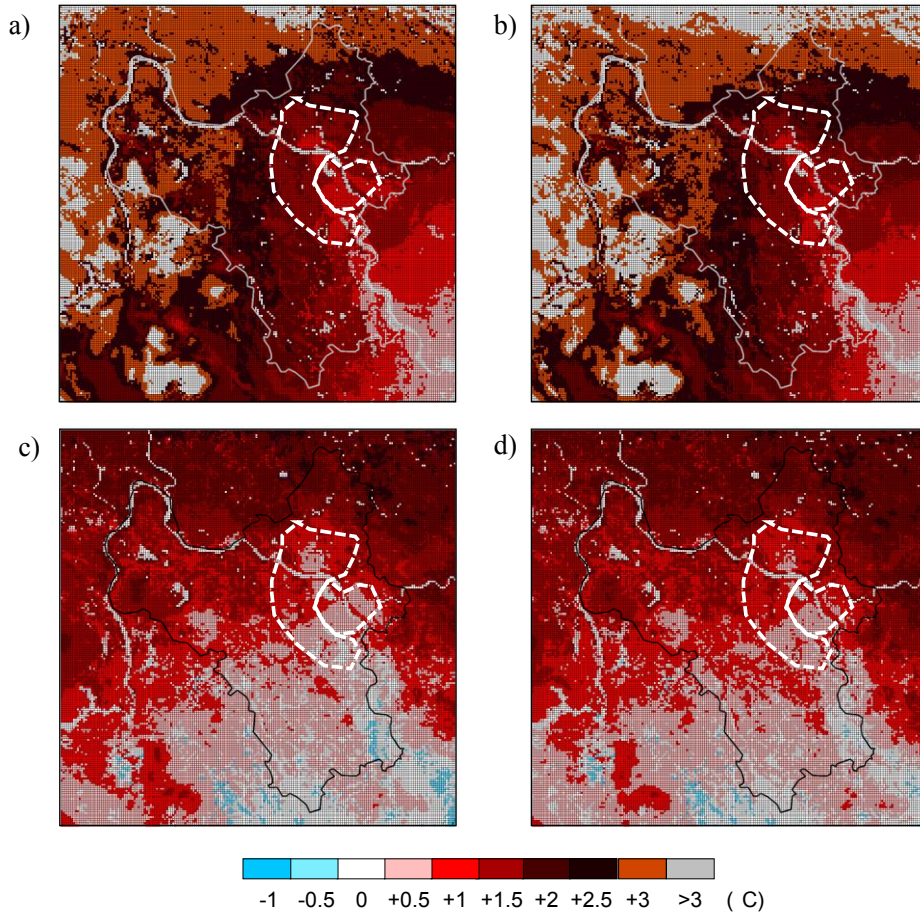


Fig. 5.3 Spatial distribution of average air temperature differences at 1:00 for (a) cases 2-1 and 2-2, (b) cases 2-1 and 2-3; and at 16:00 for (c) cases 2-1 and 2-2, (d) cases 2-1 and 2-3.

Fig. 5.4 shows the results for 10 simulated months (2026- 2035) for each RCP scenario (cases 2-2 and 2-3), calculated for existing and new urban areas. For the comparison, the results of cases 1 and 2-1 are also included. In general, the future climate conditions show a dynamic variation over the 10-year period. For instance, the year 2027 is the hottest year under RCP4.5, while 2035 is the hottest for RCP8.5. Moreover, the future air temperature can even be cooler than current conditions, as seen in 2032 and 2033 in case 2-2 (Fig. 5.4a and c). This may be due to inter-annual climate variations both in existing urban and new urban areas for RCP4.5. However, the inter-annual variability in RCP8.5 results is not distinct, and the variations in air temperature are rather confined to a narrow band. Nevertheless, hotter years would occur more often in the near future than would cooler years.

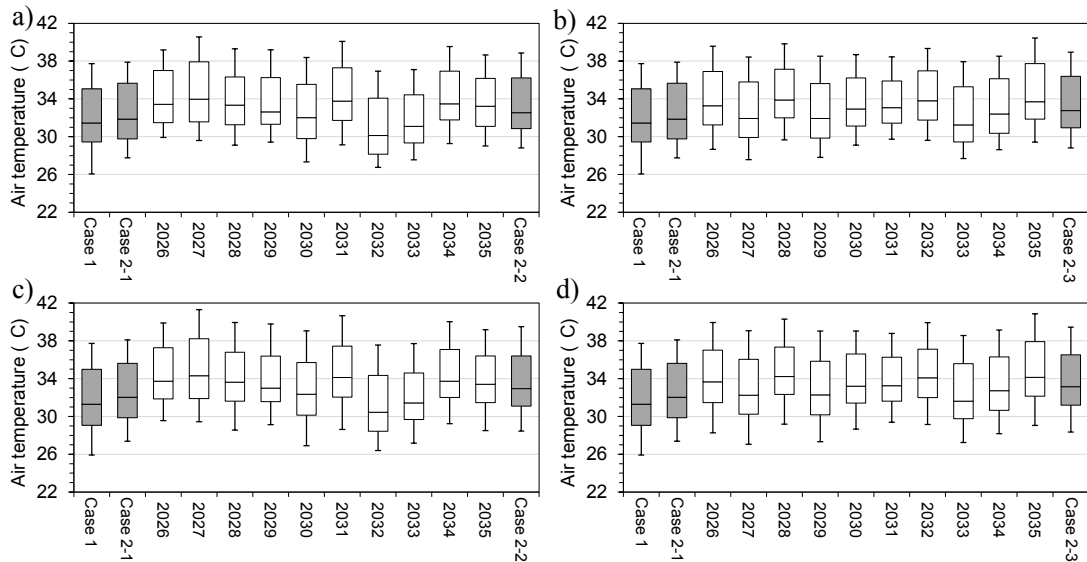


Fig. 5.4 Statistical summary (maximum, minimum, 25th percentiles, 75th percentiles, and median) of average air temperature in the existing urban area for (a) RCP4.5, (b) RCP8.5, and at the new urban area for (c) RCP4.5 and (d) RCP8.5. In order to see the climate variations over the 2030s, the results from 10 simulated months from 2026 to 2035 are shown. The box-plot at the far right of each graph is the mean value from 10 simulated months. The results from cases 1 and 2-1 are also shown for comparison.

The results also show that under the near future scenario (2026-2035), the climate response to different emission scenarios (i.e., RCP4.5 and RCP8.5) will be generally similar. The lowest average air temperature experienced by the urban areas is approximately 28.4 °C for case 2-2 and 28.5 °C in case 2-3, while the highest average air temperature is approximately 39.5 °C for both cases. The interquartile range of average air temperature in case 2-2 falls between 30.8 and 36.2 °C for existing urban areas and between 31 and 36.4 °C for the new urban areas. The ranges are slightly higher in case 2-3 by up to 0.1 °C in both existing and new urban areas.

As shown in Fig. 5.4, the maximum average temperature in the global warming conditions is up to 1.7 °C greater than that of case 1 and 1.4 °C greater than that of case 2-1. The minimum average air temperature that would be experienced by the urban areas in the future scenarios would also increase by up to 2.7 °C from case 1 and by up to 1 °C from case 2-1.

Fig. 5.5 shows the frequency of occurrence for spatially-averaged air temperatures in all urban areas, represented as the per-day frequency for cases 2-1, 2-2, and 2-3. In case 2-1, the average air temperatures in urban areas range from 28 to 37.5 °C. Two peaks in average air temperatures are observed, with mode values of 29 and 37 °C. Under cases 2-2 and 2-3, the average air temperatures in urban areas range from 28.5 to 39 °C, which are 0.5 to 1.5 °C higher than those in case 2-1. The occurrence frequency of air temperatures peaks twice, with mode values of 30 and 38 °C for case 2-2 and 31.0 and 38.5 °C for case 2-3. Moreover, in cases 2-2 and 2-3, the

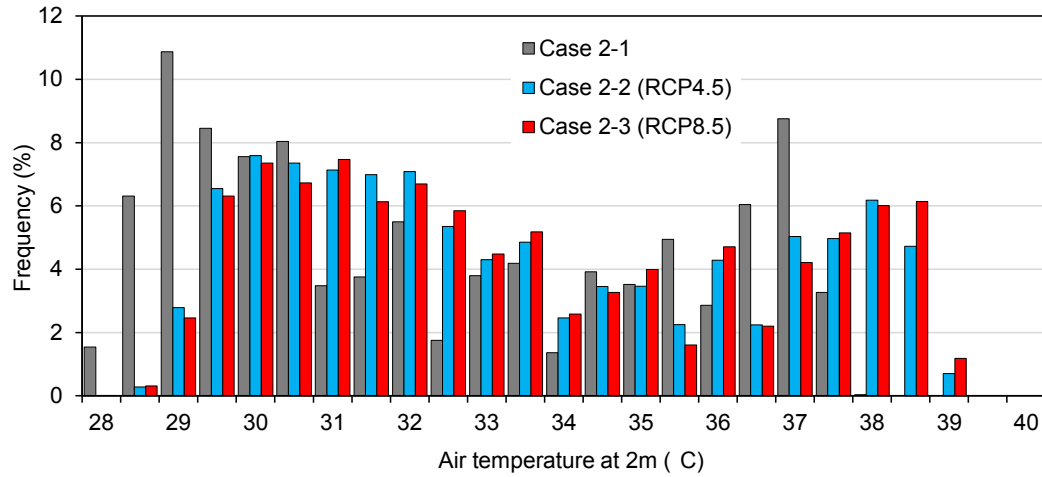


Fig. 5.5 Frequency of occurrence for spatial-average air temperatures in urban areas (both in existing and new urban areas) over the simulation periods of cases 2-1, 2-2, and 2-3, respectively. The result is represented as the per-day frequency for each future scenario.

frequency of average air temperatures ranging from 31 to 35 °C is generally greater than in case 2-1. These results show that the frequency and/or intensity of warmer nights and hotter days in urban areas of Hanoi will likely increase in the future due primarily to the influence of global warming.

5.3.2 Contributions of land use changes and global warming to the future urban warming

For elucidating the contributions of global warming ($F_{global\ warming}$) and land use changes ($F_{land\ use}$) to the temperature increase in Hanoi City, factor separation analysis was employed (Stein & Alpert 1993). In this analysis, the contribution of the interaction between land use changes and global warming to the temperature increase is not taken into account, as it is relatively small as estimated in previous studies by Yang et al. (2016). The analysis considered the following equations:

- (1) $F_{global\ warming(M)} = (Case\ 2-2\ or\ Case\ 2-3) - Case\ 2-1$
- (2) $F_{land\ use} = Case\ 2-1 - Case\ 1$
- (3) $F_{global\ warming+land\ use} = (Case\ 2-2\ or\ Case\ 2-3) - Case\ 1$

Fig. 5.6 shows the diurnal variations of spatially- and temporally-averaged air temperatures in existing and new urban areas for all cases. As shown in Fig. 5.6a, the implementation of the master plan slightly increases the average air temperature in existing urban areas both in the

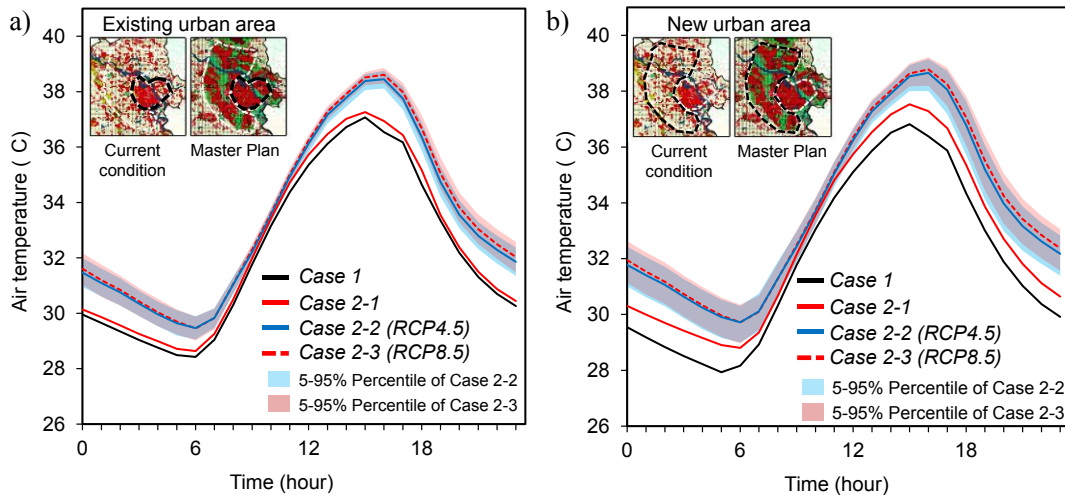


Fig. 5.6 Diurnal variations of spatial- and temporal-average air temperature in (a) existing urban area and (b) new urban area for all cases. The results are calculated from the days with prevailing south-easterly winds and only the values from the built-up land use types are taken into account. The shaded areas (blue and red shaded) indicate 5th to 95th percentile. The increasing temperatures due to the land use change are shown from the gap between the black line (case 1) and red line (case 2-1), while the impacts of global warming and land use change are represented with the blue line (case 2-2) and dashed red line (case 2-3). The maps show the location of existing and new urban areas under current and master plan situations.

daytime (06:00-17:00) and at night (00:00-05:00, 18:00-00:00). The increases in air temperature due to the land use changes in existing areas are up to 0.5 and 0.6 °C in the daytime and at night, respectively. In the new urban areas (Fig. 5.6b), the massive land use changes brought by the master plan result in a greater increase in average air temperatures than in the existing urban areas, by 0.9 and 1 °C in the daytime and at night, respectively.

Meanwhile, under the global warming scenarios, the average air temperatures for the whole day are generally higher than in the present condition. In the 2030s, the air temperatures in the existing urban areas increase by up to 1.3 and 1.5 °C for cases 2-2 and 2-3, respectively, over those in case 2-1 (Fig. 5.6a). A similar trend is also observed in the new urban areas (Fig. 5.6b), where the average air temperatures increase by up to 1.5 and 1.7 °C in case 2-2 and 2-3, respectively, over those in case 2-1. The global warming conditions in the 2030s under the RCP8.5 scenario (case 2-3) are slightly warmer than under the RCP4.5 (case 2-2), with a difference of up to 0.2°C.

In total, global warming and land use changes ($F_{global\ warming+land\ use}$) contribute to temperature increases of up to 2.1 and 2.7 °C in existing and new urban areas, respectively. According to the results from factor separation analysis, global warming contributes up to 63% of the temperature increase in new urban areas. The contribution of land use changes to the temperature increase

in new urban areas is larger than in the existing urban areas. While the land use change contributes to 29% of average air temperature increases in existing urban areas, they contribute to, at most, 37% of average air temperature increases in new urban areas.

5.4 Summary

In Hanoi, Vietnam, the Hanoi Master Plan 2030 was proposed and is being implemented by the Vietnamese government to accommodate the growing population of the city from 6.7 million in 2010 to 9.2 million by 2030. Such rapid urbanisation inevitably worsens UHIs and energy shortages. However, scientific evidence for the impacts of land use changes and global warming with the Hanoi Master Plan on the urban climate does not yet exist in the literature.

In this study, we investigated the impacts of land use changes proposed by the Hanoi Master Plan 2030 and the impacts of a future warming climate on the urban climate in Hanoi using numerical experiments with WRF modelling. Detailed land use and land cover data for the simulations were created using digital land use data for current conditions and the Hanoi Master Plan 2030, combined with Landsat 8 satellite images. For the near future climate conditions, direct dynamical downscaling with WRF was carried out with initial and boundary conditions from the MIROC5 datasets for RCP4.5 and RCP8.5.

Moreover, these following points have to be taken as limitations in the numerical experiments and considered when interpreting the results of this study. First, the impact of global warming through dynamical downscaling method were driven by one GCM output, i.e. MIROC5. However, more GCM outputs of CMIP5 used in the analysis will cover the wide range of climate variability and uncertainty. Secondly, the urban canopy model was employed with a default setting. More-detailed urban parameterisations, which are derived from the actual conditions in Hanoi City, are needed for future studies. Moreover, energy-saving policies and increases in the efficiency of cooling technologies in the future should also be reflected in the future modelling studies. Third, the influences of non-linear interaction between the gradual changes of land use and global warming on urban climate are not considered in this study but cannot be neglected. However, the quantitative analysis of the non-linear interaction need gradual or sequential scenarios of land use changes in long-term simulations and out of scope of this study.

Furthermore, it has been reported that the increase in urban temperature may prompt the emergence of heat-related illnesses and mortalities (Basu & Samet 2002). On the other hand, people living in cities may acclimate and adapt to the increased urban temperatures, to a certain extent (Toe & Kubota 2013). It will be particularly important to investigate the effects of future urban warming on health issues and the thermal comfort of urban residents of growing cities in future studies.

The following are the main findings.

1. Hotspots widely expanded following the pattern of new built-up areas in the master plan scenario. The implementation of the master plan increased the number of hotspots with peak average air temperatures in the existing urban areas, largely at night, where the number of hotspots at 30 °C increased by up to 23%.
2. The land use changes proposed in the master plan are expected to increase the average air temperature in the existing and new urban areas by up to 0.6 and 1 °C, respectively.
3. The simulation results with global warming effects from direct dynamical downscaling illustrated that the urban air temperature was expected to increase along with global warming. In the 2030s, the average air temperature increase in the existing urban areas was projected to be up to 2.1°C, of which up to 1.5 and 0.6 °C are attributable to global warming and land use changes, respectively. Global warming contributed, at most, 71% of the temperature increase in existing urban areas of Hanoi City in the 2030s.
4. The increase in air temperature for the near future (2030s) will likely offset the cooling effects from any UHI mitigation measures. The development of UHI mitigation measures must take into account the influence of future global warming, even for the short-term future such as by 2030.

References

- Basu, R. & Samet, J.M., 2002. Relation between elevated ambient temperature and mortality : A review of the epidemiologic evidence. *Epidemiologic Reviews*, 24(2), pp.190–202.
- Stein, U. & Alpert, P., 1993. Factor separation in numerical Simulations. *Journal of the Atmospheric Sciences*, 50(14), pp.2107–2115.
- Toe, D.H.C. & Kubota, T., 2013. Development of an adaptive thermal comfort equation for naturally ventilated buildings in hot–humid climates using ASHRAE RP-884 database. *Frontiers of Architectural Research*, 2(3), pp.278–291.
- Vietnam Institute of Architecture Urban and Rural Planning (VIAP), 2011. *The Hanoi Capital Construction Master Plan 2030 and Vision to 2050, Comprehensive Report*, Hanoi, Vietnam: VIAP.
- Yang, L. et al., 2016. Contrasting impacts of urban forms on the future thermal environment : example of Beijing metropolitan area. *Environmental Research Letters*, 11, pp.1–10.

6

Cooling effect of the green spaces: A case study of Hanoi

6.1 Objectives

The objective of this chapter is to investigate the cooling effect of the proposed green strategies in the Hanoi Master Plan 2030. Firstly, numerical experiments were conducted for the master plan condition with four different green strategies. Then, three new configurations of the green network were proposed, and the resulting impacts on the urban climate were also assessed. Furthermore, this chapter investigates to what extent the further urban greening would improve UHI mitigation in the Hanoi Master Plan. A scenario analysis of UHI effect in the land use conditions of the master plan with different green coverage ratios (GCRs) and vegetation types was performed.

6.2 Assessment of the cooling effect of proposed green spaces

6.2.1 WRF configuration

The WRF simulations adopted an interactive grid nesting with four domains that have horizontal resolutions of 27, 9, 3 and 1 km (Fig. 6.1). The fourth domain covers all of Hanoi City. The initial and lateral boundary conditions were imposed every 6 hours using the NCEP

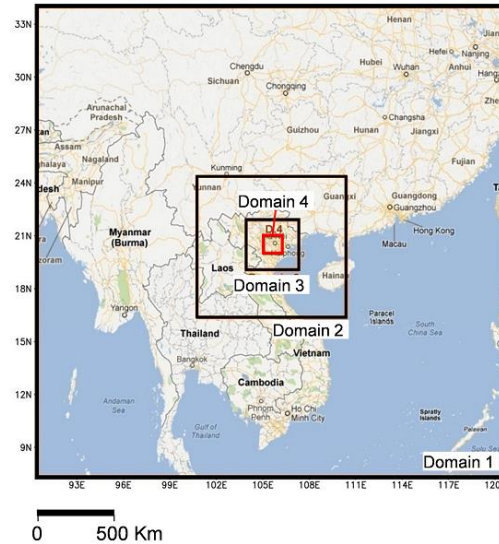


Fig. 6.1 Four computational domains for WRF modelling. The smallest domain, Domain 4, covers the entire Hanoi City with 1 km spatial grid resolution (indicated with red line square).

Table 6.1 WRF model configuration of Hanoi case study with four domains

| Physics/parameterization | Domain 1 | Domain 2 | Domain 3 | Domain 4 |
|----------------------------|---|-----------|-----------|-----------|
| Horizontal resolution (km) | 27 | 9 | 3 | 1 |
| Domain size (km) | 2700 x 2700 | 900 x 900 | 300 x 300 | 100 x 100 |
| Vertical layers | 30 | | | |
| Microphysics | WRF single-moment 3-class scheme | | | |
| Longwave radiation | Rapid Radiative Transfer Model (RRTM) scheme | | | |
| Shortwave radiation | Dudhia scheme | | | |
| Surface-layer | MM5 similarity based on Monin-Obukhov scheme | | | |
| Cumulus scheme | Kain-Fritsch scheme (only for Domain 1) | | | |
| Land surface model | Noah Land Surface Model (LSM) | | | |
| Planetary boundary layer | Yonsei University (YSU) Scheme | | | |
| Simulation period | 00:00 UTC 12 to 00:00 UTC 24 June 2013 (for validation purpose) | | | |

FNL data. Domains 1 and 2 adopted the default datasets and USGS topography data, with spatial resolutions of 10 and 2 minutes, respectively. In contrast, domains 3 and 4 had different data sources. For domain 3, the Global Land Cover by National Mapping Organizations (GLCNMO) data were used in the simulations. The GLCNMO data have an approximately 1-km (30 arc seconds) grid resolution with 20 land cover items and were created using MODIS data acquired in 2003. A 16-day composite of 2003 was used for the land cover classification. The classification was based on the land cover classification system (LCCS) developed by the Food and Agriculture Organisation (FAO). Therefore, the GLCNMO and other land cover data products can be compared and integrated based on the LCCS. For domain 4, two-source

datasets, composed of national digital land use data provided by the Vietnam Institute of Urban and Rural Planning (VIUP) and own-processed land cover data using high-resolution satellite images from the Advanced Land Observing Satellite (ALOS) Advanced Visible and Near Infrared Radiometer type 2 (AVNIR-2), were combined. Since the national digital data from VIUP were available only within the administrative boundary of Hanoi City, the surrounding areas of Hanoi City in domain 4 were covered by the ALOS images (acquired in 2009) for all the cases. The combining process of the different data sources is provided in Appendix I. Table 6.1 displays the model configurations used in the WRF simulations. The surface parameters used in the simulations were given as shown in Appendix J.

6.2.2 Scenarios for numerical experiments

The numerical experiments were conducted for the Hanoi Master Plan 2030 with four different green strategies. Scenario 1 represents the land use condition proposed by the Hanoi Master Plan 2030, whereas scenarios 2-4 were created to evaluate the effects of proposed green spaces on the UHIs. The land use category of the proposed green spaces was set to be mixed shrubland/grassland. Fig. 6.2 depicts the locations of the proposed green spaces and the water bodies. In scenario 2, the green belts were not considered, while the green buffers were removed in scenario 3. In scenario 4, both the green belts and green buffers were not taken into account, and these areas became built-up areas. The land use fraction in the newly transformed urban area is set to be 0.8 and 0.2 for built-up area and vegetation, respectively. Fig. 6.3 exhibits the LULC maps of used in the Domain 4 of numerical experiments for four scenarios. Table 6.2 shows the sources of the land use and land cover datasets for each domain in the numerical experiments.

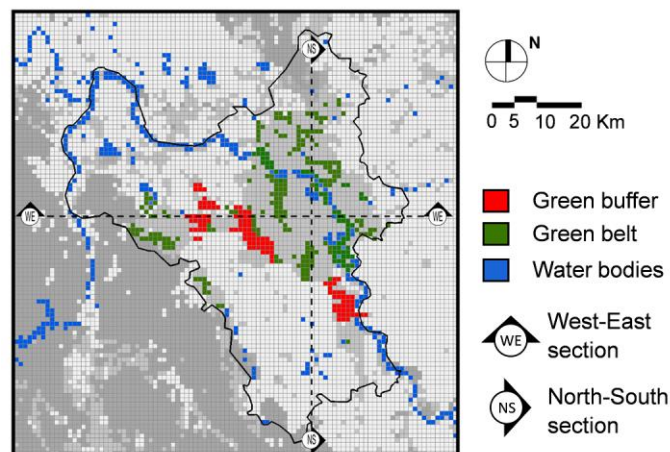


Fig. 6.2 Spatial distribution of green belts (green color) and green buffers (red color) in the Hanoi Master Plan 2030. Blue color indicates the water bodies. The dashed lines indicate the location of for north-south and west-east cross sections for the analysis in Figs. 6.12 and 6.13.

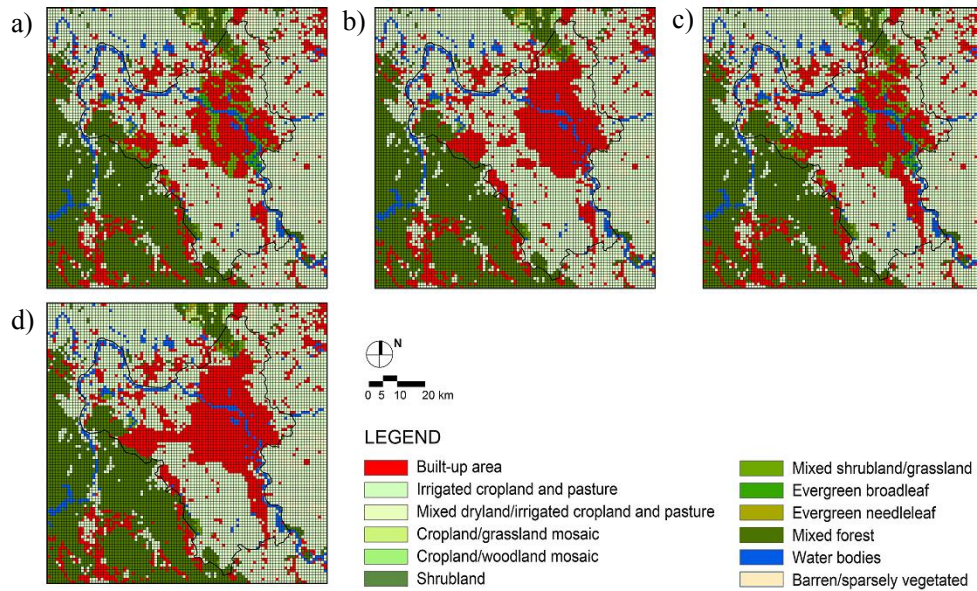


Fig. 6.3 LULC used for domain 4 in numerical experiments. (a) Scenario 1 (master plan condition), (b) scenario 2, (c) scenario 3, and (d) scenario 4. In the scenarios 2-4, the spatial distribution of green belts and green buffers are changed into built-up lands to assess their effects on urban heat island. The surrounding areas of Hanoi City remain unchanged.

Table 6.2 LULC data sources for each domain and numerical experiments.

| Experimental run | Scenario 1 (master plan) | Scenario 2 | Scenario 3 | Scenario 4 |
|---------------------------|--|--|--|--|
| Domain 1 | | USGS topography dataset (default dataset) | | |
| Domain 2 | | USGS topography dataset (default dataset) | | |
| Domain 3 | | GLCNMO 30 arc second dataset | | |
| Domain 4 | Digital land use data for Hanoi Master Plan 2030 | Modified land use data of Hanoi Master Plan 2030 | Modified land use data of Hanoi Master Plan 2030 | Modified land use data of Hanoi Master Plan 2030 |
| Green belts in domain 4 | Yes | No | Yes | No |
| Green buffers in domain 4 | Yes | Yes | No | No |

6.2.3 Model validation

The WRF simulation for validation purpose was performed for the current status of Hanoi City with the LULC for domain 4 that is shown Fig. I.6. The simulation was carried out for 7 days from 00:00 UTC 13 to 00:00 UTC 20 June in 2010. Fig. 6.4 presents the

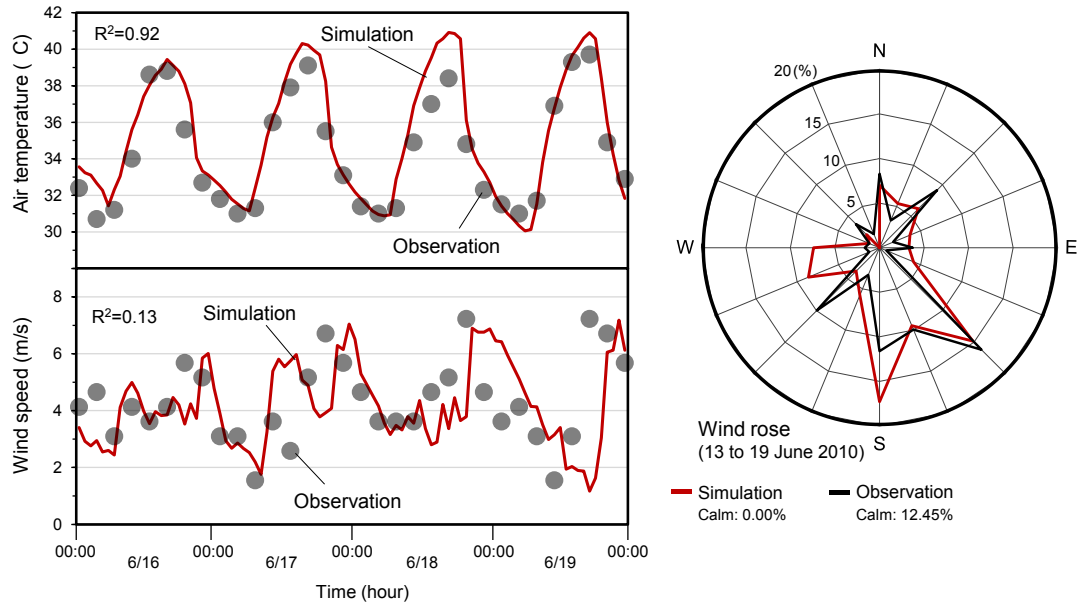


Fig. 6.4 Comparison between observed and simulated air temperature, wind speed and direction at Lang station (21.02° N and 105.8° E) in Hanoi urban center. Land use and land cover data of current status in domain 4 are used for the validation purpose.

comparisons of air temperature, wind speed, and direction between the simulated and the observed conditions at Lang Station (see the location of the station in Fig. 1.4). The simulated air temperature at 2 m above the surface showed good agreement with the observed values with a coefficient of determination of 0.92. Moreover, the calculated wind speed and direction were fairly in accordance with the observed values: the coefficient of determination for wind speed was 0.13. The observed wind speeds were adjusted to 10 m winds above ground according to the power law vertical wind profile. The calculated wind direction was not adjusted.

6.3 Proposal for new configuration of green spaces

6.3.1 Scenarios for numerical experiments

As described in the previous section, the Hanoi Master Plan 2030 proposed a large green network consists of the green belts and the green buffers. Both of those green spaces form a large and centralized green areas in the city.

In this section, a UHI mitigation strategy with the improved configuration of the proposed green spaces was proposed, namely scenario 5, 6, and 7, respectively. In scenario 5, instead of the mixed shrubland/grassland, the land use category of the green spaces was turned into the

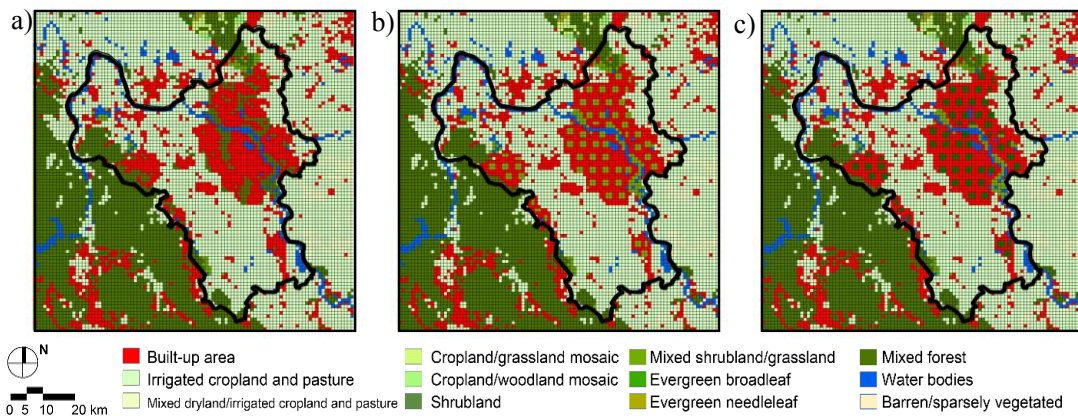


Fig. 6.5 LULC used for domain 4 in numerical experiments. (a) Scenario 5, (b) scenario 6, and (c) scenario 7.

mixed forest. In scenario 6, the same amount of the proposed green spaces in the master plan is redistributed to new locations, resulting in smaller green spaces but equally distributed in the city. While, in scenario 7, the mixed forest was used as the vegetation cover in the equally distributed green spaces. Fig. 6.5 shows the LULC dataset for scenarios 4,5 and 6.

The land use datasets for scenarios 6 and 7 were modified by making use of the dataset of scenario 4 as the base map. As shown in Fig. 6.3d, in scenario 4, all the proposed green spaces have been removed. Then, we added new green areas into the map and assigned the same land use fraction values for all newly added green spaces. The land use fraction in those areas was set to be 0.2 and 0.8 for urban and vegetation, respectively. The WRF model was set with the same configuration given in Table 6.1.

6.4 Cooling impacts of increasing the green coverage ratio in Hanoi Master Plan 2030

6.4.1 Overview

In fact, implementing the equally distributed green spaces is difficult in the already established master plan. This strategy requires new allocation of lands that would make a significant modification in the master plan. Therefore, instead of allocating any new lands for the green spaces, in this section, we proposed an additional urban greening by implementing the green coverage ratio (GCR) in each lot of built-up lands in the city.

This study aims to investigate to what extent the further urban greening would improve UHI mitigation in Hanoi Master Plan. A scenario analysis of UHI effect in the land use conditions of the master plan with different GCRs and vegetation types was performed by using the Weather Research and Forecasting (WRF).

Table 6.2 Summary of simulation cases

| | Hanoi Master Plan 2030 | | | | |
|----------------------------|--|-------------------------------|-------------------------------|-------------------------------|-----------------|
| | Case 1 | Case 2 | Case 2-1 | Case 2-2 | Case 2-3 |
| Green coverage ratio | - | - | 10% | 30% | 30% |
| Vegetation type | - | Mixed shrubland/ grassland | Mixed shrubland/ grassland | Mixed shrubland/ grassland | Mixed forest |
| LULC data | 2010 | HMP | Modified HMP | Modified HMP | Modified HMP |
| Initial boundary condition | NCEP FNL | | | | |
| Simulation period | 12-24 June 2013 | | | | |
| Radiation scheme | RRTM scheme (longwave) and Dudhia scheme (shortwave) | | | | |
| Surface-layer | Monin-Obukhov similarity scheme | | | | |
| Land-surface | NOAH LSM | | | | |
| Planetary boundary layer | YSU scheme | | | | |
| Microphysics | WRF SM 3-class scheme | | | | |
| Cumulus scheme | Kain-Fritsch scheme | | | | |

6.4.2 WRF configuration

The WRF simulations in this study were performed with three domains that have a horizontal resolution of 4.5, 1.5, and 0.5 km for domains 1, 2, and 3, respectively (Fig. 6.6a). Domain 3 covers the whole administrative boundary of Hanoi. Table 6.2 summarizes the simulation cases and the physics schemes used in the WRF simulations. As shown in Table 6.2, all the simulations were conducted under the same weather condition so that the impacts of the GCR and vegetation type to the thermal environments in Hanoi can be observed. Accordingly, the WRF simulations employed NCEP FNL (Final) Operational Global Analysis data with $1^{\circ} \times 1^{\circ}$ resolution as the initial and boundary conditions.

6.4.3 Scenarios for numerical experiments

In order to understand the impact of land use change and urban greening on the urban climate in Hanoi, this study assessed five scenarios, namely case 2-1, case 2-4, case 2-5, and case 2-6, respectively. The LULC datasets within the Hanoi administrative boundary were produced using the digital data from Vietnam Institute of Urban and Rural Planning (VIUP). Since the data only cover the areas within the city's boundary, the LULC for the area outside of the city was produced from the land cover detected from Landsat-8 imagery.

Case 2-1 depicts the proposed land use plan in the Hanoi Master Plan 2030. As the proposal of UHI mitigation through urban greening, cases 2-4, 2-5, and 2-6 assessed the land use condition of the master plan with different GCRs and vegetation type. The GCR of 10% and 30% are adopted to case 2-4 and case 2-5, respectively. The vegetation type of the green spaces in cases 2-1, 2-4, and 2-5 is mixed shrubland or grassland. Meanwhile, case 2-6 adopted the

mixed forest as the vegetation type in all proposed green spaces. The simulation cases are summarized in Table 6.2. The LULC maps of the simulation cases are shown in Fig.6.6.

The simulations for all cases were conducted in June 2013, which represents the summer month in the typical year over the period of 2000 to 2015. The results of WRF model validation is shown in Chapter 4.

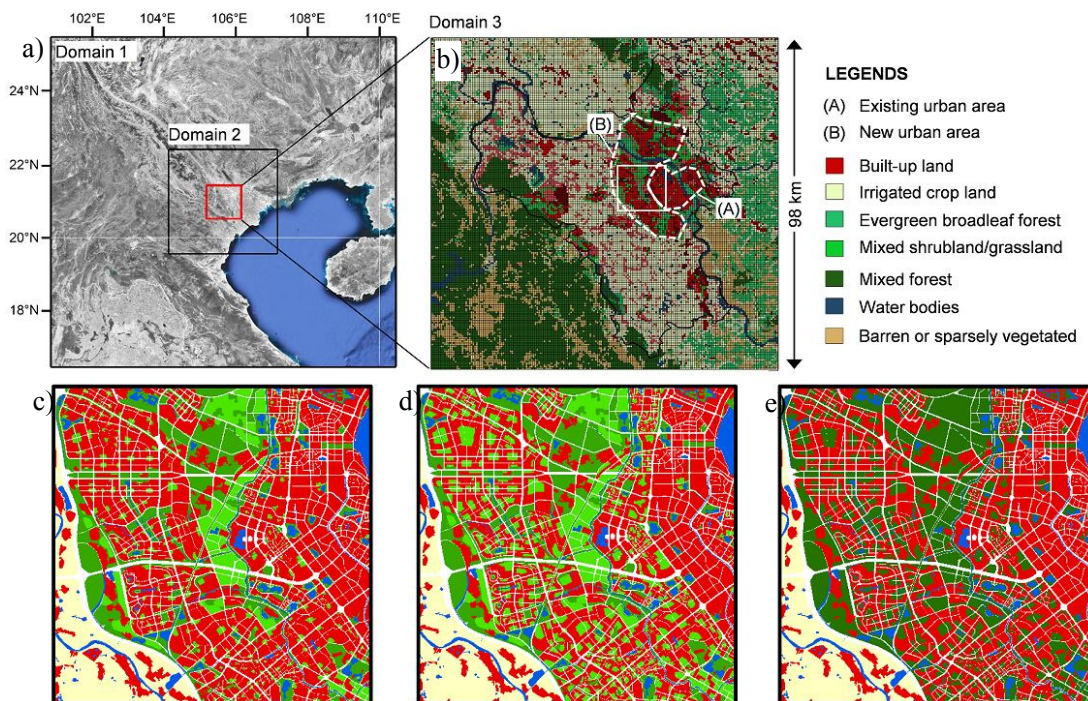


Fig. 6.6 (a) WRF 3 domains configuration. LULC of domain 3 for (b) case 2-1. The resulted LULC maps based on GCRs and vegetation types in (c) case 2-4, (d) case 2-5, and (e) case 2-6.

6.5 Results and discussion

6.5.1 The cooling effect of the proposed green spaces

Spatial distribution of air temperatures

The spatial distributions of the surface winds and air temperatures at 04:00, 10:00, 16:00, and 22:00 for scenarios 1 to 4 are shown in Fig. 6.7. Overall, the spatial pattern of the temperature

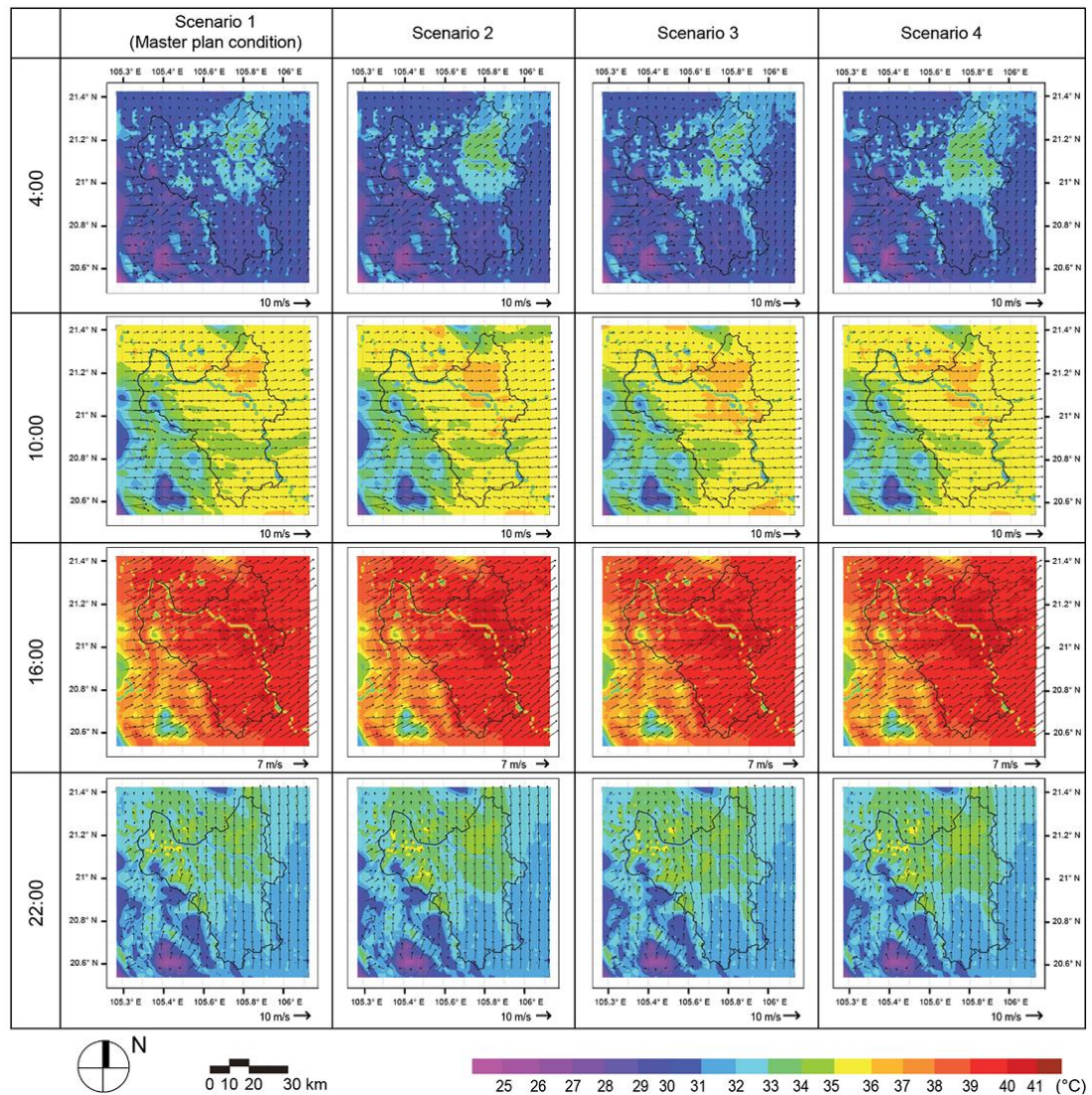


Fig. 6.7 Spatial distribution of simulated air temperature and winds at 4:00 10:00, 16:00, and 22:00 on 17 June 2010.

increments at 04:00 corresponds well to the planned built-up areas. In the results of scenario 2 without the green belts in the LULC of the master plan, the rise of the air temperature in the areas North and South of the Red River at 04:00 are very distinctive compared to the current status. The maximum difference in the air temperature between the current status and scenario 2 at 04:00 is approximately 4 to 5 °C in the expanded built-up areas. The spatial pattern of the temperature increments at 04:00 corresponds well to the planned built-up areas. At 10:00, the air temperature is over 36 °C in the area South of the Red River, and this temperature increase does not spread out much, partially due to the green buffers. During the afternoon, Hanoi City observes temperatures up to 40 °C, with the city centre becoming a hot spot. At 22:00, the spatial pattern of the air temperature is similar to the pattern at 04:00.

In scenario 3, the green buffers are not taken into account in the LULC of the master plan, while the green belts are now considered. The air temperature distribution at 04:00 shows the effects of the green belts, which is 3 to 4 °C lower than the built-up areas. The newly built-up areas near 21°N transformed from the green buffers exhibit high air temperatures. Compared to the current status of these areas, the built-up areas depict 4 to 5 °C higher temperatures in the expanded built-up areas. At 10:00 and 16:00, a higher air temperature compared to the surrounding areas appears for the planned built-up areas. The newly built-up areas transformed from the green buffers ironically express the importance of these areas for a higher air temperature. At 22:00, the higher air temperature areas within the 33 to 35 °C range become wider compared to those areas in scenario 2 because of the newly built-up areas on the formerly green buffer zones.

In scenario 4, both the green belts and green buffers are all turned into built-up areas, and no planned green spaces in the master plan are considered within domain 4 in the simulation. As expected, the air temperature pattern at 04:00 illustrates a high temperature of 33 to 35 °C over the expanded built-up areas corresponding to the master plan. At 10:00, however, the air temperatures are slightly lower than the temperatures in scenario 3 for the newly built-up areas transformed from the green buffer areas. At 16:00, high temperatures over 40 °C are found over the expanded built-up areas. The air temperature pattern at 22:00 follows the expected spatial pattern of the built-up areas.

In terms of the surface winds in Fig.6.7, the westerly or south-westerly winds prevail in the western mountainous region throughout the day except for several hours from 18:00-23:00. During this period (18:00-23:00), the south-easterly wind begins blowing at 18:00 and then proceeds to gradually pass over the entire simulated region until 19:00. After this time, the wind changes to a south-north direction. The westerly wind starts blowing over the western mountainous region at midnight (00:00), while the southerly wind still prevails in the eastern half of the simulated areas but with gradually decreasing wind speeds. Two main wind regions are formed on the West side and the East side from the meridional line at 105.65°E of simulated domain 4. Around 09:00, the hot and dry westerly wind reaches the centre of Hanoi, replacing the southerly wind. The westerly or south-westerly winds continue to flow over the entire Hanoi Region until around 17:00. In addition, the simulated results do not show any remarkable difference in terms of the wind patterns near the ground surface among the numerical experiments.

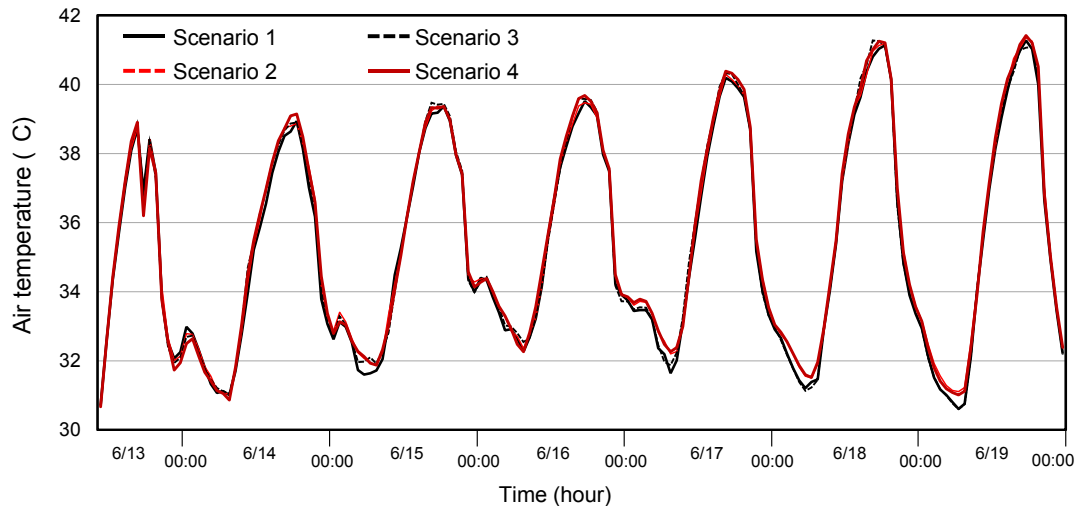


Fig. 6.8 Temporal variations of the simulated air temperatures in different scenarios at Lang Station (see Fig. 1.4 for the location). As shown, the temporal variations of scenarios 2 and 4 are similar, the same for scenarios 1 and 3.

Fig. 6.8 compares the temporal variation of air temperatures at Lang Station for all scenarios. The Lang station is located in the center of Hanoi's urban area (see location in Fig. 1.4). Therefore, from this station, we can observe the impacts of removing each green space to the thermal condition of the existing urban center. As shown in Fig. 6.8, the removal of green belts in scenario 2 increases the air temperature, particularly at the night-time. Meanwhile, if the green buffer is removed from the master plan (scenario 3), the air temperature at Lang station does not experience any significant change. It is mostly due to the location of the green buffer is far from Lang station (approx. 4 km). As has been discussed in Section 2.4, the average distance of the cooling effect is no more than 1 km. Therefore, the cooling effect of the green buffer cannot reach Lang station. Therefore, the temperature increases in scenario 4 (i.e. both proposed green spaces are removed) are also attributed to the absence of green belts instead of the green buffer. The difference between scenario 1 and scenarios 2 and 4 becomes noticeable particularly during nights, with a maximum difference of 1 °C on the 14th and 17th of June.

Spatial distribution of air temperatures differences

Fig. 6.9 depicts the differences in the air temperature at 1:00 and at 16:00 in 17 June between the current status and scenario 4 (i.e. master plan condition without the green strategies). At 1:00, considerable increases in the air temperature over the newly developed built-up areas in the northern and eastern parts of the Red River are found. In particular, in the northern part of the Red River, the temperature increase reaches up to 3 °C in scenario 4. Because no green spaces are considered in this scenario, high temperature rises are observed

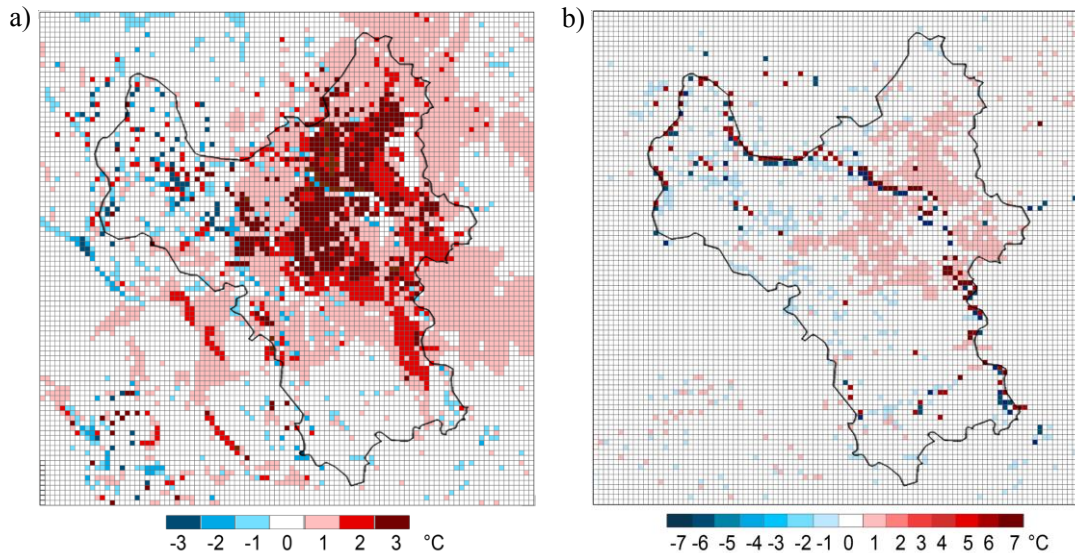


Fig. 6.9 Differences of air temperature between the current status and scenario 4 (master plan condition without green strategies) at (a) 1:00 and (b) 16:00.

over the built-up areas that were formerly green buffer spaces. The air temperature rise of 1 °C at 16:00 is found over the same transformed built-up areas (Fig. 6.9b). The incremental zones of the air temperature in scenarios 1 and 4 correspond to the expanded built-up areas and those transformed from the planned green spaces, respectively.

Figs. 6.10 and Fig. 6.11, indicate the simulated air temperature distributions for the different land categories at 01:00 (Fig. 6.10) and 16:00 (Fig. 6.11) on 17 June 2010. In the case of master plan condition, at 01:00, the built-up area ranges from 31.5 to 34.5 °C with the proportion of the area at a specific temperature peaking at less than 5% at 33.5 °C. Irrigated cropland accounts for the largest proportion ranging from 30 to 33 °C, with the peaks over 15% at 31 and 31.5 °C. The mixed forest records the minimum temperature of approximately 27 °C with the second largest proportion. In the results from scenarios 2-4, though the proportions of the built-up areas are increased due to the transformation of the strategic green spaces into built-up areas, the peak air temperatures of the built-up areas maintain the same value, 33.5 °C, compared to the original master plan condition (scenario 1). This result indicates that the green strategies proposed in the master plan are not necessarily effective at cooling all of the built-up areas at night, though these green strategies largely reduce the air temperatures within the green spaces by up to 2 to 3 °C.

At 16:00 in Fig. 6.11, on average, the air temperature ranges of all of the land categories largely increase compared to the ranges at 01:00, except for the temperature range of the water bodies. The differences in the peak air temperature between the built-up areas and the other vegetated areas become smaller in all of the cases. The proportions of the air temperatures at the peak for the built-up areas and others from scenario 1 (master plan condition) do not change in scenarios 2-4, although the amounts of proportions vary depending on the case. As previously

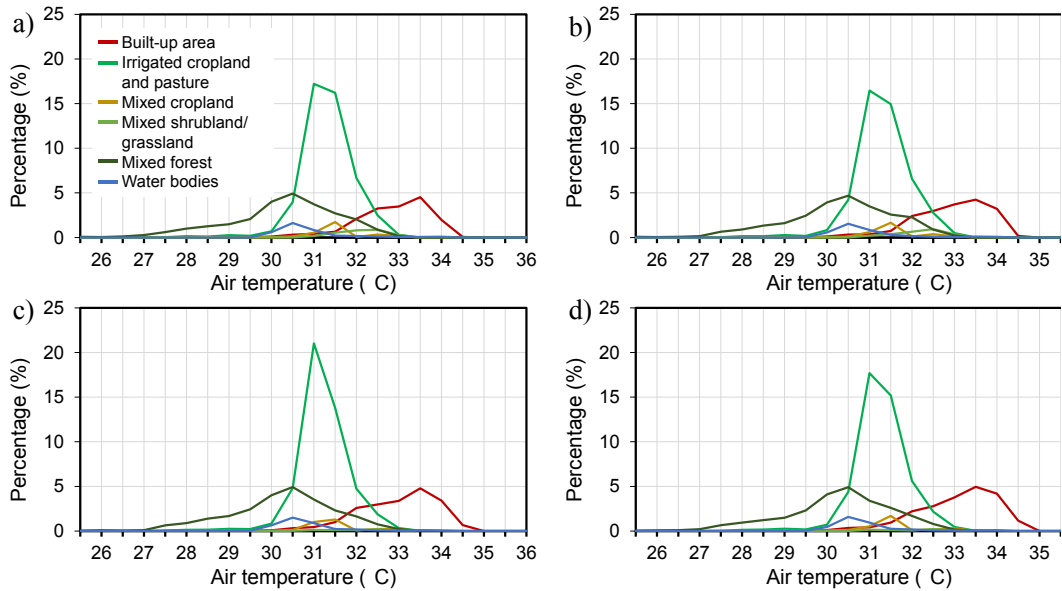


Fig. 6.10 Air temperature distribution by land use categories at 1:00 for (a) scenario 1 (master plan condition), (b) scenario 2, (c) scenario 3, and (d) scenario 4 on 17 June 2010.

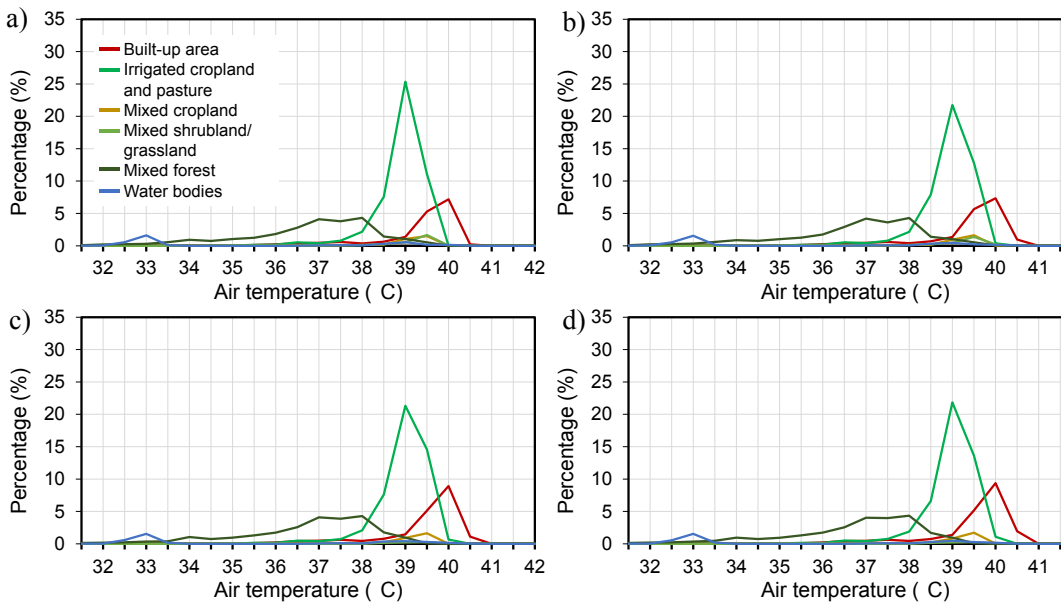


Fig. 6.11 Air temperature distribution by land use categories at 16:00 for (a) scenario 1 (master plan condition), (b) scenario 2, (c) scenario 3, and (d) scenario 4 on 17 June 2010.

discussed herein, the daily peak air temperatures in scenario 1 are not anticipated to increase very much, although the high air temperature areas would enlarge dramatically in line with the expansion of the city.

In Fig. 6.12 and 6.13, the temporal variations in the air temperature and wind speeds along the cross-sections of domain 4 are presented in terms of LULC (see Fig. 6.2 for the locations of cross-sections). Each panel further indicates the simulated air temperature and wind speed variations from scenario 1 to scenario 4 (without green spaces). The horizontal indicator for the LULC category in each panel is based on the master plan condition. Therefore, from Figs. 6.12 and 6.13, the effects of the green spaces and surface winds on the air temperature and UHIs can be discussed.

In Fig. 6.12, the air temperature and wind speeds following a west-east cross-section along the zonal line of 21.04°N are shown for 01:00, 10:00, 13:00, 16:00, and 20:00, from the top panel to the bottom. This cross-section traverses two mountains at heights of approximately 260 m and 280 m in the western region at 105.22°E and 105.40°E , respectively. As shown in Fig. 6.12, the leeward sides of both of the mountains receive relatively higher winds, particularly from 01:00 to 10:00, and the air temperatures increase while flowing down the slopes of the mountains (i.e. the Foehn effect). As discussed before, the westerly or south-westerly winds flow over the entire Hanoi Region from 09:00-17:00. As shown in Fig. 6.12, the air temperature is increased to approximately 34 to 39 °C before entering the urban areas at 105.49°E during the above period. As shown, the wind speed over the built-up areas becomes gradually higher, reaching speeds of 5 to 6 m/s during the daytime from 09:00 to 15:00. In the green strategy areas between 105.53°E and 105.6°E , the winds over the built-up areas from scenario 4 are weaker by approximately 1 to 2 m/s than those winds from scenario 1 (master plan condition). Then, from late afternoon (16:00) to evening (20:00), as the wind direction changes from west to south, the winds over the eastern half of domain 4 become gradually stronger and reach 7 m/s. Interestingly, at 20:00, when the southerly winds of 7 m/s are prevailing over the eastern half from 105.63°E , then the air temperature simulated in scenario 4 drops nearly 3 °C over the built-up areas. The air temperature in the eastern part of the Red River (105.85°E) at 20:00 is reduced even further due to the strong winds.

In general, the air temperature over the built-up areas from scenario 4 at 01:00 is 2 to 3 °C higher than the neighbouring green spaces, irrigated cropland, and forest. Then, during the daytime, when the hot westerly winds flow over the entire region, the air temperature from scenario 4 becomes higher and reaches up to 40.5 °C over the built-up areas at 16:00. The air temperature for the green strategy spaces calculated from scenario 1 also increases during the daytime, but this temperature is approximately 1 °C lower than the built-up areas. On the other hand, the effects of water bodies, specifically the Red River streams at 105.31°E and 105.85°E , are clearly found to lower the temperature near the built-up and green spaces throughout the day. The air temperature over the river streams ranges from 31 to 33.5 °C.

The discrepancies between the air temperatures in the strategic green spaces in scenario 1 and the built-up transformed areas from the above green spaces in scenario 4 are large, up to 2 to 3 °C, when the relatively strong and cool southerly winds prevail at night (e.g., at 20:00 and

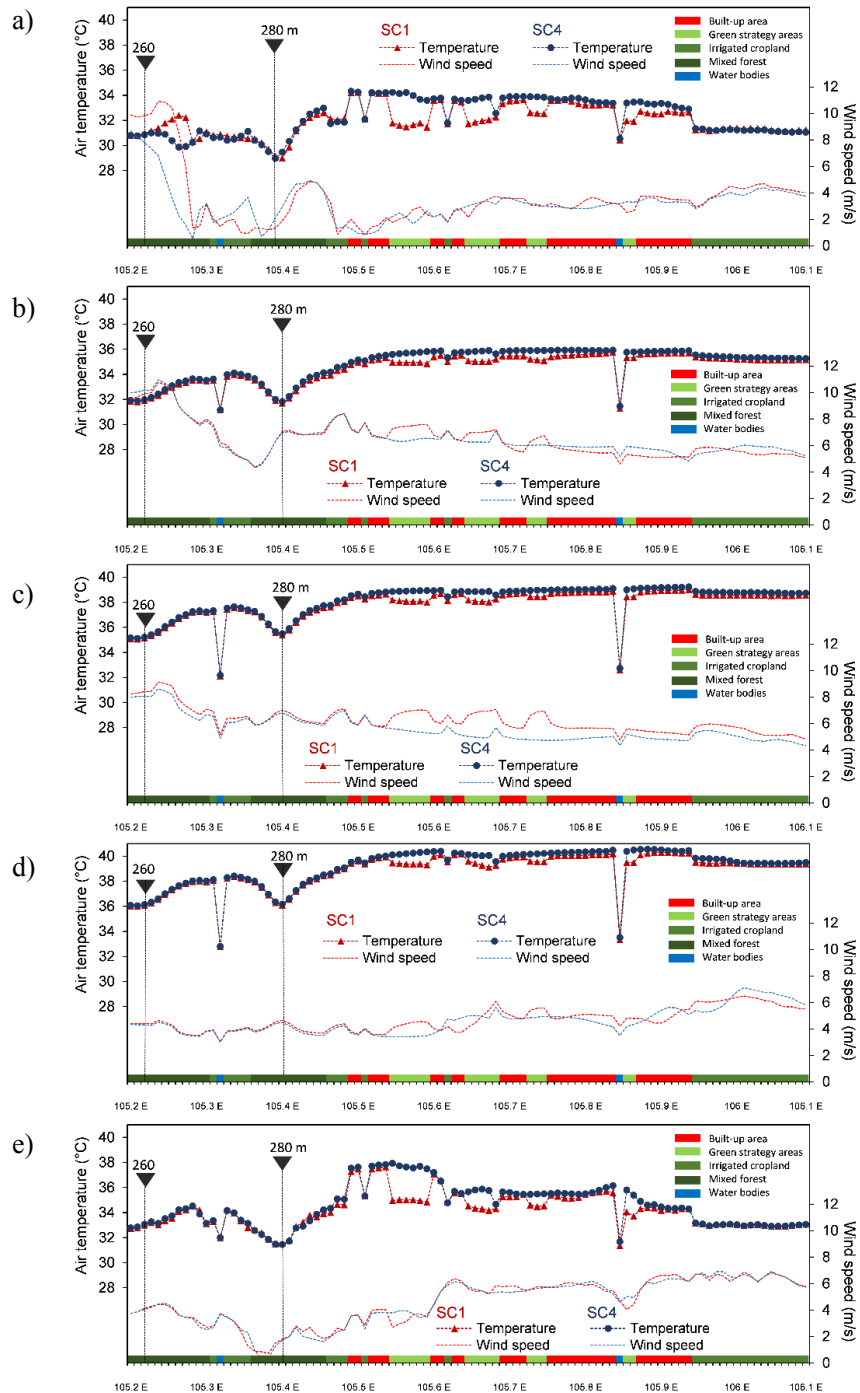


Fig. 6.12 Variations of the simulated air temperature and wind speed from scenario 1 (SC1) and from scenario 4 (SC4) along the west-east cross-section of the zonal line at 21.04° N at (a) 1:00, (b) 10:00, (c) 13:00, (d) 16:00, and (e) 20:00. The horizontal color bar indicates the land use types.

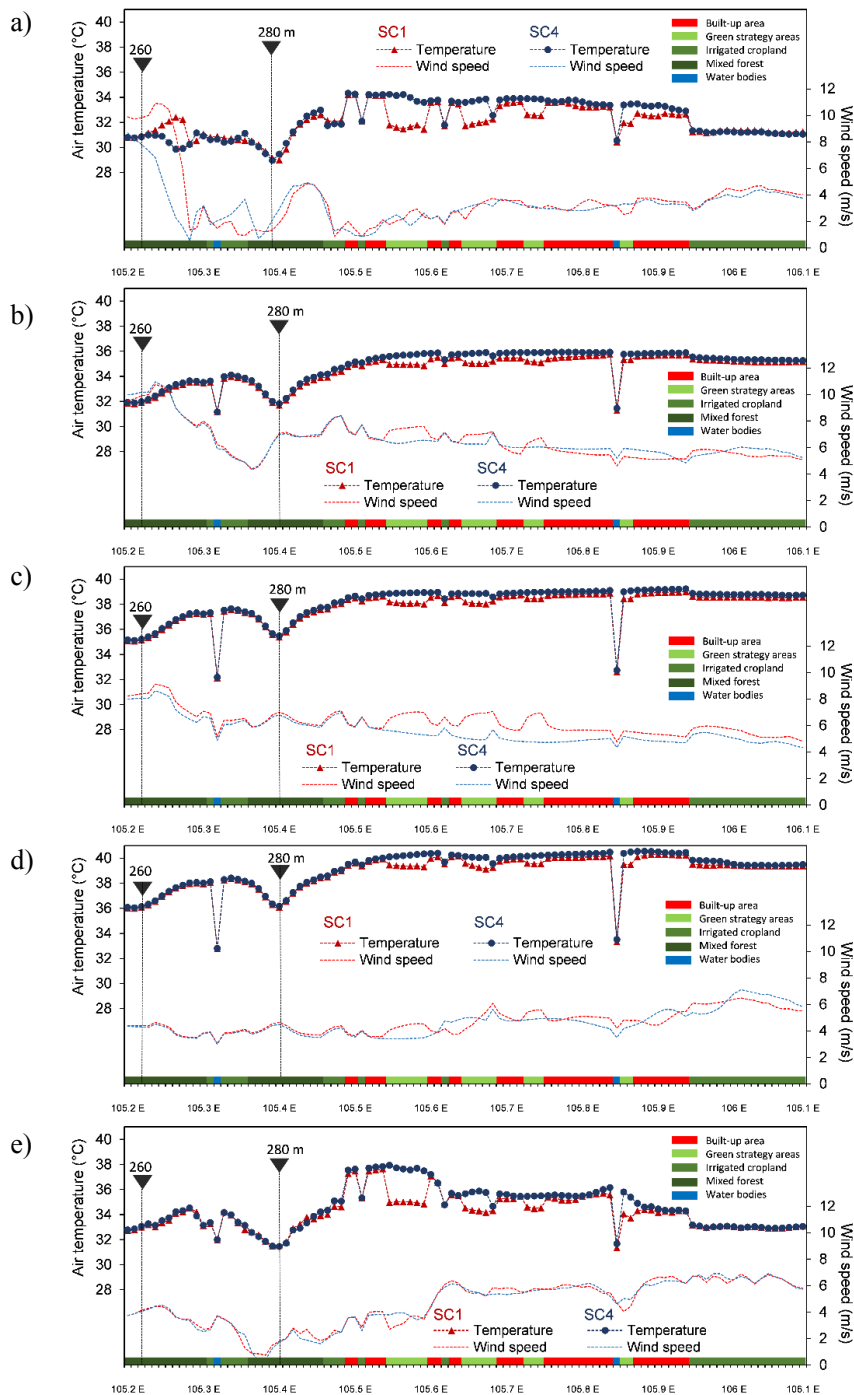


Fig. 6.13 Variations of the simulated air temperature and wind speed from scenario 1 (SC1) and from scenario 4 (SC4) along the south-north cross-section of the zonal line at 105.81° E at (a) 1:00, (b) 10:00, (c) 13:00, (d) 16:00, and (e) 20:00. The horizontal color bar indicates the land use types.

01:00 in Fig. 6.12). In this circumstance, the reduction in the air temperature due to the effects of the strategic green spaces can be observed not only within the green spaces but also in some parts of the surrounding built-up areas, up to 1 °C in scenario 1 (e.g., at 01:00 in Fig. 6.12). These discrepancies are reduced during the daytime as the wind direction changes from the South to the West and the air temperature increases over the built-up areas.

In Fig. 6.13, the air temperature and wind speeds following a south-north cross-section along the 105.81°E zonal line are presented for 01:00, 10:00, 13:00, 16:00, and 20:00, from the top panel to the bottom. The effects of the surface winds on the air temperature are clearly seen, particularly when the southerly winds prevail at night (i.e., at 01:00 and 20:00 in Fig. 6.13). At night, the relatively cool southerly winds flow from the coastal area and pass through the irrigated croplands in the south at 20.85°N. Unlike the daytime hot westerly winds, the southerly winds maintain a relatively lower air temperature of approximately 31 to 33 °C before entering the urban areas at 20.85°N at night. From the above point, the simulated air temperature of the neighbouring built-up area in scenario 4 gradually increases towards the North both at 01:00 and 20:00. The wind speed at 20:00 is relatively strong at 6 to 7 m/s in the south at 21.13°N and then rapidly decreases. Then, the air temperature simulated in scenario 4 depicts a direct and linear response to the corresponding winds. Under the stronger southerly winds at 20:00, the gradient of the air temperature curve becomes steeper than the curve for 01:00. Because the stronger southerly winds blow over consistently, the lower air temperature would be observed over the built-up areas.

6.5.2 Assessment of the new configurations of the green spaces

Spatial distribution of air temperatures

Figs. 6.14 and 6.15 present the spatial distributions of the simulated air temperatures at 2 m above the ground and the winds at 10 m above the ground for scenarios 1, 5, 6, and 7, respectively. In general, the peak air temperature maintains almost at the same level among all scenarios.

In scenario 5 (Fig. 6.14b), the spatial distribution of air temperature and winds are almost similar to those in scenario 1 (Fig. 6.14a). Nevertheless, the mixed forest in the green belt areas shows lower air temperatures than the mixed shrub/grassland in the scenario 1. As a result, the green space with mixed forest contributes to the lower air temperature at its surrounding built-up areas during the daytime, if compared with scenario 1. Therefore, this results in the reduction of the number of areas experiencing hot air temperature. In scenario 6, as shown in Figs. 6.14c and 6.15c, the distributions of air temperature are different than that of scenarios 1 and 5. The low-temperature regions are observed in the new locations of the green spaces. Moreover, the improvement of the urban green space in the built-up area located in the western mountainous region helps to relieve the occurrence of hot air temperature caused by the Foehn wind. Therefore, in scenario 6, at night, the peak air temperature is only observed in the built-up areas located in the eastern region (Fig. 6.14c).

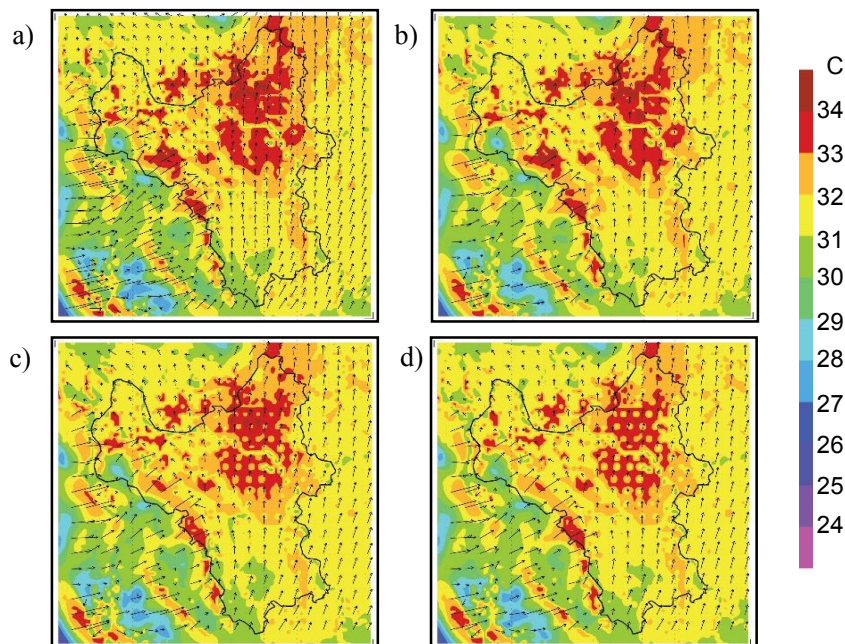


Fig. 6.14 Spatial distributions of air temperatures and winds at 1:00 on 17th June for (a) scenario 1 (b) scenario 5, (c) scenario 6, and (d) scenario 7.

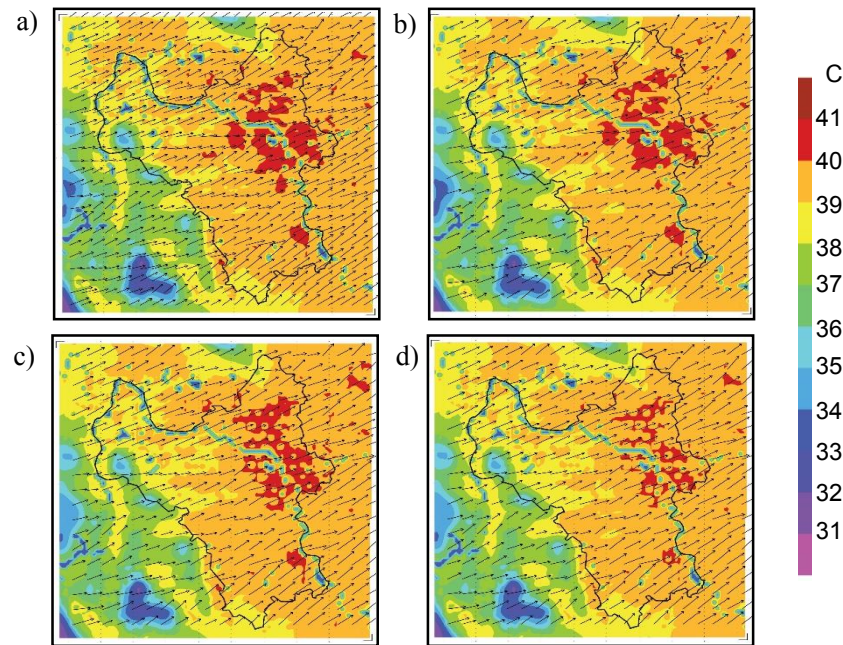


Fig. 6.15 Spatial distributions of air temperatures and winds at 16:00 on 17th June for (a) scenario 1 (b) scenario 5, (c) scenario 6, and (d) scenario 7.

The greater cooling effects of the mixed forest are also seen in scenario 7. At night, the distribution of air temperature produces similar patterns as those in scenario 6 (Fig. 6.14d). However, the air temperature of the green spaces in scenario 7 is lower by up to 2 °C than the surrounding built-up areas, resulting in more reductions of the hotspots than scenario 6. During the daytime, ameliorating effects of scenario 7 to the urban climate becomes more noticeable, with a large reduction of the areas experiencing peak air temperatures (Fig. 6.15d).

Cooling impacts of the new configurations of green spaces.

Figs. 6.16 and 6.17 show the spatial distributions of air temperature differences between scenario 1 and scenarios 5 to 7 at 1:00 and 16:00 on 17 June, respectively. Based on these figures, the cooling effect induced by the different green space configurations can be discussed.

In scenario 5, the largest nocturnal cooling occurs only within the green network itself, by up to 0.5 °C (Fig. 6.16a). The cooling effect of the green spaces is not observed in the surrounding built-up areas. Instead, the mixed forest in scenario 5 induces increases in air temperature at particular locations by up to 0.5 °C at night. This is due to the surface fraction of the mixed forest slightly reduce the wind velocity. When the wind is not strong enough, the heated air is trapped within the urban heat islands.

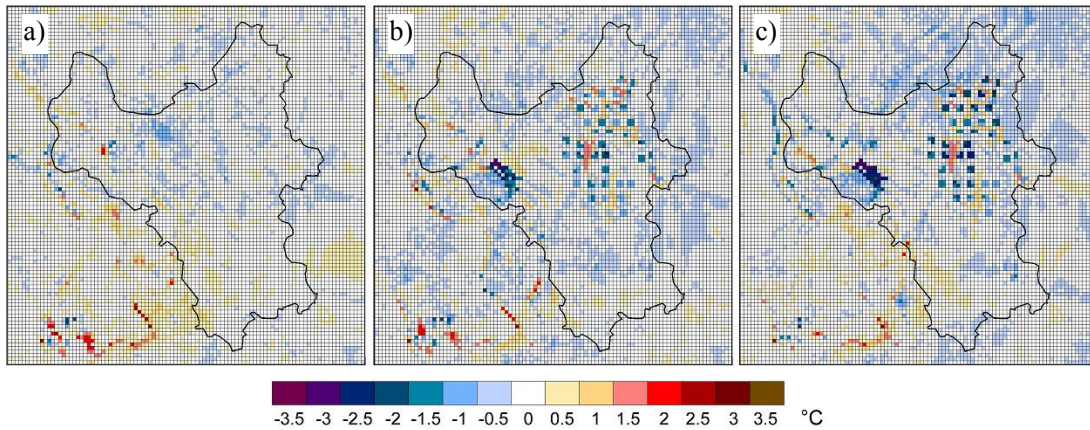


Fig. 6.16 Spatial distributions of air temperature differences between scenario 1 and (a) scenarios 5, (b) scenario 6, and (c) scenario 7 at 1:00 on 17 June.

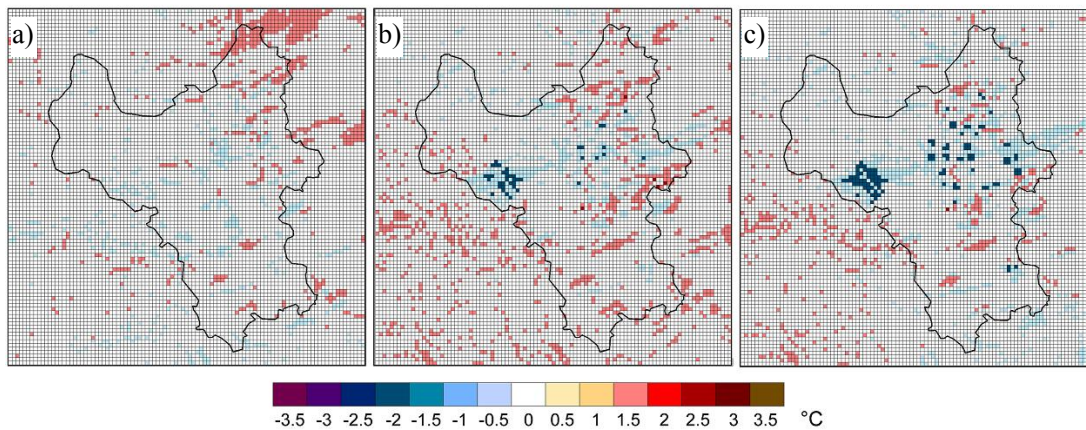


Fig. 6.17 Spatial distributions of air temperature differences between scenario 1 and (a) scenarios 5, (b) scenario 6, and (c) scenario 7 at 16:00 on 17 June.

In scenario 6, the existence of the green spaces and the relatively close distance between them produce a strong nocturnal cooling effect (Fig. 6.16b). The reduction in air temperature induced by the green spaces is evident at the built-up areas around it, with a cooling effect ranging from -0.5 to -1 °C at distances up to 1 km. Meanwhile, the air temperature inside the green spaces in scenario 7 shows lower air temperature inside the green spaces by 0.5 °C than in scenario 6, which is attributed to the cooling effect of the mixed forest (Fig. 6.16c). If the results of scenario 7 are compared with scenario 6, we can see that the reduction of hotspots in scenario 7 is more significant than in scenario 6. The increase in air temperature at particular locations is mainly caused by the changes of the land use that is transformed into the built-up land.

In the daytime, the cooling impact of the mixed forest to the surrounding areas is seen when the winds are relatively strong (6-7 m/s), with the cooling effect of $-0.5\text{ }^{\circ}\text{C}$ within up to 1 km distance (Fig. 6.17a). Regarding the nocturnal thermal condition inside the built-up areas, which is enhanced due to the new configuration of the green spaces, the daytime condition also reveals a positive effect of the equally distributed green spaces and the green space with mixed forest in scenarios 6 and 7, respectively (Figs. 6.17b and c).

Fig. 6.18 shows the air temperature distribution over the built-up areas in scenarios 1,5,6, and 7 at 1:00 and 16:00 on 17th June 2010, respectively. As shown in Fig. 6.18a, the nocturnal air temperatures in the built-up areas range from $30\text{--}34.5\text{ }^{\circ}\text{C}$, with the proportion of the area at specific temperature peaking at $33.5\text{ }^{\circ}\text{C}$. In scenario 6, the proportions of the area with the air temperature of $32.5\text{--}34\text{ }^{\circ}\text{C}$ are reduced, while the proportions of the area with the lower air temperatures of $31\text{--}32\text{ }^{\circ}\text{C}$ are increased. This air temperature shift indicates the reduction in hot air temperature areas after the green spaces are equally distributed within the city. In the daytime, the amount of areas with the air temperature of $39.5\text{ }^{\circ}\text{C}$ is reduced and shifted down to the ranges of $38.5\text{--}39\text{ }^{\circ}\text{C}$, indicating the temperature reduction by $0.5\text{--}1\text{ }^{\circ}\text{C}$ (Fig. 6.18b). The impact of the relocation of the green spaces on the reduction of UHI intensity is greater in the night-time than that in daytime. Moreover, the greater reduction of hotspots is achieved in scenario 7. The combination of equally distributed green spaces with mixed forest results in the reduction of hotspot areas by up to 56.5% in the nighttime and 16.2% during the daytime.

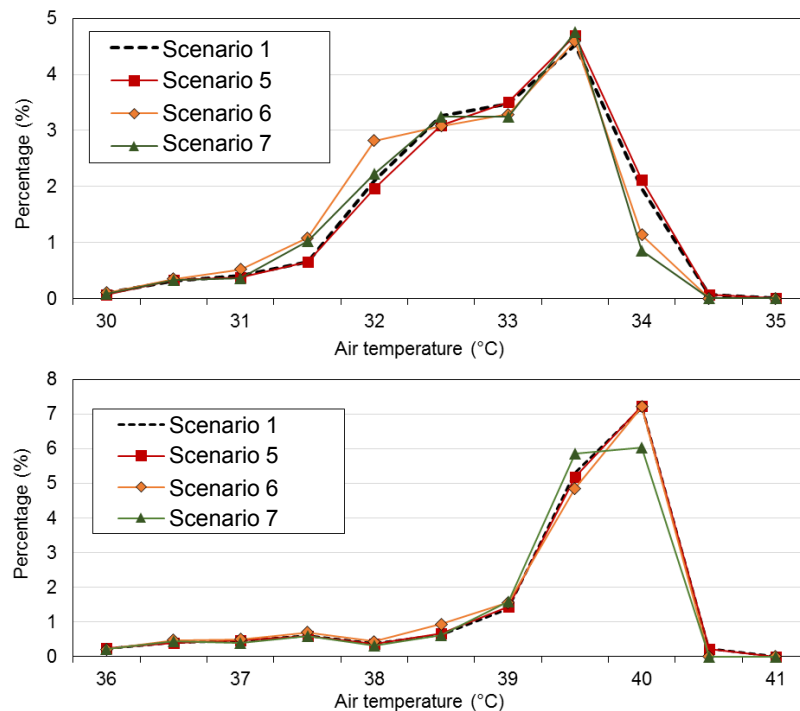


Fig. 6.18 Air temperature distribution over the built-up areas on 17th June at (a) 1:00 and (b) 16:00. The y-axis represent the percentage of built-up area to the total areas in domain 4.

6.5.3 Effects of further urban greening through GCR and vegetation type

Spatial distribution of air temperatures

Figs. 6.19 and 6.20 illustrate the distributions of average air temperature at 2 m above the surface and the winds at 10 m above the surface for cases 2-1, 2-4, 2-5, and 2-6 at 1:00 and 14:00, respectively. In general, the improvement of urban greening through the increased GCRs shows an ameliorating effect on the UHIs in Hanoi. Although it could not lower the peak average air temperature, the number of hotspots is reduced with the increase in GCR (see Fig. 6.19bcd and Fig. 6.20bcd). At night, in all cases, the average air temperatures of 30–30.5 °C are observed over the built-up areas of Hanoi (Fig. 6.19). The peak nocturnal air temperature in cases 2-4, 2-5, and 2-6 remains at the same level with that in case 2-1, which is 30.5 °C. Nevertheless, the number of areas with the peak nocturnal air temperature is reduced significantly after the improvement of GCR. The largest reduction of hotspots is observed in case 2-6 (Fig. 6.19d).

During the daytime, the built-up areas in all cases experience the average air temperatures of 37.5 to 38 °C. A relatively lower air temperature region of 33 to 36.5 °C is observed within

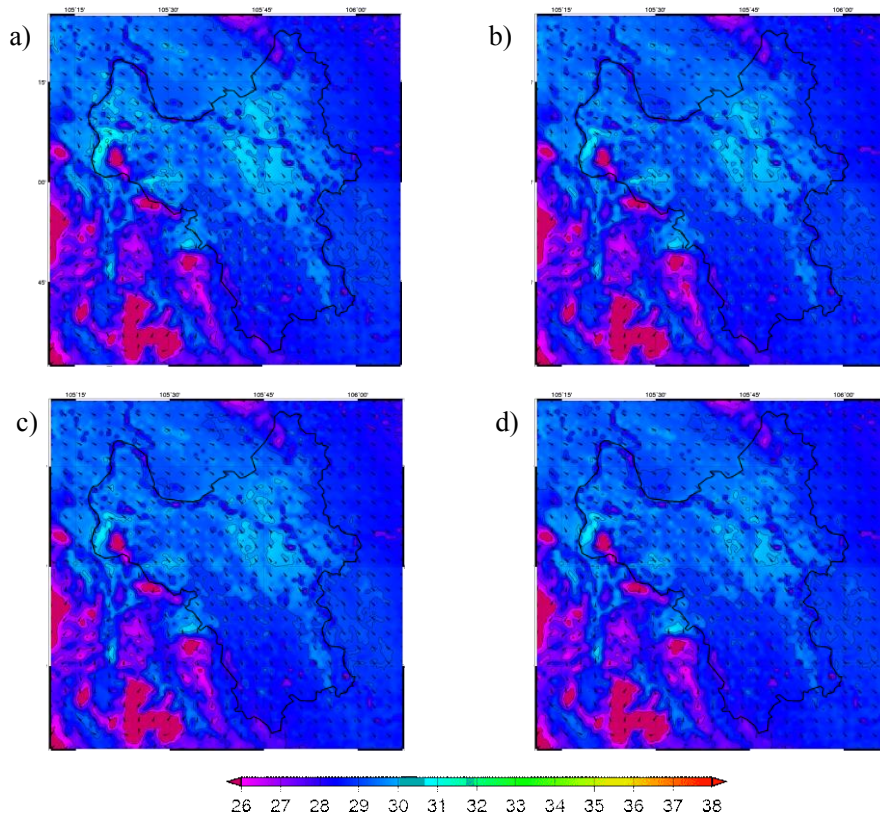


Fig. 6.19 Spatial distributions of average air temperatures at 1:00 (night-time) for (a) Case 2-1, (b) Case 2-4, (c) Case 2-5, and (d) Case 2-6.

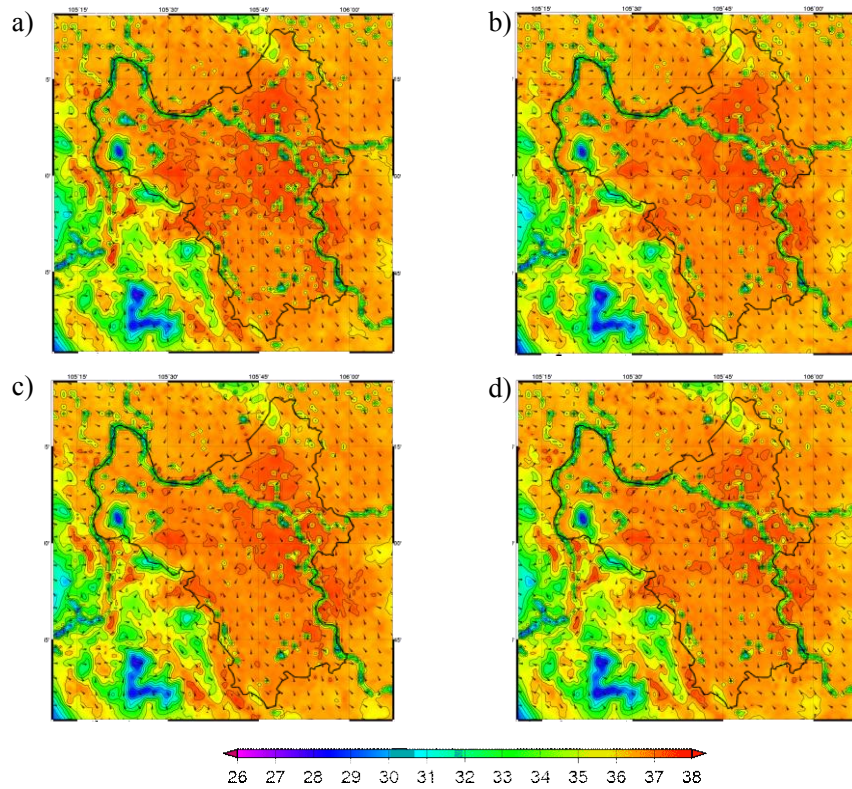


Fig. 6.20 Spatial distributions of average air temperatures at 14:00 (daytime) for (a) Case 2-1, (b) Case 2-4, (c) Case 2-5, and (d) Case 2-6.

the water bodies and vegetative land use, respectively. In case 2-4, the increased GCR of 10% slightly reduces the number of hotspots in the master plan condition (Fig. 6.20b). Moreover, the number of hotspots is further reduced when the GCR is increased to 30% in case 2-5 (Fig. 6.20c). While maintaining the same GCR of case 2-5 (i.e. 30%), the configuration of green spaces in case 2-6 results in a greater reduction of hotspots, owing to the cooling effect of the mixed forest adopted in the green spaces (Fig. 6.20d). Most of the air temperature reductions occur in the new urban areas where the improvement GCRs are employed. There is no significant reduction in air temperature observed in existing urban areas.

Distributions of air temperatures by different land use categories

Fig. 6.21 shows the distribution of average air temperature by different land use categories in existing urban areas at 1:00 for cases 2-1, 2-4, 2-5, and 2-6, respectively. In general, in all cases, the built-up land accounts for the largest proportion of land use in existing

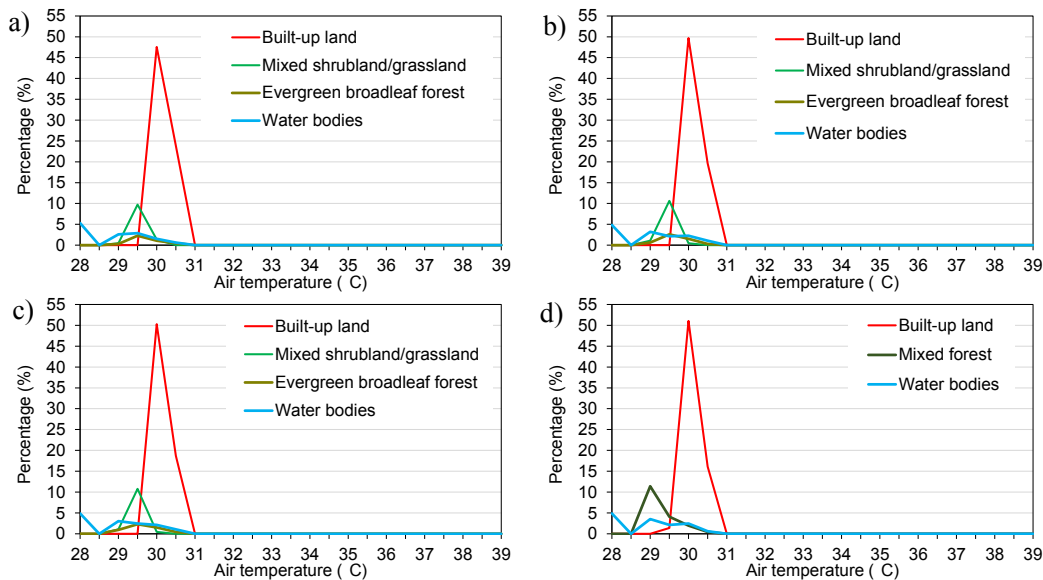


Fig. 6.21 Distribution of average air temperatures by different land use categories in existing urban areas at 1:00 for (a) case 2-1, (b) case 2-4, (c) case 2-5, and (d) case 2-6.

urban areas, with the average air temperature ranges between 29.5 and 30.5 °C, and with the mode value of 30 °C at more than 45% of the land in existing urban areas at night. On the other hand, mixed shrublands/grasslands in cases 2-1, 2-4, and 2-5 experience a lower air temperature range between 29.5 and 30 °C (Fig.6.21abc). The mixed forest in case 2-6 experiences even lower air temperature range, which is from 29 to 30 °C (Fig. 6.21d).

The peak air temperature in existing urban areas in case 2-1 reaches 30.5 °C at night, and it remains the same in the rest of cases. Nevertheless, the percentage of areas with the peak nocturnal average air temperature decreases as the GCR increases. However, the reductions are not significant since the GCR is mostly implemented in new urban areas. The maximum reductions from the master plan condition (i.e. case 2-1) are up to 4.2%, 5.2%, and 7.7% for case 2-4, case 2-5, and case 2-6, respectively.

Fig. 6.22 shows the distribution of average air temperature by different land use categories in existing urban areas at 14:00 for cases 2-1, 2-4, 2-5, and 2-6, respectively. During the daytime, in all cases, the average air temperature over the built-up land ranges between 37 and 38 °C. The mixed shrublands/grasslands in cases 2-1, 2-4, and 2-5 experience a relatively similar temperature range with that of built-up land, which is between 37 and 37.5 °C. Meanwhile, the mixed forest in case 2-6 experiences slightly lower air temperature range than the mixed shrubland/grassland, which is from 36.5 to 37.5 °C (Fig. 6.22d).

In contrast with the night-time, the increased GCRs tend to increase the number of hotspots in existing urban areas during the daytime. For instance, in case 2-4, the percentage of area with peak air temperature of 38 °C is 4% higher than that of the master plan condition (i.e. case 2-

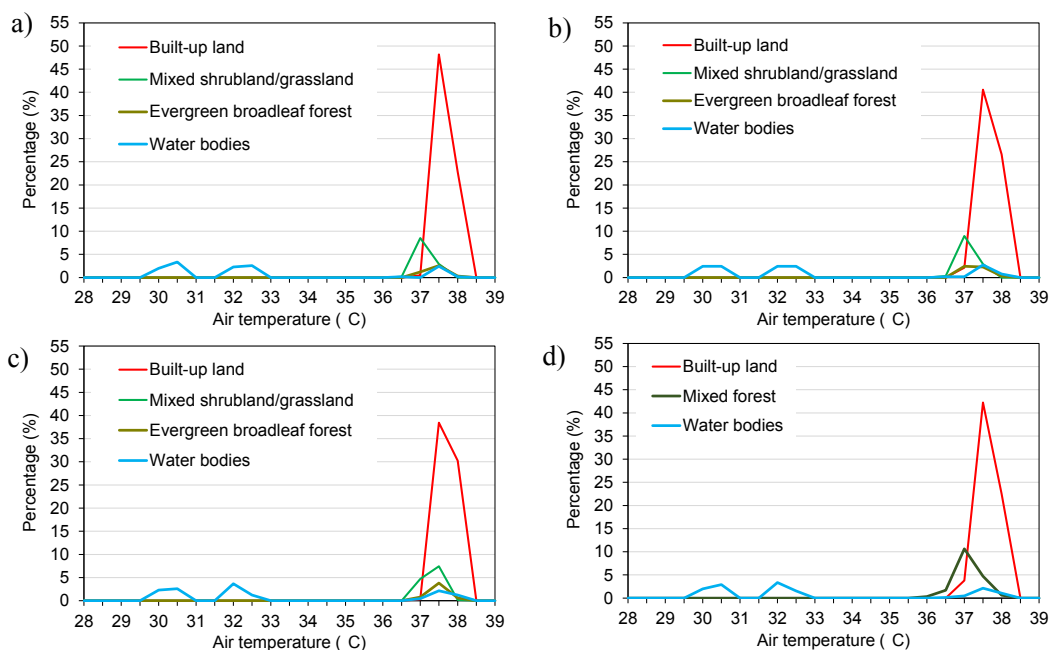


Fig. 6.22 Distribution of average air temperatures by different land use categories in existing urban areas at 14:00 for (a) case 2-1, (b) case 2-4, (c) case 2-5, and (d) case 2-6.

1). The number of hotspots with peak air temperature rises further by approximately 4% after the GCR is increased to 30% in case 2-5 (Fig. 6.22c). Nevertheless, with the same GCR of 30%, the cooling effect of the mixed forest employed in case 2-6 can reduce the hotspots to the same level as in case 2-1, which is 22.5% (Fig. 6.22d). Moreover, the number of built-up land with the relatively low air temperature of 37 °C increases by 4% in case 2-6.

Fig. 6.23 shows the distribution of average air temperature by different land use categories in new urban areas at 1:00 for cases 2-1, 2-4, 2-5, and 2-6, respectively. In case 2-1, the percentage of land experiencing the peak nocturnal air temperature of 30.5 °C is 26% (Fig. 6.23a). The reduction of hotspots reached 9% when GCR is increased by 30% (i.e. case 2-5). Moreover, while maintaining 30% GCR, the greater cooling effect was achieved when the forest species are adopted to the green areas (i.e. case 2-6). This resulted in the reduction of hotspots with peak average air temperature of 30.5 °C by up to 13% from case 2-1 (Fig. 6.23d). The reduction of air temperature in the new urban area is larger than in existing urban area. This is likely because GCR is adopted more within the new urban areas than in the existing urban areas which are already too dense.

At night, the vegetative land use categories in the proposed green spaces, such as mixed shrubland/grassland, evergreen broadleaf forest, and mixed forest; experience the average air temperatures up to 1 °C lower than that of the built-up land. The average air temperature in those land use categories ranges between 29 and 30.5 °C, with the mode value of 29.5 °C observed in all simulation cases.

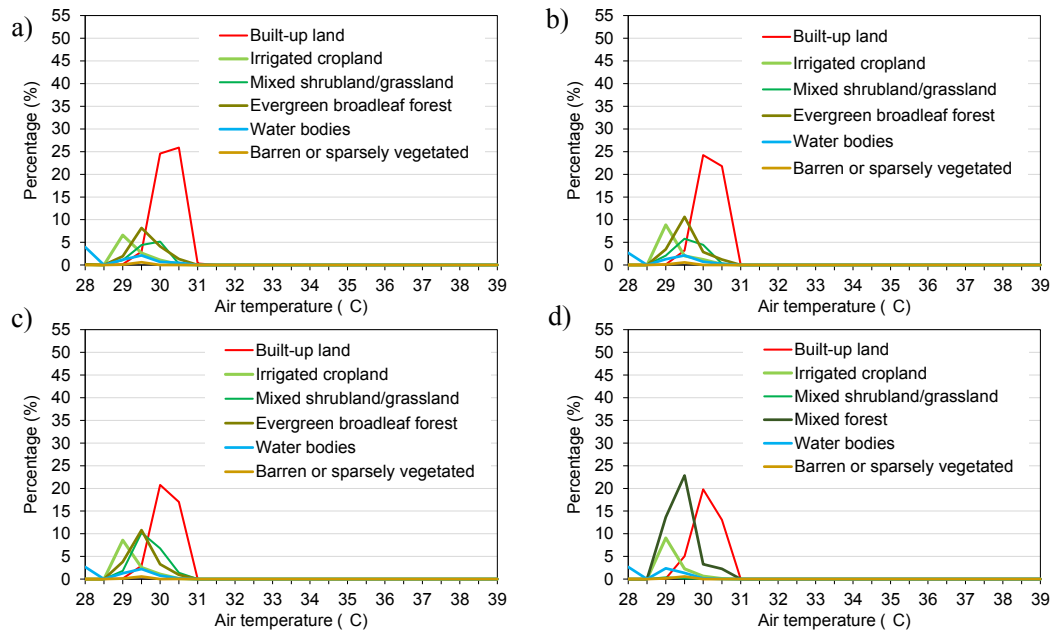


Fig. 6.23 Distribution of average air temperatures by different land use categories in new urban areas at 1:00 for (a) case 2-1, (b) case 2-4, (c) case 2-5, and (d) case 2-6.

Fig. 6.24 shows the distribution of average air temperature by different land use categories in new urban areas at 14:00 for cases 2-1, 2-4, 2-5, and 2-6, respectively. In the daytime, the average air temperature range in new built-up areas is the same with those in existing built-up areas, which is between 37 and 38 °C. The vegetative land use categories in the proposed green spaces experience the average air temperature up to 0.5 °C lower than that of the built-up land. The average air temperatures in those land use categories range between 37 and 38 °C, with the mode value of 37.5 °C in all simulation cases.

In case 2-6, the cooling effect of the mixed forest results in a notable increase in the percentage of green spaces experiencing the average air temperatures of 37 °C. With the more green spaces are within the low-air temperature region, the more built-up lands can be benefitted from their cooling effects. As a result, the percentage of areas with the peak air temperature of 38 °C can be reduced by up to 21% (i.e. from 35% in case 2-1 to 14% in case 2-6). Furthermore, from the results obtained in new urban areas, the increased GCR can lead to a greater reduction in the number of hotspots during the daytime than at night. The further reduction is achieved when the mixed forest is employed as the vegetation type in the proposed green spaces.

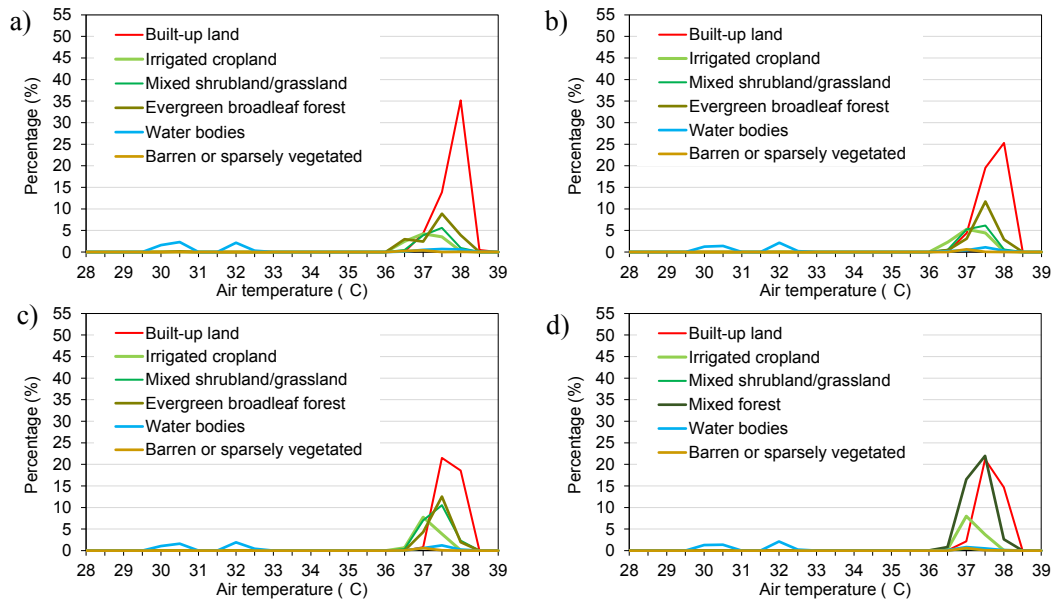


Fig. 6.24 Distribution of average air temperatures by different land use categories in new urban areas at 14:00 for (a) case 2-1, (b) case 2-4, (c) case 2-5, and (d) case 2-6.

Spatial distribution of air temperature differences

Fig. 6.25 shows the spatial distributions of average air temperature differences between the master plan condition and cases 2-4, 2-5, and 2-6, respectively. The positive values in Fig. 6.25 shows the increased air temperatures, while the negative values indicate the reductions in air temperatures due to the increased GCRs.

In general, the increased GCRs in cases 2-4, 2-5 and 2-6 result in the reductions in air temperatures by up to 1 °C, particularly in new urban areas where the improvement of GCR is implemented. Furthermore, the number of areas with reductions in average air temperatures increase as the GCR increases (Fig. 6.25).

At night, in case 2-4, the average air temperature reduction is up to 1 °C. The similar air temperature reduction of 1 °C also occurs in case 2-5. Although the magnitude of air temperature difference between cases 2-4 and 2-5 is the same, the number of areas experiencing air temperature reduction in case 2-5 is more than those in case 2-4. Furthermore, the greatest number of areas with the decreased air temperatures are observed in case 2-6.

During the daytime, in case 2-4, the maximum reduction of average air temperature by up to 0.5 °C is observed in most of the areas experiencing the reduction in average air temperature. Meanwhile, in cases 2-5 and 2-6, the maximum average air temperature reduction is up to 1 °C; however, it is only observed in a very limited area of cases 2-5 and 2-6. Most of the cooled region in cases 2-5 and 2-6 experience the reduction of air temperature of 0.5 °C. With

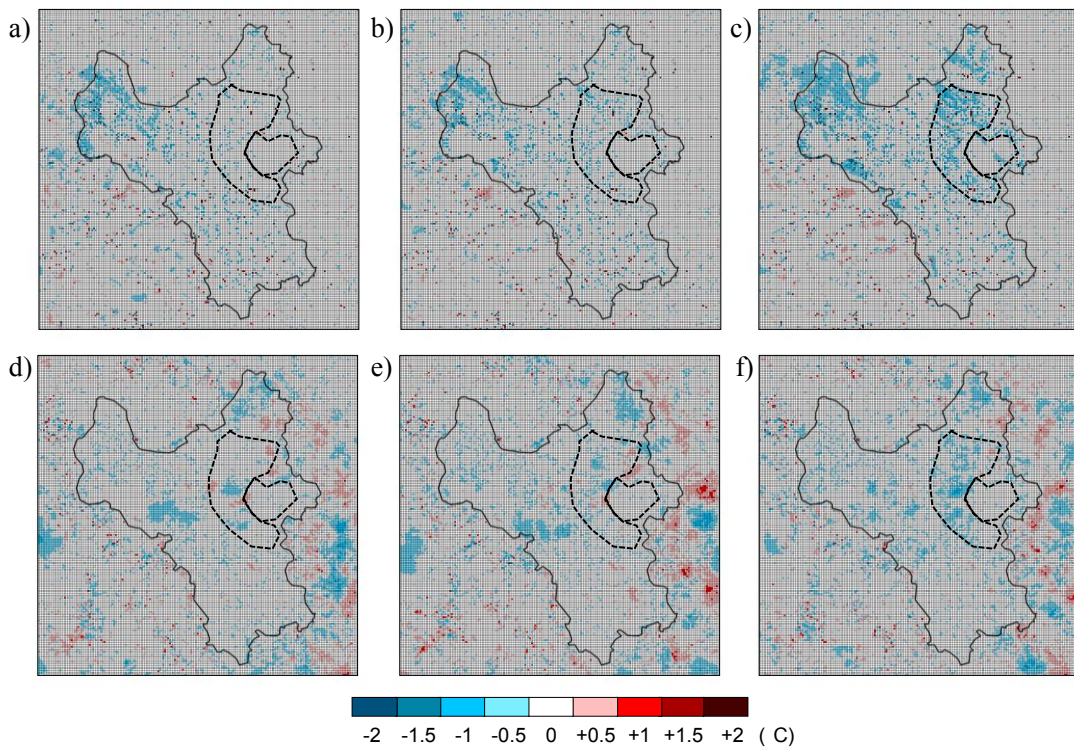


Fig. 6.25 Spatial distributions of air temperature differences. The above panels illustrated the spatial distribution of air temperature difference at 1:00 between (a) cases 2-1 and 2-4, (b) cases 2-1 and 2-5, (c) cases 2-1 and 2-6. The below panels are the spatial distributions at 16:00 between (d) cases 2-1 and 2-4, (e) cases 2-1 and 2-5, (f) cases 2-1 and 2-6.

the same GCR of 30%, more decreased temperature regions are observed in case 2-6 than in case 2-5. This is attributed to the use of mixed forest in the green spaces of case 2-6.

Diurnal variations of air temperature, relative humidity, and wind speed

Fig. 6.26 shows the diurnal variations of average air temperature, wind speed and relative humidity of all cases in existing and new urban areas, respectively. As shown in Fig. 6.26, the increased GCR in new urban areas does not influence the thermal environment as well as the wind conditions in existing urban areas (Fig. 6.26abc). The reduction of air temperatures between cases 2-1 and the other simulation cases is up to 0.1 °C, in average, both in daytime and night-time, respectively.

On the other hand, the results show that if the GCR in new urban areas is increased to 10%, then the average reduction in air temperature at night (18:00 and 06:00) in those areas is up to

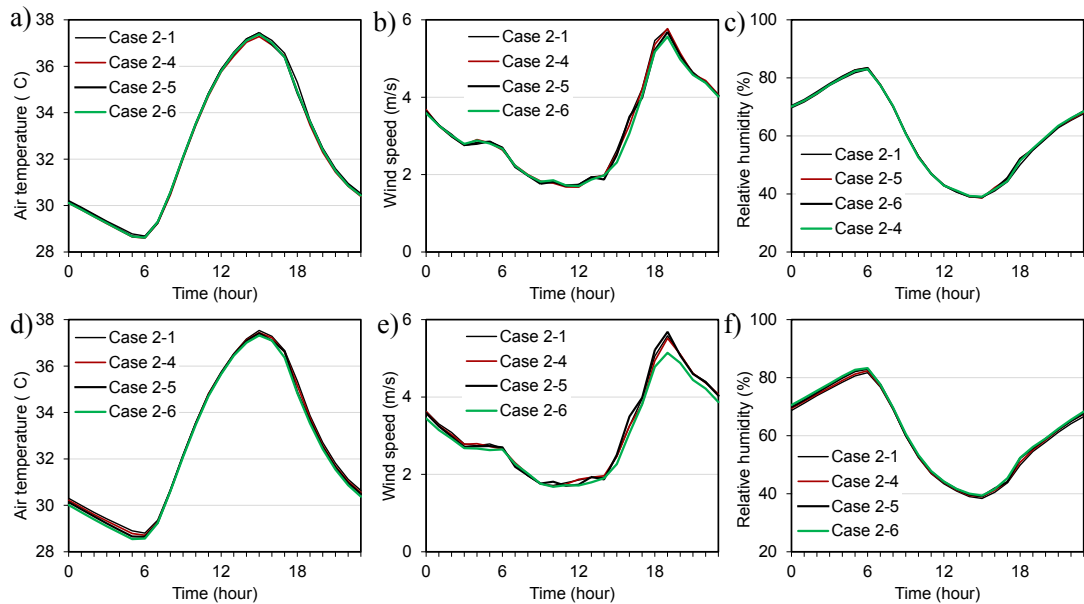


Fig. 6.26 The upper panels shows the diurnal variations of (a) air temperature, (b) wind speed, and (c) relative humidity in existing urban areas while the lower panels are for those in new urban areas.

0.1 °C lower than the average air temperature projected in the master plan. More reduction up to 0.2 °C (average air temperature reduction between 18:00 and 06:00) is achievable when the GCR is increased to 30%. Furthermore, a greater reduction was seen in case 2-6, by up to 0.3 °C in average during the night-time. In general, the reductions in air temperatures between case 2-1 and cases 2-4, 2-5, 2-6 are more notable during the night-time than those during the daytime. Meanwhile, the maximum reduction in air temperature is up to 0.52 °C which is recorded in the air temperature difference between cases 2-1 and 2-6 (Fig. 6.26d).

Nevertheless, the increase in GCR potentially raises the relative humidity and lowered the wind speed. Further, the combination of GCR and adoption of forest species in the green spaces results in lowering the wind speed in the urban areas throughout the day, notably during the night-time (Fig. 6.26e). Moreover, increasing the GCR together with the implementation of the forest species will also further increase the relative humidity by up to 2% to 4% in new urban areas (Fig. 6.26f).

Energy balance analysis

The configuration of the green spaces can help to lower the increased urban air temperature after the implementation of the master plan. The result in suggests to increase the

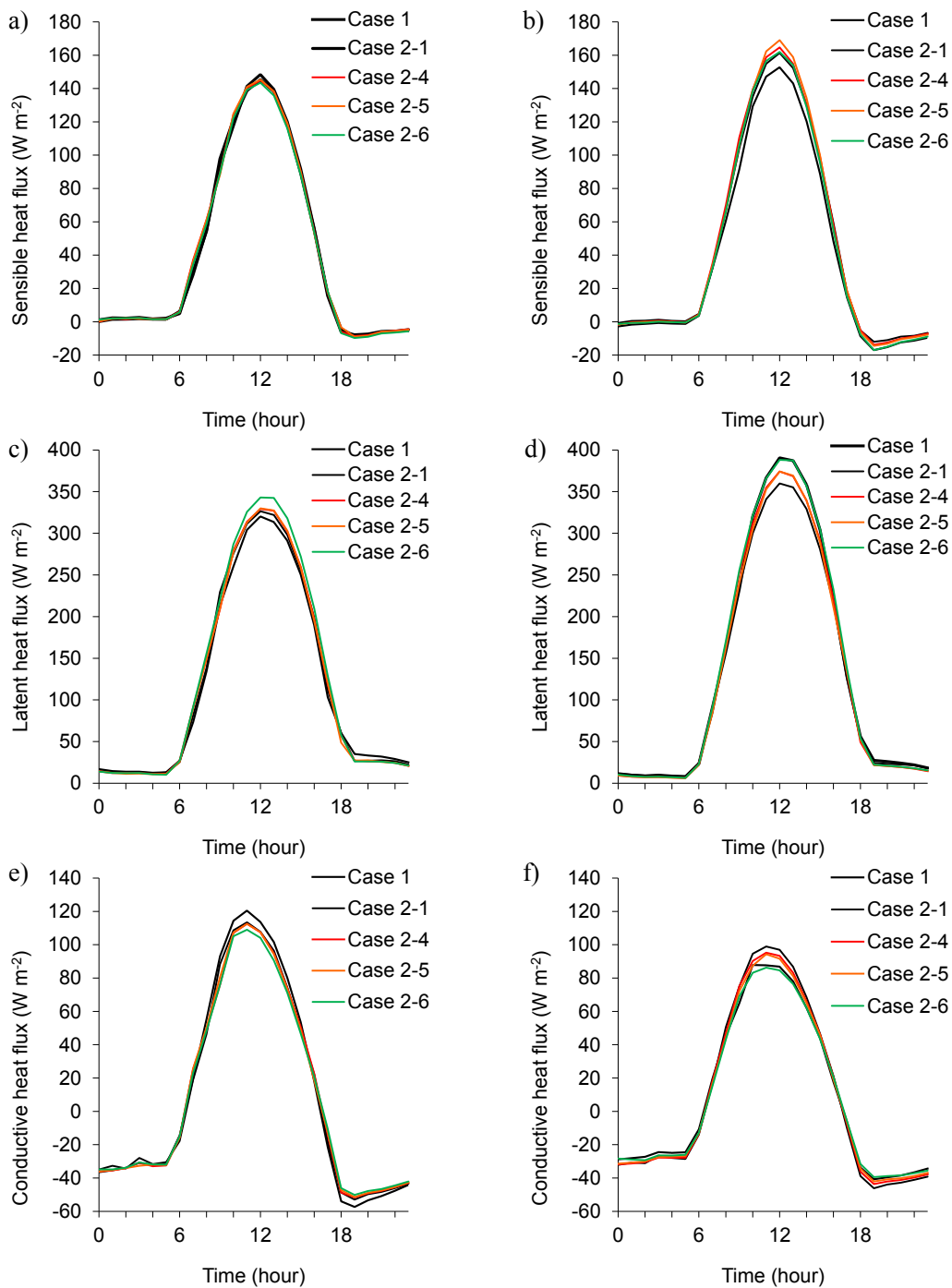


Fig. 6.27 The sensible, latent, and conductive heat fluxes in different land use conditions in existing (left panels) and new urban areas (right panels) of Hanoi case study.

GCR in new urban areas by 30% and to use the mixed forest as the vegetation type in the green spaces. This strategy results in the reduction in the average air temperature of the master plan condition by averagely 0.3 °C at night. This is particularly due to the reduction in sensible heat during the night-time (Fig. 6.27b). Furthermore, the increased vegetative surface in the city results in the increase in latent heat, particularly in new urban areas (Fig. 6.27d). The simulation results also show that the increase in GCR in new urban areas also potentially increases the sensible heat (Fig. 6.27b) during the daytime. Nevertheless, during the daytime, the influence of sun radiation is much stronger, therefore, the impact of increased sensible heat due to the increased vegetative surface is negligible during the daytime.

6.6 Summary

This chapter investigates the cooling effects of the proposed green spaces in the Hanoi Master Plan 2030 through a scenario analysis with a numerical simulation model, the WRF. Furthermore, three new configurations of green spaces for Hanoi Master Plan 2030 were proposed, and the resulting impacts on the reduction of air temperature were analyzed. Last, the additional urban greening to achieve more distributed green spaces by increasing the green coverage ratio (GCR) in each lot of built-up lands were simulated. The main findings are as follows:

1. The simulation results indicated that the green strategies proposed in the master plan are not necessarily effective at cooling all of the built-up areas during both periods, though these strategies largely reduce the air temperatures within the green spaces by up to 2 to 3 °C, particularly at night.
2. On the other hand, the equally distributed green areas show a better performance in the reduction of urban air temperature, especially at night.
3. The increased GCR results in the reduction of the number of hotspots with peak air temperature, particularly in new urban areas throughout the day.
4. The greater reduction of the hotspots during the daytime and night-time is achieved when the mixed forest is used as the vegetation cover in the equally distributed green network. This strategy can lower the temperature by averagely 0.3 °C during the night-time. Nevertheless, trees in the green spaces should be carefully planted as they may block the wind flows and increase the humidity.
5. It is difficult to increase medium-to-large scale green spaces in the existing urban areas. Since the new urban areas are still under development, it is necessary to introduce a minimum standard of GCR in those areas.

7

Influence of anthropogenic heat release on urban climate: A case study of Johor Bahru

7.1 Objectives

This chapter discusses the influence of anthropogenic heat release on urban climate. The city of Johor Bahru (JB), Malaysia, was chosen as the case study. In JB, a comprehensive climate change mitigation strategies, namely the Low Carbon Society (LCS) Blueprint, was introduced to reduce the anthropogenic emission in the future development of the city. There are two future scenarios investigated in the LCS, which are BaU (business as usual) and CM (countermeasures) scenarios (Universiti Teknologi Malaysia et al., 2009).

The main objective of this chapter is to investigate the future urban climate under the BaU and CM scenarios, respectively. In this study, the spatial and temporal distributions of present and future anthropogenic heat emissions are quantified. Then, a numerical simulation model, the WRF coupled with UCM, was employed to estimate the impacts of anthropogenic heat emissions on the urban climate.

7.2 Scenarios for numerical experiments

We formed three scenarios, namely case 1-1, case 2-1, and case 2-2, respectively. Case 1-1 depicts the LULC of the present condition with the anthropogenic heat emission in 2008. The

LULC of case 1-1 is the same with the LULC used in case 1 in Section 4.2.3 in Chapter 4. Meanwhile, cases 2-1 and 2-2 represent the master plan condition under BaU and CM scenarios, respectively. The main difference between the WRF simulation in this chapter and those in Chapter 4 is that the anthropogenic heat emission is taken into account. The LULC dataset for cases 2-1 and 2-2 is the same with the LULC for case 2 in Section 4.2.3 in Chapter 4 of this thesis.

7.3 Calculation of anthropogenic heat emission for current condition

The fundamental theory for estimating the anthropogenic heat emission is the urban (surface) energy balance (UEB) which is expressed as (Oke, 1987):

$$Q^* + Q_F = Q_H + Q_E + \Delta Q_S + \Delta Q_A \quad [\text{W m}^{-2}] \quad (1)$$

where Q^* is the net all-wave radiation flux, Q_H and Q_E are the turbulent sensible and latent heat fluxes, respectively. ΔQ_S is the net heat storage flux and ΔQ_A the net horizontal advective heat flux. Q_F is the anthropogenic heat flux and the focus of this present study. Positive values on the left-hand side of Eq. (1) are inputs to the system, while positive values on the right-hand side are outputs or losses.

Q_F is estimated as the sum of the major sources of waste heat (e.g. Sailor & Lu 2004):

$$Q_F = Q_V + Q_B + Q_M \quad [\text{W m}^{-2}] \quad (2)$$

where Q_V , Q_B , and Q_M are the contributions to the anthropogenic heat flux from traffic, buildings, and human metabolism, respectively. The three terms on the right-hand side of Eq. (2) were determined using different inventory-based modelling approach (i.e. top-down and bottom-up approach).

Due to the issues associated to the data availability, we employed a combination of top-down and bottom-up approaches. It should be noted that the inventory based analysis assumes that energy consumption equals anthropogenic heat emissions although this ignores the fact that the energy used in urban context is also embodied in other components of UEB.

7.3.1 Anthropogenic heat releases from traffic

The hourly heat emission from the combustion of vehicle fuels (Q_v) is computed by using this formula:

$$Q_v(h) = [\sum_{ijk} (n_{vijk}(h) \times EV_{ij} \times d_k) / 3600] / A \quad [\text{Wm}^{-2}] \quad (3)$$

$$EV_{ij} = (NHC_{ij} \times \rho_j) / FE_{ij} \quad [\text{Jm}^{-1}] \quad (4)$$

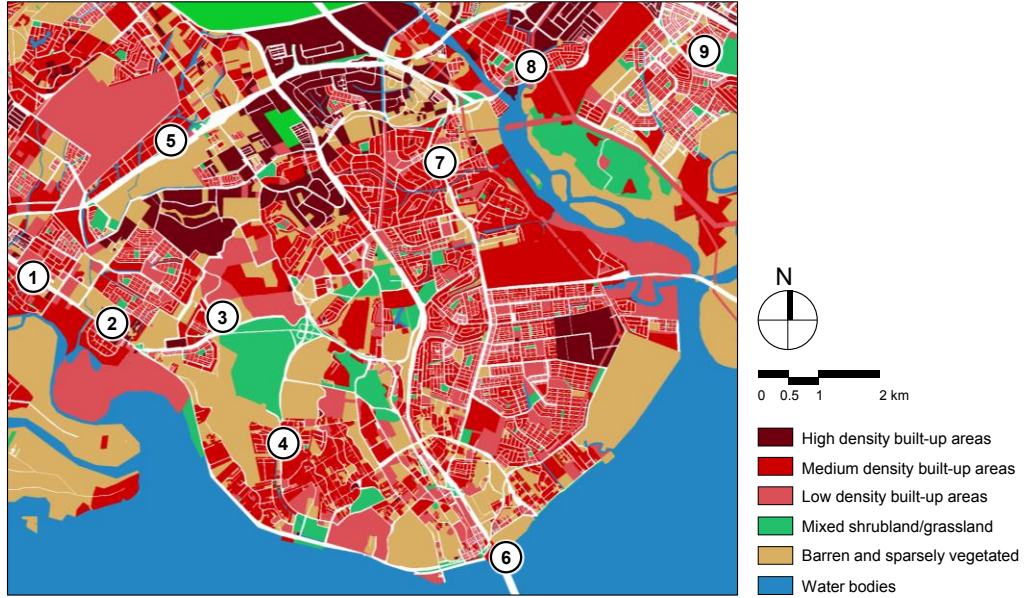


Fig. 7.1 Map showing the location of the survey stations listed in Table 7.1 and land use categories in JB.

where h is local time (hour; solar time +1 h), subscripts i, j and k indicate vehicle class, fuel type and road segment, respectively, $n_{vij k}(h)$ is the hourly total number of class i vehicles consuming fuel type j and travelling on road segment k at hour h , d_k is vehicle distance travelled on road segment k (m), EV_{ij} is the energy used per vehicle of class i consuming fuel type j (J/m), A is the size of the study area (m²), NHC_{ij} is the net heat combustion of fuel type j (J/kg), ρ_j is the density of fuel type j (kg/l) and FE_{ij} is the mean fuel economy of class i vehicles consuming fuel type j (m/l). Q_v is a function of the number of vehicles, energy used by vehicles, and distance travelled by vehicles within the study area. Two assumptions were made in using the above formula. First, the road length follows the length of the domain grid

Table 7.1 Summary of data collection at all traffic survey stations in JB.

| Survey station | Station code in RVTM | Road class | Urban type representation | Counting periods (hours) | Measurement periods (day) |
|----------------|----------------------|--------------|---------------------------|--------------------------|---------------------------|
| 1 | JR 205 | Federal road | Residential | 16 (6:00-22:00) | 7 |
| 2 | JR 206 | Federal road | Residential | 16 | 7 |
| 3 | JR 210 | Federal road | Residential | 16 | 7 |
| 4 | JR 207 | State road | Residential | 16 | 1 |
| 5 | JR 211 | Federal road | Industrial | 16 | 1 |
| 6 | JR 208 | Expressway | Commercial | 24 | 7 |
| 7 | JR 215 | Federal road | Commercial | 16 | 1 |
| 8 | JR 214 | State road | Industrial | 16 | 1 |
| 9 | JR 216 | Federal road | Industrial | 16 | 1 |

and horizontal spatial resolution in WRF model, which is 500 m. Second, the size of study area is the size of one mesh in domain 3, which is 250,000 m².

Data sources

The number of vehicles per hour ($n_{vijk}(h)$) was obtained from the digital report on Road Traffic Volume Malaysia (RTVM) 2014 by the Highway Planning Division, Ministry of Works, Malaysia (<http://rtvm.kkr.gov.my/app>). The survey took place at nine survey stations in JB as shown in the Fig. 7.1. In RVTM, the vehicles are classified into six classes, which are: motor cars and taxis, small vans and utilities, lorries and large vans, lorries with 3-axles, busses, and motorcycles. We assumed that the number of vehicles in each urban category (i.e. residential, commercial, and industrial) can be associated with the location of each survey

Table 7.2 Percentage of fuel type by vehicle type.

| Vehicle type | Petrol | Diesel | NGV | Electric | Petrol & Electric | Petrol & NGV |
|----------------|--------|--------|------|----------|-------------------|--------------|
| Motorcycle | 99.97 | 0 | 0 | 0.02 | 0 | 0 |
| Motorcar | 96.79 | 0.34 | 0 | 0 | 2.84 | 0.02 |
| Bus | 21.33 | 71.09 | 2.37 | 0 | 0 | 5.21 |
| Taxi | 18.49 | 0 | 0.16 | 0 | 0 | 81.35 |
| Hire&Drive Car | 97.71 | 0.97 | 0 | 0 | 1.06 | 0.26 |
| Goods vehicle | 27.59 | 71.82 | 0.35 | 0 | 0 | 0.24 |
| Others | 27.54 | 72.05 | 0 | 0.34 | 0.01 | 0.06 |

Source: Transport Statistic Malaysia 2013.

Table 7.3 Percentage of vehicle by types from 2008 to 2013.

| Year | Motorcycle | Motor Car | Bus | Taxi | Hire & Drive Car | Goods Vehicle | Others |
|------|------------|-----------|--------|--------|------------------|---------------|--------|
| 2008 | 1,286,032 | 1,020,978 | 9,348 | 11,461 | 103 | 113,589 | 45,351 |
| 2009 | 1,348,349 | 1,086,147 | 9,638 | 11,808 | 103 | 117,338 | 47,237 |
| 2010 | 1,414,665 | 1,160,041 | 9,982 | 12,022 | 114 | 121,729 | 49,713 |
| 2011 | 1,488,653 | 1,234,331 | 10,268 | 12,281 | 122 | 126,222 | 52,021 |
| 2012 | 1,574,475 | 1,312,016 | 10,548 | 12,392 | 120 | 131,007 | 54,398 |
| 2013 | 1,646,941 | 1,339,446 | 8,196 | 11,808 | 2740 | 139,681 | 93,883 |

Source: Transport Statistic Malaysia 2013.

Table 7.4 Net heat combustion and fuel density of fuel type.

| Vehicle type | Fuel type | Net heat combustion (MJ kg ⁻¹) | Density of fuel type (kg l ⁻¹) | FE ¹ (m l ⁻¹) | EV (J m ⁻¹) |
|---------------|---------------------|--|--|--------------------------------------|-------------------------|
| Car/Taxi * | Petrol ¹ | 46.41 | 0.75 | 10,416.67 | 3341.52 |
| Minivan | Petrol ¹ | 46.41 | 0.75 | 9900.99 | 3515.56 |
| Lorry/Big van | Diesel ² | 42.81 | 0.85 | 7092.2 | 5130.78 |
| Lorry (big) | Diesel ² | 42.81 | 0.85 | 6849.32 | 5312.72 |
| Bus | Diesel ² | 42.81 | 0.85 | 2178.65 | 16,702.32 |
| Motorcycle | Petrol ¹ | 46.41 | 0.75 | 29,411.76 | 1183.46 |

Note: Fuel density varies with ambient temperature; as such the mid-point value (in parenthesis) was used.

Sources: ¹Shell Eastern Petroleum (Pte) Ltd. in (Quah & Roth, 2012), ²world-nuclear.org.

station. The durations of the survey were mostly only 16 hours per day, from 6:00 to 22:00 (only survey station no. 6 conducted 24 hours measurement). Therefore, the minimum counts of vehicles were used to fill the remaining unmeasured time slots. Table 7.1 summarizes further details of all survey stations.

The fuel type used in JB was calculated based on the data for new registered motor vehicles by type of fuel usage in Transport Statistic Malaysia 2013 as shown in Table 7.2. In Malaysia, most of the motorcars are fueled with petrol, while most of taxis are bi-fuel vehicle which use the combination of petrol and natural gas (NGV). Nevertheless, the proportion of taxi is very small compared to motorcar (see Table 7.3). Therefore, petrol is assumed to be used for all motorcar although taxi is included in this category. The values for the net heat combustion

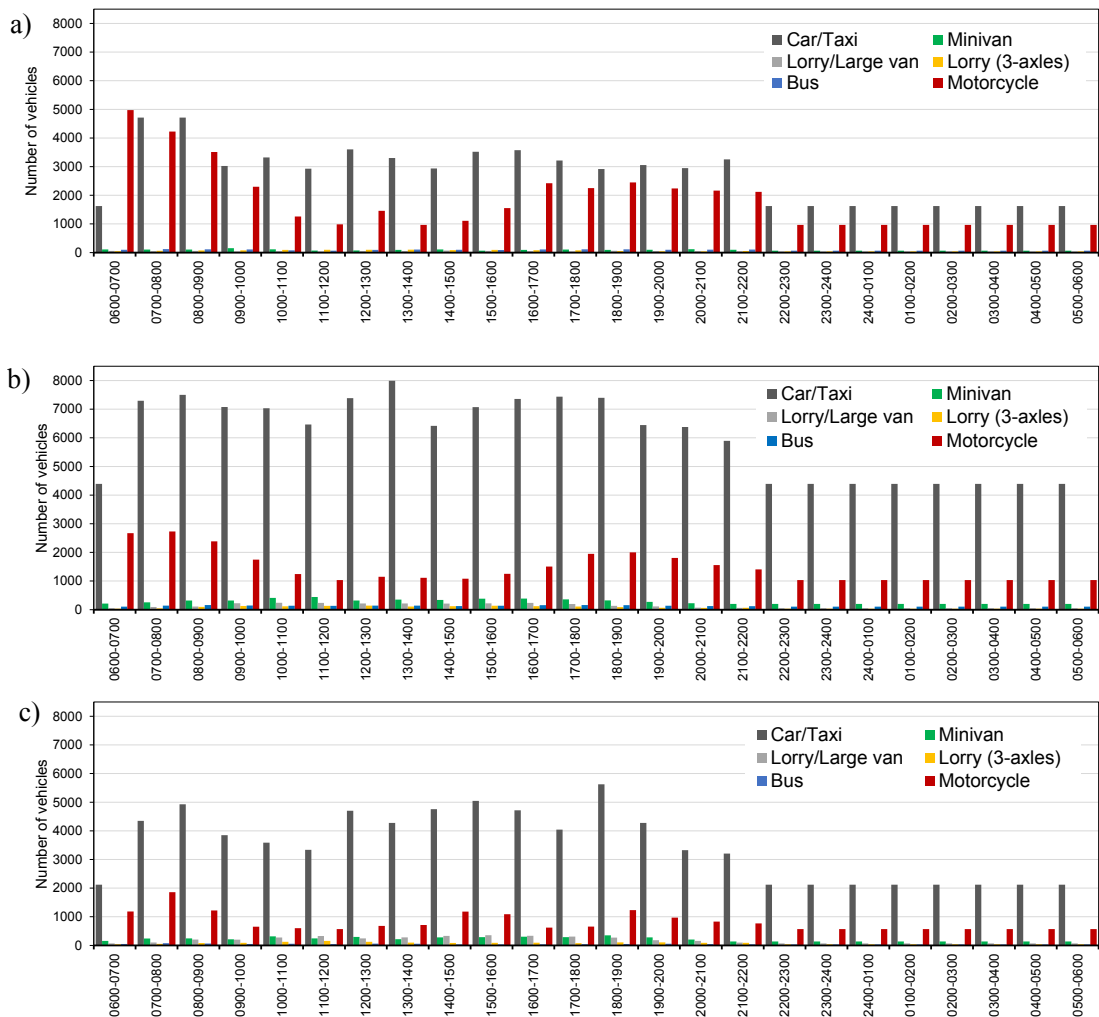


Fig. 7.2 Average traffic volume by vehicle type in (a) commercial, (b) residential, and (c) industrial. The period from 22:00-6:00 use the minimum counts of each vehicle type.

(NHC), fuel density (ρ), mean fuel economy values (FE), and energy used per vehicle class (EV) considered in JB are listed in Table 7.4.

Estimation of anthropogenic heat release in three urban categories

The anthropogenic heat releases from traffic are classified into three urban categories. The traffic counts in each urban category are the ensemble averages from the traffic counts in representative survey stations in each urban category (see Table 7.1). As previously mentioned, we assumed that the unmeasured periods (22:00-06:00) is the non-peak hours and put the minimum counts of each vehicle type to fill those periods accordingly. The average traffic volumes by vehicle types are shown in Fig. 7.2.

Diurnal variation of anthropogenic heat release from vehicles

Ensemble average of the diurnal variation of Q_v are shown in Fig. 7.3. As shown, Q_v is largest at the residential area at every hours of the day with maximum value of 18.5 W/m^2 recorded at 13:00. In the industrial area, the peak diurnal Q_v values of 10.2 and 11.88 W/m^2 were observed at 7:00 to 8:00, with smaller peak of 10 W/m^2 at 18:00. These peaks correspond to the morning and evening rush hours. Meanwhile, the peak diurnal Q_v value in commercial areas was observed during the morning period, with the values of 13.18 and 12.72 W/m^2 at 7:00 and 8:00, respectively.

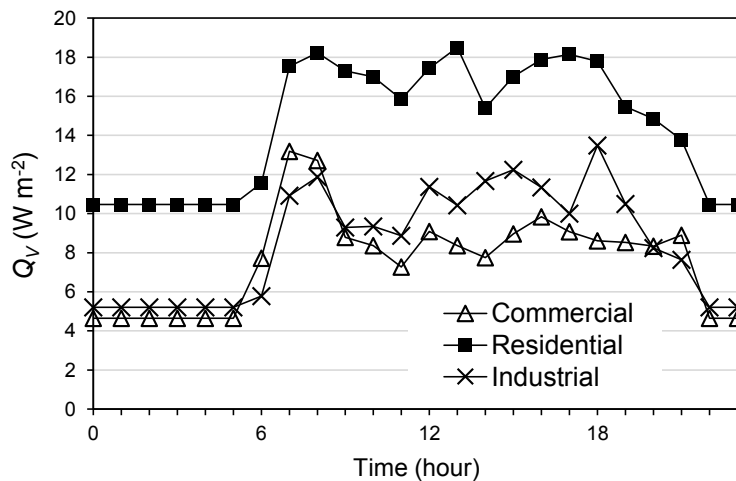


Fig. 7.3 Ensemble average of diurnal variation of Q_v at commercial, residential, and industrial urban category.

7.3.2 Anthropogenic heat releases from buildings

The hourly emission from the combustion of buildings (Q_B) is computed by using:

$$Q_B(h) = \sum_k E_k(h)/A \quad [Wm^{-2}] \quad (5)$$

where subscript k indicates building type and $E_k(h)$ is hourly electricity consumption of building k at hour h (W).

Data sources

The diurnal energy consumption pattern for residential is represented by the air conditioning usage pattern in residential buildings in Malaysia. The data were derived from the survey of energy consumption in residential buildings in Malaysia (Kubota, Jeong, Toe, & Ossen, 2011). Meanwhile, the diurnal patterns for commercial and industrial areas are derived from the energy consumption pattern of commercial buildings which were reported by Quah & Roth (2012). The hourly values of energy consumption in residential, commercial, and industrial are calculated from the annual energy consumption reported in the preliminary study of Low Carbon City 2025 – Sustainable Iskandar Malaysia (Universiti Teknologi Malaysia et al., 2009). Since the value of diurnal energy consumption should be in a daily basis, we downscaled the annual values into daily basis by dividing them with 365 days respectively.

The total numbers of unit for residential and industrial are based on the data from Property Market Report 2005. There are 12 residential categories listed in the report (see Table 7.5). In order to obtain the total floor space (A), the number of units are multiplied by the average size of each building category.

The average floor size of double story terraced house is 155 m² (Toe, Sugiyama, Yasufuku, & Kubota, 2014). This value is also applied for 2-3 story terraced house, 2-3 story semi-detached, and cluster categories. Meanwhile, the floor spaces for apartments, flats, townhouses, and single-storey terraced houses are obtained by analyzing the data provided in the Malaysia property website (<https://www.iproperty.com.my>) (Fig. 7.4). Since the number of category in the website is less than the categorization in the Property Market Report, we assumed that

Table 7.5 Supply of residential units by municipalities in Iskandar Malaysia.

| | Single story terraced | 2-3 story terraced | Single story semi-detached | 2-3 story semi-detached | Detached | Town house | Cluster | Low cost house | Low cost flat | Flat | Service apartment | Condominium/apartment | Total |
|-------------|-----------------------|--------------------|----------------------------|-------------------------|----------|------------|---------|----------------|---------------|-------|-------------------|-----------------------|--------|
| Johor Bahru | 85853 | 83032 | 6226 | 7054 | 21370 | 1031 | 152 | 56038 | 38558 | 13606 | 593 | 18064 | 331577 |
| Pontian | 4155 | 1963 | 1592 | 208 | 7039 | 0 | 0 | 4607 | 504 | 18 | 0 | 0 | 20086 |
| Total | 90008 | 84995 | 7818 | 7262 | 28409 | 1031 | 152 | 60645 | 39062 | 13624 | 593 | 18064 | 351663 |

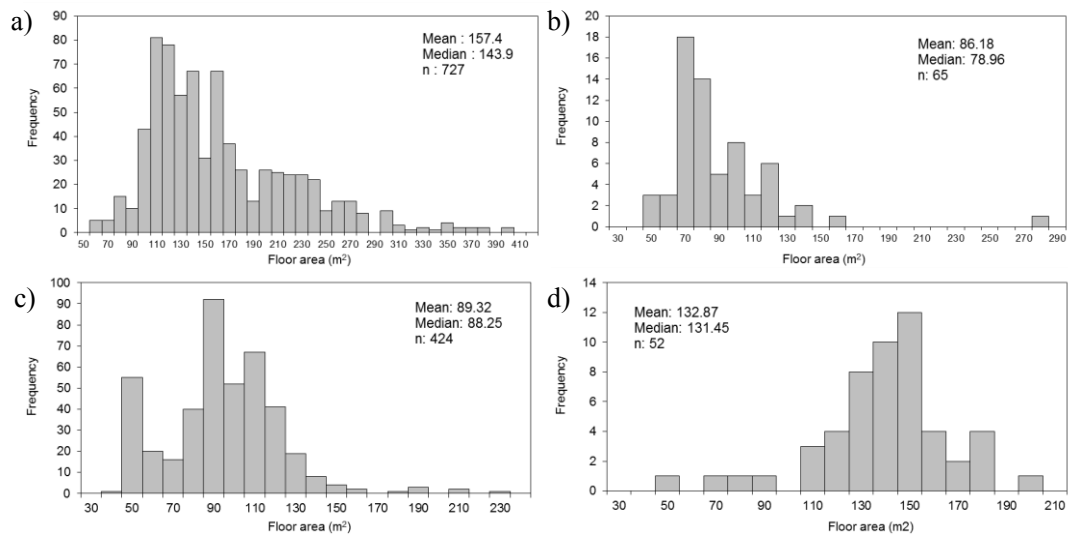


Fig. 7.4 Histogram showing the distribution of total floor areas at (a) townhouses, (b) Flats, (c) Apartments, and (d) single-story terraced house.

Table 7.6 Floor area of residential unit by type in Iskandar Malaysia.

| Residential category | Total unit ¹ | Average floor size ² (m ²) | Total floor area (m ²) |
|-----------------------------------|-------------------------|---|------------------------------------|
| Single-storey terraced house | 90,008 | 132.87 | 11,959,363 |
| 2-3 storeys terraced house | 84,995 | 155 | 13,174,225 |
| Single-storey semi-detached house | 7,818 | 132.87 | 1,038,778 |
| 2-3 storeys semi-detached house | 7,262 | 155 | 1,125,610 |
| Detached house | 28,409 | 157.4 | 4,471,577 |
| Town house | 1,031 | 157.4 | 162,280 |
| Cluster | 152 | 155 | 23,560 |
| Low cost house | 60,645 | 132.87 | 8,057,902 |
| Low cost flat | 39,062 | 86.18 | 3,366,364 |
| Flat | 13,624 | 86.18 | 1,174,117 |
| Service apartment | 593 | 89.32 | 52,967 |
| Condominium/apartment | 18,064 | 89.32 | 1,613,477 |
| Total | 351,663 | - | 46,220,216 |

Source: ¹Property Market Report 2005, ² www.iproperty.com.my, ³Toe et al. 2014.

some building category can represent the category that is not listed in the report. So, the average floor area of single-story terraced house is also used for the single-story semi-detached house and low cost house, respectively. Moreover, the average floor area of townhouse is also used for detached house. Then, the average floor area of flat is also applied for low-cost flat. In addition, the average floor area of apartment is also used for service apartment. Table 7.6 shows the total floor area of each residential category. As shown, the total floor area for residential is 46,220,216 m².

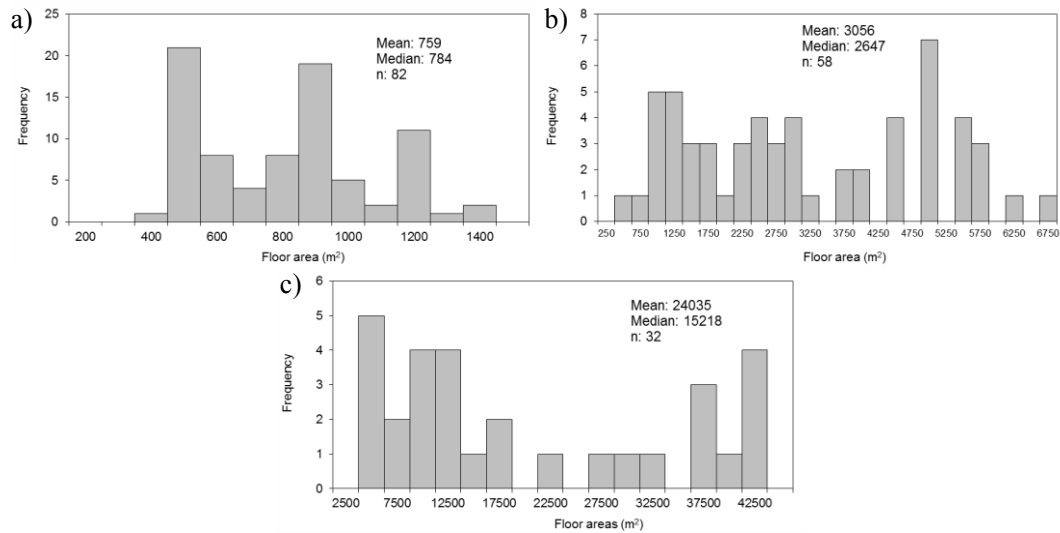


Fig. 7.5 Histogram showing the distribution of total floor areas at (a) semi-detached factories, (b) detached factories, and (c) industrial complex.

Table 7.7 Supply of industrial units by type in Iskandar Malaysia

| | Terraced | Semi-detached | Detached | Flatted factory | Industrial complex | Total |
|-------------|----------|---------------|----------|-----------------|--------------------|--------|
| Johor Bahru | 6008 | 2212 | 1440 | 0 | 274 | 9934 |
| Pontian | 89 | 44 | 75 | 0 | 6 | 214 |
| Total | 6097 | 2256 | 1515 | 0 | 280 | 10,148 |

Table 7.8 Floor area of industrial units by type in Iskandar Malaysia

| | Terraced | Semi-detached | Detached | Flatted factory | Industrial complex | Total |
|---|-----------|---------------|-----------|-----------------|--------------------|------------|
| Total unit | 6097 | 2256 | 1515 | 0 | 280 | 10,148 |
| Average floor area ¹ (m ²) | 759 | 759 | 3056 | 0 | 24,035 | - |
| Total floor area ² (m ²) | 4,627,623 | 1,712,304 | 4,629,840 | | 6,729,800 | 17,699,567 |

Source: ¹Property Market Report 2005, ² www.iproperty.com.my.

In case of industrial, the floor areas are also calculated by using the data provided in the property website in JB. According to the Property Market Report 2005, industrial buildings are divided into five categories which are: terraced factory, semi-detached factory, detached factory, flatted factory, and industrial complex. The average floor area of semi-detached factory is also used for terraced factory because the data for terraced factory are not available. Fig. 7.5 shows the distribution of total floor areas for industrial buildings. Table 7.7 shows the number of units of industrial buildings, while Fig. 7.8 shows the total floor area of industrial unit by type. As shown in Fig. 7.8, the total floor area of industrial is 17,699,567 m².

Table 7.9 Annual energy consumptions and daily energy consumptions by urban category and scenarios for numerical experiments.

| Urban category | Annual Energy Consumption ¹ (ktoe) | | | Daily Energy Consumption (MWh) | | |
|----------------|---|----------|----------|--------------------------------|-----------|-----------|
| | 2005 | 2005-BaU | 2025 LCS | 2005 | 2025 BaU | 2025 LCS |
| Commercial | 376.15 | 978 | 685 | 11985.40 | 31162.03 | 21826.16 |
| Residential | 242.44 | 1091 | 649 | 7725.01 | 34762.55 | 20679.10 |
| Industrial | 3317.5 | 6635 | 3494 | 105705.55 | 211411.10 | 111329.37 |

Source: ¹Universiti Teknologi Malaysia et al. 2009. 1 ktoe =11630 MWh

Table 7.10 Energy consumption per m² by urban category

| Urban category | Total floor area (m ²) | Daily energy consumption per m ² (W m ⁻²) |
|----------------|------------------------------------|--|
| Commercial | 6,800,000 | 1763 |
| Residential | 46,220,216 | 167 |
| Industry | 17,699,567 | 3015 |

In case of the commercial buildings, the total floor area in commercial sector for future scenario is obtained from Low Carbon City 2025 – Sustainable Iskandar Malaysia (Universiti Teknologi Malaysia et al., 2009). In the current status, the total floor area in commercial sector is 6,800,000 m², while the number increase by 2.8 times in 2025, which is 19,300,000 m².

Estimation of anthropogenic heat release in three urban categories

The hourly emissions from buildings is computed by using Eq. 5. Firstly, the annual energy consumptions of each urban category were downscaled into the daily energy consumption by dividing them with 365 days (Table 7.9). The energy consumptions in the weekday and weekend were ignored in this calculation. Then, the daily energy consumptions are divided with the total floor area of each urban category (Table 7.10). Then, the resulted energy consumption per m² is distributed into hourly energy consumption by using the proportion of diurnal pattern of energy consumption. As previously mentioned, due to lack of data availability in the diurnal of energy consumption for commercial and industrial, we referred to the diurnal pattern for commercial facility reported by Quah & Roth (2012). In case of residential buildings, the diurnal pattern of AC usage was used. Table 7.11 summarizes the input values of hourly electricity consumption (E_k). The resulted diurnal patterns of energy consumption for each urban category are shown in Fig. 7.6.

As shown in Fig. 7.6, Q_B is significantly highest in high density built-up areas at every hours of the day. It corresponds to the high energy consumption in industrial buildings, with the peak of 168 W/m² at 11:00. Meanwhile, the residential areas consume relatively low amount of energy if compared to commercial and industrial areas.

Table 7.11 Hourly energy consumptions by urban category.

| Hour | Commercial | | Residential | | Industrial | |
|--------------|------------|--|-------------|--|------------|--|
| | Fraction | Energy consumption (W/m ²) | Fraction | Energy consumption (W/m ²) | Fraction | Energy consumption (W/m ²) |
| 0 | 0.0288 | 50.73 | 0.1115 | 18.62 | 0.0288 | 86.77 |
| 1 | 0.0270 | 47.56 | 0.0974 | 16.26 | 0.0270 | 81.35 |
| 2 | 0.0276 | 48.62 | 0.0908 | 15.16 | 0.0276 | 83.16 |
| 3 | 0.0258 | 45.45 | 0.0823 | 13.75 | 0.0258 | 77.73 |
| 4 | 0.0252 | 44.39 | 0.0751 | 12.54 | 0.0252 | 75.93 |
| 5 | 0.0270 | 47.56 | 0.0698 | 11.66 | 0.0270 | 81.35 |
| 6 | 0.0294 | 51.79 | 0.0295 | 4.93 | 0.0294 | 88.58 |
| 7 | 0.0312 | 54.96 | 0.0135 | 2.26 | 0.0312 | 94.00 |
| 8 | 0.0420 | 73.99 | 0.0068 | 1.14 | 0.0420 | 126.54 |
| 9 | 0.0468 | 82.44 | 0.0054 | 0.90 | 0.0468 | 141.00 |
| 10 | 0.0552 | 97.24 | 0.0056 | 0.93 | 0.0552 | 166.31 |
| 11 | 0.0558 | 98.30 | 0.0066 | 1.09 | 0.0558 | 168.12 |
| 12 | 0.0534 | 94.07 | 0.0092 | 1.53 | 0.0534 | 160.89 |
| 13 | 0.0510 | 89.84 | 0.0161 | 2.69 | 0.0510 | 153.66 |
| 14 | 0.0516 | 90.90 | 0.0167 | 2.79 | 0.0516 | 155.47 |
| 15 | 0.0522 | 91.96 | 0.0161 | 2.69 | 0.0522 | 157.27 |
| 16 | 0.0528 | 93.01 | 0.0150 | 2.51 | 0.0528 | 159.08 |
| 17 | 0.0540 | 95.13 | 0.0134 | 2.23 | 0.0540 | 162.70 |
| 18 | 0.0492 | 86.67 | 0.0121 | 2.03 | 0.0492 | 148.24 |
| 19 | 0.0486 | 85.61 | 0.0218 | 3.63 | 0.0486 | 146.43 |
| 20 | 0.0480 | 84.56 | 0.0329 | 5.50 | 0.0480 | 144.62 |
| 21 | 0.0474 | 83.50 | 0.0528 | 8.81 | 0.0474 | 142.81 |
| 22 | 0.0390 | 68.70 | 0.0930 | 15.53 | 0.0390 | 117.50 |
| 23 | 0.0318 | 56.02 | 0.1066 | 17.80 | 0.0318 | 95.81 |
| Total | 1 | 1763 | 1 | 167 | 1 | 3015 |

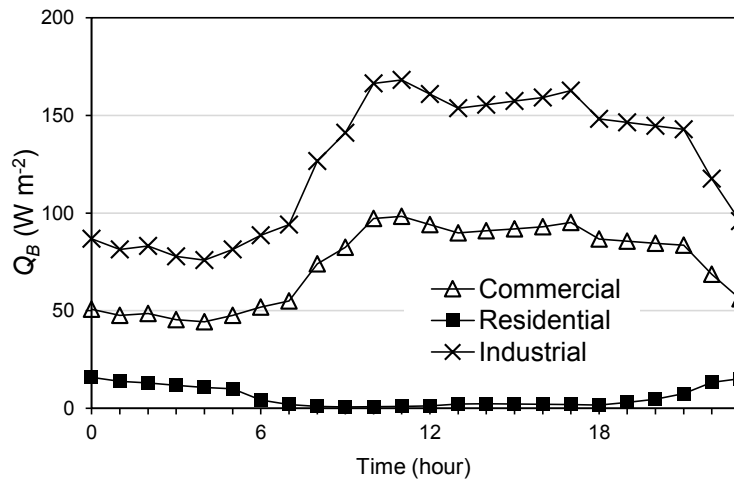


Fig. 7.6 Ensemble average of diurnal variation of Q_B at commercial, residential, and industrial buildings.

7.3.3 Anthropogenic heat releases from human metabolism

The approach used to estimate Q_m followed Grimmond (1992): Each day was divided into two periods, ‘active’ and ‘sleep’, defined as 7:00-22:59 and 23:00-6:59, respectively. Q_m was calculated by following this formula:

$$Q_m(h) = \sum [M_p \times n_p(h)]/A$$

M_p is the metabolic heat per person during the time period p , the subscript p represents the time of ‘active’ or ‘sleep’, while n_p is the number of person during the time period p in the study area. A is the total floor area of urban category k .

Data sources

Table 7.12 shows the metabolic heat production values of activity types, cited from Quah & Roth (2012). The metabolic heat per person (M_p) was estimated as 171 W (averaged of metabolic heat production the activities in ‘active’ category) and 69 W for ‘sleep’ period.

The population in residential areas during the sleep periods are represented by the whole population in Iskandar Malaysia. While the population in residential areas during the active periods is estimated by putting out the working population from the population in residential areas. The working population is estimated by multiplying the whole population with labour force participation rate, which is 65%. In CDP (Khazanah Nasional, 2006), the population in Iskandar Malaysia is 1,353,000. So, the number of workers is estimated as 879,450 people. Then, the workers are divided into commercial and industrial sectors. The percentage of worker by sector is obtained from Department of Statistics, Malaysia. Table 7.13 shows the number of workers by sector in Iskandar Malaysia.

By using the above assumptions, we estimated the weekend and weekday population at sleep and active periods in the three urban categories (Fig. 7.14). The population in the three urban categories during the ‘active’ period was considered to be equivalent to their daytime population while that for the ‘sleep’ period was assumed to be the same as the resident population.

Table 7.12 Metabolic heat production values of activity types

| Activity | Approximate metabolic heat production | |
|---------------|---------------------------------------|----------------|
| | W m ² | W ^a |
| Sleeping | 41 | 69 |
| Office work | 52-70 | 88-119 (104) |
| Driving | 58-100 | 99-197 (148) |
| Shopping | 93 | 158 |
| Domestic work | 93-198 | 158-336 (247) |
| Walking | 116 | 198 |

^a Calculated based on an adult human body surface area of 1.7 m².

^b Average value given in parenthesis were used. Source: (Fanger, 1972)

Table 7.13 Number of workers by sector in Iskandar Malaysia

| Sector | Percentage (%) | Number of workers |
|---------------------------------------|----------------|-------------------|
| Agriculture, hunting and forestry | 13.5 | 118,725.8 |
| Fishing | 1.1 | 9673.95 |
| Mining | 0.4 | 3517.8 |
| Manufacturing | 19.8 | 174,131.1 |
| Electricity, Gas, Water Supply | 0.6 | 5276.7 |
| Construction | 9 | 79,150.5 |
| Wholesale and retail trade | 16.1 | 141,591.5 |
| Hotels and Restaurant | 6.7 | 58,923.15 |
| Transport, storage, communications | 5.4 | 47,490.3 |
| Financial intermediation | 2.5 | 21,986.25 |
| Real Estate, Rental, Business service | 4.6 | 40,454.7 |
| Public administration, defense | 7.3 | 64,199.85 |
| Education | 6 | 52,767 |
| Health and Social work | 2.1 | 18,468.45 |
| Social and personal services | 2.3 | 20,227.35 |
| Private household employment | 2.6 | 22,865.7 |
| Extra-territorial organizations | 0 | 0 |
| Total | 100 | 879,450 |

Source: Department of Statistics, Malaysia.

Table 7.14 Estimated weekend and weekdays population at sleep and active periods.

| Study area | Estimated hourly population | | |
|-------------|-----------------------------|------------------|------------------|
| | Sleep period | Active (weekday) | Active (weekend) |
| Commercial | 64,213 | 418,618 | 261,197 |
| Residential | 1,294,077 | 724,667 | 980,113 |
| Industrial | 52,767 | 306,049 | 52,767 |

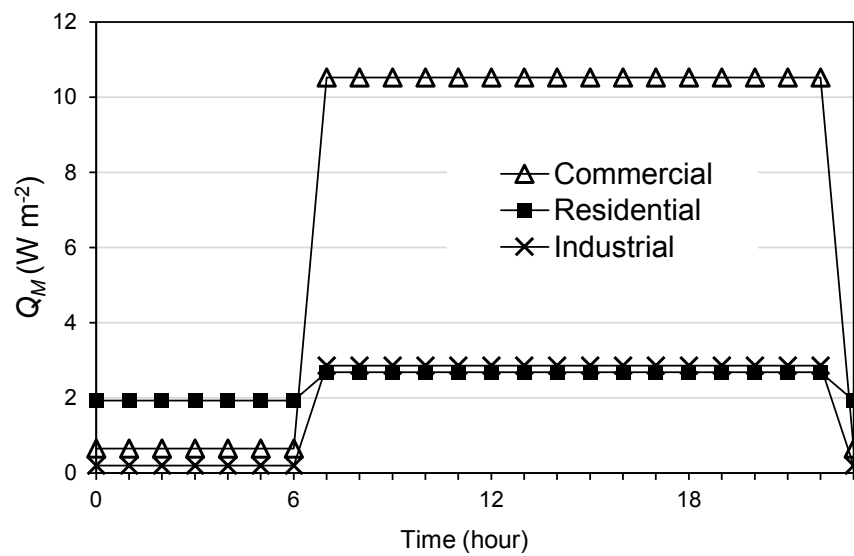


Fig. 7.7 Ensemble average of diurnal variation of Q_m at commercial, residential, and industrial

Fig. 7.7 shows the ensemble average of diurnal variation of Q_m at commercial, residential, and industrial. As shown, the Q_m is the highest during the active period, reaching 11 W/m², while the values for residential and industrial are almost at the same level. During the ‘sleep’ period, the Q_m in residential accounts as the highest, by up to 2 W/m², while the commercial and industrial were less than 1 W/m².

7.4 Calculation of anthropogenic heat emission for BaU and CM scenarios.

The estimations of anthropogenic heat emission for the future scenarios used the top-down approach. We used the value for the final energy demand in 2025 projected by the Low Carbon Society report (Universiti Teknologi Malaysia et al., 2009), for BaU and CM scenarios, respectively.

7.4.1 Anthropogenic heat releases from traffic

The calculation of anthropogenic heat releases from traffic for future scenarios is based on value of the final energy demand in 2025 from passenger transport in the LCS report. We assumed that the daily patterns do not change in the future. Table 7.15 shows the summary of daily energy consumptions in transportation sector. We used those values into the diurnal pattern of Q_v for each urban category. Fig. 7.8 shows the ensemble diurnal variation of Q_v at commercial, residential, and industrial for BaU scenario and CM scenario, respectively.

Table 7.15 Summary of daily energy consumptions for traffic

| Urban type | Energy share (%) | Daily energy consumption (W m ⁻²) | | |
|-------------|------------------|---|----------|---------|
| | | 2005 | 2025 BaU | 2025 CM |
| Commercial | 25 | 183 | 402 | 129 |
| Residential | 47 | 347 | 765 | 245 |
| Industrial | 28 | 205 | 450 | 144 |
| Total | 100 | 735 | 1617 | 518 |

7.4.2 Anthropogenic heat releases from buildings

The estimation of the anthropogenic heat releases from buildings for the future scenarios is based on the total energy consumption and total floor areas in the future. We assumed that the other variables do not change (i.e. diurnal pattern, etc.). Nevertheless, the report does not contain the data about total floor area for residential and industrial. It only provides the projection for total unit of residential and total industrial land in 2025.

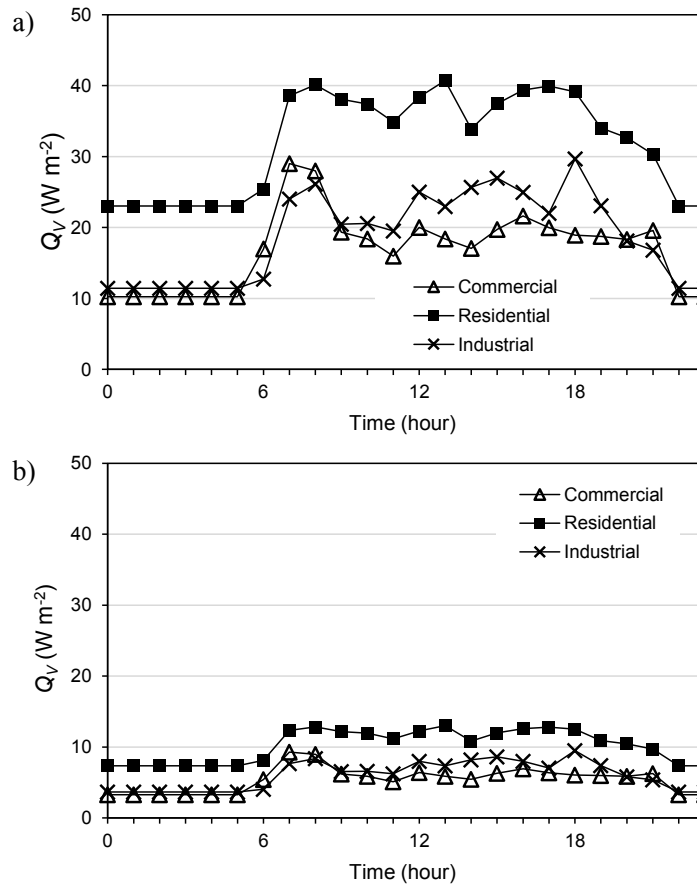


Fig. 7.8 Ensemble average of diurnal variation of Q_v at commercial, residential, and industrial buildings for (a) BaU scenario and (b) CM scenario.

Therefore, for residential, the total housing units in the future is interpolated with the proportion of housing category in Iskandar Malaysia. The result is the total number of units by housing type in the future. We put assumption that the average floor area and proportion of each housing type is unchanged. Then, the total number of units are multiplied with the average floor area of each housing type respectively.

To obtain the total floor area of industrial in the future, the total industrial land in the future is multiplied with the building coverage ratio of industrial land (i.e. 45%). The building coverage ratio is estimated by dividing the total industrial land with total floor area of industrial buildings of current condition. Again, we assumed that this ration will not change in the future.

Table 7.16 summarizes the daily energy consumption, total floor area, and energy consumption per m^2 for current and future scenarios. Fig. 7.9 shows the ensemble diurnal variation of Q_B at commercial, residential, and industrial for BaU scenario and CM scenario, respectively.

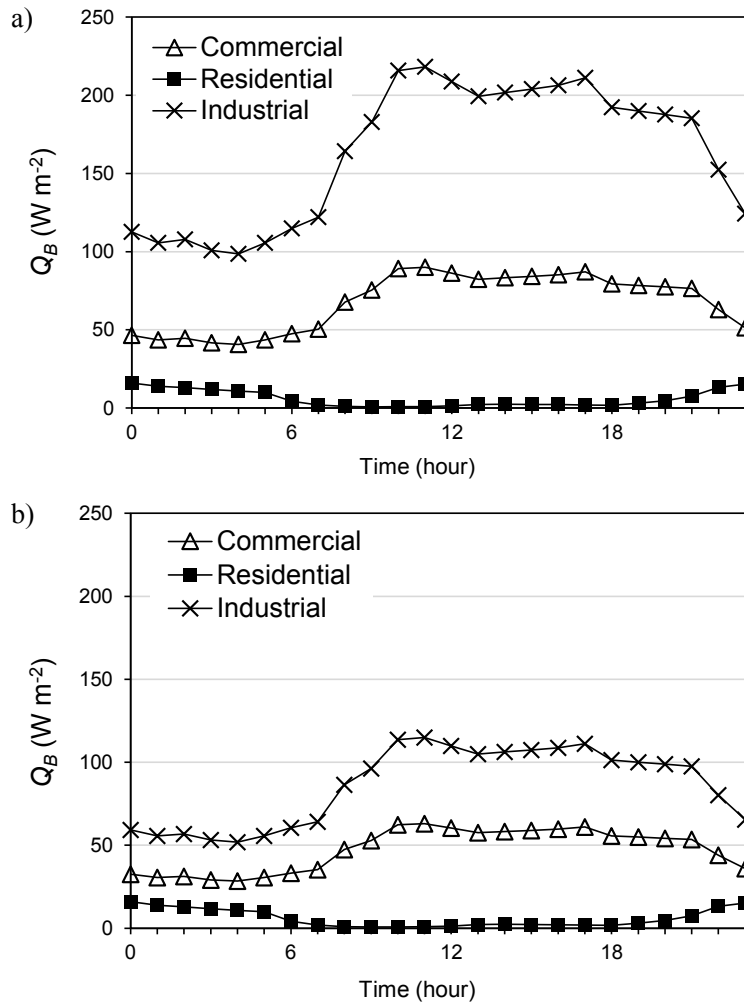


Fig. 7.9 Ensemble average of diurnal variation of Q_B at commercial, residential, and industrial buildings for (a) BaU scenario and (b) CM scenario.

Table 7.16 Summary of the daily energy consumption, total floor area, and energy consumption per m^2 for all scenarios and land use categories.

| Urban category | Daily Energy Consumption (MWh) | | | Total Floor Area (ha) | | Energy consumption per m^2 ($W m^{-2}$) | | |
|----------------|--------------------------------|----------|---------|-----------------------|------|---|----------|---------|
| | 2005 | 2025 BaU | 2025 CM | 2005 | 2025 | 2005 | 2025 BaU | 2025 CM |
| | Commercial | 11,985 | 31,162 | 21,826.16 | 680 | 1930 | 1763 | 1615 |
| Residential | 7725 | 34,763 | 20,679 | 4622 | 8753 | 167 | 397 | 236 |
| Industrial | 55,215 | 211,411 | 111,329 | 1831 | 5403 | 3015 | 3912 | 2060 |

7.4.3 Anthropogenic heat releases from human metabolism

The calculation of future anthropogenic heat release from human metabolism is based on the total floor area and number of workers in 2025. Fig. 7.10 shows the ensemble diurnal variation of Q_M at commercial, residential, and industrial for BaU scenario and CM scenario, respectively.

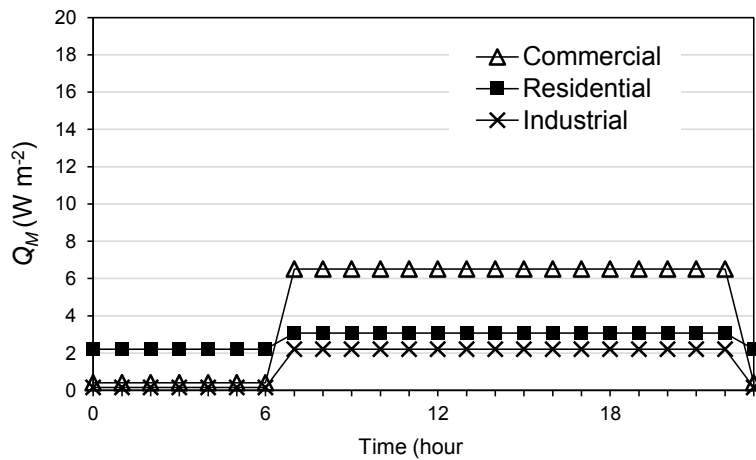


Fig. 7.10 Ensemble average of diurnal variation of Q_M at commercial, residential, and industrial buildings used in both BaU and CM scenarios.

7.5 Total of anthropogenic heat emission for current, BaU, and CM scenarios

The total anthropogenic emission Q_F is calculated using Eq. 2. It is the sum of the anthropogenic heat releases from traffic, buildings, and human metabolism for each urban category (i.e. commercial, residential, and industrial) (see Figs.7.11, 7.12, and 7.13). In general,

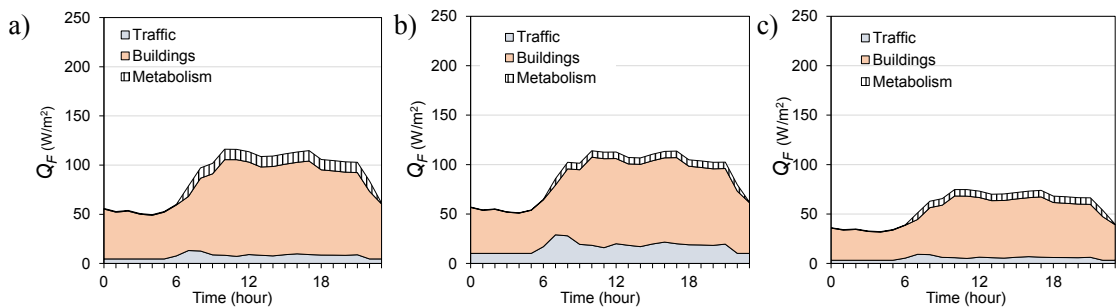


Fig. 7.11 Q_F in commercial for (a) current, (b) BaU, and (c) CM scenarios.

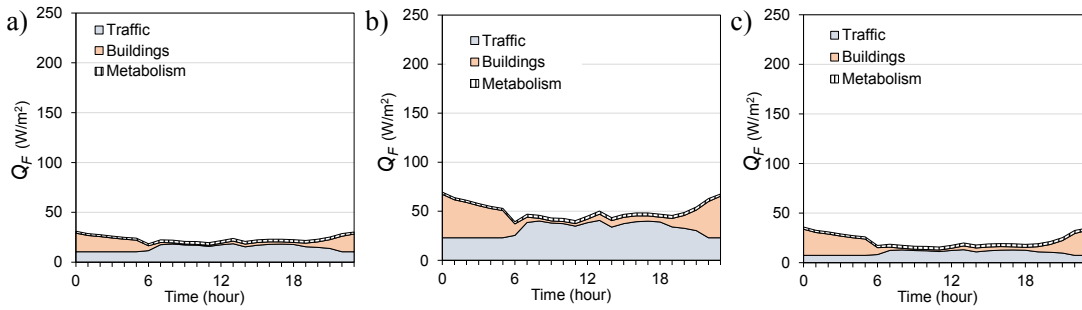


Fig. 7.12 Q_F in residential for (a) current, (b) BaU, and (c) CM scenarios.

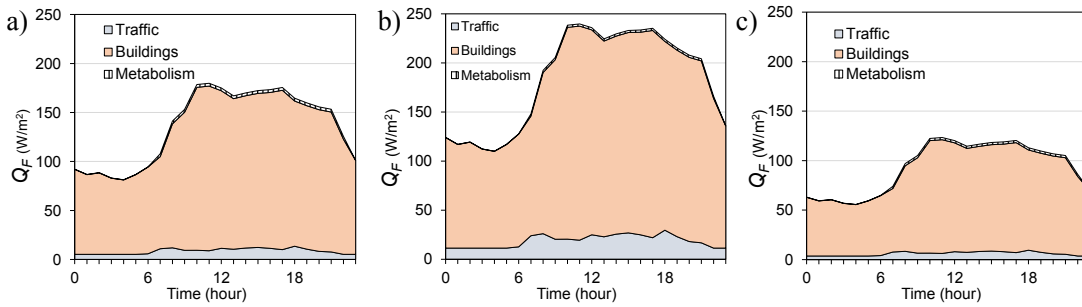


Fig. 7.13 Q_F in industrial for (a) current, (b) BaU, and (c) CM scenarios.

the major contributor of the anthropogenic heat emission is coming from the building sectors in all urban categories. As shown in Figs. 7.11, 7.12, and 7.13, the highest anthropogenic heat emission is derived from industrial areas. Meanwhile, the lowest anthropogenic heat emission is observed in residential areas. The total Q_F estimated in the CM scenario accounts as the lowest values, even lower than those of the current status.

7.6 WRF-UCM configuration

The WRF coupled with UCM simulations were conducted for current, BaU, and CM scenarios, respectively. The physical parameterization for WRF is same with the simulation for JB in Section 4.3.3. The main difference between of this chapter and Chapter 4 is that the WRF simulation in this chapter consider the additional heating from anthropogenic heat releases. The detail configuration of the URBPARM.TBL of UCM is shown in Appendix K.

7.7 Model validation

The WRF simulation for current status was conducted from 00:00:00 UTC 12 June to 00:00:00 17 June 2013. Fig. 7.14 shows the validation results for air temperature at 2 m above the ground and wind speed and direction at 10 m above the ground at Senai airport in JB and Changi airport in Singapore, respectively. The results of the WRF simulation without UCM are also included in Fig. 7.14 for comparison. In general, there is no significant difference between the WRF simulation with and without UCM (Fig. 7.14).

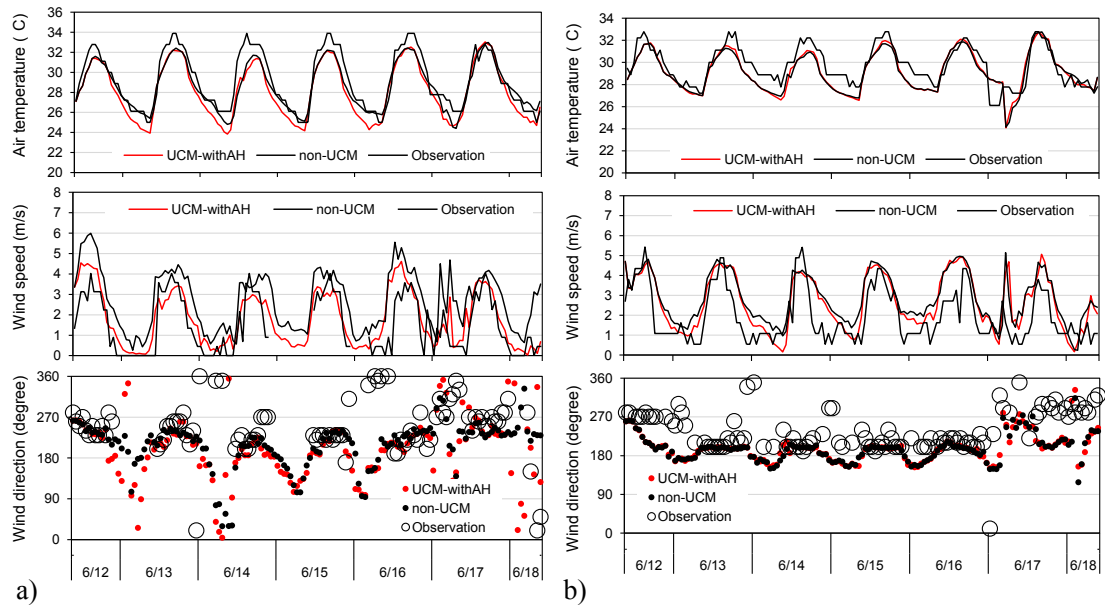


Fig. 7.14 Comparison of air temperature at 2m and wind conditions at 10 m above the ground between WRF simulations with/without UCM and the observed values at (a) Senai airport in Johor Bahru and (b) Changi airport in Singapore.

7.8 Results and discussion.

The WRF simulations were conducted for current status (case 1), master plan under BaU scenario (case 2-1), and master plan under CM scenario (case 2-2), respectively. All simulations were conducted from 7 to 16 June 2009. June is selected to represent the southwest monsoon season in JB. Furthermore, only the non-rainy days were taken into account and the temporal hourly average air temperatures of each scenario are presented for the comparison.

Figs. 7.15 and 7.16 show the spatial distributions of average air temperature of all cases in the night-time and daytime, respectively. In general, the hot air temperature region corresponds with the planned built-up areas in the master plan. Meanwhile, the low air temperature region is observed mostly in the non-built-up area. The air temperature difference between the built-up and non-built-up areas is up to 2 to 3 °C.

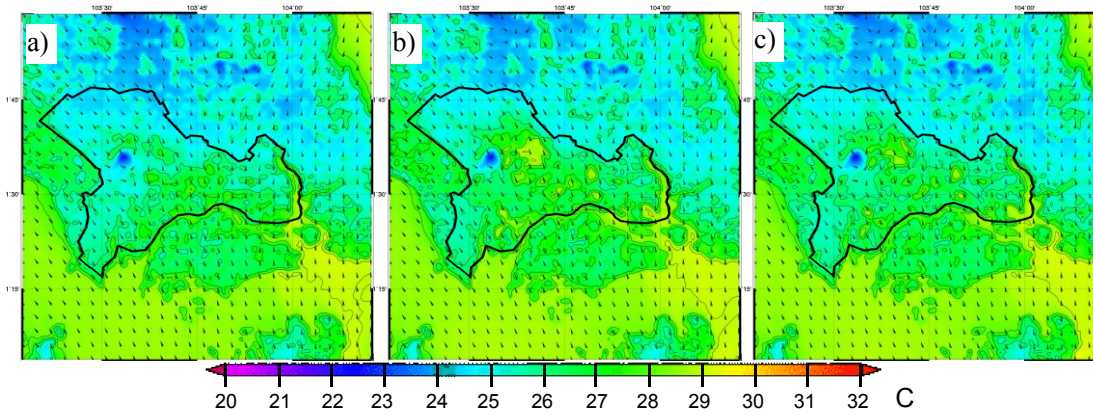


Fig. 7.15 Spatial distribution of average air temperature in (a) case 1, (b) case 2-1, and (c) case 2-2 at 1:00.

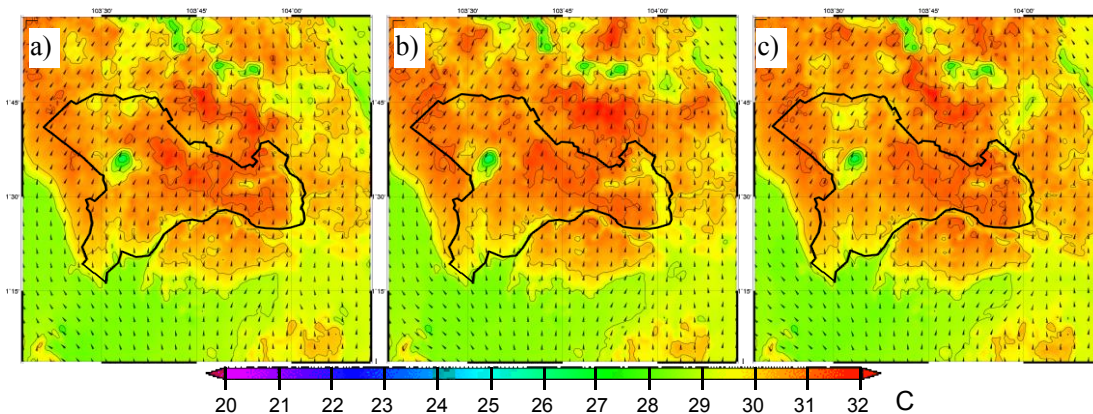


Fig. 7.16 Spatial distribution of average air temperature in (a) case 1, (b) case 2-1, and (c) case 2-2 at 16:00.

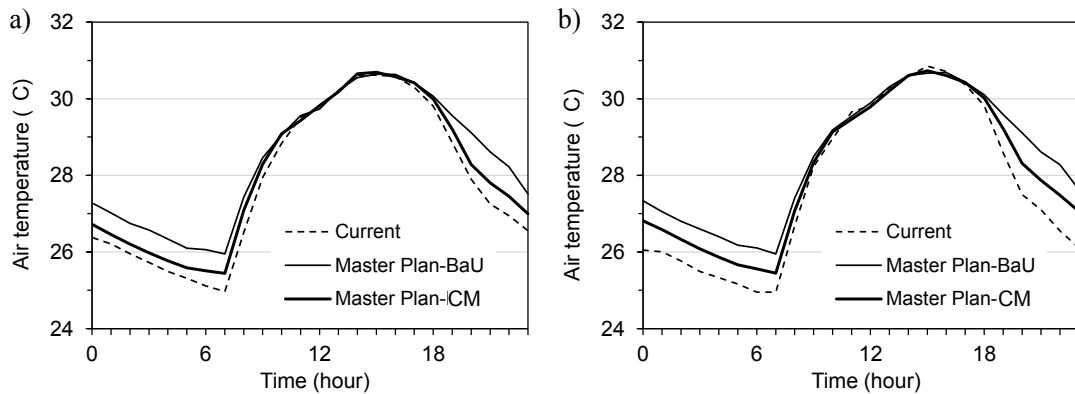


Fig. 7.17 Diurnal variation of average air temperature in built-up area for case 1 (current status), case 2-1 (BaU scenario), and case 2-2 (CM scenario) at (a) existing and (b) new urban areas.

As shown in Figs. 7.15a and b, the land use change and the increased the anthropogenic heat emissions not only increase the number of hotspots, but also raise the peak air temperature in the night-time (Fig. 7.15b). In contrast, in the daytime, both land use changes and the increase of anthropogenic heat releases do not affect the peak air temperature significantly (Fig. 7.16a and b).

Each of the future scenario (i.e. cases 2-1 and 2-2) resulted in different spatial distributions of air temperatures, respectively. As seen in Figs. 7.15c and 7.16c, the number of hotspots with peak air temperature is less in the CM scenario than in BaU scenario, both in the daytime and night-time.

Fig. 7.17 shows the diurnal variations of the temporal average air temperatures in the existing and new urban areas, respectively. As shown, the implementation of the master plan generally increases the air temperature, not only in new urban area but also in the existing urban area. Nevertheless, the temperature increases mainly occur in the night-time. The BaU scenario (case 2-1) shows the highest increment of air temperature, by up to 1.36 and 1.73 °C from case 1 in the existing and new urban areas, respectively. Meanwhile, the CM scenario (case 2-2) gives a notable reduction of air temperature from BaU scenario although it is still higher than that of the current status by up to 0.58 and 0.96 °C in the existing and new urban areas, respectively. Moreover, the CM scenario can lower the air temperatures by up to 0.84 °C from the BaU scenario. The land use changes followed with either the increase or decrease of anthropogenic emissions do not affect the air temperature in the daytime. Nevertheless, the air temperatures may increase even higher if the increased ambient temperature due to the global warming, which is the direct effect of anthropogenic emission, is considered in this simulation.

Contribution of anthropogenic heat emission to the urban climate

In order to understand the contribution of the additional heat from anthropogenic heat emission on the urban climate, we compare the results of WRF simulation of cases 2-1 and 2-2 with

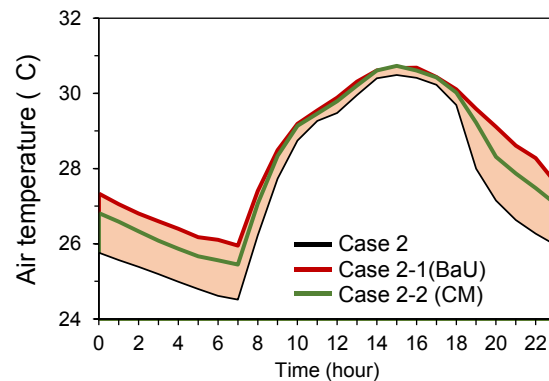


Fig. 7.18 Diurnal variation of average air temperatures in new urban areas for case 2 (master plan without anthropogenic heating), case 2-1 (BaU scenario), and case 2-2 (CM scenario). The shaded area indicates the air temperature increase due to the added heat from anthropogenic heat emissions.

case 2 (i.e. without added heat from anthropogenic heat releases). Fig. 7.18 shows the diurnal variation of temporal average air temperature in the new urban areas of cases 2, 2-1, and 2-2.

In general, the added heat from anthropogenic heat emission raises the air temperature throughout the day with the larger increments at night than those during the daytime, reaching 2°C and 1.2°C for BaU and CM scenarios, respectively. The added heat from anthropogenic emission raise the peak air temperature by up to 0.3°C in average. Nevertheless, the peak air temperatures of cases 2-1 and 2-2 remain at the same level although the anthropogenic emissions in the daytime in case 2-2 have been cut to averagely 48% from case 2-1.

Energy budget analysis

Fig. 7.19 shows the surface energy balance in the new urban areas of JB. As shown, the anthropogenic heat emission scenarios significantly influence the sensible heat in the city. The highest increase of the anthropogenic heat emission in BaU scenario accordingly results in the highest sensible heat flux among other scenarios. On the other words, the magnitude of the sensible heat flux strongly depends on the magnitude of anthropogenic heat emission in the city. In JB, the BaU scenario accounts for the largest anthropogenic heat emission, therefore, its sensible heat also accounts as the highest. On the other hand, the reduction in anthropogenic heat emission in case 2-2 (i.e. CM scenario) results in the reduction of sensible heat throughout the day. Nevertheless, due to a stronger influence of sun radiation in the daytime, the cooling effect of the anthropogenic heat reduction is more apparent at night. As a result of the reduction in sensible heat in CM scenario, the average air temperature in master plan condition can be lowered by up to 0.84 °C from the BaU scenario (see Fig. 7.18).

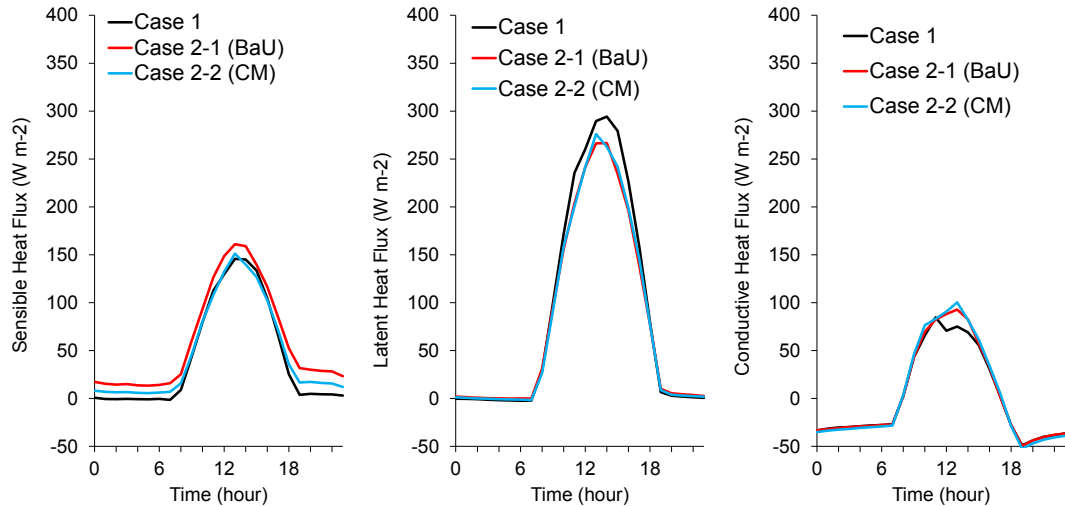


Fig. 7.19 The sensible, latent, and conductive heat fluxes in different scenarios in new urban areas of JB.

7.9 Summary

The main findings in this Chapter are summarize as below:

1. A combination of top-down and bottom-up approaches was used in the estimation of anthropogenic heat emission in JB. A combined approach is necessary due to the issues of data availability.
2. The total anthropogenic emissions for commercial, residential and industrial areas are expected to be cut by averagely 40%, 62% and 50%, respectively, under the CM scenario.
3. The reduction of anthropogenic emission under the CM scenario also significantly reduce the urban air temperatures, particularly in the night-time, by up to 0.84°C if compared to the BaU scenario.
4. The daytime air temperature increases by 0.3°C in average due to the added heat from the anthropogenic releases. Nevertheless, the peak air temperatures of cases 2-1 and 2-2 remain at the same level although the anthropogenic emissions during the daytime in case 2-2 have been cut to averagely 48% from case 2-1.
5. Anthropogenic heat emissions produced by the human activities are one contributor to UHI. It is also clear that the reduction of anthropogenic heat emission should be among the strategy to counter the UHI effect.

References

- Fanger, P. O. (1972). *Thermal comfort : analysis and applications in environmental engineering*. New York, USA: McGraw-Hill. y
- Grimmond, C. S. B. (1992). The Suburban Energy-Balance: Methodological Considerations and Results for a Mid-latitude West Coast City Under Winter and Spring Conditions. *International Journal of Climatology*, 12, 481–497.
- Kubota, T., Jeong, S., Toe, D. H. C., & Ossen, D. R. (2011). Energy Consumption and Air-Conditioning Usage in Residential Buildings of Malaysia. *Journal of International Development and Cooperation*, 17(3), 61–69.
- Oke, T. R. (1987). *Boundary Layer Climates* (2nd ed.). New York, USA: Routledge.
- Quah, A. K. L., & Roth, M. (2012). Diurnal and weekly variation of anthropogenic heat emissions in a tropical city, Singapore. *Atmospheric Environment*, 46, 92–103.
- Sailor, D. J., & Lu, L. (2004). A top-down methodology for developing diurnal and seasonal anthropogenic heating profiles for urban areas. *Atmospheric Environment*, 38(17), 2737–2748.
- Toe, D. H. C., Sugiyama, S., Yasufuku, S., & Kubota, T. (2014). Numerical Simulation of Passive Cooling Strategies for Urban Terraced Houses in Hot-Humid Climate of Malaysia. In *30th International PLEA Conference* (pp. 1–8). Ahmedabad, India.
- Universiti Teknologi Malaysia, Kyoto University, Okayama Univeristy, & Ritsumeikan University. (2009). *Low Carbon City 2025 - Sustainable Iskandar Malaysia*. Johor Bahru.

8

Impacts of urban warming on thermal comfort and cooling load in residential buildings: A case study of Hanoi

8.1 Urban houses in Hanoi

In Vietnam, the influence of foreign architectural trend, building codes and standards have transformed the country's building environment, especially in the densely populated cities like Hanoi and Ho Chi Minh. Although the contemporary housing styles in Vietnam are diverse in nature, they can be divided into three common types, which are row house, detached house, and apartments (Phuong, Birkeland, & Demirbilek, 2010). In another terminology, these housing types are often named as pencil-type house (i.e row house) and villa (for detached house) (Vuong & Yoshino, 2010). Other housing types such as semi-detached house, student or worker dormitories are still exist in Vietnam but their numbers are not significant.

The first housing type is the row house. It is a multi-storied structure in a rectangular plot which has the width much shorter than the length, with the main façade facing the street. This

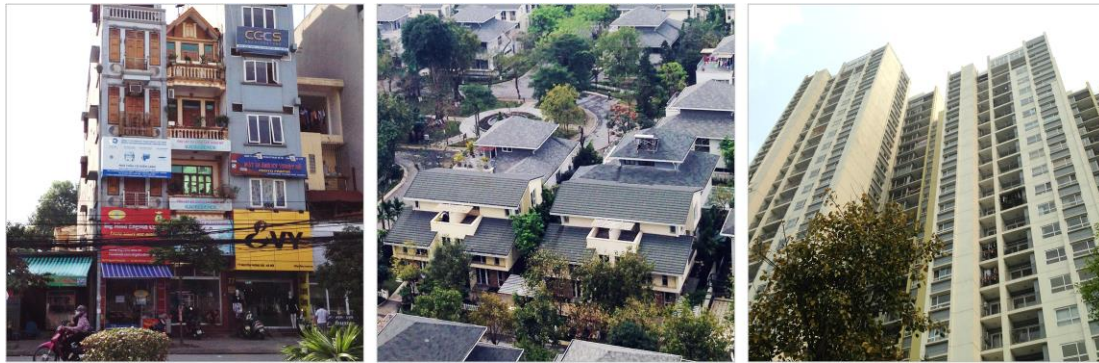


Fig. 8.1 The residential buildings in Hanoi. (a) Row house, (b) villa and (c) apartments.
Source: Author's documentation.

housing style is very prominent in Hanoi. The number of stories is commonly up to 5 stories but some extreme cases can even reach 10 stories. The second category is the detached house. It is a single-family house with all façade facing the surrounding environment (i.e backyard/garden). The plot ratio of a detached house is less than 50% and the number of stories is commonly up to 3 levels. Meanwhile, apartment is the multi-stories housing used by many families or occupants where there are shared facilities. According to the survey in 2009, the percentages of row house, detached house and apartments in Vietnam were 61%, 3% and 36%, respectively (Vuong & Yoshino, 2010).

8.2 Energy saving techniques for residential buildings in Vietnam

In 1995, the Ministry of Construction of Vietnam accepted the application of the national building code. The National Building Code of Vietnam is a legal document which stipulates the minimum technical requirement mandatory to all construction activities. It consists of the solutions and standards that must be applied in order to satisfy the requirements. The main objective of the national building code is to ensure the safety, hygiene, and amenity conditions for occupants in urban areas. In addition, it also promotes the protection of living environment, cultural heritage, landscape, public property, and so on. Nevertheless, the building code did not cover the effort to achieve energy efficiency in buildings. Therefore, in 2013, the Ministry of Construction ratified the National Technical Regulation on Energy Efficiency Buildings. This regulation applies to the envelope of the buildings and mechanical system in buildings such as lighting, AC, water heating, elevators, etc. However, the regulation is designated only to buildings with a gross floor area of 2,500 m² or larger.

A comprehensive green building rating for Vietnam, namely LOTUS, was established by the Vietnam Green Building Council (VGBC). It is said that LOTUS is more compatible to the Vietnamese context compared with other green building rating system like LEED from US, BCA Green Mark from Singapore, BREEAM from UK or CASBEE from Japan.

Table 8.1 Summary of energy saving techniques for residential buildings in Hanoi

| Building's part | Descriptions |
|---------------------|--|
| Wall | <ul style="list-style-type: none"> • All the external walls are made with any or any combination of the following: <ul style="list-style-type: none"> - AAC blocks, - A layer of insulation material (material with a thermal conductivity ≤ 0.05 W/m.K) with a thickness of at least 40mm, - Lightweight hollow blocks - Materials, techniques with an equivalent performance (subject to VGBC approval) • 95% of the solid roof surface meet any or any combination of the following: <ul style="list-style-type: none"> - Have a Roof solar reflectivity > 0.4 - Be a green wall - Have external shadings. |
| Roof | <ul style="list-style-type: none"> • All the roofs are made with any or any combination of the following: <ul style="list-style-type: none"> - An air layer of at least 40mm, - A layer of insulation material (material with a thermal conductivity ≤ 0.05 W/m.K) with a thickness of at least 40mm - A fixed sunshade (it must be installed at a minimum clearance of 0.3 m from the roof surface to have ventilation between the roof and the sunshade) - A green roof - Materials, techniques with an equivalent performance (subject to VGBC approval) • 95% of the solid roof surface meet any or any combination of the following: <ul style="list-style-type: none"> - Have a Roof solar reflectivity > 0.7 - Be a green roof - Have external shadings (PV panels and solar collectors can be considered external shadings for opaque roofs). • Countermeasures to UHI effects <ul style="list-style-type: none"> - 30% or 50% of the paved and roof area limits the heat island effect (using shading devices, high solar reflective material, green roof) |
| Windows and glazing | <ul style="list-style-type: none"> • Window to wall ration of east and west facades is lower than 30% (2 points) or 15 % (1 point). • Shading devices should be installed appropriately in south and north, east and west facades. • All the glazing systems installed are any or any combination of the following: Solar control glasses or low solar heat gain low-E double glazing windows. |

Source: LOTUS Homes Pilot.

VGBC has developed various rating tools. One of them is the LOTUS Homes Pilot which proposes energy saving strategies for individual residential houses (VGBC, 2016). The strategies comprise the proper application of materials and passive design techniques to reduce energy consumption, overexploitation of resources, negative local environmental impacts and to maintain good indoor air quality during occupancy. Table 8.1 summarises the energy saving techniques proposed by LOTUS which were investigated in this study.

8.3 Objectives

This study aims to investigate the indoor thermal comfort conditions and cooling load under the future climate in a residential building in Hanoi by taking into consideration the impacts of land use change and the global warming by the 2030s. A row house type residential

unit, which accounts for 60% of the building stock in Vietnam was selected as the case study house. We assess the effectiveness of multiple energy saving techniques as the countermeasures to the changing climate for ensuring thermal comfort as well as cooling load reduction.

8.4 Simulation conditions

Indoor thermal condition in the current and future weather conditions

The simulations were conducted under the daily average weather conditions for the current status (i.e. June 2013) and after the implementation of the master plan (June in the 2030s), respectively. The input weather data for TRNSYS simulation were produced from the results of WRF simulations in Chapter 5. The weather condition in June 2013 represents the summer month of the typical year, while the weather condition of the future scenario is a 10-year average of June from 2026 to 2035 under RCP4.5 scenario projected by MIROC5. Additionally, only the days with prevailing southerly wind direction were selected. Six

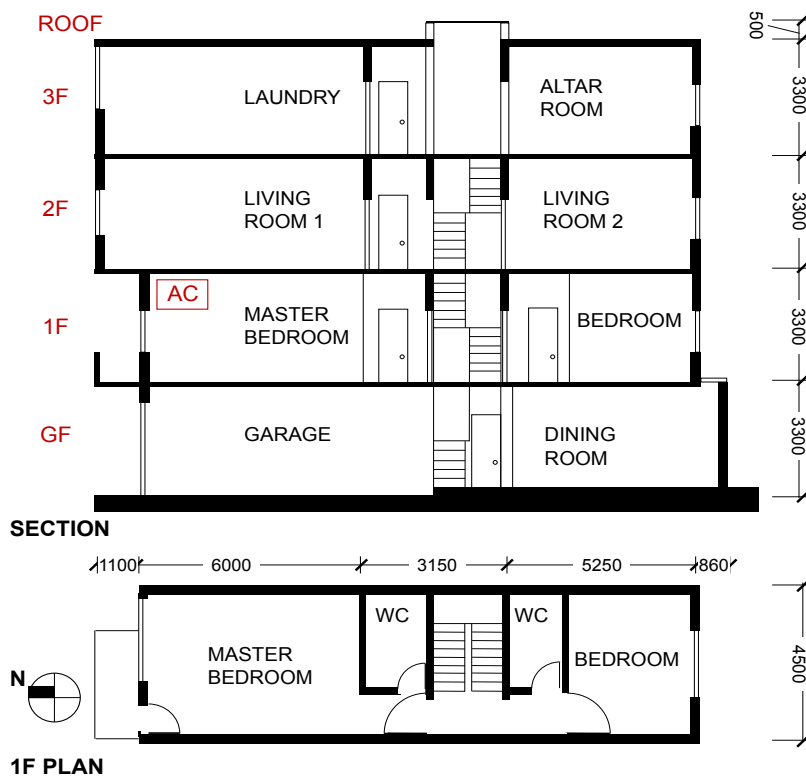


Fig. 8.2 Floor plan and cross section of the case study house.

Table 8.2 Schedule of the window “open” and “closed” mode in all ventilation techniques.

| Window condition | Ventilation techniques | | |
|------------------|---------------------------------|---------------------------------|----------------------|
| | Daytime ventilation | Night ventilation | Full day ventilation |
| Open | 8:00 to 20:00 | 20:00 to 8:00 (of the next day) | 24 hours |
| Closed | 20:00 to 8:00 (of the next day) | 8:00 to 20:00 | Never |

weather components were taken into account: air temperature, relative humidity, wind speed, wind direction, solar radiation, and pressure. Further, the analyses were divided into the existing urban areas and new built-up areas respectively and the resultant simulated weather data were used as initial conditions for building simulations using TRNSYS.

Case study house

An actual house in Hanoi was chosen as the case study house. It is constructed with reinforced concrete frame filled with hole-burned bricks as envelopes. The total floor area of this house is 295.2 m². It consists of four floors and with the front-side of the house is facing north. Fig. 8.2 shows the spatial arrangement of the house. AC is installed only in the master bedroom. The field measurement was conducted in this house from August to September 2014 (Tung et al., 2015). The house was occupied during measurement, so occupancy for each room, door and window opening conditions were considered in this model. In addition, internal heat gain, moisture from cooking, showering and cleaning were also included in this model.

Cooling effects of the ventilation techniques

We investigated the impacts of three ventilation conditions, i.e. (1) daytime ventilation, (2) night ventilation and (3) full day ventilation on the indoor thermal environment. All ventilation techniques are tested under the current and future weather conditions. Table 8.2 shows the schedule and duration of the window opening of the three ventilation techniques. Under the window “open” mode, the windows are opened in the rooms of first, second and third floor at the same time (there is no window in the ground floor of the model house). Meanwhile, under the full-day ventilation condition, the windows are opened for 24 hours.

Cooling effects of the energy saving techniques

In this study, the impacts of different energy saving techniques on the improvement of thermal comfort and the cooling load reduction were explored by means of a parametric study. Parametric study has been used by many research to optimize the design of the models. The methodology consists in evaluating each energy saving technique at different four levels of modification intensity, respectively, under the current and future weather conditions. The levels distributed in the studies parameters are listed in Table 8.3.

Table 8.3 Levels distributed to each energy saving techniques.

| Building techniques | Parameters | Level 0 (base) | Level 1 (low) | Level 2 (medium) | Level 3 (LOTUS ¹) | Level 4 (High) |
|----------------------------------|-------------------------------|----------------|---------------|------------------|-------------------------------|----------------|
| Roof reflectance | Albedo | 0.3 | 0.5 | 0.6 | 0.7 | 0.8 |
| Roof insulation | Thickness (mm) | none | 20 | 30 | 40 | 50 |
| | U-value (W m ⁻² K) | 2.05 | 0.88 | 0.69 | 0.57 | 0.49 |
| Internal and external insulation | Thickness (mm) | none | 20 | 30 | 40 | 50 |
| | U-value (W m ⁻² K) | 2.05 | 0.88 | 0.69 | 0.57 | 0.49 |
| Wall | U-value (W m ⁻² K) | 2.25 | 0.96 | 0.74 | 0.61 | 0.51 |
| Ceiling | U-value (W m ⁻² K) | 3.44 | 1.12 | 0.84 | 0.67 | 0.56 |
| Floor | Reach of sunshade (m) | none | 0.07 | 0.13 | 0.26 | 0.39 |
| | b/H | none | 0.05 | 0.1 | 0.2 | 0.3 |
| Glazing performance | Glass type | Single glass | Pair glass | Pair glass+ | Low-E | Low-E+ |
| | U-value (W m ⁻² K) | 5.61 | 2.54 | 2.3 | 1.05 | 1.05 |
| | G-value | 0.83 | 0.44 | 0.30 | 0.33 | 0.22 |

Notes: ¹The given values in level 3 are recommended by LOTUS Home Pilot.

H: Window height, b: reach of shading.

As listed in Table 8.3, the techniques used for the building envelope were the main focus of this study. This is because the indoor thermal environment is highly dependent of thermal response of materials used in building envelope, beside the other parameters, such as ventilation techniques (i.e. also investigated in this study). In the base case (level 1), no energy saving techniques were applied. The given values in level 1 are derived from the actual condition of the case study house. Further, the design and operational parameters of HVAC system are not considered though it is acknowledged that the improvement of HVAC system could affect optimal energy use in buildings. Moreover, we also do not consider the increase of AC unit in the future scenario although it may increase along with the improvement of household's financial condition.

8.5 Model validation

The simulation results of the base model were compared with the observation data from field measurement which was carried out from 16th to 21th August 2014 (see Fig. 8.3). As shown, the RMSE and R² values for air temperature and operative temperature are satisfactory: RMSE and R² for air temperature are 0.40 and 0.86, respectively, while those for operative temperature are 0.39 and 0.87, respectively.

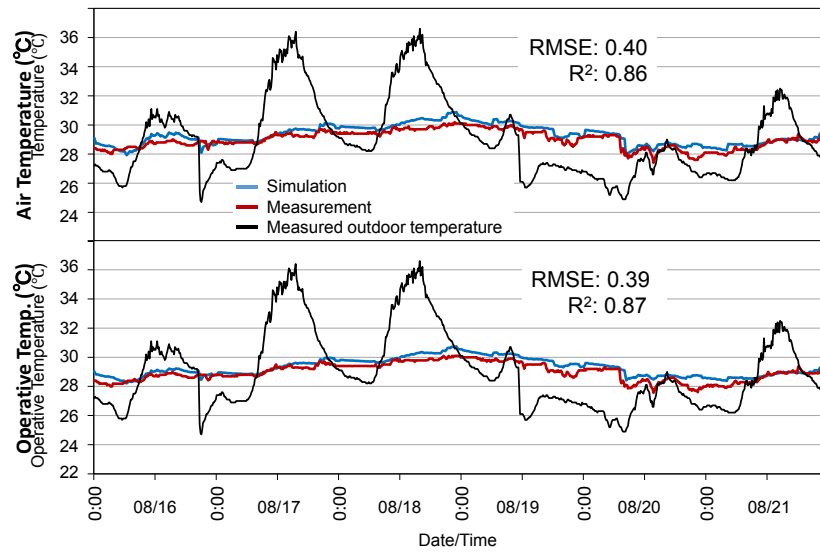


Fig. 8.3 Comparisons between the simulated and measured temperatures in the master bedroom. The measured outdoor temperature is also included.

8.6 Results and discussion

8.6.1 Impacts of future urban warming on indoor thermal environments

This section discusses the impact of the future urban warming on the indoor thermal conditions under three ventilation conditions i.e. (1) daytime ventilation, (2) night ventilation, and (3) full-day ventilation. Fig. 8.4 shows the diurnal variations of operative temperatures under the three ventilation conditions (i.e. A, B, C for daytime, night, and full-day ventilation, respectively) for current and future conditions with the corresponding outdoor temperature, respectively. As shown, in the current status, the maximum outdoor temperature was 35.7°C,

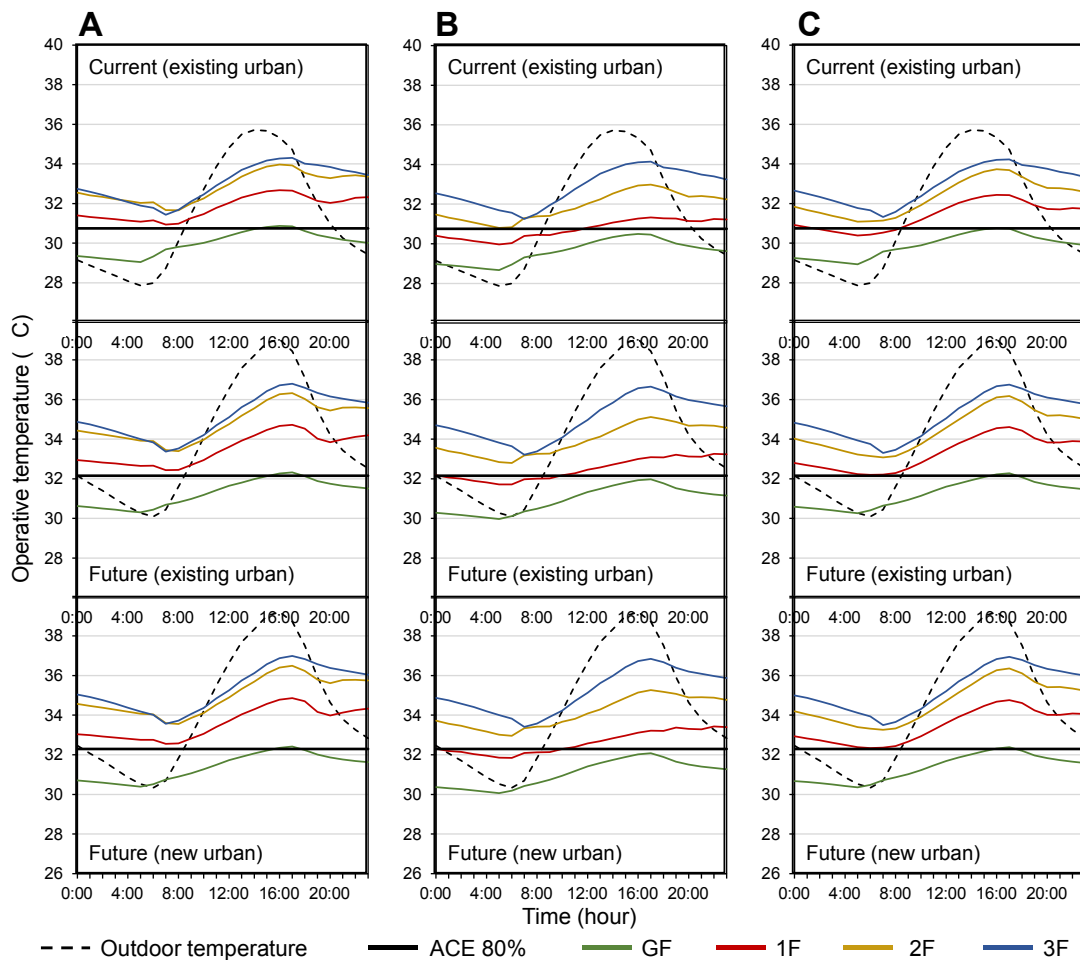


Fig. 8.4 Outdoor and indoor operative temperatures for each floor for existing urban area in current condition and existing urban area and new urban area in future condition (A: Day time ventilation B: Night time ventilation C: Full day ventilation).

while the minimum was 27.9°C. On the other hand, in the future condition, the maximum outdoor temperature is 39.0°C and 30.1°C at minimum in both urban areas. This shows that the outdoor temperature is projected to increase approximately 3.3°C in the daytime and 2.2°C at night in Hanoi. In all scenarios, the night ventilation showed the best performance among all ventilation techniques in terms of the reduction of operative temperature, especially on the first and second floor. In the current condition, the night ventilation lowered the operative temperature in master bedroom by up to 1.4°C as compared to the daytime ventilation. Application of full-day ventilation also resulted in the reduction in operative temperature although the magnitudes of reduction (up to 0.7°C) were still less than those by the night ventilation. The indoor thermal comfort was evaluated by using the 80% upper limit of Adaptive Comfort Equation (ACE) for naturally ventilated buildings in hot and humid climates developed by Toe & Kubota (2013). As shown in Fig. 8.4, under the current condition, although the night ventilation could lower the operative temperature of all rooms, this technique alone was not able to meet the required adaptive comfort limit throughout the day. For instance, the operative temperature of master bedroom slightly exceeded the comfortable 80% upper limit. As shown, the exceeding period will further increase even if the night ventilation is performed in the future condition.

8.6.2 Cooling effect of energy-saving techniques on indoor thermal conditions

In a naturally ventilated building, generally, as the outdoor temperature rises, the indoor temperatures follow and this affects the thermal comfort. This section investigates the effect of energy-saving techniques on indoor thermal conditions under naturally ventilated conditions. Six energy-saving techniques were examined, i.e. (1) increase in roof reflectance, (2) roof insulation, (3) external wall insulation (outside), (4) external wall insulation (inside), (5) external shading, and (6) improvement of glazing performance. The effectiveness of the techniques was analyzed in different levels respectively as shown in Table 8.2. Level 0 (base case) indicates the case study house without the energy-saving techniques. Levels 1–4 represent low to high qualities/standards of each energy-saving technique. In particular, Level 3 follows the criteria proposed in LOTUS (VGBC, 2016), which is a green building rating system recommended for residential buildings in Vietnam.

Fig. 8.5 shows the diurnal variations of resultant operative temperatures in respective rooms when each of the energy-saving techniques (Level 4) is adopted under night ventilation condition in the future conditions. As shown, increase in roof reflectance and roof insulation can reduce daytime operative temperature on the 3rd floor. However, the resulting cooling effect would not reach the lower floors. Outside and inside insulation of the external wall can reduce nocturnal operative temperature in all rooms except for the 3rd floor. At night, the resulting cooling effects are almost the same between outside and inside insulation. However, the outside insulation can reduce daytime operative temperature more compared with inside insulation. External shading has no significant effect on the operative temperature reduction throughout the day. Improvement of glazing performance can reduce daytime operative temperature, especially on GF, 1st floor and 2nd floor.

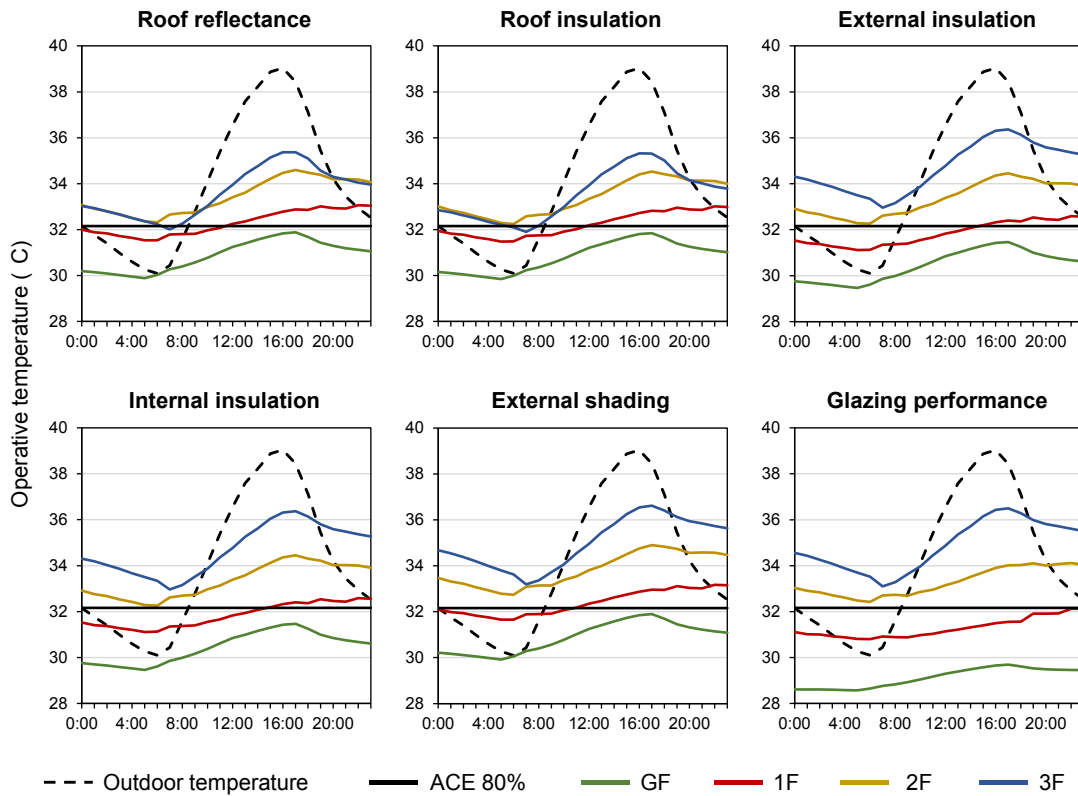


Fig. 8.5 Outdoor temperature and indoor temperature for each floor with energy saving techniques in the case of level 4 under night ventilation condition for existing urban area in future condition.

Fig. 8.6 shows the simulated operative temperatures on each floor when each of the energy-saving techniques is adopted under night ventilation condition in the existing urban areas in the future condition. The results showed that by increasing the roof reflectance and applying roof insulation, the operative temperature on the 3rd floor significantly decreased. In the Level 4, the temperature reduction was up to 1.72°C and 1.89°C for roof reflectance and roof insulation, respectively. Nevertheless, the operative temperatures still exceed the adaptive comfort limit (80%) during most of the time. On the 2nd floor, improvement of glazing performance resulted in the largest reduction in daily mean and maximum operative temperatures. In addition, installation of insulation for external wall (outside and inside) could also reduce the daily mean and maximum operative temperatures. However, the 80% adaptive comfort limit cannot be achieved on the 2nd floor by applying external wall insulation. On the 1st floor, installation of insulation for external wall (outside and inside) and improvement of glazing performance reduced the operative temperature by 0.72, 0.64, and 1.54°C, respectively in the case of Level 4. The 80% comfort limit was achieved in master bedroom by applying these techniques respectively (Fig. 8.6b). On the ground floor, installation of insulation for external wall (outside and inside) and improvement of glazing performance reduced the operative temperature by 0.54, 1.13, and 2.28°C, respectively in the case of level 4 (Fig. 8.6a).

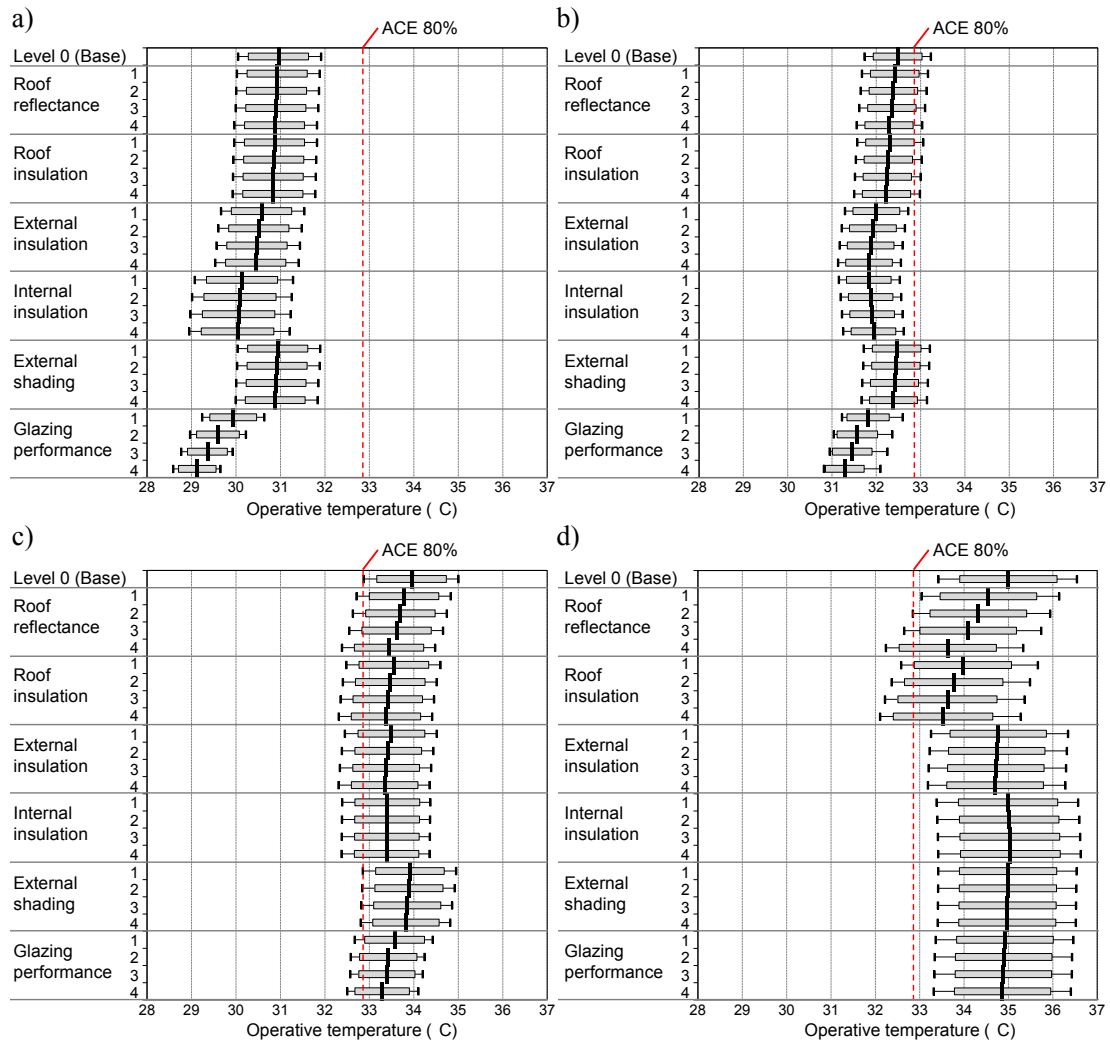


Fig. 8.6 Thermal comfort evaluation of simulated indoor operative temperatures with energy saving techniques under night ventilation conditions for existing urban area in future condition at (a) GF, (b) 1F, (c) 2F and (d) 3F.

8.6.3 Effect of energy-saving techniques on cooling load reduction

Given an air-conditioning (AC) is used in the master bedroom, the resulting cooling load was calculated when each of the energy saving techniques is adopted (Fig. 6). The AC settings were determined as shown in Table 8.4, which was based on the survey results conducted in Vietnam (Vuong & Yoshino, 2010). Fig. 8.7 shows the cooling loads under the night ventilation and full-day ventilation, respectively. As shown in Fig. 8.7a, when the night ventilation was adopted to all rooms (with the exception of master bedroom due to AC usage),

Table 8.4 AC setting in simulation.

| Variables | Description |
|-----------------------|---------------------------------|
| AC location | 1F (Master bedroom) |
| Set-point temperature | 26°C |
| Relative humidity | 60% |
| Operating time | 20:00 to 4:00 (of the next day) |

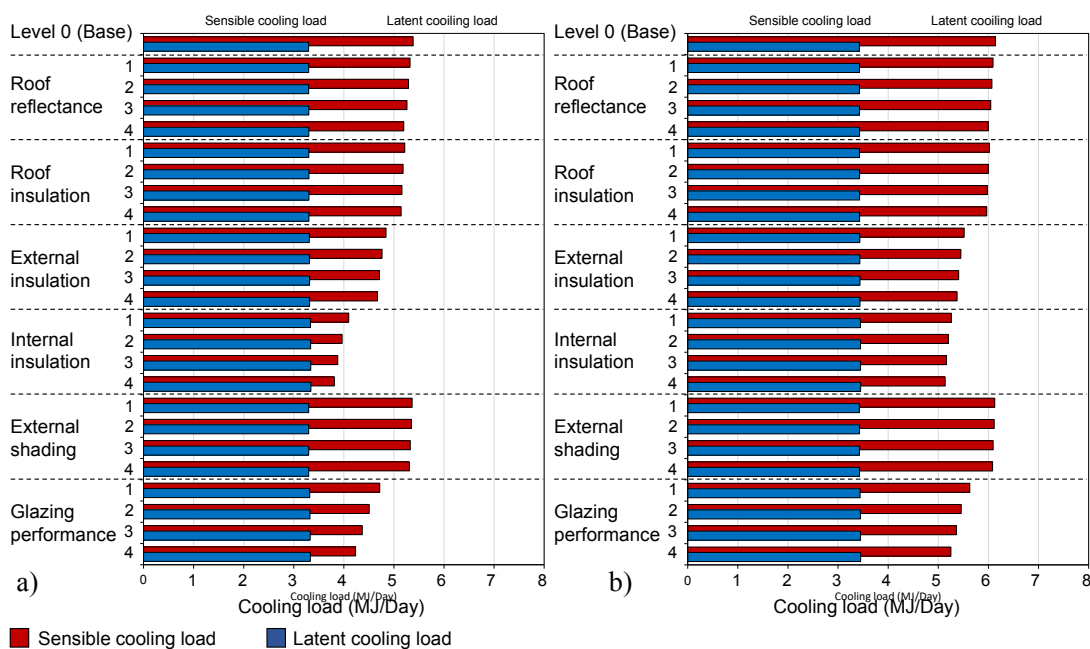


Fig. 8.7 Cooling load of base and each level for single energy saving techniques in master bedroom for (a) night-time ventilation and (b) full day ventilation

the sensible cooling load became smaller than that of the full-day ventilation in the base case (no energy saving technique is applied) by up to 12%. Under the night ventilation condition, installation of inside insulation in all rooms was the most effective to reduce the cooling load with the maximum reduction rate of 29%. In addition, improvement of glazing performance also resulted in a large reduction of sensible cooling load by up to 21%. When the full-day ventilation is adopted to all rooms (except in master bedroom during AC usage), installation of inside insulation in all rooms was the most effective to reduce sensible cooling load by up to 16% (Fig. 8.7b). Increase in roof reflectance and installation of roof insulation were not able to reduce the cooling load sufficiently. The roof insulation of Level 4 reduced the cooling load by only up to 4%. The installation of external shading has no notable cooling load reduction at all levels under any ventilation conditions.

8.7 Summary

Key findings of this study are summarized as follows:

1. Night ventilation showed the largest reduction of operative temperature in current and future conditions. Nevertheless, in future condition, the exceeding period will further increase even if the night ventilation is employed.
2. Among the energy-saving techniques considered in this study, the glazing performance for windows was the most influential in reducing operative temperature in the master bedroom, which had the reduction of up to 0.8 °C. Inside/outside insulation for external wall was also effective in reducing operative temperature.
3. Increase in roof reflectance and installation of roof insulation can sufficiently reduce the operative temperature in the room beneath the roof. Since the cooling effect of both techniques on the indoor thermal conditions is almost the same, increase in roof reflectance is more preferable since it can also contribute to mitigate UHI at the urban scale.
4. In particular, installation of inside insulation for external wall and improvement of glazing performance for windows under night ventilation were found to be effective energy-saving techniques in reducing cooling load in the master bedroom, with the reduction rates of up to 29% and 21%, respectively.

Reference

- Phuong, L. Y., Birkeland, J., & Demirbilek, N. (2010). Towards sustainable housing for Vietnam. In *Proceedings of the 4th International Conference on Sustainability Engineering and Science* (pp. 1–20). Auckland: University of Auckland, New Zealand.
- Toe, D. H. C., & Kubota, T. (2013). Development of an adaptive thermal comfort equation for naturally ventilated buildings in hot–humid climates using ASHRAE RP-884 database. *Frontiers of Architectural Research*, 2(3), 278–291.
- Tung, N. H., Trihamdani, A. R., & Kubota, T. (2015). Field investigation and numerical simulation of indoor thermal environments in urban row houses in Hanoi : Impact of urban heat island on indoor thermal comfort. In *The 7th International Conference of SuDBE 2015* (pp. 1–8). Reading, UK.
- VGBC. (2016). LOTUS Homes Pilot-Technical Manual.
- Vuong, L. P. T., & Yoshino, H. (2010). Survey on energy consumption of residential buildings in Vietnam. *Proceedings of Annual Meeting Architectural Institute of Japan*, 2010, 417–418. Retrieved from <http://ci.nii.ac.jp/naid/110008111174/en>

9

Countermeasures to urban warming for growing cities of Southeast Asia

9.1 The potential factors causing future urban warming

The previous chapters have investigated the potential factors that influence the increased urban temperature, which is the UHIs and global warming effect. Those two factors are different in terms of the scale. The UHI is a local to regional scale with the causes of the phenomenon are derived from local scales, such as the land use changes and anthropogenic heat emission in the city. Meanwhile, the global warming effect is rather a global phenomenon where the causes are difficult to be identified in time and space. Nevertheless, most of the climate scientists believe that the main cause of the current global warming is due to human expansion that leads to the increased GHG emissions.

Land use change

The massive land use change proposed in the master plan generally alters the thermal environment in a city. The obvious impact of this land use change is the increases of the number of hotspots, particularly in new urban areas where the land use conversions from

vegetative land into built-up land mostly occur. As discussed in Chapter 4, the increased built-up land and the absence of vegetative surface in new urban areas result in the increase of the sensible heat. Accordingly, the latent heat in new urban areas is significantly decreased because many vegetative covers in those areas are transformed into built-up lands. As a result, the number of hotspots increases because more energy is transformed into sensible heat and less into latent heat.

Meanwhile, in the Hanoi case study, the configuration of the green spaces can help to lower the increased urban air temperature after the implementation of the master plan. The results in Chapter 6 suggest to increase the GCR in new urban areas by 30% and to use the mixed forest as the vegetation type in the green spaces. This strategy results in the reduction of the average air temperature by averagely 0.3 °C at night. This is particularly due to the reduction in sensible heat during the night-time. Furthermore, by increasing the vegetative surface in the city, the transformed energy into latent heat also increases.

Anthropogenic heat emission

The additional heat from anthropogenic heat emission significantly raises the air temperature in a city. The influence of the anthropogenic heat emission is very apparent at night due to the absence of sun radiation. As discussed in Chapter 7, the anthropogenic heat emission significantly influences the energy balance in the city. The highest increment of the anthropogenic heat emission in BaU scenario accordingly results in the highest increment of the sensible heat flux compared to other scenarios. The significant reductions in the anthropogenic heat emissions in the CM scenario result in the reduction of sensible heat throughout the day. Nevertheless, due to a stronger influence of sun radiation in the daytime, the cooling effect of the reduction of anthropogenic heat emission becomes more apparent at night. As a result of the reduction in sensible heat in CM scenario, the average air temperature in master plan condition can be lowered by up to 0.84 °C from the BaU scenario.

Global warming

The result of this study shows that the global warming effect causes a considerable increase in urban air temperature in the near future. It will amplify the UHI and future problems related to this phenomenon. In the Hanoi case study, the urban air temperature is projected to increase by up to 2.7 °C in the 2030s. Moreover, the result from Hanoi case study also shows that the frequency and/or intensity of warmer nights and hotter days in urban areas will likely increase in the future.

9.2 The UHI mitigation measures through urban greening and reduction of anthropogenic heat emission

The previous chapters have discussed the UHI mitigation measures in urban scale such as the cooling effect of the urban green and the mitigation potential of anthropogenic heat reduction as well the adaptation measures in the building scale (i.e. Chapter 8). Table 9.1 summarizes the cooling effect of the UHI mitigation measures investigated in this thesis.

As shown in Table 9.1, most of the UHI mitigation measures are effective at cooling the cities at night in particular. The maximum cooling effect was obtained from the reduction of anthropogenic heat in the JB case study. However, even this technique gives the largest temperature reduction, it should also be noted that the reduction target in the LCS Blueprint is an ambitious target and the might be difficult to achieve, especially in the growing cities in developing countries.

Meanwhile, the result in Chapter 5 suggests that the urban air temperature will increase far beyond the cooling effect of any UHI mitigation measures. This means that the UHI mitigation measures cannot only depend on one single technique. Instead, it should comprise a combination of various techniques in order to obtain the maximum cooling benefits. Moreover, the urban dwellers should also be prepared to cope with the warmed urban temperature in the near future.

Table 9.1 Summary of the cooling effect of the UHI mitigation measures.

| UHI mitigation measures | Techniques | Cooling effects | | Descriptions |
|-------------------------------------|---|---|--|---|
| | | Daytime | Night-time | |
| Urban green spaces | Small and equally distributed green spaces all over the city | up to 0.1°C of T_{avg} | up to 0.5°C of T_{avg} | The cooling effect is larger than the large and centralized green space. |
| | Increase the green coverage ratio by 10% in new urban areas | up to 0.05°C of T_{avg} | up to 0.2°C of T_{avg} | This technique was applied only in new urban areas. |
| | Increase the green coverage ratio by 30% in new urban areas | up to 0.1°C of T_{avg} | up to 0.5°C of T_{avg} | This technique was applied only in new urban areas. |
| | Increase the green coverage ratio by 30% and use mixed forest in new urban areas | up to 0.2°C of T_{avg} | up to 0.52°C of T_{avg} | The mixed forest largely reduce the hotspots during the daytime. |
| Reduction of the Anthropogenic heat | Anthropogenic emission cut by 40%, 62% and 50% in the commercial, residential and industrial areas. | up to 0.1°C of T_{avg} from the BaU scenario. | up to 0.84°C of T_{avg} from the BaU scenario. | The magnitudes of anthropogenic heat emission do not significantly affect the temperature in the daytime. |

9.3 Adaptation to urban warming in buildings

The increased urban warming affects the quality of life of urban dwellers. Higher temperatures decrease the indoor and outdoor comfort levels and also affect human health. The results of this study found that the existing urban house, in Hanoi for instance, is not able to provide thermal comfort condition when the house was simulated under the global warming condition in the 2030s. Consequently, this will lead to the increased energy consumption for cooling, which will again lead to the further heating and CO₂ release.

In fact, buildings under the warmed urban temperature require more air conditioning in order to provide the comfort condition to the building's occupants. Meanwhile, buildings play a very important role in the urban thermal balance. The building materials determine strongly the energy consumption and comfort conditions of individual buildings as well as of its surrounding environment. Therefore, the reduction of energy consumption, through passive cooling techniques, for instance, can lower the anthropogenic heat emissions which also help to mitigate the urban warming. The energy saving technique in buildings will benefit both indoor and outdoor environment.

One example of the energy saving technique is the cool material. Cool materials are characterized by high solar reflectance and high thermal emittance. The use of the cool material in buildings can benefit the indoor as well as the outdoor environment. Nevertheless, the cooling effect of cool materials on the outdoor environment is only expected if this technique is used in most buildings in the city. Therefore, this implies that the building code or green building standard and/or guidelines on climate sensitive design are necessary to ensure the growth and development of cities can has less impacts on human health and environment.



Fig. 9.1 (a) The large and centralized “Central Park” in New York, US and (b) the garden city concept in Savannah, Georgia, US.

Sources: Keith Sherwood Photography (left) and www.hunterphotography.net (right).

9.4 Recommendations

9.4.1 Tacking global warming or UHI? Global or local?

The scale at which interventions to counter the urban warming is important. Considering that the 71% of the increased temperature in the future is attributed to the global warming, we suggest that the growing cities of Southeast Asia should take a serious consideration to the global warming mitigation measures.

The key concept of mitigating urban warming is to reduce the sensible heat as much as possible, while also trying to maintain or increase the transformed energy into the latent heat. One of the effective measures is the countermeasures through the reduction in the anthropogenic heat emissions. This strategy has co-benefits. First, the reductions in anthropogenic heat emissions contributed to the reduction of GHG emissions to the atmosphere. Second, the emission reduction also benefits the local climate, such as in the reduction of the air temperature at night.

Related to the reduction of anthropogenic heat emission, the city municipality should strongly encourage the use of public transportation in order to reduce the waste heat from traffic. Furthermore, given that the building sector is the major contributor of the total anthropogenic heat releases (in JB for instance), the government should encourage the stakeholders in the building and construction sector to comply with the green building code/standard. It should be noted that the potential of each technology for an area, for different scales, should be evaluated and adapted to the local conditions.

9.4.2 Focus on the reduction of nocturnal air temperature

The sun radiation play a major role at governing the urban temperature during the daytime. On the other hand, this study found that the magnitude of anthropogenic heat emission as well as the land use change have relatively less impact on the peak air temperature during the daytime. Nevertheless, those two factors play major role on the increased nocturnal air temperature at night, when the impact on sun radiation is less. There are several strategies to reduce the nocturnal temperature as discussed below.

Equally distributed green spaces

The presence of greenery in urban areas helps to cool the environment at night through the process of evapotranspiration. We suggested the growing cities provide a smaller green space and equally distributed in the city rather than designing a large and centralized ones. Moreover, small parks should be preferred when considering the cooling efficiency in the urban area with pricy space. Further, the vegetation type in the green spaces should be carefully planted. Our study found that employing mixed forest in the green spaces increases the humidity and tend to reduce the wind velocity.

Building and construction materials

The building and constructions material should not store the heat until the night-time. The common materials in urban areas have relatively high thermal capacity. This materials store the heat in the daytime and release the heat slowly during the night-time, resulting in warm urban air temperature at night. To solve this problem, building should use materials with relatively low-thermal capacity and/or cool materials with high reflectivity and thermal emittance.

Reduction of anthropogenic heat emission

As has been previously discussed, the reduction of anthropogenic heat emission at night significantly lowers the nocturnal air temperature. One of the anthropogenic heat sources at night is the exhaust heat released from AC. In the warmed urban temperature in the future, it is expected that more exhaust heat from AC will be released. Therefore, more attention should be put on the use of AC in cities of Southeast Asia in the future.

9.4.3 Adaptation measures at building scale

Energy saving techniques/Passive cooling techniques

Under the warmed urban environment, the energy saving technique or passive cooling technique, which maintain indoor thermal comfort and reduce the cooling load, become more important. Among several technologies, we investigated the performance of reflective roof material (i.e. cool roof), building insulations (for roof, floor, ceiling and wall), the window glazing material and the shading devices to improve the thermal comfort and to reduce the cooling load in an urban row house in Hanoi.

The cool roof and roof insulation perform similarly in terms of the reduction of cooling load. However, we recommend using the cool roof since it can help to cool the urban environment. Moreover, it is necessary to use low-e glass for windows. Low-E glass reduces the emission of infrared energy while letting the visible light pass. Therefore, it limits the heat originating from outdoor to enter the building.

Improving the efficiency of air-conditioned room

The use of AC is inevitable under the warmed urban temperature in the future. Therefore, we suggest to use the insulation layer, especially in the room with the AC installed. The insulated room will improve the efficiency of AC and therefore reduce the cooling load.

9.5 Remarks

There have been ongoing project of the real applications of UHI mitigation technologies. The lesson learned from that project is that the UHI mitigation measures should be a design-oriented outcomes that could link between the complicated results of the urban climatology research with the town planners, architects, and building contractors.

The growing cities of Southeast Asia are facing urban climate challenges in the near future, associated with the UHI and global warming effects. Regardless the growing problems associated with the growth of the city, there are several opportunities remain.

1. In many growing cities, there is a continuous conflict between conservation and development. Decision-makers must act effectively to preserve, restore and even create urban greenery and urban water bodies. This requires them to implement tough, innovative and proactive planning, with a holistic perspective and cooperation across sectors.
2. The growing cities are the drivers of the green economy. Cities must attract large-scale investments in order to help address the climate challenge and develop sustainably. Investing for sustainable development will entail managing significant commitments and capitals– but would also generate large profits in the long run

10 Conclusions

10.1 Key findings of this study

10.1.1 Literature review on existing UHI studies

The review focuses on the existing studies that investigated the impact of land use change on the urban climate. The review shows that very few studies on UHI was conducted in the developing countries to project the urban climates after the implementation of the proposed master plans. Further review on the urban warming studies also found that there is a research gap in the existing studies on UHI.

The review also discussed various UHI mitigation measures that have been widely studied and developed. Nevertheless, given the fact that the anthropogenic heat emissions have an important role in deteriorating or ameliorating the urban climates, few works were carried out to investigate the impacts of the future possible changes in the anthropogenic heat emission derived from plausible scenarios on mitigating the UHIs.

We also conducted a literature review on the cooling effect of UHI countermeasures in the building scale. We found that most of the studies were conducted in a single story building. Moreover, if the study focused on the multi-story buildings, the thermal comfort and cooling load were investigated in the room underneath/adjacent to the roof. The residential building in Hanoi, however, are 4-5 story building. The master bedroom, where the AC is installed, is mostly located at 2nd or 3rd floor. On the other words, the target room where the AC is installed may be not affected directly by the cooling benefits of cool roof or roof insulation. Given the fact that factors affecting the performance of UHI countermeasures might be different among countries or geographical location, the countermeasure strategies should be adapted to the local condition in each case study or location.

10.1.2 Impact of land use change and global warming on the urban climate

In this study, we investigated the impacts of land use changes proposed by the Hanoi Master Plan 2030 and CDP 2025 in Hanoi and JB, respectively. In general, the implementation of the masterplan will increase the sensible heat flux in a city. On the other hand, the latent heat flux in new urban area significantly decreases because many evaporative surfaces (e.g. vegetation) in the new urban area are turned into built-up land. This results in the expansion of the areas with relatively high air temperatures. These newly emerged hotspots correspond well with the locations of the planned built-up area in the master plan. The increases in air temperature due to the land use change in those area is more apparent during the night-time.

In Hanoi case study, we conducted the urban climate simulations using the future climate conditions in 2030s, which were produced via direct dynamical downscaling with WRF under RCP4.5 and RCP8.5 scenarios. The simulation results shows that the urban air temperature is expected to increase along with global warming. In the 2030s, the average air temperature is projected to increase by 2.1°C, of which up to 1.5 and 0.6 °C are attributable to global warming and land use changes, respectively. Global warming contributed, at most, 71% of the temperature increase in existing urban areas of Hanoi City in the 2030s. Nevertheless, the results of this study is only derived from one GCM output (i.e. MIROC5) which is not able to represent the variabilities of global warming projections from many other GCMs. In addition, we also found that the increased temperature in the future will likely exceed the cooling effect of any UHI mitigation measures.

10.1.3 Cooling effect of the green spaces: A case study of Hanoi

The cooling effects of the proposed green spaces were investigated and further proposal to improve the cooling effect of the green spaces in the city were also studied. The results show that the proposed green spaces are not necessarily effective to cool the entire urban areas. On the other hand, when the same amount of the proposed green spaces were distributed equally in the city, this strategy resulted in a better reduction of urban air temperature, especially at night.

Moreover, by distributing the green spaces more equally in the city, the number of hotspots can be reduced. The cooling effect of the small and equally distributed green spaces is larger than the large and centralised green spaces on cooling the entire urban areas. Consequently, this also lowers the risk for urban dwellers to be exposed to the areas with high temperature. Nevertheless, the idea of equally distributed green spaces is difficult to be implemented in the already established master plan. Therefore, we proposed an additional urban greening by implementing the green coverage ratio (GCR) in each lot of built-up lands in the city. The result shows that the increased GCR results in the reduction of the number of hotspots with peak air temperature, particularly in new urban areas throughout the day. Based on the result in this chapter, we suggested the growing cities to set a minimum standard of GCR, especially in the areas that are still under development.

10.1.4 Influence of anthropogenic heat release on the urban climate

The additional heat from anthropogenic heat emission are found to be one of the significant factors that raises the urban air temperature mainly during the night-time. Meanwhile, the LCS Blueprint that aims to reduce the anthropogenic emission can significantly reduce the urban air temperature particularly at night, if compared to the business as usual scenario. The influence of anthropogenic heat emission to urban climate is more apparent at night due to the absence of sun radiation and relatively stable air circulation during the night-time.

10.1.5 Impacts of urban warming on thermal comfort and cooling load in residential building

The study found that the existing building in Hanoi cannot provide the occupants a thermal comfort condition under a warmed urban environment. This condition is expected to further increase the energy consumption for cooling in the future. Therefore, we proposed to retrofit the existing building with energy saving techniques. The results show that among the energy-saving techniques considered in this study, the glazing performance for windows was the most influential in reducing operative temperature in the master bedroom. Inside/outside insulation for external wall was also effective in reducing operative temperature. Increase in roof reflectance and installation of roof insulation can sufficiently reduce the operative temperature in the room beneath the roof. Since the cooling effect of both techniques on the indoor thermal conditions is almost the same, increase in roof reflectance is more preferable since it can also contribute to mitigate UHI at the urban scale.

10.1.6 Countermeasures to urban warming for growing cities of Southeast Asia

Considering that the 71% of the increased temperature in the future is attributed to the global warming effect, we recommend the growing cities of Southeast Asia to take serious consideration to the countermeasures to global warming. This countermeasures include the adaptation and mitigation actions, respectively.

One of the recommended countermeasures is to reduce the anthropogenic heat emission in the city. This measure has co-benefits. First, it reduces the GHG emissions to the atmosphere. Second, the emission reduction benefits the local climate, such as the reduction in urban air temperature at night. Furthermore, the countermeasures should focus on the reduction of nocturnal air temperature. It can be achieved through the improvement of green spaces and reduction of anthropogenic heat emission in the city.

Moreover, the use of AC will become inevitable under the warmed urban environment in the future. We highly recommend to improve the insulation in the air-conditioned rooms. The well-insulated rooms will improve the efficiency of AC and therefore reduce the energy consumption for cooling.

10.2 Limitation and suggestion for the future research

We described the simulation results for the impacts of land use changes proposed in master plan and the impacts of global warming in 2030 through the numerical experiments. In general, however, the following points have to be taken as limitations in the numerical experiments and considered when interpreting our modeling results. Furthermore, some relevant studies to urban climate are discussed in the followings.

1. The impacts of global warming through direct dynamical downscaling were driven by one GCM output, MIROC5. However, more GCM outputs from CMIP5 will be used to take into account the wide range of climate variability and uncertainty in our future works.
2. In Hanoi case study, the urban canopy model was employed with a default setting. More-detailed urban parameterisations, which are derived from the actual conditions in Hanoi City, are needed for future studies. Moreover, energy-saving policies and increases in the efficiency of cooling technologies in the future should also be reflected in the future modelling studies.
3. The influences of non-linear interaction between the gradual changes of land use and global warming on urban climate are not considered in this study but cannot be neglected. However, the quantitative analysis of the non-linear interaction need gradual or sequential scenarios of land use changes in long-term simulations and out of scope of this study.
4. It has been reported that the increase in urban temperature may prompt the emergence of heat-related illnesses and mortalities (Basu & Samet, 2002). On the other hand, people living in cities may acclimate and adapt to the increased urban temperatures, to a certain extent (Toe & Kubota, 2013). It will be particularly important to investigate the effects of future urban warming on health issues and the thermal comfort of urban residents of growing cities in future studies.

References

- Basu, R., & Samet, J. M. (2002). Relation between elevated ambient temperature and mortality : A review of the epidemiologic evidence. *Epidemiologic Reviews*, 24(2), 190–202.
- Toe, D. H. C., & Kubota, T. (2013). Development of an adaptive thermal comfort equation for naturally ventilated buildings in hot–humid climates using ASHRAE RP-884 database. *Frontiers of Architectural Research*, 2(3), 278–291.

Appendix A

Creation process of the LULC datasets for WRF simulation

To improve the accuracy of the simulation results, the default LULC datasets were replaced with an own-created dataset for domain. The detailed processes of creating the LULC dataset are provided below:

Land use detection of Landsat 8 images

The LULC data for areas within the metropolitan boundary of Hanoi City are provided by the digital land use data from VIUP. Therefore, the additional data from Landsat 8 satellite images were used for the surrounding areas, covering the whole region for domain 3. The digital land use data for the current and master plan conditions from VIUP are presented in Fig. A1. Firstly, the land use categories of the digital VIUP data were converted into USGS24 land cover categories. Landsat 8 is the land-observing satellite launched in May 2013 as a joint initiative between U.S. Geological Survey (USGS) and NASA. Landsat 8 carries two instruments. The

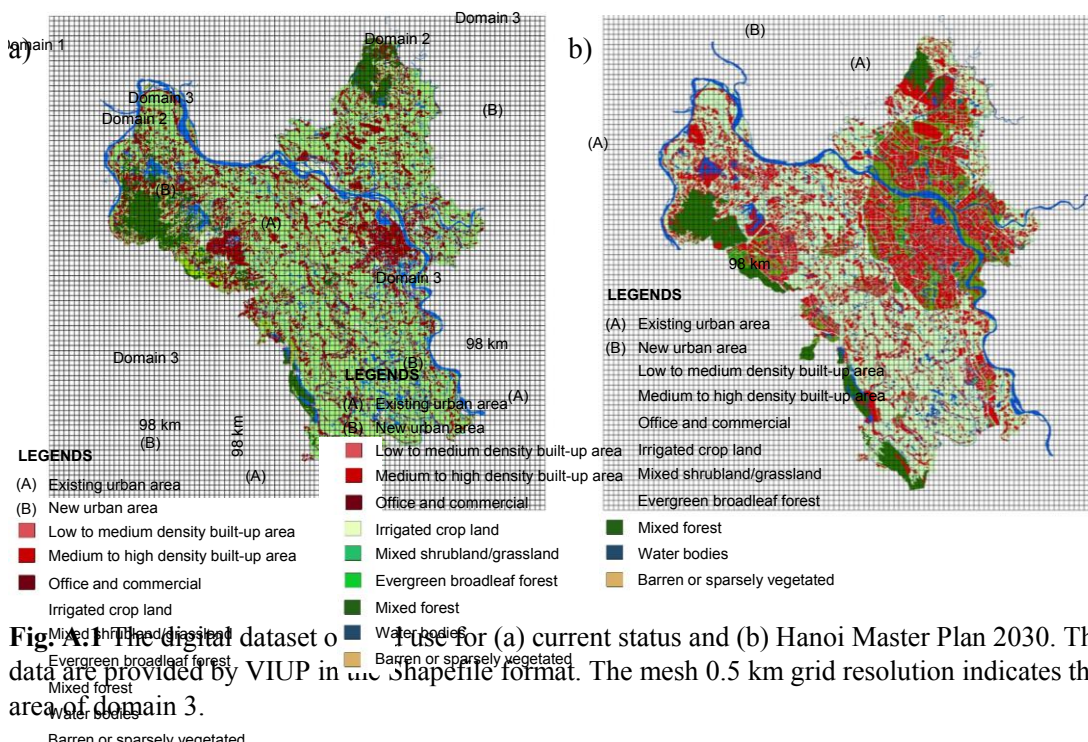


Fig. A.1 The digital dataset of LULC use for (a) current status and (b) Hanoi Master Plan 2030. The data are provided by VIUP in the shapefile format. The mesh 0.5 km grid resolution indicates the area of domain 3.

Table A.1 Wavelength and resolution of Landsat 8's bands

| Band number | in μm | Resolution |
|-------------|------------------|------------|
| 1 | 0.433 – 0.453 | 30 m |
| 2 | 0.450 – 0.515 | 30 m |
| 3 | 0.525 – 0.600 | 30 m |
| 4 | 0.630 – 0.680 | 30 m |
| 5 | 0.845 – 0.885 | 30 m |
| 6 | 1.560 – 1.660 | 30 m |
| 7 | 2.100 – 2.300 | 30 m |
| 8 | 0.500 – 0.680 | 15 m |
| 9 | 1.360 – 1.390 | 30 m |
| 10 | 10.6 - 11.2 | 100 m |
| 11 | 11.5 - 12.5 | 100 m |

Source: NASA, 2014.

Operational Land Imager (OLI) sensor includes refined heritage bands, along with three new bands: a deep blue band for coastal/aerosol studies, a shortwave infrared band for cirrus detection, and a quality assessment band. The Thermal Infrared Sensor (TIRS) provides two thermal bands.

As images from Landsat 8 provide good spatial land-coverage maps and land-use classification maps with 30-m spatial resolution, we use two images (see Fig. A2) that can fully cover domain 3. Both images were acquired in the same month (acquired on 30 May 2015). One image has 11 multispectral bands, and the wavelengths of these bands are listed in Table A1.

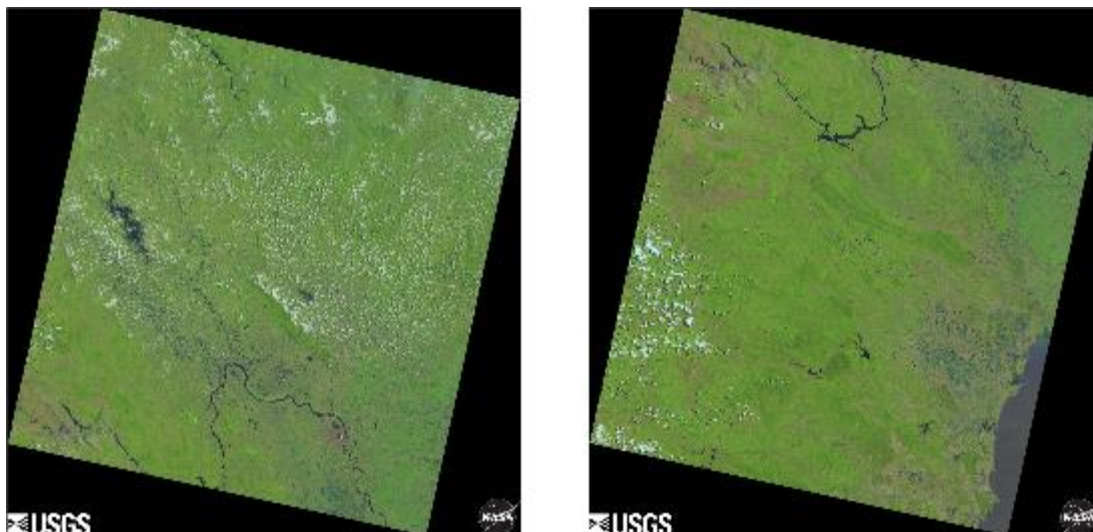


Fig. A.2 Two Landsat 8 satellite images used to cover the area in domain 3. Source: NASA

Landsat 8 imageries were quantitatively analysed using a supervised classification method (Richards & Jia, 2006). Supervised classification is based on the use of suitable algorithms to label pixels in an image. Labelled pixels represent particular ground cover types or classes. The available algorithms vary from those based on probability distribution for the classes of interest to those in which the multispectral space is divided into class-specific regions using optimally located surfaces. In this research, the Maximum Likelihood Classification (MLC) was used to label pixels based on USGS 24-land cover categories. Of various algorithms, the MLC is the most commonly used with remote sensing image data (Richards & Jia, 2006).

In the process, the classes resulting from the supervised classification were spectral classes, which, based on the natural grouping of the image values, were compared with the digital land use data from VIUP and Google Maps for determination of the identity and information value of the spectral classes. The final classes determined are water, mixed forest, built-up land, wet

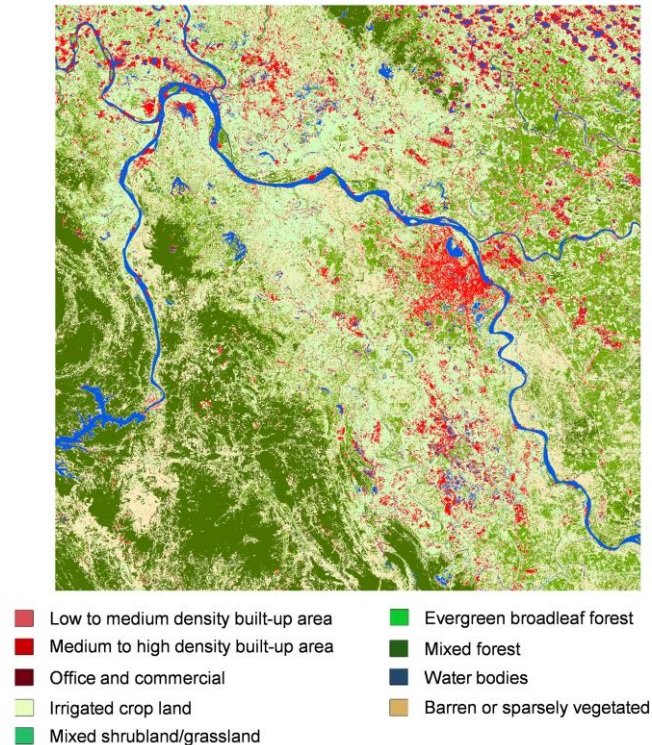
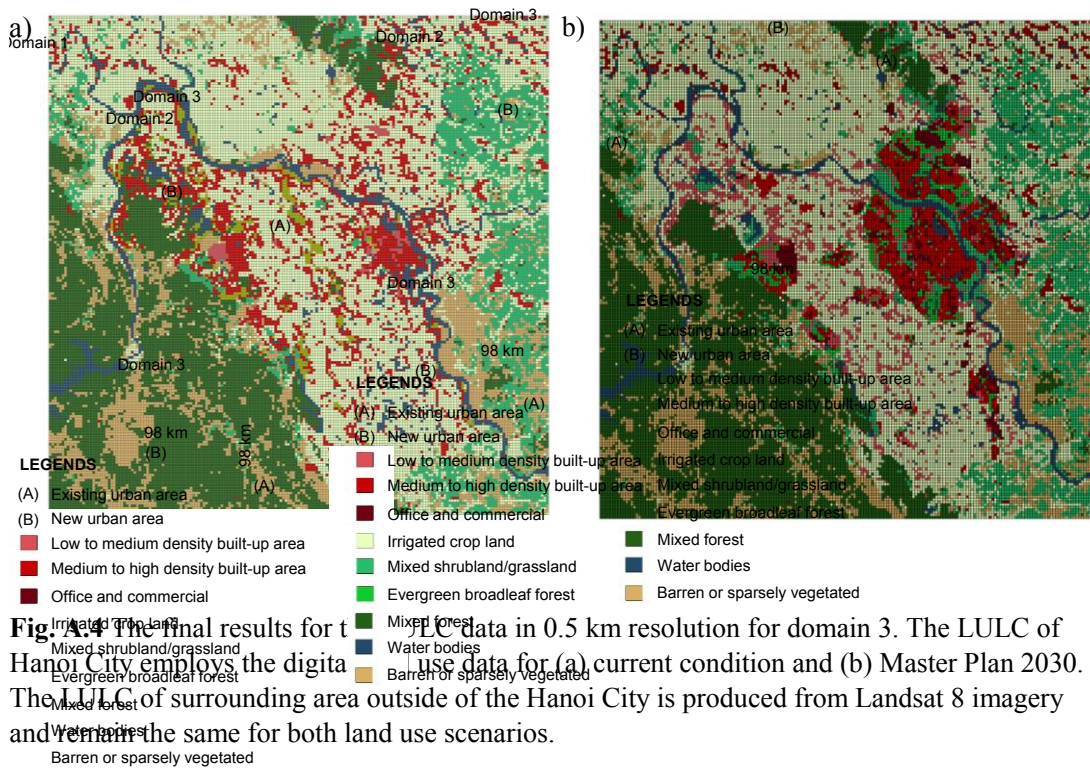


Fig. A.3 The results of land cover classification of the merged satellite images shown in Fig. A2.

cropland, dry cropland and clouded area. The merged product of the detected LULC from Landsat 8 imagery for the region of domain 3 is shown in Fig. A3.

Clouded areas were then replaced by values from VIUP data using ArcGIS. After the overlaying of Landsat 8 data with VIUP data for the current condition, all data were converted into 0.5-km resolution for WRF simulations and into USGS24 categories (Fig. A4a). The same process was also applied to the master plan condition within the Hanoi City administrative area, whereas the surrounding areas were assumed to be the same as current conditions (Fig. A4b).



Appendix B

Analysis of weather data in Hanoi

Determining period that could represent the average current climate conditions is important in this study in order to compare fairly between the future climate and the current climate. An analysis on the air temperature records between 2000 and 2015 was conducted. Firstly, we chose a year that has the closest value to the average air temperature over 15-year. Then, we chose the month during the summer season in that year which has the closest value of the average air temperature in June over 15-year period. The results show that June 2013 could represent the average climate conditions for current climate. The monthly average air temperature in June 2013 was 33.6°C, relatively close to the average air temperature in June over 15-year period. Table B.1 shows the monthly average air temperatures in Hanoi from 2000-2015.

Table B.1 The monthly average air temperature in Hanoi (Lang weather station) 2000-2015.

| | '00 | '01 | '02 | '03 | '04 | '05 | '06 | '07 | '08 | '09 | '10 | '11 | '12 | '13 | '14 | '15 | Average |
|---------|-------|-------|-------|-------|-------|-------|-------|-------|-------|-------|-------|-------|-------|-------|-------|-------|---------|
| Jan | 21.00 | 21.20 | 20.90 | 20.70 | 19.70 | 18.40 | 21.10 | 20.20 | 18.40 | 19.90 | 20.50 | 14.70 | 16.50 | 17.20 | 21.60 | 21.70 | 19.61 |
| Feb | 18.80 | 19.70 | 21.70 | 24.30 | 21.20 | 20.00 | 20.90 | 25.40 | 16.30 | 26.00 | 24.50 | 20.60 | 18.60 | 22.30 | 19.40 | 21.70 | 21.34 |
| Mar | 22.80 | 23.80 | 25.00 | 25.00 | 23.10 | 21.70 | 23.00 | 23.80 | 25.10 | 23.70 | 24.90 | 19.40 | 22.50 | 27.00 | 21.90 | 23.80 | 23.53 |
| Apr | 28.40 | 27.20 | 29.40 | 29.80 | 27.50 | 27.50 | 29.00 | 27.00 | 28.00 | 28.10 | 26.60 | 26.90 | 30.00 | 28.20 | 27.10 | 28.70 | 28.09 |
| May | 31.00 | 30.30 | 31.90 | 33.10 | 30.50 | 33.50 | 31.50 | 31.30 | 31.40 | 30.60 | 32.40 | 31.00 | 32.60 | 32.60 | 33.10 | 34.50 | 31.96 |
| Jun | 31.90 | 32.70 | 33.40 | 33.80 | 33.40 | 34.20 | 34.30 | 34.40 | 32.70 | 34.30 | 34.90 | 33.40 | 34.10 | 33.60 | 33.70 | 34.50 | 33.71 |
| Jul | 33.10 | 32.70 | 32.70 | 33.70 | 32.00 | 33.30 | 33.50 | 34.40 | 33.20 | 33.10 | 34.70 | 33.70 | 33.00 | 31.90 | 33.30 | 33.50 | 33.24 |
| Aug | 32.50 | 32.00 | 31.90 | 32.90 | 32.60 | 32.40 | 31.60 | 33.20 | 32.50 | 34.00 | 32.20 | 32.60 | 33.20 | 32.80 | 32.20 | 33.20 | 32.61 |
| Sep | 30.90 | 31.80 | 31.50 | 31.30 | 31.70 | 32.50 | 32.20 | 31.10 | 32.00 | 33.10 | 32.50 | 31.00 | 31.20 | 30.30 | 32.30 | 31.70 | 31.69 |
| Oct | 28.60 | 29.20 | 28.90 | 30.10 | 29.60 | 29.50 | 31.50 | 29.40 | 30.30 | 30.40 | 29.10 | 27.50 | 30.40 | 28.90 | 30.40 | 30.50 | 29.64 |
| Nov | 25.60 | 25.80 | 24.70 | 27.40 | 26.80 | 26.00 | 29.00 | 26.20 | 25.00 | 25.90 | 25.80 | 27.60 | 26.30 | 25.60 | 25.70 | 27.40 | 26.30 |
| Dec | 23.90 | 20.70 | 21.60 | 22.00 | 23.20 | 20.30 | 22.00 | 23.40 | 22.10 | 23.00 | 22.70 | 20.60 | 20.90 | 20.00 | 20.20 | 22.50 | 21.82 |
| Average | 27.38 | 27.26 | 27.80 | 28.68 | 27.61 | 27.44 | 28.30 | 28.32 | 27.25 | 28.51 | 28.40 | 26.58 | 27.44 | 27.53 | 27.58 | 28.64 | 27.79 |

Appendix C

Creation process of the LULC datasets for WRF simulation for JB case study

The preparation of a LULC map for JB was mainly based on the spatial and spectral information retrieved from the Landsat 8 satellite imagery. The Landsat 8 imagery used for land cover classification in this research are shown in Fig. C1. Scene 1 consists of the western coast of Peninsular Malaysia in the north, the Strait of Malacca in the centre, and several islands belonging to Sumatra (Indonesia) in the south of the image. The western part of scene 1 is highly contaminated by smoke caused mainly by biomass burning, which originates from Sumatra and reaches until the western coast of Peninsular Malaysia. Scene 2 comprises of the southern-most tip of Peninsular Malaysia and Singapore Island in the centre, Batam, Bintan and several other Indonesian islands in the south, and the South China Sea in the east of the image. Larger cloud formations cover areas east and west of JB as well as larger parts of Indonesian islands in the south. The formation of clouds over several areas in scene 1 and 2 limits the observation capabilities of Landsat 8 in the visible and infrared spectral regions.

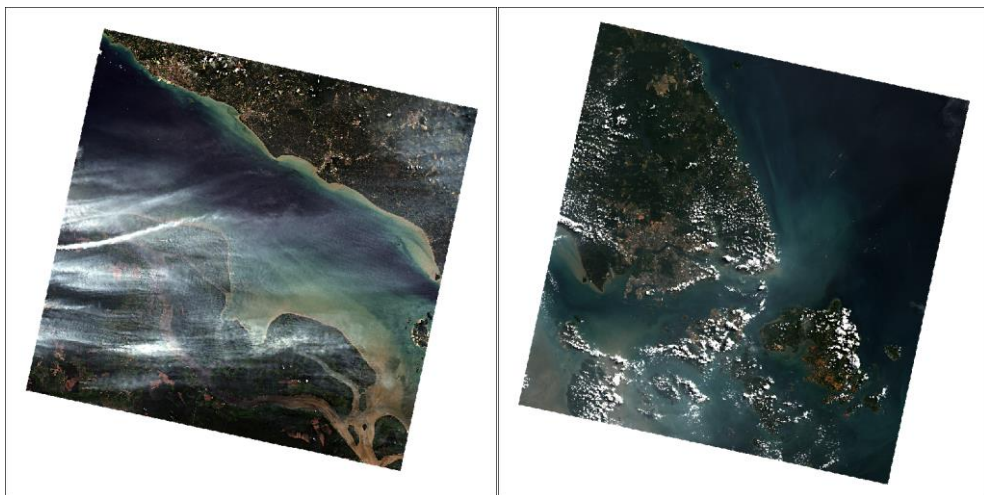


Fig. C.1 Landsat 8 imagery (a) 18 June 2013 - Scene 1 (b) 27 June 2013 - Scene 2.

Before processing and analysing Landsat 8 imagery, various pre-processing steps were applied. Pre-processing aimed at enhancing quality of the image data by reducing radiometric errors caused by internal and external conditions, and by reducing in-scene contamination by haze.

Radiometric calibration

Radiometric calibration was performed to compensate for radiometric errors from sensor defects, variations in scan angle, and system noise to produce an image that represents true radiance at the Landsat 8 OLI/TIRS sensor. Landsat 8 OLI/TIRS imagery were calibrated to radiance.

Atmospheric correction

Landsat 8 satellite collects solar radiation emitted by earth's surface in an altitude of 705 km. On the way to the satellite, solar radiation passes through the atmosphere. The opacity of the atmosphere influences the surface reflectance that reaches the sensor of the satellite. Water vapour and carbon dioxide molecules as well as ozone layer in the upper atmosphere are known to have an impact on the absorption of radiation. Compensation of the atmospheric effect through atmospheric correction tools is necessary for the analysis of surface reflectance in the scope of land cover classification. The Fast Line-of-sight Atmospheric Analysis of Hypercubes (FLAASH) tool was applied to retrieve spectral reflectance from multispectral as well as hyperspectral radiance images.

Land cover classification

Supervised Classification Landsat 8 imagery were quantitatively analysed using supervised classification method. Supervised classification is based on the use of suitable algorithms to label pixels in an image. Labelled pixels represent particular ground cover types or classes. In this research, the Maximum Likelihood Classification (MLC) was used to label pixels based on USGS 24-land cover categories. Among other algorithms, the MLC represents a method that is used most commonly with remote sensing image data (Richards & Jia, 2006).

Appendix D

Historical weather analysis for JB case study

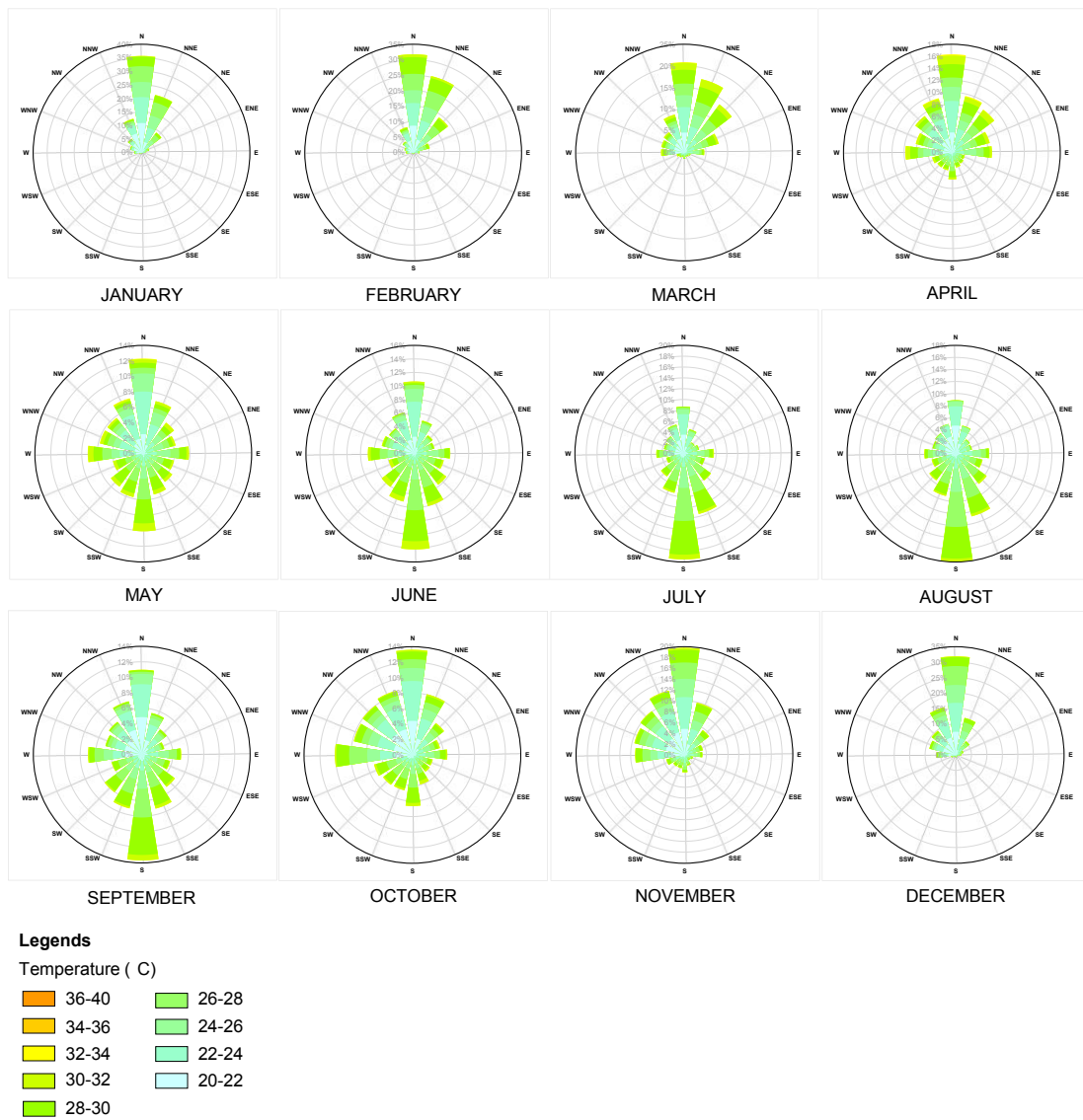


Fig. D.1 Wind pattern analysis. The wind direction for each month is a temporal average from 2000 to 2017.

Table D.1 The monthly average air temperature in JB (Senai weather station) 2000-2013.

| | '00 | '01 | '02 | '03 | '04 | '05 | '06 | '07 | '08 | '09 | '10 | '11 | '12 | '13 | Average |
|---------|-------|-------|-------|-------|-------|-------|-------|-------|-------|-------|-------|-------|-------|-------|---------|
| Jan | 25.7 | 26.6 | 26.6 | 26.25 | 26.4 | 26.1 | 26.55 | 26.2 | 26.5 | 26.4 | 27.15 | 26.05 | 27.2 | 27.35 | 26.50 |
| Feb | 25 | 27.1 | 26.65 | 26.7 | 27.1 | 27.9 | 27.3 | 26.85 | 26.45 | 27.2 | 28.35 | 27.1 | 27.35 | 27.15 | 27.01 |
| Mar | 27.4 | 27.55 | 27.65 | 27.85 | 27.6 | 27.85 | 27.95 | 27.45 | 26.2 | 27.3 | 28.2 | 27.35 | 27.45 | 28.7 | 27.61 |
| Apr | 26.2 | 27.85 | 27.85 | 27.65 | 28.05 | 28.35 | 27.55 | 27.65 | 27.35 | 27.7 | 28.5 | 28.2 | 27.65 | 28.25 | 27.77 |
| May | 28.15 | 27.85 | 27.95 | 27.9 | 27.85 | 28.05 | 27.7 | 27.45 | 27.2 | 27.95 | 28.85 | 28.25 | 27.8 | 28.1 | 27.93 |
| Jun | 27.2 | 27.35 | 27.3 | 27.5 | 27.55 | 27.95 | 27 | 27.6 | 27.05 | 27.9 | 27.55 | 27.85 | 28.05 | 29 | 27.63 |
| Jul | 27.35 | 27.4 | 27.2 | 26.7 | 26.6 | 27.25 | 27.2 | 26.85 | 26.55 | 27.2 | 27 | 27.85 | 27.2 | 27.95 | 27.16 |
| Aug | 27.05 | 27.3 | 27 | 26.95 | 26.75 | 27 | 26.95 | 26.45 | 26.55 | 27.3 | 27.2 | 27.45 | 27.25 | 27.8 | 27.07 |
| Sep | 27.2 | 27.15 | 26.5 | 26.55 | 26.55 | 27.3 | 26.8 | 26.8 | 26.85 | 27.5 | 27.45 | 27.45 | 27.45 | 27.55 | 27.08 |
| Oct | 27.6 | 27.55 | 27.25 | 26.6 | 27 | 27.15 | 27.5 | 27.1 | 26.9 | 27.5 | 27.45 | 27.55 | 27.75 | 28.25 | 27.37 |
| Nov | 27.15 | 27.2 | 26.75 | 26.8 | 26.8 | 26.8 | 26.95 | 26.65 | 27.2 | 27.2 | 27.5 | 27.65 | 27.8 | 28.2 | 27.19 |
| Dec | 27.3 | 26.95 | 26.85 | 26.1 | 26.05 | 26.95 | 26.4 | 26.35 | 26.75 | 27 | 27.05 | 27 | 27.15 | 26.9 | 26.77 |
| Average | 26.94 | 27.32 | 27.13 | 26.96 | 27.03 | 27.39 | 27.15 | 26.95 | 26.80 | 27.35 | 27.69 | 27.48 | 27.51 | 27.93 | 27.26 |

Appendix E

Process of urban land use classification in Hanoi for UCM

In order to run the WRF simulation with UCM, the built-up areas should be further classified into three categories as required by UCM. Therefore, we classified the built-up areas in Hanoi were classified based on the building density, energy pattern, building height and roof material.

Analyse the building footprint in each land use category

The land use classification for urban areas for the master plan from Vietnam Institute of Urban and rural Planning (VIUP) is our reference. There are 13 categories specified by VIUP. We further classified 13 types of land use from the digital land usedata into three categories as required by urban canopy model (UCM).

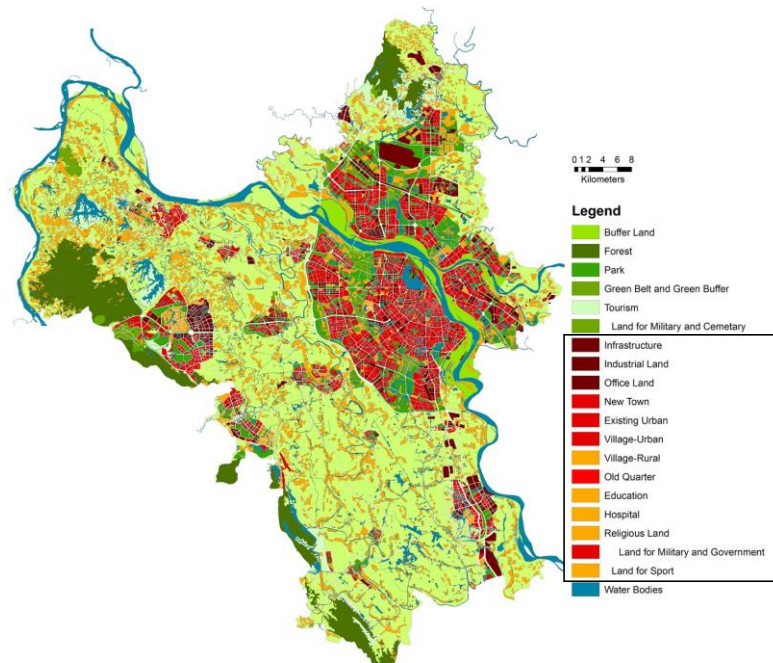


Fig. E.1 Land use of Hanoi Master Plan 2030. The land uses inside the box are the land use for urban areas specified by VIUP.



Fig. E.2 This is a sample taken from ‘New Town’ category. We traced the building’s footprint (as seen in the figure on the right-hand side). We calculated the total area of the buildings located within the boundary of the sample. Then, the building’s density is calculated by dividing the total area of building with total area of sample.

Then, we randomly selected 4 to 5 samples from each land use and analysed the building’s footprint inside the area of the sample. An example is given in Fig. E.2. We calculated the total area of the buildings located within the boundary of the sample. Then, the building’s density is calculated by dividing the total area of building with total area in each sample. After that, we calculated the average building’s density for each urban category. Table E.1 shows the building densities in all urban land use categories.

Cluster analysis to classify three urban categories

Cluster analysis was conducted to classify the urban categories into three categories. Table E.2. shows the variables used in the cluster analysis. Two methods were performed in the cluster analysis (i.e. building’s density, roof height, energy usage pattern, and roof materials). The former method is Hierarchical Cluster Analysis (HCA) to see the hierarchy of cluster. The latter method is K-Mean Cluster Analysis (KCA) to show the resulting final clusters. Since the urban canopy model (UCM) only requires three urban categories, the number of cluster was set to three clusters in both methods.

Fig. E.3 shows the dendrogram resulted from HCA. Table 3 shows the final urban categories and their definitions. The land use map with three urban categories is shown in Fig. E.4.

Table. E.1 Building densities in all urban land use categories.

| Landuse | Sample name | Total area | Area | | Building density |
|---------------------------------------|----------------|------------|------------------------|-------|------------------|
| | | | Building coverage area | Other | |
| Infrastructure (IF) | S1 | 0.087 | 0.046 | 0.041 | 0.53 |
| | S2 | 0.026 | 0.005 | 0.021 | 0.20 |
| | S3 | 0.021 | 0.007 | 0.015 | 0.31 |
| | S4 | 0.062 | 0.012 | 0.051 | 0.19 |
| | S5 | 0.081 | 0.012 | 0.069 | 0.14 |
| | Average | | | | |
| Industrial land (IN) | S1 | 0.250 | 0.124 | 0.127 | 0.49 |
| | 0.36 | 0.250 | 0.114 | 0.136 | 0.46 |
| | S3 | 0.250 | 0.099 | 0.151 | 0.40 |
| | S4 | 0.250 | 0.121 | 0.129 | 0.48 |
| | Average | | | | |
| Office land (OF) | S1 | 0.051 | 0.028 | 0.023 | 0.55 |
| | S2 | 0.081 | 0.029 | 0.052 | 0.35 |
| | S3 | 0.262 | 0.102 | 0.160 | 0.39 |
| | S4 | 0.044 | 0.017 | 0.027 | 0.39 |
| | S5 | 0.048 | 0.018 | 0.031 | 0.36 |
| | Average | | | | |
| New Town (NT) | S1 | 0.094 | 0.043 | 0.051 | 0.46 |
| | S2 | 0.061 | 0.033 | 0.028 | 0.54 |
| | S3 | 0.311 | 0.158 | 0.153 | 0.51 |
| | S4 | 0.040 | 0.018 | 0.022 | 0.44 |
| | S5 | 0.132 | 0.052 | 0.079 | 0.40 |
| | Average | | | | |
| Existing Urban (EU) | S1 | 0.250 | 0.168 | 0.082 | 0.67 |
| | S2 | 0.030 | 0.018 | 0.012 | 0.61 |
| | S3 | 0.030 | 0.021 | 0.009 | 0.70 |
| | S4 | 0.250 | 0.167 | 0.084 | 0.67 |
| | Average | | | | |
| Village Urban (UV) | S1 | 0.040 | 0.016 | 0.024 | 0.40 |
| | S2 | 0.040 | 0.014 | 0.026 | 0.36 |
| | S3 | 0.010 | 0.005 | 0.006 | 0.45 |
| | S4 | 0.010 | 0.004 | 0.006 | 0.43 |
| | Average | | | | |
| Village Rural (RV) | S1 | 0.088 | 0.032 | 0.056 | 0.36 |
| | Average | | | | 0.36 |
| Old quarter (OL) | S1 | 0.250 | 0.147 | 0.103 | 0.59 |
| | S2 | 0.250 | 0.180 | 0.070 | 0.72 |
| | S3 | 0.250 | 0.178 | 0.072 | 0.71 |
| | Average | | | | 0.67 |
| Education (ED) | S1 | 0.054 | 0.016 | 0.038 | 0.29 |
| | S2 | 0.042 | 0.012 | 0.030 | 0.28 |
| | S3 | 0.059 | 0.023 | 0.036 | 0.39 |
| | S4 | 0.024 | 0.009 | 0.016 | 0.36 |
| | S5 | 0.059 | 0.021 | 0.039 | 0.35 |
| | Average | | | | 0.33 |
| Hospital (HO) | S1 | 0.048 | 0.016 | 0.032 | 0.33 |
| | S2 | 0.021 | 0.011 | 0.011 | 0.50 |
| | S3 | 0.003 | 0.002 | 0.002 | 0.45 |
| | Average | | | | 0.43 |
| Religious Land (RL) | S1 | 0.021 | 0.003 | 0.018 | 0.15 |
| | S2 | 0.032 | 0.006 | 0.026 | 0.19 |
| | S3 | 0.025 | 0.009 | 0.016 | 0.34 |
| | S4 | 0.056 | 0.004 | 0.052 | 0.07 |
| | S5 | 0.011 | 0.002 | 0.009 | 0.21 |
| | Average | | | | 0.19 |
| Land for Military and Government (GO) | S1 | 0.146 | 0.037 | 0.109 | 0.25 |
| | S2 | 0.054 | 0.011 | 0.042 | 0.21 |
| | S3 | 0.035 | 0.009 | 0.026 | 0.26 |
| | Average | | | | 0.24 |
| Land for sport (SP) | S1 | 0.258 | 0.061 | 0.197 | 0.24 |
| | S2 | 0.028 | 0.007 | 0.021 | 0.25 |
| | Average | | | | 0.25 |

Table. E.2 Variables used in the cluster analysis

| Land use categories | Density | Average Width | Roof Height (m) | Energy usage ¹ | Roof cover ² |
|----------------------------------|---------|---------------|-----------------|---------------------------|-------------------------|
| Old quarter | 0.67 | 57.43 | 4 | 1 | 1 |
| Existing Urban | 0.66 | 48.15 | 4 | 1 | 1 |
| New town | 0.47 | 24.79 | 4 | 1 | 1 |
| Industrial Land | 0.46 | 90.24 | 4 | 3 | 1 |
| Village Urban | 0.41 | 14.40 | 4 | 1 | 1 |
| Village Rural | 0.36 | 14.40 | 3 | 1 | 1 |
| Hospital | 0.43 | 34.75 | 4 | 3 | 2 |
| Education | 0.33 | 21.05 | 4 | 2 | 2 |
| Infrastructure | 0.28 | 21.92 | 3 | 3 | 1 |
| Land for Sport | 0.25 | 45.40 | 4 | 5 | 1 |
| Land for Military and Government | 0.24 | 30.71 | 2 | 2 | 2 |
| Religious Land | 0.19 | 21.07 | 2 | 5 | 2 |
| Office land | 0.41 | 47.79 | 10 | 2 | 2 |

¹For energy usage: 1) residential, 2) office, 3) commercial, 4) 24-hous, 5) Other.

²For roof materials: 1) metal roof and 2) clay roof.

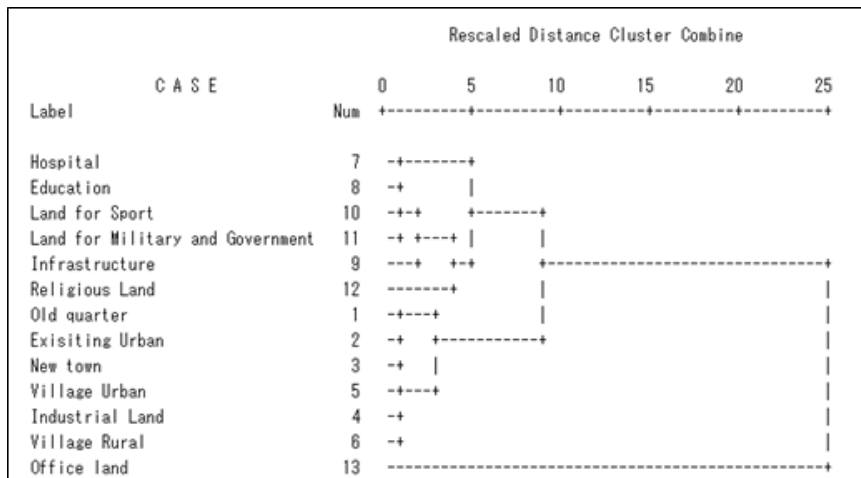


Fig. E.3 Dendrogram resulted from HCA

Table. E.3 Final urban categories and their definitions.

| Urban Category | Definition | Land use | Density | Roof Height | Usage | Roof cover |
|----------------|-----------------------------------|----------------------------------|---------|-------------|-------|------------|
| Urban I | Medium-High Density Built-up Area | Old quarter | 0.67 | 4 | 1 | 1 |
| | | Exisiting Urban | 0.66 | 4 | 1 | 1 |
| | | New town | 0.47 | 4 | 1 | 1 |
| | | Industrial Land | 0.46 | 4 | 3 | 1 |
| | | Village Urban | 0.41 | 4 | 1 | 1 |
| | | Village Rural | 0.36 | 3 | 1 | 1 |
| Urban II | Low Density Built-up Area | Hospital | 0.43 | 4 | 3 | 2 |
| | | Education | 0.33 | 4 | 2 | 2 |
| | | Infrastructure | 0.28 | 3 | 3 | 1 |
| | | Land for Sport | 0.25 | 4 | 5 | 1 |
| | | Land for Military and Government | 0.24 | 2 | 2 | 2 |
| | | Religious Land | 0.19 | 2 | 5 | 2 |
| Urban III | Office and commercial | Office land | 0.41 | 10 | 2 | 2 |

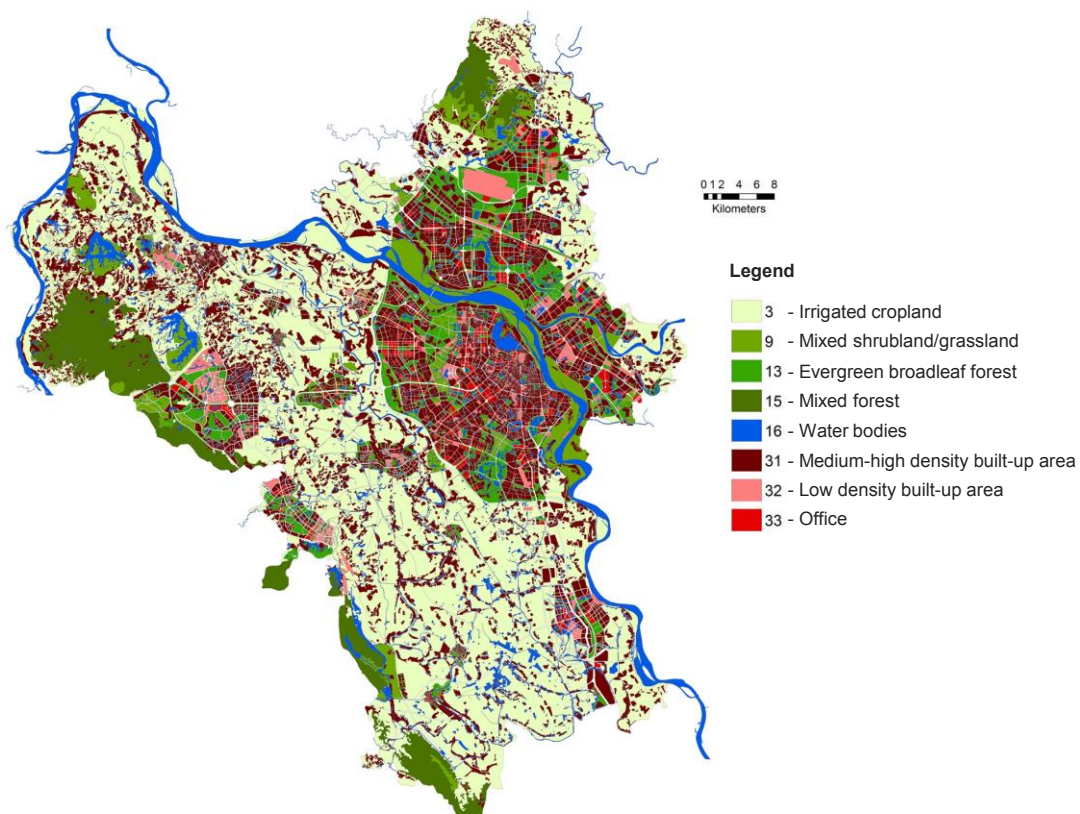


Table. E.4 Land use map with three urban categories.

Appendix F

Process of urban land use classification in JB for UCM

The similar method for land use classification for UCM in Hanoi was also employed in JB case study. Nevertheless, the land use categories are different between current condition (land use data in 2008) and master plan (i.e. CDP 2025). In general, we use the land use categories in the digital land use data in 2008 as reference. Table F.1 shows the list of land use categories in the digital land use data in 2008 and CDP 2025, respectively. The building densities were calculated through three methods.

Table. F.1 Final urban categories and their definitions.

| Land use categories of current condition | Land use categories in the master plan | Density |
|--|--|---------|
| Business and service | Commercial | 0.39 |
| Construction (Business) | | |
| | Enterprise | 0.31 |
| Construction (Housing) | Established housing | 0.32 |
| Houses | | |
| Planned housing | | |
| Under construction | | |
| Heavy industry | Established industry | 0.49 |
| Medium industry | | |
| Light industry | | |
| | High density residential | 0.61 |
| | Industrial park | 0.38 |
| Electricity supply | Infrastructure and utility | 0.3 |
| Water supply | | |
| Sewerage | | |
| Solid waste disposal | | |
| Religious | | |
| Security | | |
| Telecommunication | | |
| Construction (Education) | Institutional and commercial facility | 0.24 |
| Education | | |
| Health | | |
| Other community facility | | |
| | Low density residential | 0.3 |
| | Medium density residential | 0.38 |
| | Medium high density residential | 0.53 |
| Village housing | Villages | 0.13 |

As shown in Table F.1, the calculation of building densities for the master plan are divided into three groups with their own calculation method, respectively. The first group used the building density values which have been specified in the master plan. This group is highlighted with orange color in Table F.1. The second group use the sampling data from the urban categories of the master plan which also have been already established in the current condition (indicated with green color in Table F.1. The third group use the sampling data from the building density in current condition because the land use category in this group have not been established/constructed and not their densities are not stated in the master plan. This group is highlighted with blue color in Table F.1.

Based on the classification in Table F.1, cluster analyses to classify the land uses into three categories were conducted for current and master plan conditions, respectively. Tables F.2 and F.3 show final urban classifications for current and master plan conditions, respectively.

Table. F.2 Final urban categories of current condition.

| Urban category | Ave. Density | Ave. Roof height | Dominant Roof material | Land use category | Density | Roof height (m) | Energy usage pattern ¹ | Roof material ² |
|----------------|--------------|------------------|------------------------|--------------------------|---------|-----------------|-----------------------------------|----------------------------|
| Industrial | 0.45 | 6.3 | 3 | Medium industry | 0.53 | 7 | 3 | 1 |
| | | | | Heavy industry | 0.52 | 7 | 3 | 1 |
| | | | | Light industry | 0.43 | 6 | 3 | 1 |
| | | | | Solid waste disposal | 0.41 | 5 | 3 | 1 |
| | | | | Other community facility | 0.36 | 7 | 2 | 1 |
| Residential | 0.31 | 4.6 | 1 | Sewerage | 0.37 | 3 | 3 | 1 |
| | | | | Construction (Housing) | 0.35 | 5 | 1 | 2 |
| | | | | Houses | 0.34 | 4 | 1 | 1 |
| | | | | Village housing | 0.32 | 5 | 1 | 2 |
| | | | | Security | 0.33 | 4 | 2 | 1 |
| | | | | Planned housing | 0.31 | 6 | 1 | 1 |
| | | | | Telecommunication | 0.14 | 4 | 2 | 1 |
| Commercial | 0.28 | 6.3 | 2 | Business and service | 0.46 | 7 | 2 | 3 |
| | | | | Religious | 0.33 | 8 | 4 | 2 |
| | | | | Construction (Business) | 0.33 | 6 | 2 | 2 |
| | | | | Under construction | 0.28 | 7 | 3 | 3 |
| | | | | Water supply | 0.28 | 5 | 3 | 3 |
| | | | | Electricity supply | 0.25 | 5 | 3 | 3 |
| | | | | Construction (education) | 0.21 | 7 | 2 | 2 |
| | | | | Education | 0.21 | 6 | 2 | 2 |
| Health | 0.17 | 6 | 2 | 2 | | | | |

¹For energy usage: 1) residential, 2) office, 3) commercial, 4) Other.

²For roof materials: 1) metal roof, 2) clay roof and 3) concrete roof.

Table. F.2 Final urban categories of current condition.

| Urban category | Ave. Density | Ave. Roof height | Dominant Roof material | Land use category | Density | Roof height (m) | Energy usage pattern ¹ | Roof material ² |
|----------------|--------------|------------------|------------------------|--------------------------------------|---------|-----------------|-----------------------------------|----------------------------|
| Industrial | 0.39 | 6.3 | Metal | Established industry | 0.49 | 7 | 3 | 1 |
| | | | | Industrial park | 0.38 | 7 | 3 | 1 |
| | | | | Infrastructure and utility | 0.3 | 5 | 3 | 1 |
| Residential | 0.27 | 5.4 | Clay roof | Medium density residential | 0.38 | 5 | 1 | 2 |
| | | | | Established housing | 0.32 | 6 | 1 | 2 |
| | | | | Low density residential | 0.3 | 4 | 1 | 2 |
| | | | | Institutional and community facility | 0.24 | 7 | 2 | 2 |
| | | | | Villages | 0.13 | 5 | 1 | 2 |
| Commercial | 0.46 | 6.8 | Concrete | High density residential | 0.61 | 7 | 1 | 3 |
| | | | | Medium high density residential | 0.53 | 6 | 1 | 3 |
| | | | | Commercial | 0.39 | 7 | 3 | 3 |
| | | | | Enterprise/RD zone | 0.31 | 7 | 2 | 3 |

¹For energy usage: 1) residential, 2) office, 3) commercial, 4) Other.

²For roof materials: 1) metal roof, 2) clay roof and 3) concrete roof.

Appendix G

Validation results of WRF simulation at all weather stations in JB case study

Fig. G.1 shows the locations of the weather stations within the domain 3. As shown, there is only one weather station in JB while the other stations are located in Singapore. Table G.1 summarizes the validation results at Chango, Paya Lebar and Seletar weather stations.

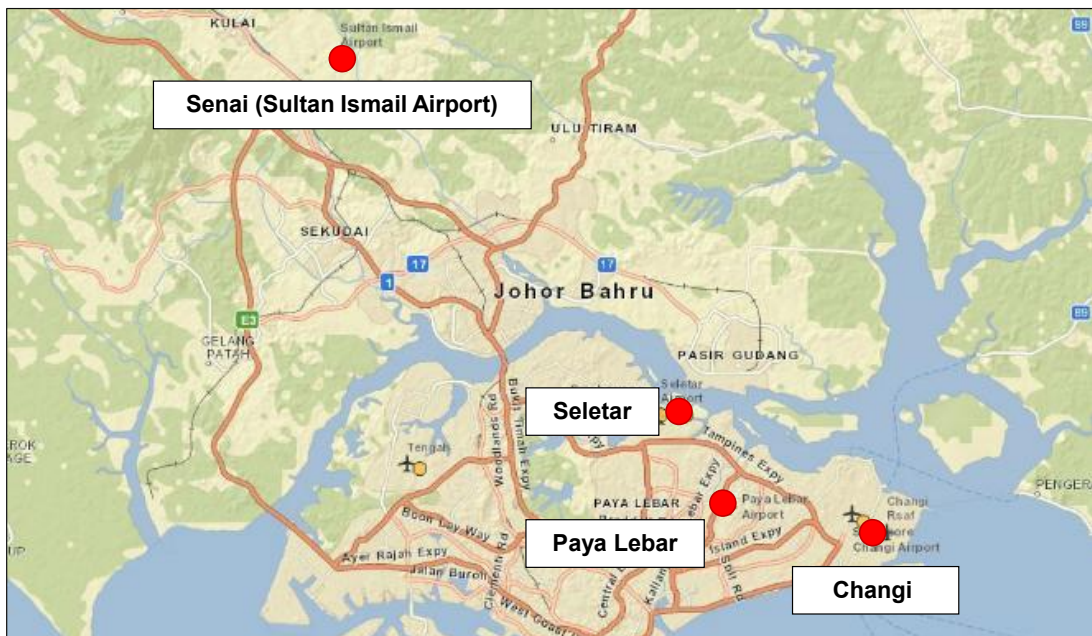


Fig. G.1 Locations of the weather stations in domain 3.

Table G.1 Summary of validation results at Changi, Paya Lebar, and Seletar weather stations.

| | Air temperature | | | Wind speed | | |
|------------|-----------------|------|-------|------------|------|------|
| | R | RMSE | Bias | R | RMSE | Bias |
| Changi | 0.74 | 2.74 | 0.15 | 0.29 | 3.31 | 1.31 |
| Paya Lebar | 0.64 | 3.89 | -1.00 | 0.33 | 2.99 | 0.92 |
| Seletar | 0.73 | 1.55 | 0.25 | 0.17 | 6.86 | 2.01 |

Validation results at Changi weather station

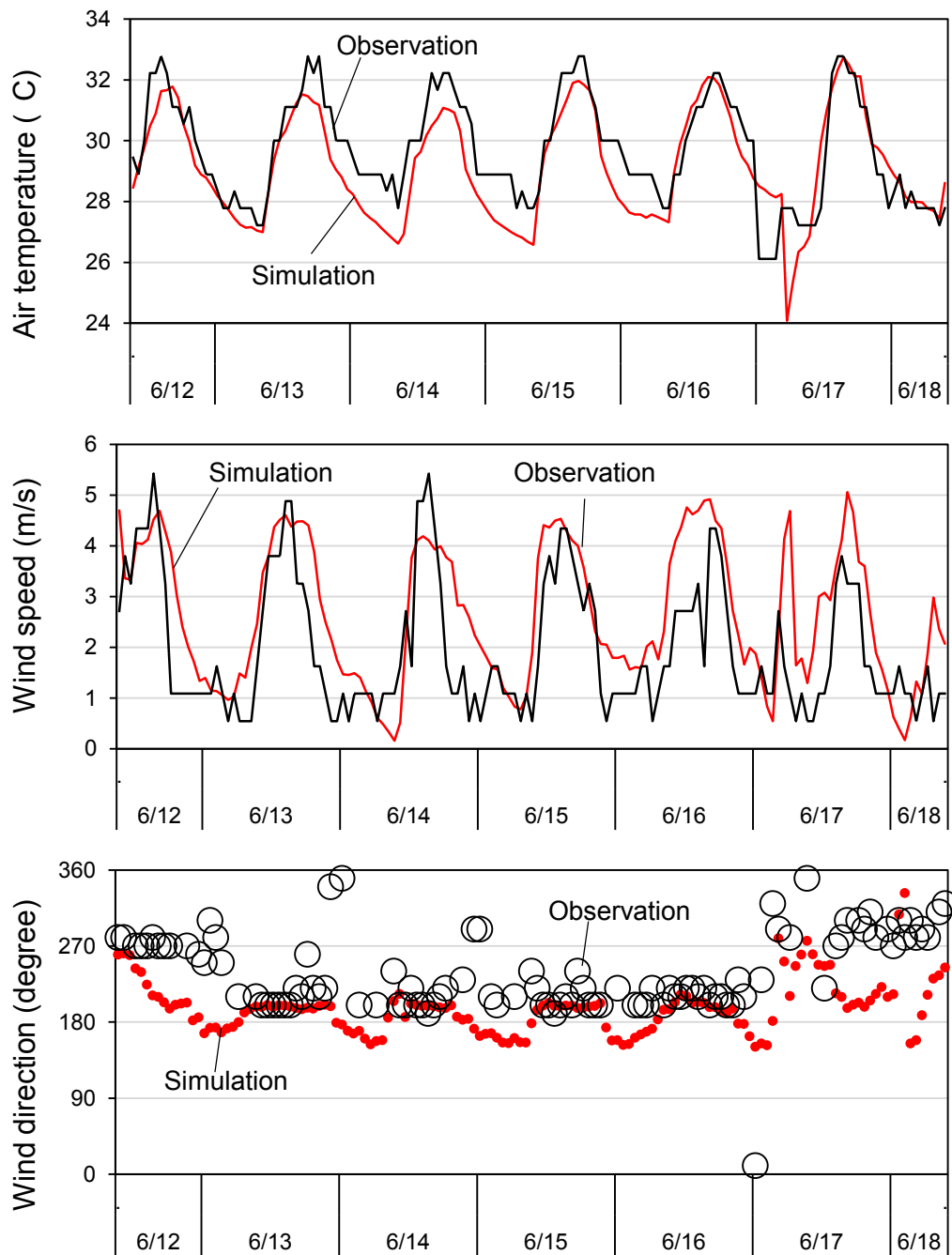


Fig. G.2 Comparisons between the observed and simulated air temperature at 2 m and wind conditions at 10 m above the ground at Changi weather station.

Validation results at Paya Lebar weather station

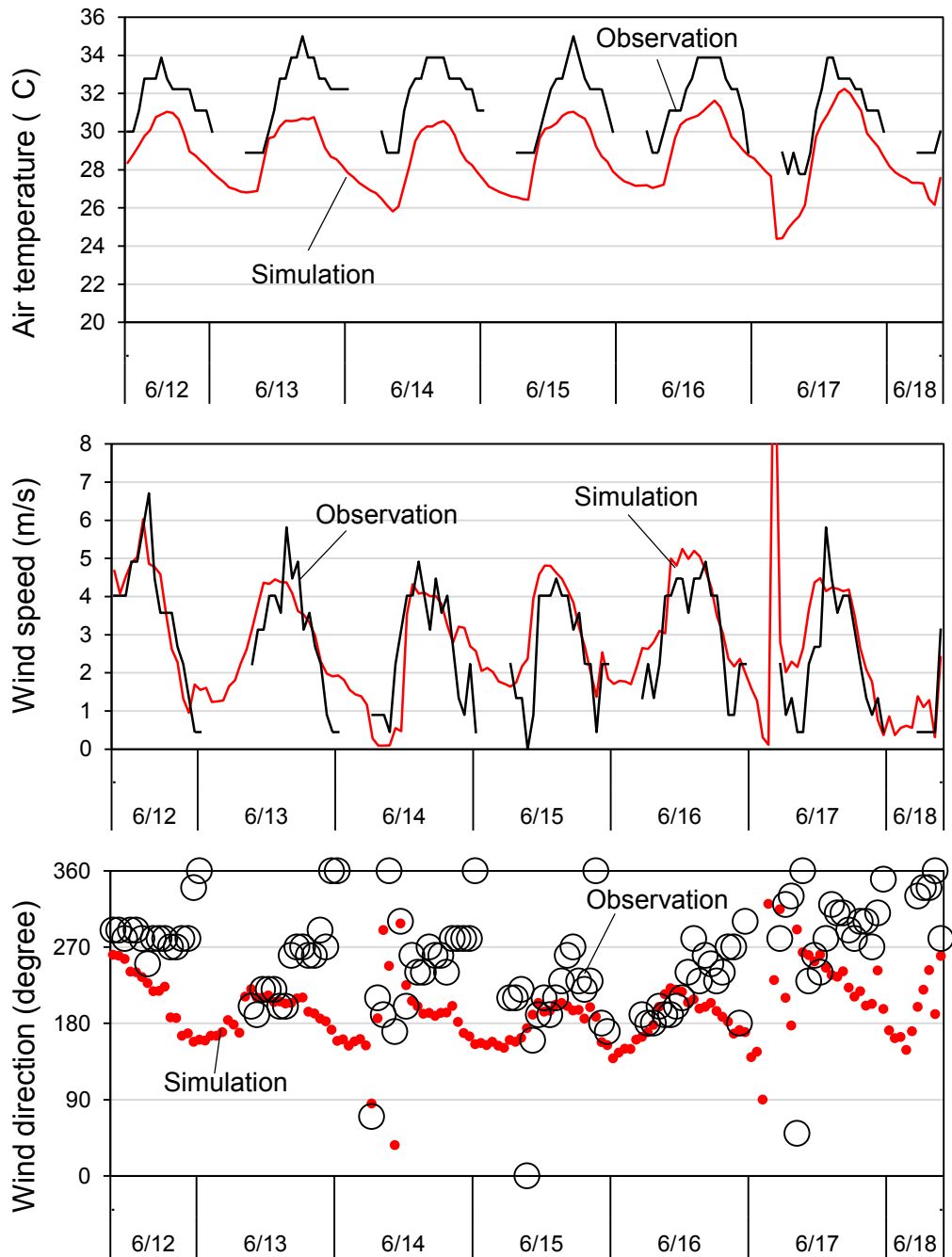


Fig. G.3 Comparisons between the observed and simulated air temperature at 2 m and wind conditions at 10 m above the ground at Paya Lebar weather station.

Validation results at Seletar weather station

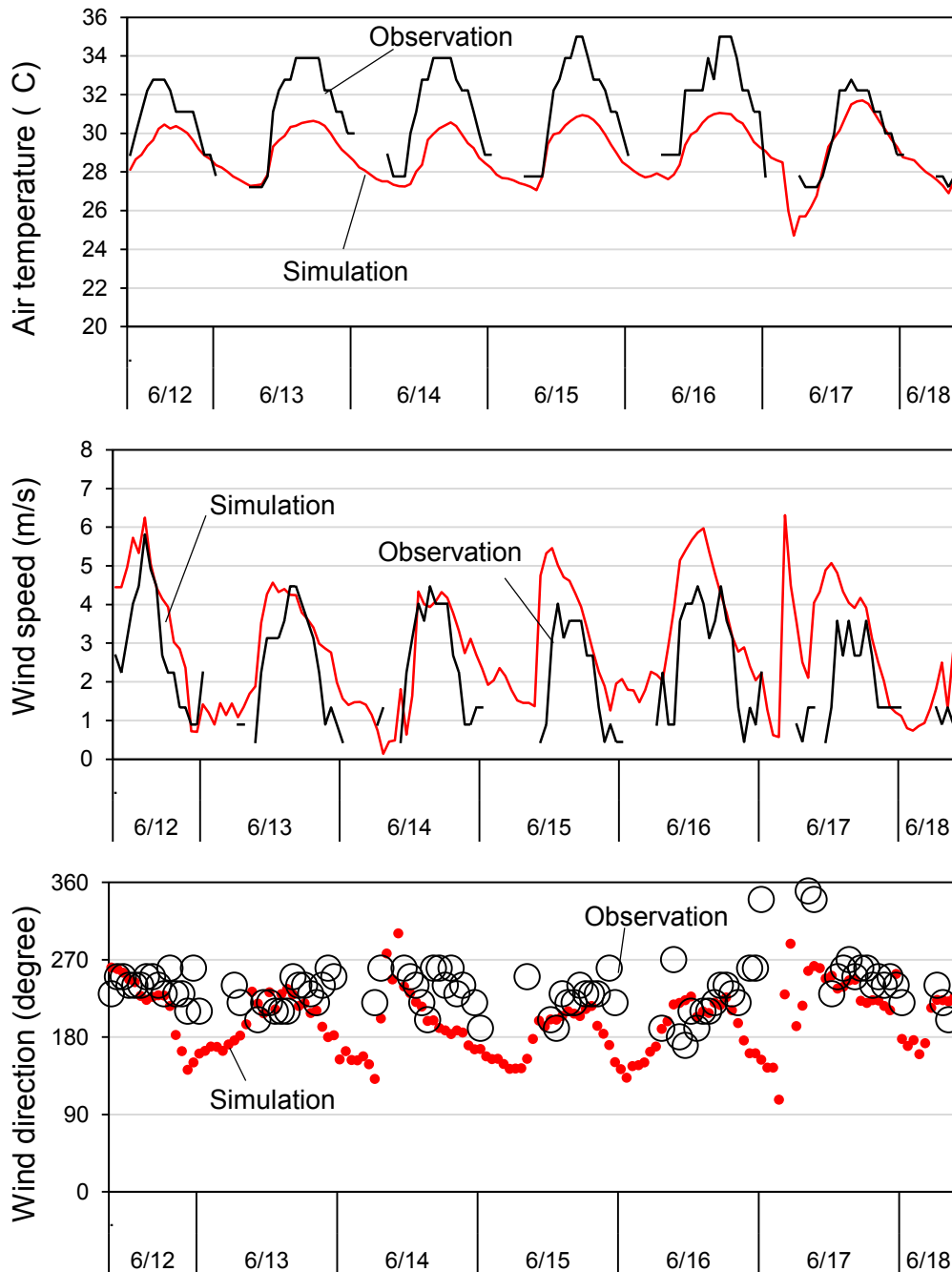


Fig. G.4 Comparisons between the observed and simulated air temperature at 2 m and wind conditions at 10 m above the ground at Seletar weather station.

Appendix H

Effects of monsoon winds on UHI in JB

Many previous studies showed that the sea breeze plays an important role to reduce the urban air temperature. However, JB is located about 20km away from the Southern coastal line of Singapore and therefore sea breeze is not expected to reach the city sufficiently even during the southwest monsoon season (Fig. H.1). As shown in Fig. H.1a, the southern part of Singapore received relatively cool sea breeze. After entering built-up areas, the air temperature gradually increased towards the north though it was decreased when passing through the Johor Strait. Meanwhile, in the case of northeast monsoon season, the northeasterly winds flowed from the palm plantation areas and brought cool air before entering the built-up areas (Fig. H.1b). The air temperature depicts a direct and linear response to the corresponding winds.

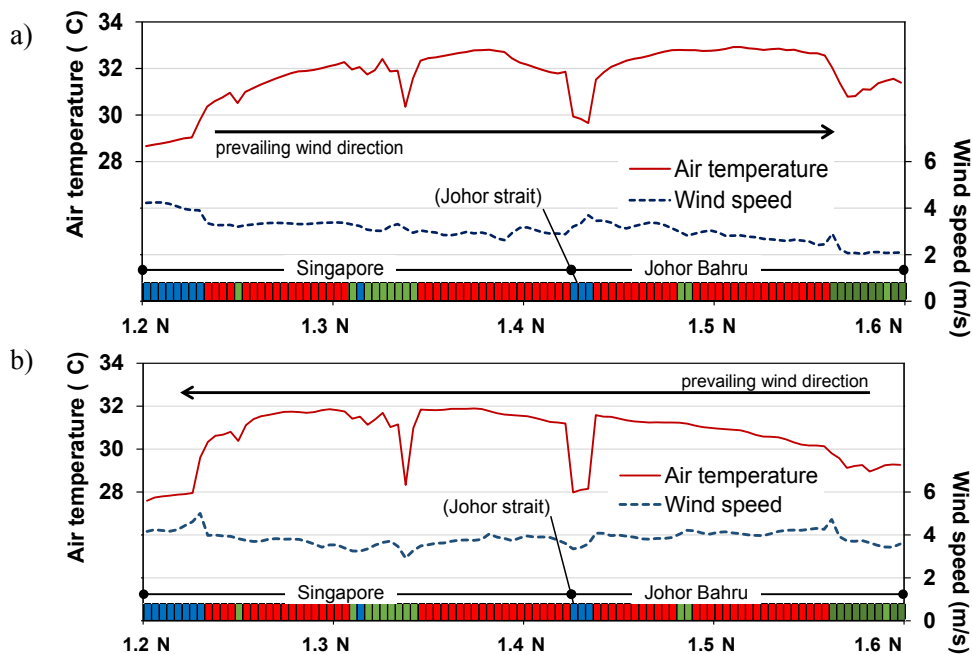


Fig. H.1 North-south cross section of the master plan condition for (a) southwest monsoon and (b) northeast monsoon at 15:00 (daytime). The horizontal color bar indicates the LULC of the master plan.

Appendix I

Creation process of the LULC datasets for WRF simulation with four domains configuration

To improve the accuracy of the simulation results, the default LULC datasets were replaced with an own-created dataset for domains 3 and 4. The detailed processes for creating LULC are provided herein.

Domain 3

The Global Land Cover by National Mapping Organizations (GLCNMO) data are used for domain 3. Fig. I.1a shows the original 30 arc-sec GLCNMO data with 20 land cover categories for domain 3, which is derived from MODIS images observed in 2003. A 16-day composite of 2003 is used for land cover classification. Then, the original GLCNMO data are converted over a 3-km mesh for domain 3 and its category is changed into USGS24 land cover categories by using ArcGIS (Fig. I.1b).

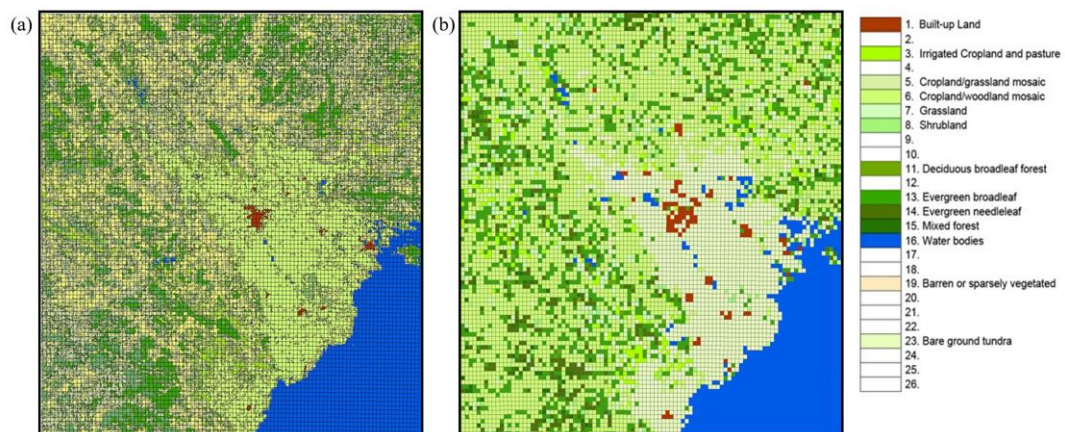


Fig. I.1 (a) The original GLCNMO LULC data and (b) converted 3-km resolution LULC data for domain 3.

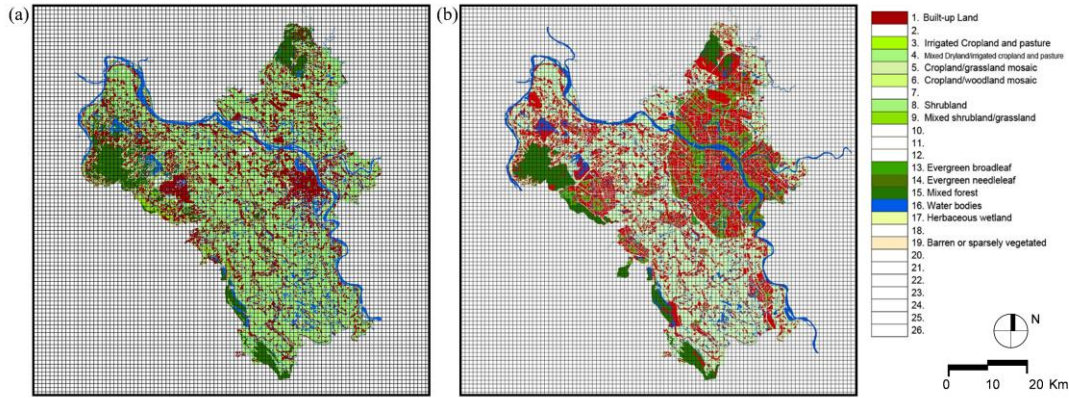


Fig. I.2 The original LULC datasets of (a) current status and (b) Hanoi Master Plan 2030 provided by VIAP.

Domain 4

Two datasets, namely digital current land use data from VIUP and ALOS satellite images, are used for domain 4, because the digital current land use covers only the Hanoi City. The original digital LULC data for the current situation and master plan condition from VIUP are presented in Fig. I.2. First, the land use categories of the digital VIUP data are converted into USGS24 land cover categories. Because the VIUP data are only available within the administrative boundary of Hanoi City, additional data from ALOS satellite images are used for the surrounding areas to cover the whole region for domain 4. ALOS is the land-observing satellite launched in January 2006 by the Japan Aerospace Exploration Agency (JAXA). ALOS has three earth-observing sensors such as the Panchromatic Remote-sensing Instrument for Stereo Mapping (PRISM) to detect elevations with high precision, Advanced Visible and Near Infrared Radiometer type 2 (AVNIR-2) for observing land coverage highly accurately, and Phased Array type L-band Synthetic Aperture Radar (PALSAR) for observing land areas during the day and night regardless of the atmospheric weather conditions.

As images from the AVNIR-2 sensors provide good spatial land-coverage maps and land use classification maps with 10-m spatial resolution and 70-km swath width at nadir, we use six images (Fig. I.3) that can fully cover domain 4 as indicated in Fig. I.4. All six of the images

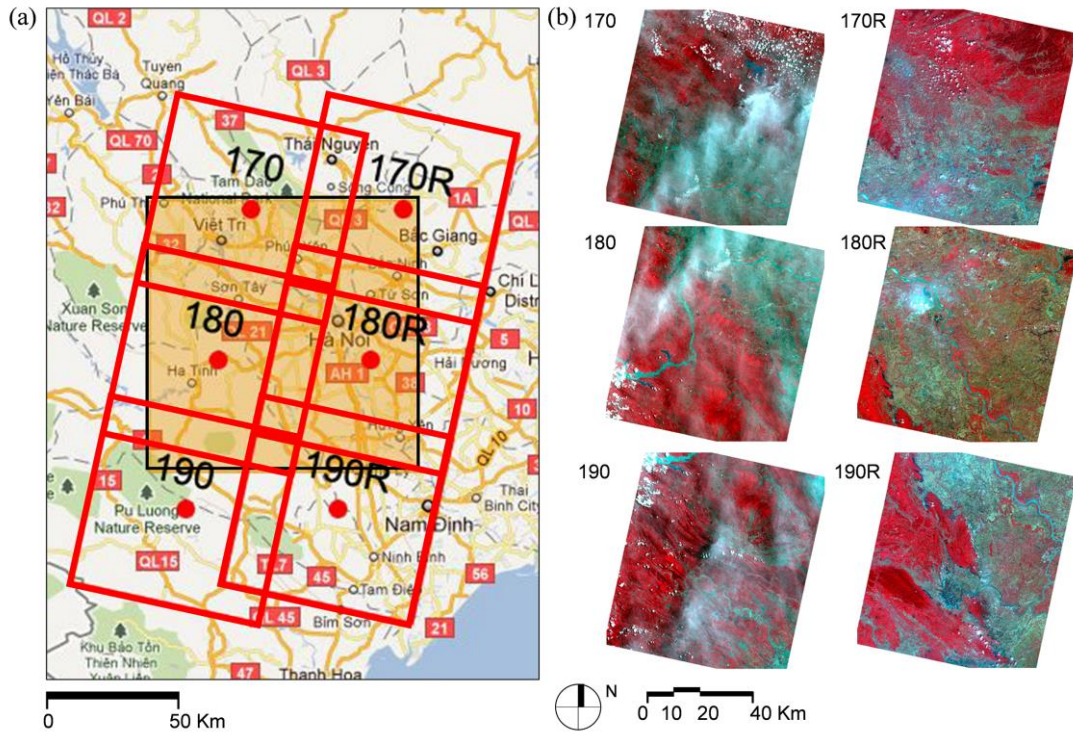


Fig. I.3 (a) Spatial coverage of six ALOS images and domain 4. (b) Six ALOS images used for covering the domain 4. Source: PASCO (<http://en-alos-pasco.com/alos/avnir/>).

were acquired in the same year but in different months (Fig. I.3a to I.3c in June 09, 2009 and Fig. I.3d to I.3f in October 08, 2009). All images have good data quality with a cloud coverage < 2%. One image has four multispectral bands, and the wavelengths of these bands are listed in Table I.1.

Table I.1. Multispectral bands of AVNIR-II

| Description | Band | Wavelength (micrometer) |
|---------------|------|-------------------------|
| Blue | 1 | 0.42 – 0.5 |
| Green | 2 | 0.52 – 0.6 |
| Red | 3 | 0.61 – 0.69 |
| Near-infrared | 4 | 0.76 – 0.89 |

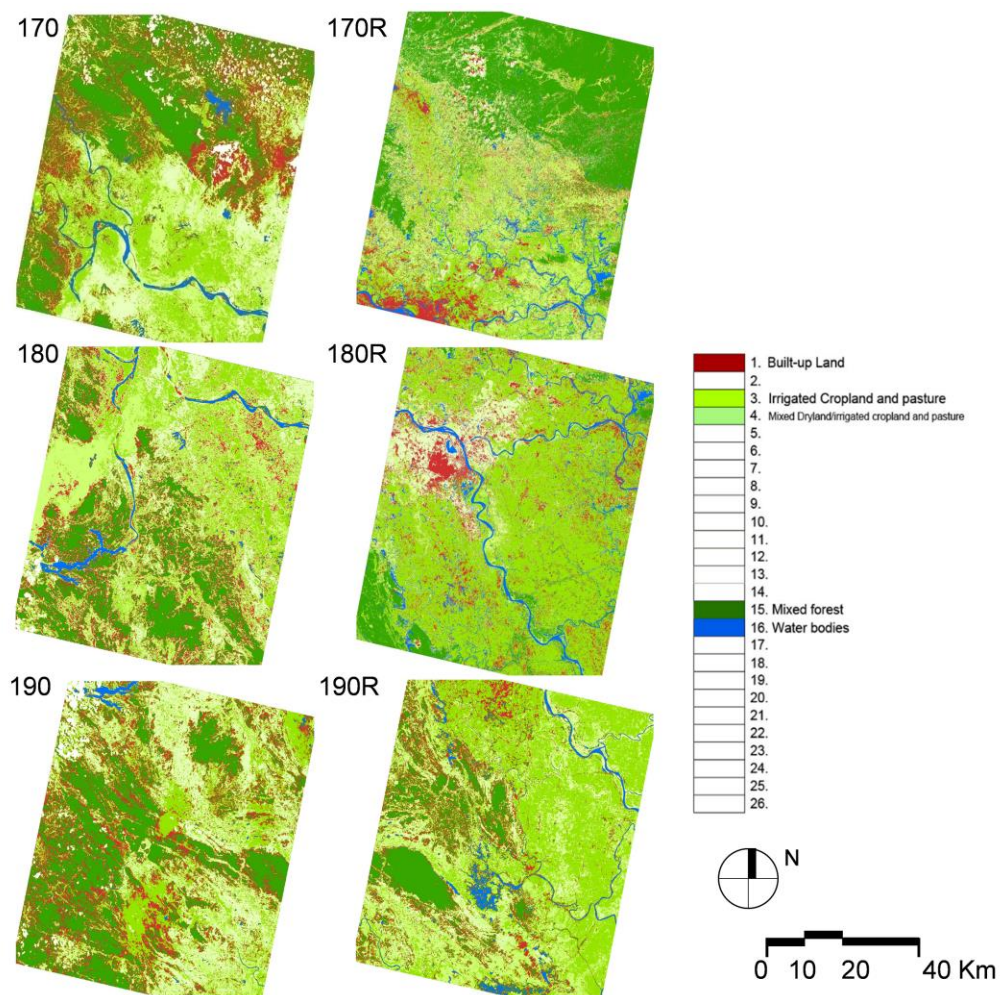


Fig. I.4 Detected land covers from six ALOS images.

To detect land cover from the ALOS images, all of the pixels of a digital image of one of several land cover classes are categorised using the MultiSpec tool. In this process, an unsupervised classification method is applied. Unsupervised classification is a method that examines a large number of unknown pixels and divides these pixels into a number of classes, based on the natural groupings presented in the image values. This method does not require analyst-specified training data. The basic premise of unsupervised classification is that the values within a given cover type should be close together in the measurement space, whereas data in different classes should be comparatively well separated (Eastman, 1995; Lillesand & Kiefer, 2000).

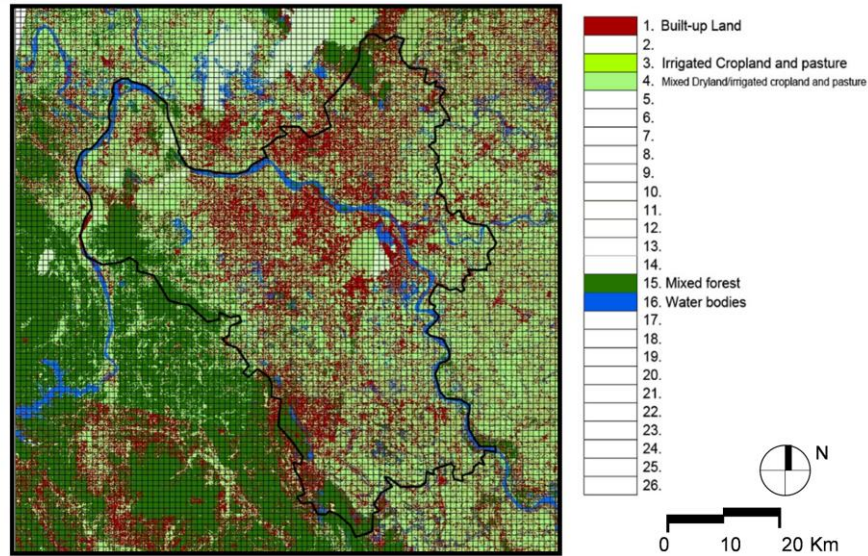


Fig. I.5 Land cover merged from the six detected land cover data in Fig. I.4.

In the process, the classes resulting from the unsupervised classification are spectral classes, which, based on the natural grouping of the image values, are compared to the digital land use data from VIUP and Google Maps to determine the identity and information value of the spectral classes. The final classes determined are water, mixed forest, built-up land, wet-cropland, dry-cropland and clouded area. The merged product of the detected LULC for the region of domain 4 is exhibited in Fig. I.5. The reliability and accuracy of the classification results are calculated by the MultiSpec tool and are shown in Table I.2.

Table I.2 Reliability and accuracy (%) of unsupervised classification results

| Land cover categories | Scene 170 | Scene 170R | Scene 180 | Scene 180R | Scene 190 | Scene 190R |
|---------------------------|-----------|------------|-----------|------------|-----------|------------|
| Water | 95.2 | 94.4 | 92.5 | 95.6 | 98.0 | 97.7 |
| Forest | 98.8 | 99.7 | 99.4 | 93.2 | 99.4 | 98.7 |
| Built-up areas | 79.9 | 70.7 | 76.7 | 88.9 | 38.6 | 62 |
| Wet-cropland | 62.6 | 82.0 | 69.9 | 68.1 | 69.5 | 79.6 |
| Dry-cropland | 66.4 | 42.5 | 77 | 66 | 49.9 | 58.3 |
| Overall class performance | 92 | 88.6 | 91.1 | 85.3 | 95.3 | 90.3 |
| Kappa Statistic | 89.1 | 83.8 | 86.7 | 81.8 | 89.7 | 84.0 |

The clouded areas were then replaced by values from GLCNMO data and VIUP data using ArcGIS. After overlaying ALOS data with VIUP data for current status (Fig. I.6a), all data were converted into 1-km resolution for simulations and to USGS24 categories (Fig. I.6b). The same process is also applied to the master plan condition within the Hanoi City administrative areas, whereas the surrounding areas are assumed to be the same as the current status (Fig. I.7).

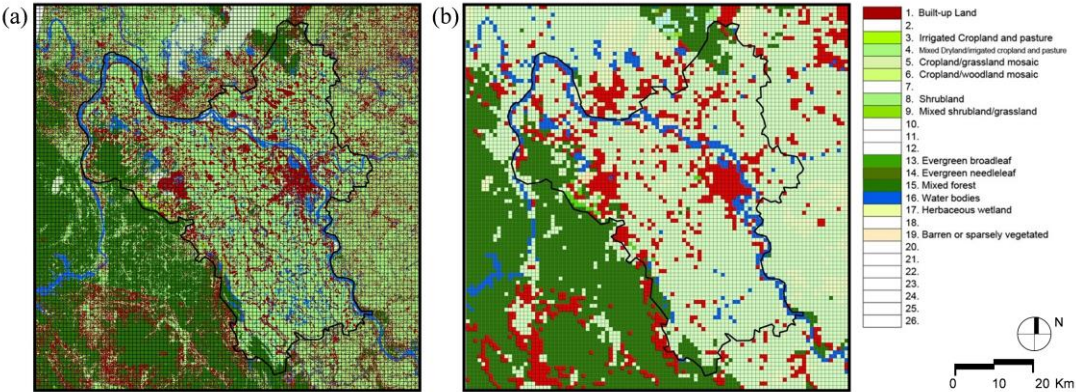


Fig. I.6 (a) Combined LULC product by using Fig. I.2a and Fig.I.5 and (b) final LULC product with 1-km spatial resolution used for current status in simulations.

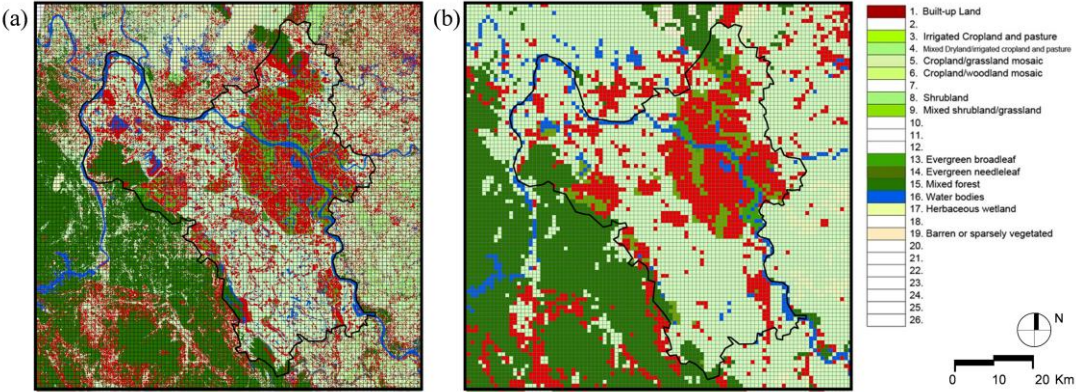


Fig. I.7. (a) Combined LULC product by using Fig. I.2(b) and Fig. I.5 and (b) final LULC product with 1-km spatial resolution used for the master plan condition (scenario 1) in simulations.

Appendix J

Surface parameters used in the simulations

Table J.1 Surface parameters used in the simulations.

| Land category | Albedo (-) | Moisture availability (-) | Emissivity (-) | Roughness length (cm) | Thermal inertia (kJ/m ² K s ^{0.5}) | Heat capacity (J/m ³ K) |
|-----------------------------------|---------------|---------------------------------|-------------------|-----------------------------|--|--|
| Urban and built-up land | 0.15 | 0.1 | 0.88 | 80 | 3 | 1.89×10^6 |
| Irrigated cropland and pasture | 0.18 | 0.5 | 0.985 | 10 | 4 | 2.50×10^6 |
| Mixed shrubland/grassland | 0.2 | 0.15 | 0.95 | 6 | 3 | 2.08×10^6 |
| Evergreen broadleaf forest | 0.12 | 0.5 | 0.95 | 50 | 5 | 2.92×10^6 |
| Mixed forest | 0.13 | 0.3 | 0.97 | 50 | 4 | 4.18×10^6 |
| Water bodies | 0.08 | 1 | 0.98 | 0.01 | 6 | 9.00×10^{25} |
| Barren or sparsely vegetated | 0.25 | 0.02 | 0.9 | 1 | 2 | 1.20×10^6 |

Appendix K

URBPARM.TBL

| Variable | Description | Unit | Current condition | | | 2025 BaU Scenario | | | 2025 CM Scenario | | |
|------------|--------------------------------|-----------------------------------|------------------------|-----------------------|------------------------|------------------------|-----------------------|------------------------|------------------------|-----------------------|------------------------|
| | | | Industrial | Residential | Commercial | Industrial | Residential | Commercial | Industrial | Residential | Commercial |
| ZR | Roof height | m | 8 | 8 | 10 | 8 | 8 | 10 | 8 | 8 | 10 |
| ROOF_WIDTH | - | m | 10 | 8 | 10 | 10 | 8 | 10 | 10 | 8 | 10 |
| ROAD_WIDTH | - | m | 10 | 10 | 10 | 10 | 10 | 10 | 10 | 10 | 10 |
| AH | Anthropogenic Heat | W m ⁻² | 180 | 31 | 116 | 240 | 70 | 113 | 123 | 36 | 75 |
| FRC_URB | - | - | 0.5 | 0.3 | 0.4 | 0.5 | 0.3 | 0.4 | 0.5 | 0.3 | 0.4 |
| CAPR | Heat capacity of roof | J m ⁻³ K ⁻¹ | 3.5 x 10 ⁶ | 1.5 x 10 ⁶ | 1.75 x 10 ⁶ | 3.5 x 10 ⁶ | 1.5 x 10 ⁶ | 1.75 x 10 ⁶ | 3.5 x 10 ⁶ | 1.5 x 10 ⁶ | 1.75 x 10 ⁶ |
| CAPB | Heat capacity of wall | J m ⁻³ K ⁻¹ | 1.75 x 10 ⁶ | 1.5 x 10 ⁶ | 1.75 x 10 ⁶ | 1.75 x 10 ⁶ | 1.5 x 10 ⁶ | 1.75 x 10 ⁶ | 1.75 x 10 ⁶ | 1.5 x 10 ⁶ | 1.75 x 10 ⁶ |
| CAPG | Heat capacity of ground | J m ⁻³ K ⁻¹ | 1.6 x 10 ⁶ | 1.6 x 10 ⁶ | 1.6 x 10 ⁶ | 1.6 x 10 ⁶ | 1.6 x 10 ⁶ | 1.6 x 10 ⁶ | 1.6 x 10 ⁶ | 1.6 x 10 ⁶ | 1.6 x 10 ⁶ |
| AKSR | Thermal conductivity of roof | J m ⁻¹ s ⁻¹ | 30 | 1 | 1.3 | 30 | 1 | 1.3 | 30 | 1 | 1.3 |
| AKSB | Thermal conductivity of wall | J m ⁻¹ s ⁻¹ | 1.3 | 0.8 | 1.3 | 1.3 | 0.8 | 1.3 | 1.3 | 0.8 | 1.3 |
| AKSG | Thermal conductivity of ground | J m ⁻¹ s ⁻¹ | 0.7 | 0.7 | 0.7 | 0.7 | 0.7 | 0.7 | 0.7 | 0.7 | 0.7 |
| ALBR | Albedo of roof | - | 0.8 | 0.3 | 0.65 | 0.8 | 0.3 | 0.65 | 0.8 | 0.3 | 0.65 |
| ALBB | Albedo of wall | - | 0.6 | 0.6 | 0.6 | 0.6 | 0.6 | 0.6 | 0.6 | 0.6 | 0.6 |
| ALBG | Albedo of ground | - | 0.2 | 0.2 | 0.2 | 0.2 | 0.2 | 0.2 | 0.2 | 0.2 | 0.2 |
| EPSR | Surface emissivity of roof | - | 0.3 | 0.9 | 0.9 | 0.3 | 0.9 | 0.9 | 0.9 | 0.9 | 0.9 |
| EPSB | Surface emissivity of wall | - | 0.9 | 0.9 | 0.9 | 0.9 | 0.9 | 0.9 | 0.9 | 0.9 | 0.9 |
| EPSG | Surface emissivity of ground | - | 0.95 | 0.95 | 0.95 | 0.95 | 0.95 | 0.95 | 0.95 | 0.95 | 0.95 |

Appendix L

Development of biomass-based ecotourism in Kita-Hiroshima, Japan

Prepared by:

Andhang R. Trihamdani, David P. Barbosa, Mattana Tunchai, and Nattacha Paksung

1. Background of the project

In Japan, the rural areas are experiencing problem of depopulation, aging farmers and stagnant income growth. Those make the Japanese agriculture at the critical point. Meanwhile, the traditional view of rural areas as the source of agricultural product is still predominant at this moment. However, with the liberalization of world open trade of agricultural products, a new and different understanding of rural areas should be strongly considered.

Several comprehensive development plan have been implemented by Japanese government to fight rural depopulation. However, persuading people to reside in rural areas is not an easy task. As the alternative solution, Japanese government is looking at the importance of urban-rural exchange. One typical example is rural tourism in depopulating areas (Asamizu, 2012).

Ecotourism is one of the most advocated concepts in tourism studies (Cobbinah, 2015). The concept of ecotourism is often interpreted in Japan as a tool for local community development that utilizes various local resources. An even broader view of ecotourism would also consider environmental education and 'cultural exchange' between urban dwellers and rural communities. (Japan Ecotourism Center, 2016).

What the rural people think is uninteresting can be amazing attraction for visitor from outside. Far from boring, the rural areas is full of wonderful things that can never be experienced in the cities. Therefore, in order to attract more visitors, ecotourism activity should be promoted and the attraction should be further diversified. This TAOYAKA Onsite Team project aims to discover the potential of the site that can be promoted as the ecotourism activity at one rural area in Japan and makes propose recommendation for the future.

About the study area of Kita-Hiroshima Town

The Onsite Team Project is developed in Kita-Hiroshima Town, Hiroshima Prefecture, Japan. It has an area of 646.24 km² and situated in the mountainous area in the north western part of Hiroshima Prefecture (see Figure 1). Kitahiroshima was formed on February 1, 2005 from the merger of the towns of Chiyoda, Geihoku, Ōasa and Toyohira, all from Yamagata District.



Fig. L1 Location of Kita-Hiroshima town in Hiroshima Prefecture (indicated by red color).

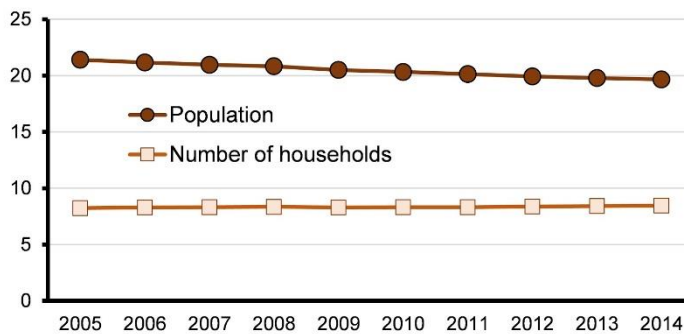


Fig. L2 Population and number of households in Kita-Hiroshima town
Source: Kita-Hiroshima town office.

Kita-Hiroshima has a population of 19,566 people in 2015 (a March, 2015), while the number of households is 8,474 households. Over the last 10 years, the population has been continuing to decline (see Figure 2). The population density is 30.9 people per 1 km² (Hiroshima average is 337.4/km²). Moreover, the statistical data surveyed in 2014 showed that over a decade, the youth and the working age groups are on the decline while the elderly population is on the rise. This shows that the declining birth and the aging society are on progress in this town.

The main agricultural product of Kita-Hiroshima is rice. Its production shares more than half of the total agricultural products in the area. Kita-Hiroshima town is also one of top vegetable producer. The largest vegetable product is tomato, thus makes the town becomes one of the top tomato producer in Hiroshima’s regions.

Moreover, the number of farmers shows a declining trend over the last decade. In 2005, the number of farmers was 2200 units, while the number was reduced to 1784 units in 2015. This trend is expected to continue in the future because the number of secondary industry (e.g. manufacturing industry) is now growing rapidly in the region.

Problem findings by the TAOYAKA Onsite Team

Firstly, a team consists of four students conducted several fieldtrips to the site. As a part of the fieldtrips, the team conducted homestays in one farmer's house in Chiyoda, Kita-Hiroshima. During the homestay, they got involved in the farming activities. They also involved in the activities held by the local non-profit organization called INE OASA. Further, they did interviews with people who are running businesses in the area. Through those activities, they could learn about the daily life in the target area. In the same time, they also got chances to listen to the need of the people, understanding their condition and the most important, is to build a trust between the team with the local people they will collaborate with.

Secondly, the fieldtrips put the focus on the tourism activity in Kita-Hiroshima. Observations on the potential sightseeing spots and some local festivals which are held in Oasa and Chiyoda area were conducted.

The findings from the observation are as follows:

1. Small scale farmers cannot depend on the income from agriculture only. In other words, they are basically not a full-time farmer. Most of them do another job for living.
2. The residues from tomatoes are gone to waste. Less of them are utilized for composting or energy production.
3. There are still lack of options for tourism activity in summer, especially for sport tourism. Whereas Kita-Hiroshima is very rich in natural and cultural heritage.
4. Tomato is the largest vegetable product in Kita-Hiroshima. However, we rarely found the unique tomato-based product (i.e. added value product) from this area.

The findings led to these following research questions:

1. Can the production of agricultural product be increased? So that farmers could get additional income?
2. How much income can be generated by selling the added value product based on tomato?
3. How much energy can be produced by converting the tomato residue into renewable energy (e.g. biofuel)?
4. What kind of sport tourism that could be a good option in summer, that make use of the resources in Kita-Hiroshima?

This project aims to conduct a pilot study in the town of Oasa and Chiyoda, Kita-Hiroshima, Japan. In order to answer the research question mentioned previously, six main objectives were designed. Then, the objectives are followed with some specific activities in order to achieve the goal. The main objectives of the project are as follow;

1. To increase the production of greenhouse tomatoes.

2. To develop a renewable energy production by using of the residue from tomato production.
3. To introduce a new business model (biomass eco-tour, tomato harvesting festival, tomato based product) with less impact to the environment.
4. To invite more people to reside in the area
5. To make the place more attractive to the tourists by making use of strategies for ecotourism, sports and cultural tourism.
6. To analyze the factibility of tomato crops as a key element to boost a sixth-industry in Kita-Hiroshima

2. Project activities

This project is divided into two main activities. They are tomato related activity and cycling related activity. Both activities have their own more specific activities in order to achieve the objectives of this project.

As shown in Figure 3, the tomato related activity consists of tomato cultivation, elaboration and product development of dried tomato product, experiments of energy production, and life cycle and energy analysis. While the cycling related activity is about surveying the routes for cycling tour and the preparation of cycling map. There are four major events that involved a large number of people. They are sensory test survey, market survey, dried tomato workshop, and cycling tour.

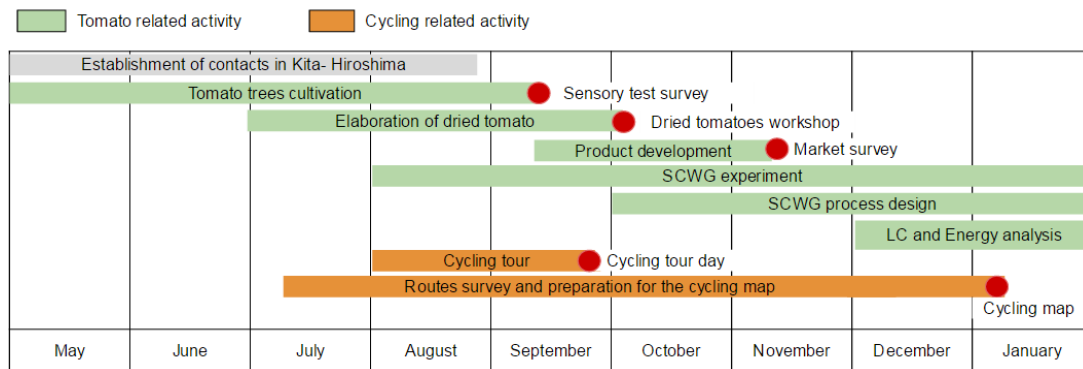


Fig. L3. Timeline of the project

2.1 Tomato related activities

Tomato was chosen as the main theme of this project based on these following considerations:

1. Tomato is the largest vegetable product in Kita-Hiroshima. However, we rarely found the special tomato-based product from this area.
2. Since the are of tomato planting is large, we would like to make use of the area not only for producing food, but also energy.
3. Tomato and biomass energy production suit with on-going research of our team members.

2.1.1 Biomass energy production

To convert tomato residue into useful secondary energy, supercritical water gasification (SCWG) is considered as a proper technology. SCWG is a technology that is suitable to convert wet biomass into hydrogen-rich gas because water is the reaction medium, and thus drying process is not necessary. Furthermore, water is safe, non-toxic and cheap. Hence, tomato residue in this area can be considered a good feedstock for implementing the SCWG.

In this section, process design for SCWG of tomato residue in Kita-Hiroshima town was evaluated. The procedure includes:

1. SCWG process design
2. Evaluation of SCWG of tomato residue in Kita-Hiroshima

SCWG process design

The SCWG process consists mainly of liquefier, pump, heat exchanger, carbon dioxide absorber and gas/liquid separator as shown in Figure 4. The feedstock slurry is fed at room temperature of 25 °C and heated to 200 °C in terms of liquefaction process. It is cooled to 25 °C again to avoid damage of a pump using to send the solution into high pressure state of 25 MPa. The feed is then heated to 600 °C before entering the reactor and after the reaction product flows out of the reactor

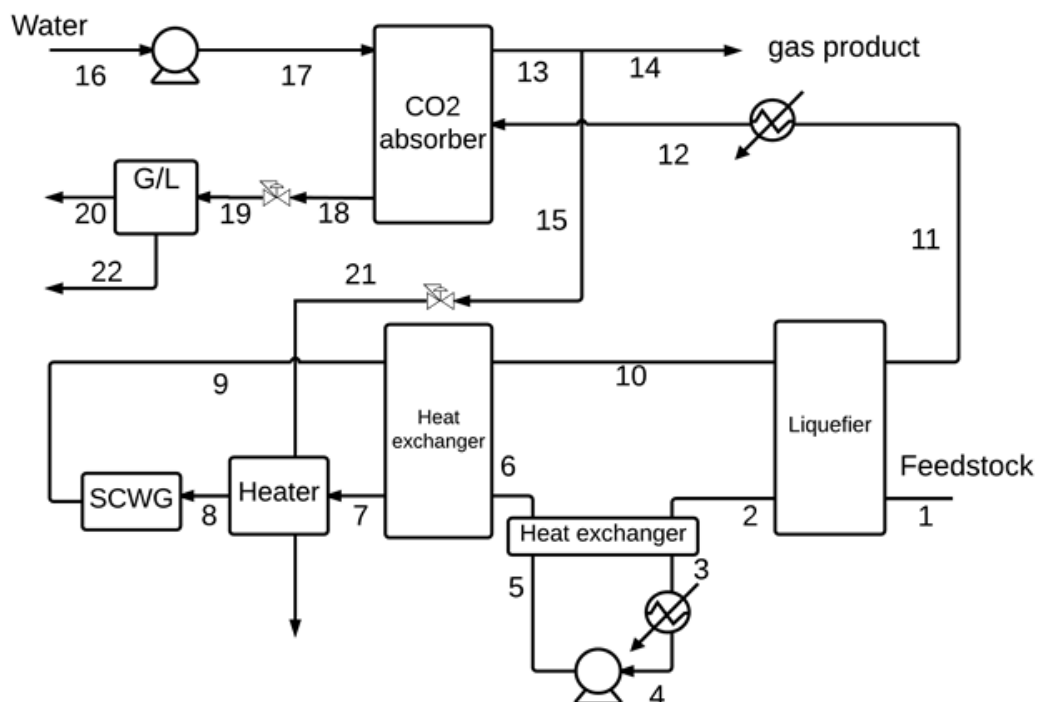


Fig. L.4 Process flow diagram of SCWG

and the flow is cooled to 25 °C. Setting minimum temperature difference for heat transfer at 10 °C and heat exchanger efficiency is 75%. After the product of the reaction is cooled down, CO₂ was absorbed out from the gas product. Assuming that no CO₂ remaining in the gas product, the heating value of the final gas product is 17,215 kJ/Nm³. The product gas is partially combusted for heating the heater and supply heat to SCWG reactor to keep the process isothermal. That is 48% of product gas is to be combusted to supply the additional heat. Therefore, the total energy produced in 1 mole basis of tomato residue is 506.1 kJ/mol or 2.31 MJ/kg tomato residue.

Evaluation of SCWG of tomato residue in Kita-Hiroshima

In this section, we compared different three cases of utilization of energy produced from SCWG of tomato residue in Kita-Hiroshima.

Case 1: current production

Currently, potential of tomato production in Kita-Hiroshima area is 705 t/y in a crop area of 16 ha. Tomato can be planted seasonally during April to September (period of 6 months). The assumptions for the evaluation are in the followings:

- Initial cost, transportation and labor cost are not taken into account.
- For 1 tomato tree, 5 kg (wet weight) of tomato residue is left.
- Moisture of tomato residue is averagely 88.29 %
- Heat is converted to electricity by gas engine, whose efficiency is 30 %.
- Electricity costs around 20 yen/kWh
- 0.05 kg of CO₂ is emitted per 1 MJ of electricity produced by natural gas

From the assumption, tomato residue is available in Kita-Hiroshima town for SCWG approximately 82.6 t (dry weight). The gas product from SCWG of tomato residue gives HHV of 2.31 MJ/kg of feedstock, which is in total 200 GJ. Assuming heat is converted to electricity by gas engine, whose efficiency is 30 %, the electricity production is finally 60 GJ or 17 MWh, which is convertible to 340,000 yen.

To consider how much carbon dioxide emission can be reduced by substitution of electricity produced by natural gas, 0.05 kg of carbon dioxide is assumed to be emitted for every 1 MJ of electricity produced, while carbon dioxide emission is considerably zero when biomass is energy resource due to its carbon neutral feature. In conclusion, 3 t carbon dioxide is reduced by using biomass conversion. The flow of case 1 is as shown in Figure 5.



Fig. L.5 Process flow of case 1

Case 2: A whole year production

Instead of converting gas product into electricity by gas engine, gas is burned in gas-fired boiler (80% efficiency) to heat up hot water on a purpose of maintaining temperature in the greenhouse at 25 °C. Supplied heat required is different depending on air temperature of each season. The supplied heat is supposed to the heat loss from the greenhouse to the atmosphere. For gas-fired boiler, whose efficiency is 80 %, 160 GJ is provide to heat greenhouse. Therefore, 2 houses can be supplied (see Appendix D). The production in one greenhouse is 0.141 t thus makes 0.3 t increase when greenhouses are utilized.

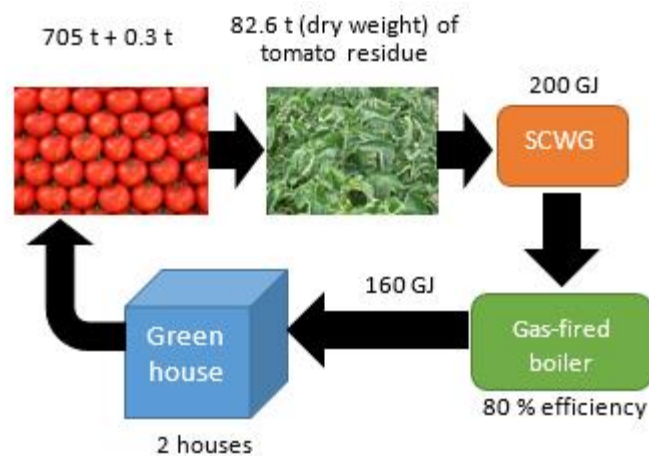


Fig. L.6 Process flow of case 2.

Case 3: A whole year production including dried tomato production

In the case that gas product from SCWG of tomato residue is utilized for heating in dried tomato cooking process, heat that is required for cooking 70 t, which is 10 % of the whole production of tomato is 24 GJ (see Appendix D).

The remaining energy is utilized for heating greenhouse and heat losses for each month. Remaining 141 GJ can supply 1.7 houses. The production in one greenhouse is 0.141 t thus makes 0.2 t increase in tomato production.

Considering economical perspective, cash flow was determined and is shown in Figure 8. Income after the project is implemented in the target area comes from three parts including fresh tomato, dried tomato as a value-added product and electricity produced as a final energy from tomato residue. The whole production of tomato is 705.2 t/y.

According to statistical data from Kita-Hiroshima town database, selling price of tomato in the market is 530 yen/kg. The production costs include of logistic cost and commission (31%) and planting cost (43%), thus make profit of 26%. Therefore the profit from 1 kg of tomato is 137.8 yen. 90% of the whole production, which is 635.2 t, is sold to the market so in total 87.5 million yen is the total profit from fresh tomato.

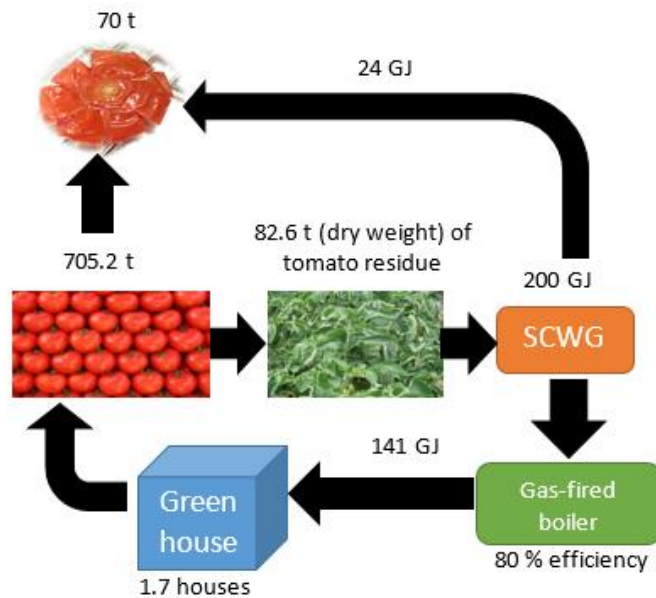


Fig. L.7 Process flow of case 3.

For value added product, which is dried tomato, 10% of the whole tomato production is to be used for material to produce dried tomato. Heat for cooking is obtained from fuel gas from SCWG of tomato residue, so that no additional heat energy required from outside the process boundary. 0.28 kg of sugar, which costs 70 yen is necessary for 1 kg of tomato to make 60 pieces of dried tomato. One pack of dried tomato contains 6 pieces and is sold at the price of 250 yen, thus make 10 packs sold at 2500 yen per 1 kg tomato. Assuming packing cost is 35 yen and commission fee is 10% (25 yen). The cost for planting tomato 228 yen. Therefore, a profit from 1 kg tomato is $2500 - 70 - (35 + 25) \times 10 - 228 = 1602$ yen or 160.2 yen per package. In total, 0.7 million packages are to be sold and 112 million yen is total profit from dried tomato.

2.1.2 Added value product: Dried tomato

In order to maintain and expand demand for domestically produced vegetables, domestic production for processing and manufacturing uses should be promoted. Therefore, we conducted the activities to promote the greater value-added product based on tomato. They are many choice of available value-added products of tomato such as ketchup, tomato juice, ice cream, candy, tomato ramen and dried-tomato. We choose dried-tomato due to the main reason as follow;

1. No need such sophisticated facility, a normal kitchen will do for the production
2. Long-storage life product (without preservation)
3. Light-weight product that will reduce the transportation cost

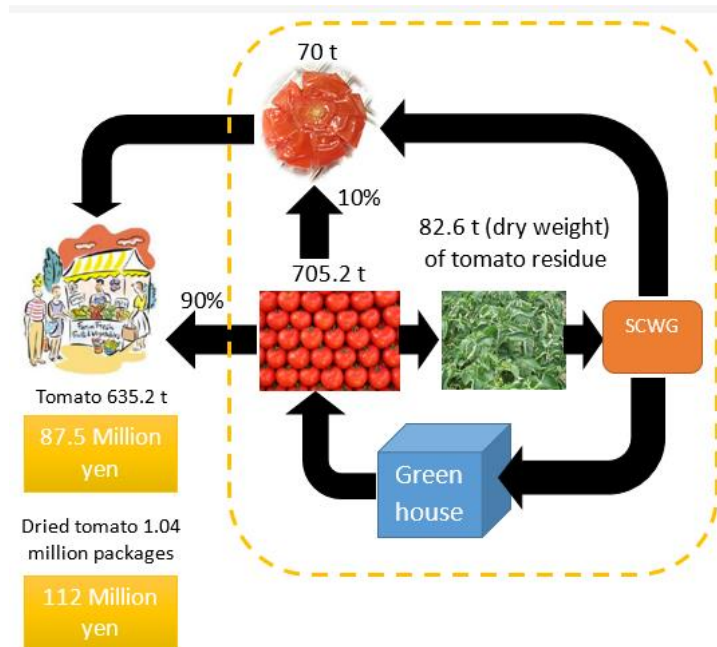


Fig. L.8 Cash flow of tomato related activities.

General consumer awareness of dried fruits still remains low because tomatoes are traditionally used as food ingredients. However, the high nutritional value of dried fruits such as dietary fiber and abundant vitamins, has started to be recognized, and a health food image has started to form as the health-consciousness and beauty interests of consumers increase. Popularity is expected to increase and demand is expected to expand (Ministry of Finance trade statistics).

Dried-tomato activities flow were conducted as follow;

1) Tomato planting

On early June 2015, during homestay activity at Makura's farm, which is located in Chiyoda area, Kita-Hiroshima town, we had learned about tomato cultivation.

2) Harvesting

Tomato can be harvested from early July until October, but the high production period is July to August.

3) Product development

We used open home-made recipe of dried-tomato from Thai website (www.KimLeng.net) as reference recipe.



Fig. L.9 Photo of our dried-tomato product using modified recipe.

After that the storage-life of the product was studied. Dried-tomatoes were kept in ordinary plastic box (without any silica gel or oxygen absorber) and had been check on its condition every day and taste it every week. The storage-life result was varied on the production batch from 3 to 6 months. All batch products could be kept up to 3 months without any fungi or bacterial infection in our storage condition. I am positive that with the good packaging, such as seal plastic bag and oxygen absorber, will result to prolong storage-life of this product.

4) Sensory test survey

Starting from September 18th, we conducted a sensory test survey of our dried-tomato product on consumer. The objective of this survey is to test consumer acceptable on physical, chemical and sensorial characteristics as well as the potential of our product for commercial scale production. This type of studies are essential for food industry during the product development stage which allow them to be able to determine the potential market for a certain product, to optimize processes, assess new ingredients and technologies as well as to decide whether or not to launch a product in the market (Lawless & Heymann, 1998).

The survey was conducted in Hiroshima University, Higashi-Hiroshima campus. Due to our target consumer is typical Japanese people, this tests used Japanese panelists who have not been trained to participate in this studies and who normally consume or use food products. So, we could assessed the response to a product, a product idea or feature from real or potential consumers. We decided the questionnaire to test the preference of our dried-tomato product comparing with Daiso dried-tomato (Figure 11), which is only one available commercial brand sale nationwide. To avoid the bias, we did the blind test without reveal source or name of both products and referred the products by color different of food cup containers. By asking panelists acceptance on appearance, color, aroma, sweetness, flavor, chewing texture, and total likeness used 9-point hedonic scales on both products, our and Daiso, we could gain consumer acceptance and preference information. Besides, we also asked purchase intent of our and Daiso product using 5-point hedonic scales. We did the test to both genders and various age groups panelists including professors, staffs and students. Japanese version questionnaire were distributed with our product (referred as foil-cup) and Daiso product (referred as color cup).



Fig. L.10 Daiso's dried-tomato product

ID:

Sensory evaluation of Dried-tomatoes

**Make a circle in the appropriate answer.*

Gender : Male Female
 Age : <14 15-24 25-34 35-44 45-54 55-64 >65
 Nationality : Japanese Non-Japanese

Instruction:

If possible, please take a sip of water before starting.
 You have just received 2 dried-tomato samples, each in the color-cup and foil- cup.
 Please take a look at the appearance and smell the samples before trying it.
 Please try the two samples, starting from the sample in the color-cup to the one in the foil-cup.

| Scale | |
|-------|--|
| 9 | – I liked it very much |
| 8 | – I like it a lot |
| 7 | – I like it moderately |
| 6 | – I liked it slightly |
| 5 | – I didn't like it/I didn't dislike it |
| 4 | – I didn't like it slightly |
| 3 | – I didn't like it moderately |
| 2 | – I didn't like it very much |
| 1 | – I didn't like it at all |

Rating your preference on the scale of 1 to 9, each scale meaning is described in the box on the right.
 Make a circle in the scale that matches what you think about the dried-tomato.

Your rating (1 to 9)

| Color-cup | | | | | | | | | |
|-----------------|---|---|---|---|---|---|---|---|---|
| Appearance | 1 | 2 | 3 | 4 | 5 | 6 | 7 | 8 | 9 |
| Color | 1 | 2 | 3 | 4 | 5 | 6 | 7 | 8 | 9 |
| Aroma | 1 | 2 | 3 | 4 | 5 | 6 | 7 | 8 | 9 |
| Sweetness | 1 | 2 | 3 | 4 | 5 | 6 | 7 | 8 | 9 |
| Flavor (total) | 1 | 2 | 3 | 4 | 5 | 6 | 7 | 8 | 9 |
| Chewing texture | 1 | 2 | 3 | 4 | 5 | 6 | 7 | 8 | 9 |
| Total likeness | 1 | 2 | 3 | 4 | 5 | 6 | 7 | 8 | 9 |

| Foil-cup | | | | | | | | | |
|-----------------|---|---|---|---|---|---|---|---|---|
| Appearance | 1 | 2 | 3 | 4 | 5 | 6 | 7 | 8 | 9 |
| Color | 1 | 2 | 3 | 4 | 5 | 6 | 7 | 8 | 9 |
| Aroma | 1 | 2 | 3 | 4 | 5 | 6 | 7 | 8 | 9 |
| Sweetness | 1 | 2 | 3 | 4 | 5 | 6 | 7 | 8 | 9 |
| Flavor (total) | 1 | 2 | 3 | 4 | 5 | 6 | 7 | 8 | 9 |
| Chewing texture | 1 | 2 | 3 | 4 | 5 | 6 | 7 | 8 | 9 |
| Total likeness | 1 | 2 | 3 | 4 | 5 | 6 | 7 | 8 | 9 |

Purchase intent

Make a circle in the scale that matches how your attitude would be if you find the sample for sale:

| | | | | | |
|------------------|----------------------------|------------------|-------------------------------|--------------|------------------------|
| Color-cup | Certainly would not buy it | Might not buy it | Might buy it/might not buy it | Might buy it | Certainly would buy it |
| Foil-cup | Certainly would not buy it | Might not buy it | Might buy it/might not buy it | Might buy it | Certainly would buy it |

Comments:

Fig. L.11 English version of questionnaire for sensory evaluation of dried-tomato

From total 76 panelists, our product gained higher scores on all tested attributes (Figure 13). The sensory score on appearance, color, sweetness and total likeness of our product showed statistically significant higher than Daiso product. Furthermore, our product obtained sensory scores more than 6 in a 9 points scale for all the attributes, except the aroma. These data indicated a good acceptance and more preference on our product than Daiso. Also, these data likely suggested that our product have potential for commercial-scale production.



Fig. L.12 Acceptability test of our dried-tomato comparing with Daiso product (n=76) used 9-point hedonic scales. Lines represent the average scores from all panelists. Asterisk (*) indicate a significant difference ($P < 0.05$) between our dried-tomato and Daiso product according to Dependent Samples t-test.

To study gender effect on the test, our dried-tomato scores data was analyzed on different gender, female (n=36) and male (n=40) panelists. As shown in Figure 14, female gave higher scores to all attributes except flavor which was equal with that of male. And female score showed significant higher on appearance and color. The result on purchase intent test (Figure 15) showed no significant different between 2 products but the average score of our product was slightly higher than Daiso.

Finally, we received some interesting idea from panelists comment. For example, our dried-tomato product seem to be fit to drink with Japanese-sake. And our dried-tomato product have potential to be sale as souvenir due to good appearance and color, especially the color which was brighter than the other dried-tomato the panelist ever seen.



Fig. L.13 Acceptability test of our dried-tomato in different gender (female n=36, male n=40) used 9-point hedonic scales. Lines represent the average hedonic scores from each genders. Asterisk (*) indicate a significant difference ($P < 0.05$) between our dried-tomato and Daiso product according to Z-test.

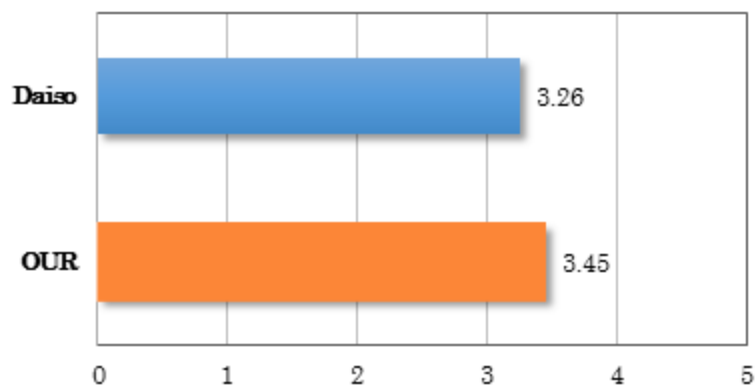


Fig. L.14 Purchase intense used 5-point hedonic scales (n=76). Bars represent the average scores from all panelists. Score 5: Certainly would buy it → score 1: Certainly would not buy it.

(5) Workshop

To introduce the local resident about the possibility of developing value-added product of tomato, we hold the workshop at Makura's farm, Chiyoda, Kita-Hiroshima. The workshop was conducted on October 8th, 2015. There were 9 local people participants joining the workshop. The participants learned step-by-step procedure for making the dried tomatoes. Interestingly, they also did their own experiment by trying their own recipe.

(6) Willingness-to-pay survey

The result of product's willingness-to-pay (WTP) survey conducted from the potential customer plays a crucial role in marketing management for pricing decisions of a new product. Therefore, WTP survey is essential for our dried tomato product. But before we conduct this survey, we need packaging for our product. The design of packaging is shown in Figure 16. We packed the dried tomatoes inside a plastic cup that is available in stores (e.g. Nafco). Firstly, we put the oxygen absorber and followed by putting 6 pieces of dried tomatoes inside each cup. Then, the cup is sealed using specially designed sticker paper as shown in Figure 16. The sticker includes a typographic logo and a unique character derived from a red tomato wearing sunglasses. The sunglasses is a symbol of the drying process which was done partly under the sun. Besides, we came up with the idea branding our product as "Dr. Tomato". The reason behind the name are as follows:

1. The word "Dr." is usually used as abbreviation for Doctor, which is related to healing and curing. This could represent our product as a healthy snack.
2. Based on our observation, some people refer "Dr." for "Dried".
3. The labors who prepared the product are doctoral students.

WTP survey was conducted on early November at Hiroshima University, Higashi-Hiroshima campus. We prepared WTP questionnaire as shown in Figure 17. Our panelists were professors, students, and staffs. Our detail method was showing Dr. Tomato product (with packaging), telling them the story of product such as making from organic tomato, and asking them to taste the product before filling the questionnaire. We were asking three questions as follows:

1. Above which price would you definitely not buy the product, because you can't afford it or because you didn't think it was worth the money?
2. Below which price would you say you would not buy the product because you would start to suspect the quality?
3. Please take a look at the dried-tomatoes' packaging. In which price you would buy for that product?

We recruited 36 panelists to participate the survey. WTP result shows in Figure 18. The price which consumer would buy the product was 220 ± 84 JPY. Usually WTP result expresses as a range of price which can be considered as price elasticity. Therefore, for next market survey, selling the product in the real market, we set the product price at 250 JPY.

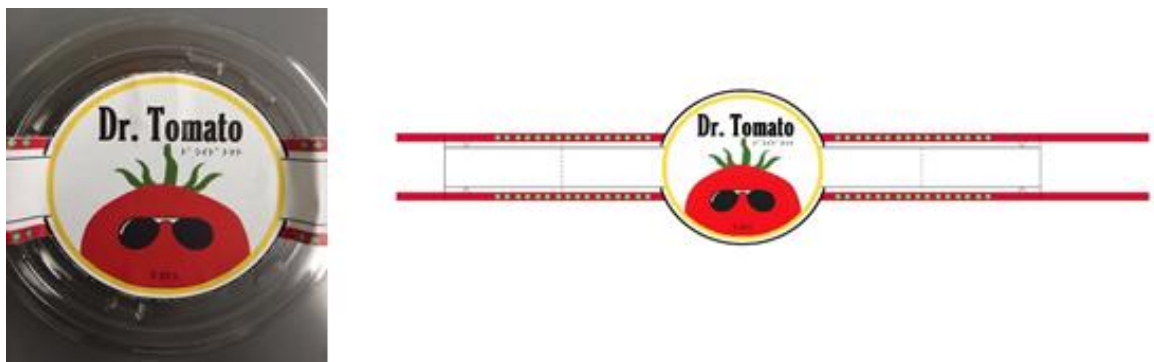


Fig. L.15 Packaging and seal of Dr. Tomato

調査を支払う意欲
Willingness to Pay Survey

性別 : 男 女

選択肢の中から一つを選んで○をつけて下さい

Please choose your age range:

15-24 25-34 35-44 45-54 55-64 >65

Above which price would you definitely not buy the product,
because you didn't think it was worth the money?

(Too expensive)

¥ _____

Below which price would you say you would not buy the
product because you would start to suspect the quality?

(Too cheap)

¥ _____

Please take a look at the dried-tomatoes' packaging.

In which price you would buy for this product?

¥ _____

ありがとうございます

Thank you!

Fig. L.16 Willingness-To-Pay (WTP) questionnaire

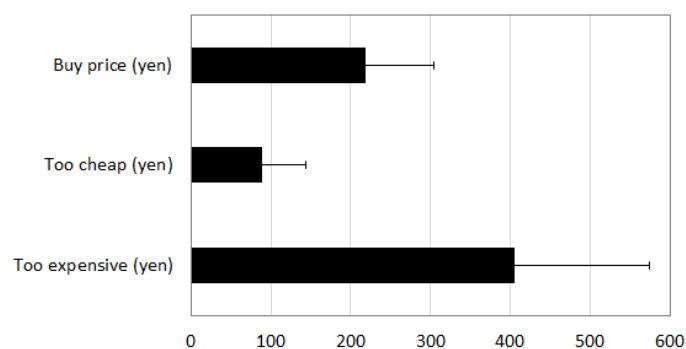


Fig. L.17 Willingness-To-Pay (WTP) result (n=36). Bars represent the average prices from all panelists.

(7) Market survey

Finally, we conducted the field experiment of market survey by selling Dr. Tomato product in real market. The field experiment aims to observe how the market reacts to our product and also their willingness to buy our product in the price range from previous WTP result. This experiment was held in the real-life situation, in this case is Green Ground Market (GGM) at Hiroshima city at November 8th, 2015. GGM is the organic market which is organized by the local Non-Profit Organization, namely Hiroshima-jin University Network (<http://hirojin.univnet.jp/>). It aims to directly connect between the producers (i.e. farmers, local shops, artists, etc.) and the consumers. GGM is held twice a year, which is in April (spring) and November (fall). The person in charge of the event, Mr. Minamisawa Katsuhiko, had agreed to have our dried tomatoes product sold in GGM. Our product was put in the booth of Tanbo Seminar (田んぼゼミ). Since we have been involved in Tanbo Seminar’s activities during the implementation of the project, they kindly accept to sell the product for us. So, our product was sold by using the name of Tanbo Seminar. Consequently, all the profits from the selling goes for them.

We prepared and packed our products using the packaging same like when we conducted WTP survey. After, expiration date’s sticker was putted at the bottom of the cup, our product is ready for sale (Figure 19). At GGM, our product was displayed as shown in Figure 20.



Fig. L.18 Final packaging of Dr. dried-tomato

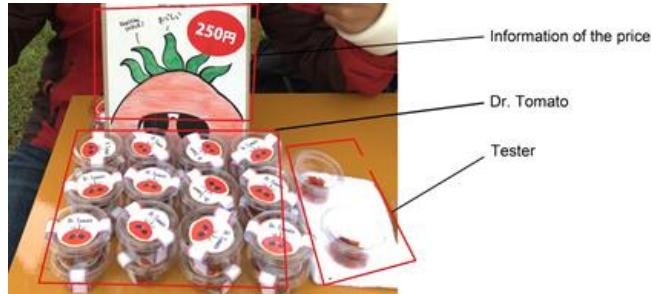


Fig. L.19 The display of the product in GGM

As shown in Figure 20, we provided the sample of the product so that people can freely taste it although they don't buy it. Through this method, we could observe their spontaneous comments. The observation is summarized in Figure 21.

We also observed how the market reacts to the price of our product. For that purpose, we intentionally change the price of the product. Starting from 10 am to 2 pm, we set the price at 250 JPY. While the price of 200 JPY was set from 2 pm to 3 pm. In total, we could sell 15 packs during the event. In the first 4 hours, we could sell 9 packs with the selling price of 250 JPY, while 6 packs were sold in the last one hour (from 2 pm to 3 pm) with the selling price of 200 JPY.



Fig. L.20 Spontaneous comments from visitors with various age range and gender.

The field experiment at GGM activity concludes the dried-tomatoes project. Through the workshop which is done in October, we have introduced the local people and the NPO in Oasa about the possibility to develop value-added product based on the tomatoes that were grown in their neighborhood. We have also completed the sensory evaluation survey which investigated people's preferences on the taste of different dried-tomatoes products. Moreover, the results obtained from the field experiment activities in GGM could show that the dried-tomatoes product is accepted by the market. The results from this study could be a useful insight for people in Kita-Hiroshima when they want to develop their own dried-tomatoes product in the future.

2.2 Cycling related activities

As part of the cultural creation and social implementation activities, we conducted the following cycling related activities: cycling tour (on September 27 th 2015), cycling tour survey (October 2015) and cycling map of Kita-Hiroshima. The objectives of these activities were:

1. To examine the potential of selected areas in Kita-Hiroshima for sports tourism and cycling.
2. To make the place more attractive to the tourists by making use of sports tourism,
3. To attract visitors to the sightseeing points of Kita-Hiroshima, and
4. To collect opinions and suggestions from visitors to improve the cycling related activities in the area.

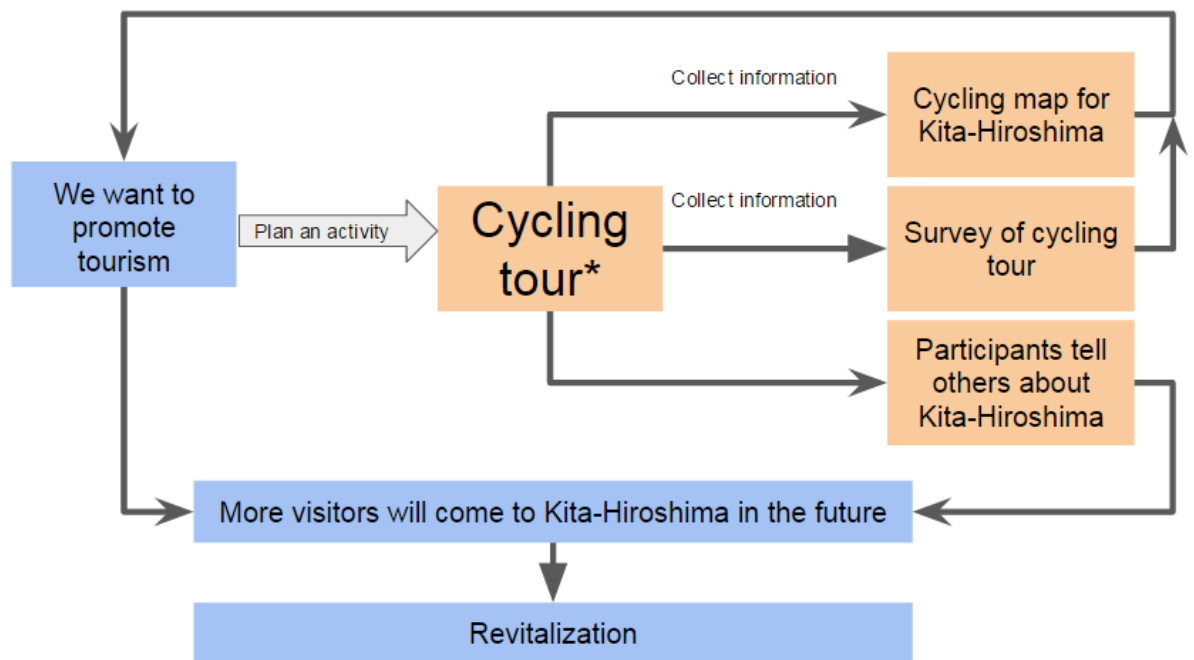


Fig. L.21 Cycling-related activities for the onsite team project in Kita-Hiroshima

2.2.1 Cycling tour

On September 27th, 10 cyclists from GULLS - Hiroshima University Triathlon Team agreed to join the cycling tour to Kita-Hiroshima. The idea was to reach Kita-Hiroshima from Higashi-Hiroshima and then return on the same day. The total distance covered was 151 km, from Hiroshima University to several locations in Kita-Hiroshima and back.

2.2.2 Cycling tour survey

After the cycling tour, the participants were asked to answer a survey questionnaire. The designed questionnaire was answered via Internet, as a web-based survey. Hereafter the design of the questionnaire and the results of the survey are exposed in more detail.



サイクリングツアーin北広島 / Cycling tour in Kita-Hiroshima

今回サイクリングツアーで訪れた場所について、皆さんの意見をお聞かせください。 / We would like to know your opinions about the cycling tour!

* Required

1.1 年齢（任意） / Your age? (optional)

1.2 このイベントより以前に、以下の場所に行ったことがありますか？ / Had you been in these places before the event? *

北広島内の場所 / Places in Kita-Hiroshima

| | はい、行ったことがあります。 / Yes | 行ったことはないが、聞いたことはあった。 / I had not been before but I heard of it | 行ったことはないし、聞いたこともない。 / I had not been nor heard of it |
|---|-----------------------|--|--|
| 千代田 / Chiyoda town | <input type="radio"/> | <input type="radio"/> | <input type="radio"/> |
| 大朝 / Oasa town | <input type="radio"/> | <input type="radio"/> | <input type="radio"/> |
| 天狗シデ / Tengushide | <input type="radio"/> | <input type="radio"/> | <input type="radio"/> |
| 北広島内の別の地域 / Other places of Kita-Hiroshima area | <input type="radio"/> | <input type="radio"/> | <input type="radio"/> |

Fig. L.22 Survey questionnaire of the Kita-Hiroshima cycling tour

2.2.3 Cycling map

Considering the results of the cycling tour survey, and additional surveys conducted by the team in the roads of the rural area of Chiyoda and Oasa, we proposed 5 different cycling routes to be introduced in a cycling map.

For the elaboration for the cycling map we followed systematically these steps:

1. Determine an optional route

2. Along each route, we listed points, elevations and distances
3. Calculate slopes (classify them into difficult, easy, medium)
4. Width of road section (bidirectional traffic, standard width, narrow, with/without sidewalks)
5. Register location of the places (and say nn km from the point zero)
6. Register location of convenience stores, vending machines and other services
7. Evaluate alternative options until finding the best routes that connect the sightseeing places, urban areas and other service areas. (back to 1 if necessary)

After the evaluation of possible routes, we decided 5 different routes to be added on the cycling map.

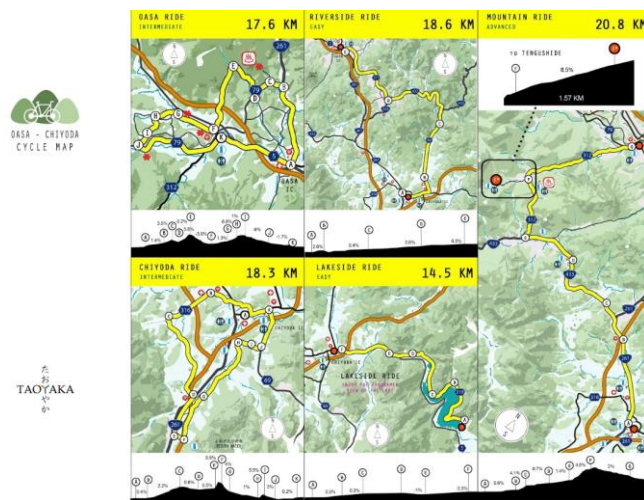


Fig. L.23 Cycling map front page.



Fig. L.24 Cycling map back page

4. Conclusions and findings from the Onsite Team Project activities

The findings from the research during the Onsite Team Project activities are summarized as follows:

1. The energy resulted from the whole tomato residue in the area could only cover the energy for heating two greenhouses in winter. This slightly increase the tomato production by 0.03%.
2. It would be possible to add non-greenhouse agricultural waste as the additional feedstock (e.g. rice straw) and some other renewable energy source.
3. Dried tomato produced by using the heat from SCWG is 1062% value-added from fresh tomato. It was successfully introduced to local people through dried-tomato-making workshop. The product's evaluation was done through questionnaire survey and market survey.
4. Results from routes survey and cycling tour held in Kita-Hiroshima were advantaged for cycling map designing. The map is to be distributed aiming at cycling tour promotional body.
5. Inspired with the rice planting festival, we would like to propose eco-tourism activity based on the cycle of tomato cultivation. For example, the tomato planting workshop can be held at the beginning of production while dried tomato making workshop can take place at peak of harvesting season. Furthermore, we propose the Tomato Matsuri (i.e. Festival). It is an event where all the businesses related to tomato can show off their specialty products, such as dried tomato or tomato based pasta for instance. This activity can be integrated to the current festivals in Kita-Hiroshima.

3. Effects to education and research of Hiroshima University

The Onsite Team Project in Kita Hiroshima was conducted to overcome the issues faced by the study area based on the uniqueness of the society, culture, and environment of the target site. This project had tried to create a cycle of science and technology with the cultural and social condition which have been nurtured in the region.

During the implementation of the project, the Onsite team faced many challenges and obstacles. These challenges and obstacles could be the reflections for the on-going educational practice and research in Hiroshima University. There are three main issues as follows:

1. A multidisciplinary approach

During the implementation of the project, the students worked closely with the teammates who are coming from many different disciplines. This experience trained students to redefine problems outside the normal boundaries and reach solutions based on the new understanding from multiple point of views.

The multidisciplinary approach should be further enhanced in the education practice in Hiroshima University. Most of the cases, student only focuses on their own field, with less knowledge of other disciplines, whereas, the problems faced by the world are complex, therefore, solutions which are derived from multidisciplinary perspectives are required.

2. Onsite reverse innovation

The solutions proposed in this project were generated from regional and social issues, designed to respond local needs, and produced by using the resources abundantly available from the site. This method of reserve innovation could lead to a new research topic that could contribute to the development of science in university. With this method in mind, students also could gain a sensitivity to diagnose the problem faced by our society and could provide an appropriate solution for them.

3. Business and management skill

Some drawbacks from this project are the reflection to the education and researches of Hiroshima University. It should be admitted that the feasibility of the project is still questionable because the lack of proper economic assessment in this project.

Business and management are the bridge between researches in the university with their implementation in the society. It is also becoming necessary for the students to be equipped with the entrepreneurship skill during their study in Hiroshima University.

4. Concrete plan or next steps in the future

The Onsite Team Project was conducted within duration of nine months. Many activities had been carried out. However, there are still some unsolved issues that required actions as follows:

1. Economic assessment on the proposed technology.

The SCWG proposed in this study has provided a good solution to treat the relatively wet feedstocks which are abundantly available in the rural areas. However, the system should be further assessed, especially about the feasibility of the system to be implemented in the area. Once the technology can be made feasible, the local government and people will be assured for having that technology in their area.

2. Realization of the dried-tomato product

The dried tomato produced in this study could give insight to the local people that the added value product could be very profitable. As we had conducted the workshop with the people in Kita-Hiroshima, we hope that they will create some businesses based on the idea we had given. The team will provide assistance to the people once they need want to develop a business in the future.

3. Distribution of cycling map

In order to enhance promotion of sport tourism in Kita-Hiroshima, we had given the cycling map to INE OASA, they will take part on the distribution of cycling map. The map will be updated based on feedbacks from the users. The Onsite Team will be in charge with any update and modification of the map.

As another batch of students will develop their project, the experiences from this activity could provide recommendations for the next team. The recommendations are summarized as follows:

1. Communication with the local people is important. Therefore, take as long as necessary to interact and learn as much as possible from the local communities.
2. The term “disadvantaged region” needs to be handled carefully. For academic discussion is fine, but for locals in the regions can be confusing, misleading, and to some extent even offensive.
3. It is better to focus on the advantages that a site has to offer to make it better (rather than the disadvantages).
4. Different approaches lead to different outcomes: “go to a place, find a problem”. Or “find a problem to solve, find a place, go to the place”.